ABSTRACT

The role of CCL25 and CCR9 in intestinal inflammation

Emily Wendt, Magdalen College & Nuffield Department of Clinical Medicine
Submitted for the degree of D. Phil in Clinical Medicine, Michaelmas Term 2013

Leukocyte extravasation is mediated in part by tissue specific chemotactic cytokines (chemokines) and specific chemokine receptors expressed on the surface of circulating cells. C-C chemokine ligand CCL25 is expressed exclusively in the intestine and thymus and mediates chemotaxis by cells expressing receptor CCR9. This chemokine and receptor pair may be relevant in the pathogenesis of intestinal inflammation, in diseases such as Crohn's disease (CD) and coeliac disease. In this thesis I investigated CCR9 expression in situ, in tissues affected by intestinal inflammation, and also examined the effects of CCR9 antagonist treatment in patients. *In vitro* I investigated CCR9 function using human peripheral blood T cells enriched for CCR9 by cell sorting or all-*trans* retinoic acid treatment.

Using tissues collected as part of a clinical trial in CD testing CCR9 antagonist, CCX282-B, I investigated ways of measuring if treatment reduced the number of CCR9 expressing cells in the intestinal mucosa. However, in situ staining for CCR9 by immunohistochemistry was unsuccessful, and in this thesis, I explored reasons why this might be the case. Treatment with CCX282-B did however, show a tendency to reduce T cell density in the intestinal mucosa, although results were highly variable between individuals.

In an examination of human CCR9 function *in vitro* I demonstrate for the first time that CCL25 stimulates CCR9 surface internalization. These data clarify the observation that CCR9 staining by IHC produces poor results in tissues where ligand is abundant, such as the intestine and thymus. I describe a novel technique for measuring calcium flux in two populations simultaneously by flow cytometry, which confirmed that in a heterogeneous population of cells, only CCR9 expressing cells respond to CCL25 by calcium flux.

Variability in clinical trials is partly created by the use of concomitant medications, and in CD, corticosteroids are widely used. For the first time I show that glucocorticoids (GC) impair CCR9 mediated chemotaxis, calcium flux and intracellular signalling without changes to CCR9 mRNA and surface protein expression. Reduced CCR9 mediated signalling was accompanied by an enhanced expression and function of co-expressed CXCR4, demonstrating that the effects of GC were receptor-specific and not mediated by non-specific toxicity or inhibition of cell signalling.

In a second study CCX282-B was tested in patients with coeliac disease, and in this trial, there was no reported concomitant use of GCs. It was confirmed that dietary gluten stimulates significant T cell recruitment to the intestinal mucosa with a pronounced accumulation of intraepithelial lymphocytes (IEL) and a rise in the frequency of FoxP3 expressing cells. Patients on CCX282-B had lower IEL counts, and an equivalent proportion of FoxP3 expressing T cells, suggesting that CCR9 blockade restricted the recruitment of effector T cell subsets. This thesis confirms that the accumulation of T cells is central to inflammation in the intestine and that modulating chemokine receptor function may affect this. Furthermore, this thesis demonstrates that the function of CCR9 is suppressed by GCs, which are widely used therapeutically and therefore could identify a novel mechanistic basis for their activity in CD.

ACKNOWLEDGEMENTS

I would like to thank my supervisor Satish Keshav, for giving me the opportunity to pursue a DPhil, and for integrating me into a talented scientific community. I am sincerely grateful for the excellent guidance, time spent improving my scientific thinking and for the constant moral support.

Professor David Greaves, who from very early on adopted me as a member of his laboratory despite my working on a cell type more 'fashionable' (but less cake worthy) than the macrophage. I sincerely appreciate all of the time spent discussing the vision, technical details and direction of my work, all the while reminding me to consider my life post DPhil.

I am also exceedingly grateful to the many talented students and postdocs I have met over the past four years. In particular Gemma White who graciously and always with tremendous insight could answer questions out of left field. I must also thank Asif Iqbal, who from some saintly place agreed to read my entire thesis, providing exceptional advice and invaluable support. To Michael Hunn, thank you for great discussions and scientific advice and for having an enviable ability to see the best in all data and to never get discouraged. And to Alex and Marianne, who have been wonderful to work with and have inspired me with their talents for medicine, Apple devices and serious multitasking.

I would like to thank my second chemokine-loving extended family at ChemoCentryx, without which I would not have had the means nor the confidence to pursue a DPhil. To Tom Schall, for graciously giving me the opportunity to contribute to exciting new and clinically relevant work in the chemokine field (without which Chapters 3 and 6 would not exist). To Matt Walters and Karen Ebsworth for their words of encouragement and invaluable insight into the British culture. And to Helen Wang and Dan Dairaghi for being wonderful mentors.

To my parents, for giving me all of their love and support over the past 28 years and for showing me that life only gets better with hard work. For allowing me to 'ride an elephant' throughout my life, with unfailing encouragement while sending me delicious care packages full of the "three essential food groups: cheese, chocolate and wine". I love you both.

Lastly I owe a huge thank you to Oliver, who has been the perfect partner through this journey. Thank you for supporting me through the good and the less good days, for making me laugh, for cooking me dinner when I get home late and for helping me keep this all in perspective.

ABBREVIATIONS

AM	acetoxymethyl
ANOVA	analysis of variance
AP-1	activator protein 1
APC	antigen presenting cells / allophycocyanin
ATRA	all *trans* retinoic acid
bp	base pair
BSA	bovine serum albumin
CCRL1	chemokine receptor like 1
CCX282-B	CCR9 small molecule antagonist (ChemoCentryx, Inc.)
CD	Crohn's disease
CDAI	Crohn's disease activity index
cDNA	complementary deoxyribonucleic acid
CRP	C reactive protein
Ct	threshold cycle
DAB	3,3'-diaminobenzidine tetrahydrochloride substrate-chromagen
DC	dendritic cell
ddH_20	distilled deionized water
DEPC	diethylpyrocarbonate
DEX	dexamethasone
DEOXY	deoxycorticosterone
DMSO	dimethyl sulfoxide
DNA	deoxyribonucleic acid
dNTP	deoxynucleotide triphoshates
DSS	dextran sulfate sodium
EDTA	ethylenediaminetetraacetic acid
ELISA	enzyme-linked immunosorbent assay
FACS	fluorescence-activated cell sorting
FCS	fetal calf serum
FITC	fluorescein isothiocyanate
FSC-A	forward scatter area
FSC-H	forward scatter height
GAG	glycosaminoglycan
GAPDH	glyceraldehyde 3-phosphate dehydrogenase
GC	glucocorticoid
GCR	glucocorticoid receptor
GPCR	G-protein coupled receptor
GRE	glucocorticoid response elements
HBSS	Hank's buffered salt solution
HEPES	4-(2-hyroxyethyl) piperazine-1-ethanesulfonic acid
HRP	horseradish peroxidase
IBD	Inflammatory Bowel Disease
ICAM	intercellular adhesion molecule
IFN-γ	interferon gamma
Ig	immunoglobulin
IHC	immunohistochemistry
IκB	inhibitor of κB

IL	interleukin
mAB	murine antibody
MAdCAM-1	mucosal addressin cell adhesion molecule 1
MIF	mifepristone
MFI	mean fluorescence intensity
mRNA	messenger ribonucleic acid
NFκB	nuclear factor κB
NK	natural killer
NP-40	nonidet P-40
NSAID	non-steroidal anti-inflammatory drug
PBL	peripheral blood leukocyte
PBMC	peripheral blood mononuclear cell
PBS	phosphate buffered saline
PCR	polymerase chain reaction
pDC	plasmacytoid dendritic cell
PE	phycoerythrin
PHA	phytohemagglutinin
PI(4,5)P_2	phosphoinositide (4,5)-bisphosphate
PLC	phospholipase C
PMA	phorbol-12-myristate-13-acetate
PRED	prednisolone
PSC	Primary Sclerosing Cholangitis
RIN	RNA integrity number
RNA	ribonucleic acid
RPMI	Roswell Park Memorial Institute medium
RT	Room temperature
qRT-PCR	quantitative real time polymerase chain reaction
SD	standard deviation
SDS-PAGE	sodium dodecly sulphate polyacrylamide gel electrophoresis
SEM	standard error mean
SSC-A	side scatter area
SSC-H	side scatter height
STAT	signal transducer and activator of transcription
TBS	tris buffered saline
TBS-T	tris buffered saline with 0.05% Tween-20
TNF	tumor necrosis factor
UC	Ulcerative Colitis
VCAM-1	vascular cell adhesion molecule 1
WT	wild type

TABLE OF CONTENTS

ABSTRACT i

ACKNOWLEDGEMENTS ii

ABBREVIATIONS iii

TABLE OF CONTENTS v

CHAPTER 1: Introduction 1

1.1 Overview of leukocyte extravasation 1

1.2 Chemokines and chemokine receptors 5

1.2.1 Chemokine structure and families 5

1.2.2 Chemokine receptors 6

1.2.3 Chemokine signalling mechanisms 7

1.2.4 Homeostatic and inflammatory chemokines 9

1.2.5 Regulation of chemokine receptor expression 10

1.3 CCR9 and CCL25 13

1.3.1 Identification of CCL25 (TECK) 13

1.3.2 Localization of CCL25 expression 13

1.3.3 Deorphanization of CCR9 14

1.3.4 Human CCR9 expression 15

1.3.5 Induction of CCR9 expression (all *trans* retinoic acid) 17

1.3.6 CCR9/CCL25 signalling 18

1.3.7 Phenotype and cytokine production by human $CCR9^+$ T cells 19

1.3.8 The role of CCR9 and CCL25 in human inflammation 20

1.3.9 CCR9 and CCL25 deficient mice and murine models of intestinal inflammation 23

1.4 Intestinal anatomy and immunity 27

1.4.1 Histology 28

1.4.2 Components of the intestinal immune system 29

1.4.3 Barrier defense and innate immunity 31

1.4.4 Adaptive immunity 32

1.4.5 Th1 cells 36

1.4.6 Th17 cells 37

1.4.7 Regulatory T cells 38

1.5 Inflammatory Bowel Disease (IBD) 40

1.5.1 Current prevalence and incidence 40

1.5.2 Health costs and economic impact 40

1.5.3 Crohn's disease 41

1.5.4 Ulcerative colitis 41

1.5.5 Cytokine environment in IBD 42

1.5.6 Chemokines implicated in intestinal inflammation 42

1.6 Corticosteroids in the treatment of IBD 49

1.6.1 Steroid hormones 49

1.6.1 Anti-inflammatory effect of glucocorticoids 50

1.7 Coeliac disease 51

1.7.1 Pathophysiology 52

1.8 Experimental Aims 53

CHAPTER 2: Materials and Methods 54

2.1 Materials 54

2.1.1 Cells 54

2.1.2 Cell culture materials 54

2.1.3 Immunohistochemistry reagents 54
2.1.4 Flow cytometry reagents 55
2.1.5 Migration assay reagents 55
2.1.6 Intracellular calcium flux reagents 55
2.1.7 Cell isolation and sorting reagents and equipment 56
2.1.8 Cytokine quantification by flow cytometry 56
2.1.9 Quantitative real time polymerase chain reaction (qRT-PCR) reagents 56
2.1.10 Phospho-kinase array and Western blotting reagents 56
2.1.11 Antibodies (flow cytometry, immunohistochemistry, and Western blotting) 58
2.1.12 Cytokines and chemokines 59
2.1.13 Primers 60
2.1.14 Steroids 60
2.2 Cell culture 61
2.2.1 Molt-4 cell culture 61
2.2.2 HEK-293 cell culture 61
2.2.3 CCR9 antibody collected from hybridoma supernatant 61
2.2.4 Long term cell storage 62
2.3 ATRA-cultured cell preparation 63
2.3.1 Primary cell isolation 63
2.3.2 All *trans* retinoic acid (ATRA)-culturing conditions 63
2.4 Immunohistochemistry 63
2.4.1 Introduction 63
2.4.2 Tissue and slide storage 64
2.4.3 Preparing cell cytospins 64
2.4.4 Slide preparation and antibody staining by IHC 65
2.4.5 Quantification of cell population stained by IHC 67
2.5 Flow cytometry 68
2.5.1 Measuring surface protein expression 68
2.6 Chemotaxis assay 69
2.6.1 Chemotaxis protocol 69
2.6.2 CellTiter-Glo® quantification of live cells 70
2.6.3 Steroid treated cell chemotaxis 70
2.7 Calcium flux assay 71
2.7.1 Introduction 71
2.7.2 Cell preparation 72
2.7.3 Ratiometric calcium flux measured by flow cytometry 73
2.7.4 Calcium flux assay ± DEX treatment 75
2.8 Internalization assay 76
2.8.1 Cell treatment 76
2.8.2 Analysis by flow cytometry 76
2.8.3 Preparation as cell cytospins 76
2.9 Measuring cytokine production by flow cytometry 76
2.9.1 Cell treatments 76
2.9.2 Staining for intracellular cytokines for analysis by flow cytometry 77
2.10 Sorting CCR9^{+} cells 77
2.11 Measuring cytokine concentrations in the cell supernatant by FlowCytomix™ Multiplex Technology 79
2.11.1 Introduction 79
2.11.2 Protocol 79
2.12 Human tissue and ethics 80
2.13 Quantitative reverse transcriptase polymerase chain reaction (qRT-PCR) 80
2.13.1 Tissue collection, storage and handling 80
2.13.2 RNA isolation 80
2.13.3 DNAse treatment 81

2.13.4 RNA quantification ... 81
2.13.5 RNA quality analysis ... 81
2.13.6 Reverse transcription ... 81
2.13.7 Primer design ... 82
2.13.8 Primer validation ... 83
2.13.9 qRT-PCR ... 83
2.13.10 Quantification ... 84
2.14 Phospho-kinase array and Western blotting ... 86
2.14.1 Cell stimulation ... 86
2.14.2 Lysate preparation ... 86
2.14.3 Determination of protein concentration ... 86
2.14.4 Phospho-kinase array ... 87
2.14.5 SDS-PAGE ... 87
2.14.6 Western blotting ... 87
2.14.7 Western blot stripping ... 88
2.15 Data analysis ... 88

CHAPTER 3: Quantifying changes to lymphocyte populations following CCR9 antagonist treatment during active Crohn's disease ... 90
3.1 Introduction ... 90
3.1.1 CCR9 antagonist, CCX282-B ... 90
3.1.2 Quantification by IHC ... 91
3.1.3 Aims of this chapter ... 92
3.2 Results ... 94
3.2.1 Evaluation of CCR9 staining by IHC ... 94
3.2.2 Alternative for estimating $CCR9^+$ cells in the small intestine by IHC (CD3 and CD8 double staining) ... 106
3.2.3 Lamina propria lymphocytes ... 108
3.2.4 Intraepithelial lymphocytes ... 110
3.2.5 Comparison between placebo and CCX282-B treatment in LPLs and IELs ... 110
3.3 Discussion ... 112
3.3.1 CCR9 staining by IHC ... 112
3.3.2 Utility in quantifying changes to intestinal lymphocyte density ... 114
3.3.3 Alternative mechanisms ... 115
3.3.4 Limitations of this study ... 116
3.3.5 Future experiments in this thesis ... 116

CHAPTER 4: Analysis of CCR9 signalling in human T cells and CCL25 mRNA expression from intestinal biopsies ... 118
4.1 Introduction ... 118
4.1.1 All *trans* retinoic acid induces CCR9 expression on T cells ... 118
4.1.2 Chemokine receptor internalization ... 119
4.1.3 Calcium flux ... 119
4.1.4 Cytokine secretion stimulated by integrins and chemokines ... 120
4.1.5 Characterization of CCL25 expression during intestinal inflammation ... 120
4.1.6 Aims of this chapter ... 121
4.2 Results ... 123
4.2.1 Characterization of human ATRA-cultured T cells used in this thesis ... 123
4.2.2 Chemokine-mediated migration by ATRA-cultured cells ... 127
4.2.3 Characterizing chemokine receptor expression by Molt-4 cells ... 130
4.2.4 Surface CCR9 internalization with CCL25 treatment ... 130
4.2.1 CCL25-mediated calcium flux in ATRA-cultured cells ... 136
4.2.2 Cytokines produced by ATRA-cultured cells and measured by flow cytometry ... 139
4.2.3 Effect of CCL25 on cytokine production ... 143

4.2.4 Measuring RNA quantity and quality isolated from human intestinal biopsies.....145
4.2.5 Chemokine mRNA expression along the gastrointestinal tract.....146
4.2.6 CCL25 mRNA expression in the small intestine with and without inflammation ..149
4.2.7 CCL25 mRNA expression during intestinal inflammation comparing colonic and small intestinal tissue.....149
4.3 Discussion.....152
4.3.1 ATRA-cultured cell characterization compared to primary CCR9+ T lymphocytes152
4.3.2 CCL25-mediated calcium flux in ATRA-cultured cells.....154
4.3.3 CCL25-mediated CCR9 internalization.....154
4.3.4 The effect of MAdCAM-1 on CCR9+ cell cytokine production.....155
4.3.5 Cytokine production following CCL25 treatment.....156
4.3.6 CCL25 production in the gastrointestinal tract ± inflammation.....157
4.3.7 Limitations to these studies.....158
4.3.8 Future experiments in this thesis.....159

CHAPTER 5: The effect of corticosteroids on CCR9-mediated cell signalling and chemotaxis 160
5.1 Introduction.....160
5.1.1 The effects of glucocorticoids on T cells.....160
5.1.2 The effect of steroids on chemokine receptor expression.....160
5.1.3 Rationale for the experiments.....162
5.1.4 Aims of this chapter.....162
5.2 Results.....163
5.2.1 *In vitro* glucocorticoid treatment and controls.....163
5.2.2 The effect of dexamethasone on chemokine receptor expression in ATRA-cultured cell 163
5.2.3 The effect of dexamethasone on ATRA-cultured cell migration.....165
5.2.4 The effect of dexamethasone on Molt-4 cells.....167
5.2.5 Isolation of primary CCR9+ T cells.....169
5.2.6 Optimizing sorted CCR9+ T cell migration conditions.....169
5.2.7 The effect of dexamethasone on chemokine receptor expression in primary CCR9+ T cells 170
5.2.8 The effect of dexamethasone on chemokine mediated cell migration in primary CCR9+ T cells.....170
5.2.9 The effect of dexamethasone on CD4 and CD8 T cell migration.....171
5.2.10 Calcium assay.....174
5.2.11 The effect of dexamethasone calcium flux.....174
5.2.12 The effect of corticosteroids on CCR9-mediated chemotaxis.....178
5.2.13 The effect of mifepristone on chemokine receptor expression.....180
5.2.14 The effect of mifepristone on chemokine mediated cell migration.....181
5.2.15 The effect of dexamethasone on CCL25-mediated CCR9 internalization.....184
5.2.16 Phospho-kinase array of CCR9+ ATRA cultured cells ± CCL25.....184
5.2.17 The effect of dexamethasone on total PLCγ1 and phospho-PLC-γ1.....187
5.2.18 The effect of dexamethasone on PLCγ1 mRNA.....187
5.2.19 CCRL1 expression by CCR9+ T cells.....188
5.2.20 The effect of dexamethasone on CCRL1 expression in human CCR9+ T cells.....191
5.3 Discussion.....194
5.3.1 Divergent effect of DEX on CCR9, CXCR4 and CXCR3.....196
5.3.2 The role of PLCγ1 in CCR9 signalling.....197
5.3.3 Potential clinical relevance.....198
5.3.4 Translating in vitro results in vivo.....198
5.3.5 Effects of GCs on CCL25 stimulated adhesion.....199
5.3.6 CCRL1 expression by CCR9+ T cells.....200
5.3.7 Limitation to these studies and potential future considerations.....200

5.3.8 Future experiments in this thesis 201

CHAPTER 6: Quantifying changes to lymphocyte populations following CCR9 antagonist treatment (CCX282-B) during active Coeliac disease 202

6.1 Introduction 202

6.1.1 Aims of this chapter 204

6.2 Results 205

6.2.1 CD3 and FoxP3 double labelling by immunohistochemistry 205

6.2.2 Lamina propria $CD3^+$ cells 208

6.2.3 Lamina propria $FoxP3^+$ T cells 210

6.2.4 Intraepithelial $CD3^+$ cell 212

6.3 Discussion 214

6.3.1 Effect on IELs 214

6.3.2 FoxP3 expressing cell accumulation 216

6.3.3 Limitations of this study 216

CHAPTER 7: Final Discussion 217

7.1 Summary of key advances in this thesis 217

7.2 Future directions and outstanding issues 221

7.2.1 Quantifying the effect of CCX282-B (or other therapies) on lymphocyte density in the intestine 221

7.2.2 *in situ* Hybridization 221

7.2.3 Investigating the effect of MAdCAM-1 on cytokine production 222

7.2.4 Studying the effect of glucocorticoids on CCR9 function *in vivo* 223

7.2.5 Examining the effect of glucocorticoids on CCL25 expression 223

7.2.6 Studying the mechanism of CCR9 inhibition by glucocorticoids 224

7.2.7 Designing intestinal specific glucocorticoids 224

REFERENCES 225

APPENDIX 1: Solutions used in this thesis 247

APPENDIX 2: Manuscripts and published work 249

APPENDIX 3: Anti-human CCR9 antibodies rejected from used by IHC 250

APPENDIX 4: Representative PROTECT-1 biopsies 253

APPENDIX 5: Representative biopsies from the duodenum (Clinical trial in coeliac disease) 259

LIST OF TABLES AND FIGURES

Figure 1.1 Mediators of leukocyte extravasation. 4
Figure 1.2 Chemokine structure and family relationship. 5
Figure 1.3 Generalized schematic of chemokine receptor mediated intracellular signalling pathways. 8
Table 1.1 Human chemokines receptors, their cognate ligand(s) and the cells which express them. 11
Table 1.2 Frequency of CCR9 expression by cell type (human). 15
Figure 1.4 Schematic representation of the healthy gastrointestinal tract. 30
Table 1.3 Cytokines, their sources and activities. 34
Figure 1.5 $CD4^+$ effector cell subsets distinguished by Th cell polarization. 39
Table 2.1 Antibodies used in this thesis for flow cytometry. 58
Table 2.2 Antibodies used in this thesis for immunohistochemistry. 59
Table 2.3 Antibodies used in this thesis for Western blotting. 59
Table 2.4 Recombinant proteins used in this thesis. 59
Table 2.5 Primers used in this thesis. 60
Table 2.6 Steroids used in this thesis. 60
Figure 2.1 Separation of epithelium from lamina propria and subsequent quantification of tissue area and cell number using Photoshop 'laso' and 'count' tool. 68
Figure 2.2 Transwell® chemotaxis assay. 69
Figure 2.3 CellTiter-Glo® and Trypan Blue Stain are equivalent measures of live cells. 71
Figure 2.4 Fura Red ratiometric analysis of calcium flux. 74
Figure 2.5 Predicted $CCR9^+CD3^+$ cell isolation from buffy coat derived PBMC. 78
Master mix 1 83
Figure 2.6 Sample output from real time SYBR green PCR experiment and validation of primer pairs. 85
Figure 2.7 Standard curve for BCA Protein Assay. 87
Figure 3.1 PROTECT-1 trial design and clinical response to CCX282-B measured in Crohn's disease. 93
Figure 3.2 Cell cytospins stained by IHC. 95
Figure 3.3 Human tonsil and thymus stained by IHC. 98
Figure 3.4 Human intestinal tissue stained for CCR9. 99
Figure 3.5 Human intestinal lymphoid follicle stained for CCR9. 100
Figure 3.6 CCR9 stained intestinal epithelial cells and intraepithelial lymphocytes. 101
Figure 3.7 CCR9 and CD3 double staining in human small intestinal tissue. 103
Figure 3.8 CCR9 and CD8 double staining in human small intestinal tissue. 104
Figure 3.9 CCR9 and CD68 double stained of human large intestine by IHC. 105
Figure 3.10 CD3 and CD8 double staining and quantification of biopsies from PROTECT-1. 107
Figure 3.11 Quantification of lamina propria lymphocytes. 109
Figure 3.12 Quantification of intraepithelial lymphocytes. 111
Figure 4.1 All *trans* retinoic acid (ATRA) induces CCR9 surface expression in human T cells. 124
Figure 4.2 Characterization of ATRA-cultured cells used in this thesis. 125
Figure 4.3 Chemokine receptor expression by ATRA-cultured cells. 126
Figure 4.4 CCL25 stimulates a dose-dependent increase in ATRA-cultured cell chemotaxis. 128

Figure 4.5 ATRA-cultured cells migrate to increasing concentrations of CXCL11 and CXCL12 and do not migrate to CCL5. 129
Figure 4.6 Chemokine receptor expression by Molt-4 cells. 131
Figure 4.7 Surface CCR9 is internalized upon treatment with CCL25 in a dose dependent manner. 132
Figure 4.8 CCL25-mediated CCR9 internalization is time dependent. 134
Figure 4.9 CCR9 internalization on Molt-4 and ATRA-cultured cells visualized by IHC on cell cytospins. 135
Figure 4.10 $CCR9^+$ ATRA-cultured cells calcium flux in response to CCL25. 137
Figure 4.11 CCL25 stimulates a dose-dependent increase in calcium flux in $CCR9^+$ ATRA cultured cells. 138
Figure 4.12 Cytokine production by ATRA-cultured cells following PMA/ionomycin activation. 140
Figure 4.13 $CCR9^+$ T cell cytokine production. 142
Figure 4.14 The effect of CCL25 on $CCR9^+$ T cell cytokine production. 144
Figure 4.15 Validating RNA isolation from intestinal biopsies. 147
Figure 4.16 Chemokine expression along the gastrointestinal tract from a single patient. 148
Figure 4.17 CCL25 mRNA expression in the terminal ileum during active Crohn's disease. 150
Figure 4.18 CCL25 mRNA expression during active IBD. 151
Figure 5.1 Chemokine receptor expression following dexamethasone treatment in ATRA-cultured cells. 164
Figure 5.2 Chemokine-mediated cell migration following dexamethasone treatment in ATRA-cultured cells. 166
Figure 5.3 Dexamethasone does not affect CCR9- nor CXCR4-mediated cell migration in Molt-4 cells. 168
Figure 5.4 Optimizing chemotaxis conditions for primary human $CD3^+CCR9^+$ cells. 172
Figure 5.5 The effect of dexamethasone on CCR9 and CXCR4 surface expression and CCR9- and CXCR4-mediated chemotaxis in primary human $CCR9^+$ T cells. 173
Figure 5.6 Calcium assay design to simultaneously monitor vehicle- and dexamethasone-treated T cells. 176
Figure 5.7 Dexamethasone reduces CCL25-mediated calcium flux in $CCR9^+$ T cells. 177
Figure 5.8 Corticosteroids with glucocorticoid and not mineralocorticoid activity reduce CCR9-mediated cell migration. 179
Figure 5.9 Titrating mifepristone (MIF) on ATRA-cultured cells. 182
Figure 5.10 The effect of mifepristone on CCR9 and CXCR4 receptor expression and receptor-mediated chemotaxis. 183
Figure 5.11 Dexamethasone has no effect on CCL25-mediated CCR9 internalization. 185
Figure 5.12 Phospho-kinase array of $CCR9^+$ T cells ± CCL25. 186
Figure 5.13 Dexamethasone reduces total PLCγ1 and CCL25-stimulated P-PLCγ1 in $CCR9^+$ T cells 189
Figure 5.14 Effect of dexamethasone on PLCγ1 mRNA in $CCR9^+$ T cells. 190
Figure 5.15 $CCR9^+$ ATRA-cultured cells express CCRL1 mRNA. 192
Figure 5.16 The effect of dexamethasone on CCRL1 mRNA expression. 193
Figure 5.17 Suggested model of GC mediated effects on human $CCR9^+$ T cells. 195
Figure 6.1 Double blind Phase II study of CCX282-B in patients with coeliac disease. 204
Figure 6.2 Human tissue double stained for CD3 and FoxP3 by IHC. 206
Figure 6.3 Matched coeliac patient biopsies at Baseline and Day 91 stained for CD3 and FoxP3 by IHC. 207
Figure 6.4 Lamina propria $CD3^+$ cells. 209

Figure 6.5 FoxP3^{+} cells within the lamina propria. 211
Figure 6.6 Intraepithelial CD3^{+}....213
Figure 7.1 The role of CCL25 and CCR9 in human small intestinal inflammation based on published data and novel data presented in this thesis.....220
CCR9 R&D Clone 248605.111 250
CCR9 R&D Clone 96-1.5 251
CCR9 R&D Clone 248601 252
Representative PROTECT-1 clinical trial biopsy (1 of 6)....253
Representative PROTECT-1 clinical trial biopsy (2 of 6)....254
Representative PROTECT-1 clinical trial biopsy (3 of 6)....255
Representative PROTECT-1 clinical trial biopsy (4 of 6)....256
Representative PROTECT-1 clinical trial biopsy (5 of 6)....257
Representative PROTECT-1 clinical trial biopsy (6 of 6)....258
Matched Coeliac patient biopsies page 1 of 2 (placebo treatment). 259
Matched Coeliac patient biopsies page 2 of 2 (placebo treatment) 260
Matched Coeliac patient biopsies page 1 of 2 (CCX282-B treatment) 261
Matched Coeliac patient biopsies page 2 of 2 (CCX282-B treatment) 262

CHAPTER 1: Introduction

Inflammation can be classified as an acute or chronic response, the former distinguished by the accumulation of neutrophils (and to a lesser extent mononuclear cells) within hours and days, while the later is largely comprised of lymphocytes, differentiated macrophages and plasma cells accumulating over weeks, months and years [1]. Acute inflammation, as originally described by Cornelius Celsus in the first century AD, is characterized by 'rubor et tumour cum calore et dolore,' which translates to 'redness and swelling with heat and pain.' If left unresolved, acute and chronic inflammation can produce the fifth element of inflammation, 'functio laesa' or 'loss of function' [2]. While cell mediated inflammation is described in the innovative experiments of 1867 by Julius Cohnheim, observing leukocyte migration through the inflamed mesentery and transparent tongue of a frog [2-4]; and in 1882 by Elie Metchnikoff, describing cell recruitment and phagocytosis of a rose thorn in the transparent starfish larvae [2,5]; in the last 30 years, many key molecular mediators of leukocyte trans-endothelial migration have been discovered, and their mechanism of action better defined.

1.1 Overview of leukocyte extravasation

The extravasation of leukocytes during an inflammatory response is a multistep process mediated by members of the selectin, integrin and chemokine families [6-8]. Inflammatory mediators such as histamine, thrombin, complement fragments, and pro-inflammatory cytokines (eg IFN-γ, TNF-α, IL-1β) stimulate the expression, presentation and activation of these molecules, in addition to increasing vascular permeability, coordinating cell recruitment to the source of insult [9,10]. The multistep paradigm of cell attachment/rolling, activation and arrest are illustrated in Figure 1.1, the first step of which is mediated by selectins.

Selectins are a family of C-type lectins (E-selectin, P-selectin and L-selectin) expressed by endothelial cells and leukocytes [11]. Interactions between selectins and selectin ligands form weak bonds which slow the flow of leukocytes as they pass along the vasculature, promoting initial cell capture and rolling [6-8]. Selectin ligands are glycoproteins such as sialyl-Lewis X (sLe^x) expressed on the surface of endothelial cells and P-selectin glycoprotein ligand 1 (PSGL1) expressed by leukocytes [9,11-14]. P-selectin is stored in Weibel-Palade bodies of endothelial cells and upon cell activation, is rapidly mobilized to the plasma membrane, binding neutrophils and monocytes during acute and chronic inflammation [6,15]. E-selectin in contrast requires *de novo* mRNA and protein synthesis before externalization, and is inducibly expressed following various inflammatory stimuli (eg TNF-α, LPS, IL-1β) [16,17]. L-selectin is constitutively expressed by the majority of leukocytes, excluding subsets of memory and effector T cells, and has a critical role in lymphocyte and dendritic cell movement to secondary lymphoid tissues in addition to mediating rolling at peripheral sites of injury and inflammation [6,13,18].

Leukocyte rolling allows surface chemokine receptors to come into contact with cognate chemokines presented on the surface of endothelial cells by glycsoaminoglycans (GAGs). Chemokines are a family of chemotactic cytokines which induce directional migration though interaction with specific cell surface chemokine receptors (to be discussed in section 1.2). Chemokines also stimulate 'inside-out' signalling,' a term to describe the rapid conformational change and activation of surface integrins from a low affinity, to high affinity state [8,19]. Activated integrins in turn promote firm adhesion to the vascular endothelium through interactions with specific adhesion molecules.

Integrins are cell surface receptors composed of an α and β subunit. On resting leukocytes, integrins are present in an inactive conformation but are rapidly activated in response to inflammatory mediators and chemokine stimulation [20-22]. Activated integrins bind members

of the immunoglobulin superfamily referred to as cell adhesion molecules (CAMs) which include intercellular-CAM (ICAM-1)($\alpha_L\beta_2$ and $\alpha_M\beta_2$), vascular-CAM (VCAM-1)($\alpha_4\beta_1$ and $\alpha_4\beta_7$), and mucosal addresssin-CAM (MAdCAM-1)($\alpha_4\beta_7$) [23]. The binding between integrin and CAMs leads to integrin clustering, stabilizing a firm adhesion between leukocyte and the vascular endothelium [8,24].

The final step in cell extravasation involves the transmigration or *diapedesis* of leukocytes across the endothelium. This process can be achieved trancellularly (through the endothelial cells) or more commonly, paracellularly (between endothelial cells). Endothelial cells actively participate in this process, forming homophilic interactions with leukocytes via platelet/endothelial cell adhesion molecule 1 (PECAM-1), junctional adhesion molecules (JAMs) and CD99 [8,25,26]. A cell that has transversed the endothelium and underlying basement membrane must migrate through the interstitial extracellular matrix to reach the final site of inflammation [27]. This is achieved through directional migration, which requires the presence of a chemokine concentration gradient and is referred to as chemotaxis.

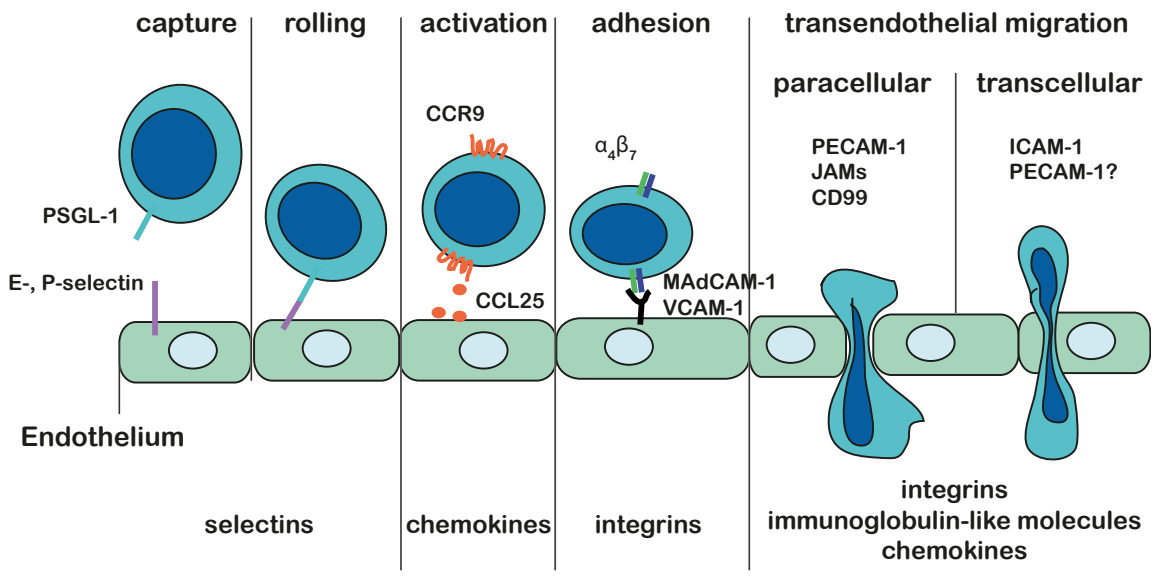


Figure 1.1 Mediators of leukocyte extravasation.
Schematic summary of molecules responsible for different stages of leukocyte extravasation with CCR9 and integrin $\alpha_4\beta_7$ used as an example. Data compiled from Springer *et al* (1994), Stefanelli *et al* (2008), Ley *et al* 2007 [6,8,28].

1.2 Chemokines and chemokine receptors

1.2.1 Chemokine structure and families

Chemokines are a family of small (70 – 130 amino acids or 8 – 10 kDa) structurally related cytokines best characterized for their chemotactic properties. The 48 identified chemokines in the human genome share between 20 – 90% sequence homology and are classified into four families: C, CC, CXC, and CX_3C (C = Cysteine; X = other amino acid) based upon the position and interaction of four conserved cysteine residues (Figure 1.2) [29,30]. A final family of chemokine, XC chemokines, are the exception to the four cysteine paradigm as XCL1 and XCL2 contain only two cysteine residues [30].

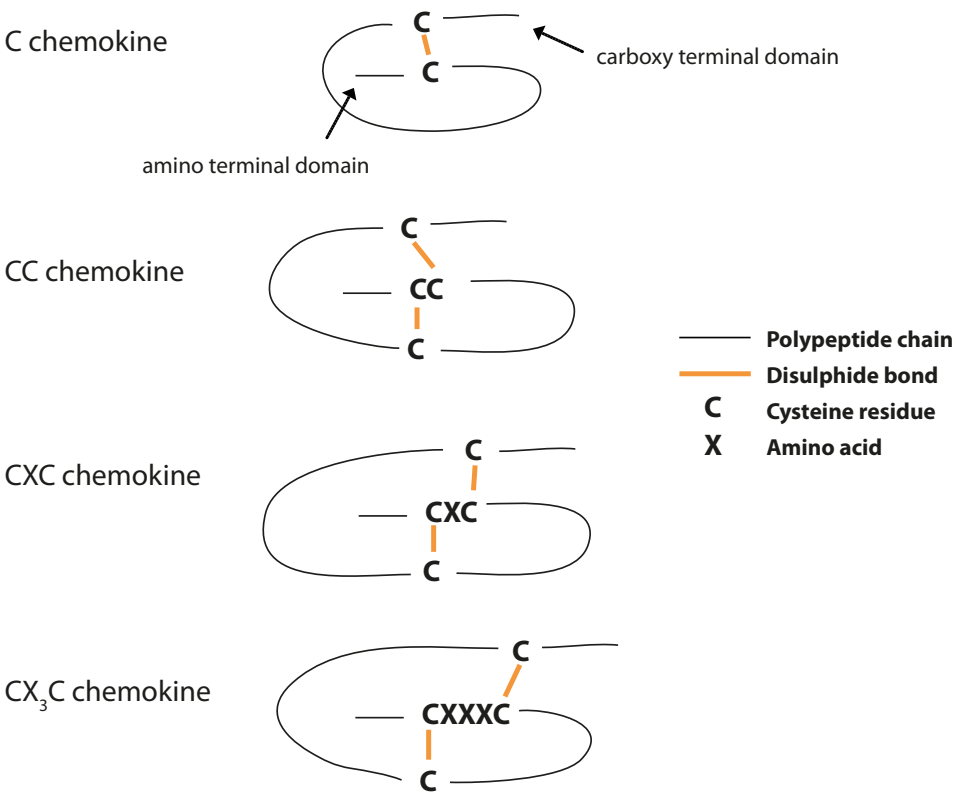


Figure 1.2 Chemokine structure and family relationship.
The four chemokine families are defined on the basis of conserved cysteine residues. Figure adapted from Burke-Gaffney *et al* (2002) [31].

1.2.2 Chemokine receptors

Chemokines bind to seven transmembrane, G-protein coupled chemokine receptors, predominantly expressed on the surface of leukocytes. The 19 chemokine receptors identified in the human genome are named in relation to the chemokines they bind: XCR1 (binds XC chemokines), CCR (bind CC chemokines), CXCR (bind CXC chemokines) and CX_3CR1 (binds CX3C chemokine, Fractalkine) [32]. As there are many more chemokines than chemokine receptors, most chemokine receptors interact with multiple chemokines and moreover, most chemokines interacting with multiple chemokine receptors. Table 1.1 summarizes the chemokine/chemokine receptor pairing and the leukocytes on which each receptor is expressed.

Structurally, transmembrane chemokine receptors are composed of an extracellular N-terminus, seven transmembrane domains and an intracellular C-terminus. The N-terminus is responsible for chemokine binding and specificity, while the C-terminus is the site of phophorylation following activation [33,34]. Chemokine receptors share a conserved Aspartic acid-Arginine-Tyrosine (DRY) motif in the second intracellular transmembrane loop which is thought to be critical for signalling [35]. In the human genome, three non-signalling chemokine receptors have been identified which lack the DRY motif: DARC (Duffy Antigen Receptor for Chemokines), D6, and CCRL1 (Chemokine Receptor Like 1) [34]. These atypical chemokine receptors bind cognate ligand but do not signal and are believed to act as a scavenger receptors, modifying levels of chemokine *in vivo* [35,36].

1.2.3 Chemokine signalling mechanisms

Chemokine receptor activation involves several secondary messengers that ultimately effect cell polarity and promotes directed cell movement. Between different chemokine receptors and across different cell types, the kinetics and specifics of signalling are variable, however a general schematic is illustrated by Figure 1.3. Chemokine receptor activation causes the dissociation of Gα and Gβγ subunits. The majority of chemokine receptors are Gαi coupled which is critical for chemotaxis as demonstrated by functional sensitivity to the Gαi inhibitor, pertussis toxin [37]. Some chemokines including CCL2, CCL5 and CXCL8 are demonstrated to activate alternative G proteins such as Gq and Gz, although their role in chemotaxis is not well defined [38,39]. Dissociated Gαi protein inhibits adenylate cyclase activity, reducing intracellular cAMP levels [37]. Free Gβγ subunit in turn, rapidly catalyzes the phosphorylation and activation of Phospholipase C (PLC).

One example of the complexity to chemokine signalling is the involvement of PLC. Over 13 PLC isoforms exist and mutational studies suggest that several isoforms can contribute to chemotaxis to varying degrees and different isoforms can be activated depending on the chemokine receptor and cell type studied [40,41]. PLC in turn catalyzes the hydrolysis of phosphoinositide (4,5)-bisphosphate (PIP_2) in the plasma membrane, releasing 1,4,5-triphosphate (IP_3) and diacylglycerol (DAG).

Cytosolic IP_3 interacts with IP_3 receptors expressed on the surface of the endoplasmic reticulum (ER), stimulating the release of intracellular calcium stored in the ER. DAG in turn activates Protein kinase C (PKC) which is responsible for subsequent phosphorylation and desensitization events. Chemokine receptor activation is also demonstrated to activate phosphoinositide 3-kinase (PI3K) and members of the mitogen-activated protein kinase (MAPK) cascade including ERK1/2, p38 and c-Jun N terminal kinase (JNK) [37,41,42].

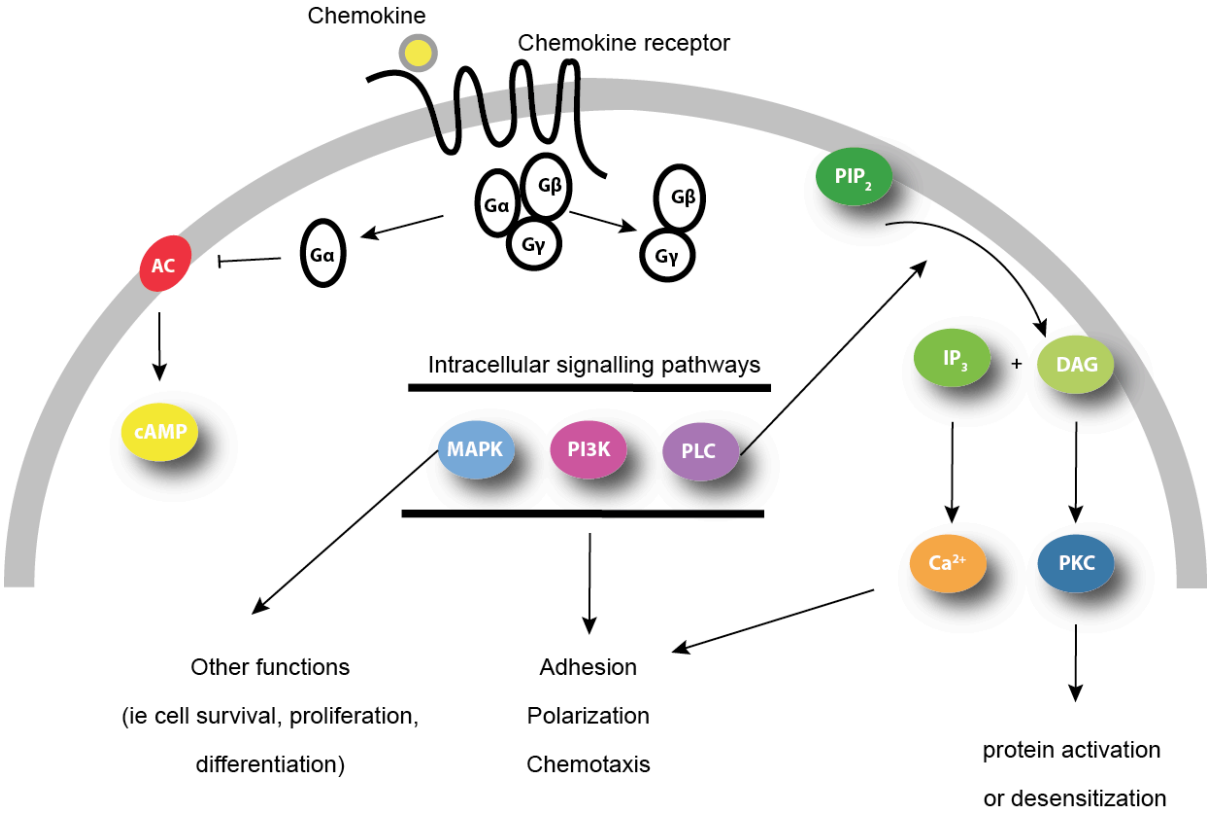


Figure 1.3 Generalized schematic of chemokine receptor mediated intracellular signalling pathways.
Abbreviations: AC = adenylate cyclase, cAMP = cyclic adenosine monophosphate, MAPK = mitogen activated protein kinase, PI3K = phosphoinositide 3-kinase, PLC = Phospholipase C, PIP_2 = phosphoinositide (4,5)-bisphosphate, IP_3 = 1,4,5-triphosphate, DAG = diacylglycerol, PKC = Protein kinase C.

1.2.4 Homeostatic and inflammatory chemokines

Chemokines that are constitutively expressed coordinate the homeostatic circulation of leukocytes; this has a critical utility in establishing the architecture of secondary lymphoid follicles and maintaining immune surveillance at peripheral tissues. Other chemokines are only found at sites of inflammation, inducibly expressed by activated cells and are involved in recruiting appropriate subsets of effector cells to the site of infection or injury. Table 1.1 distinguishes homeostatic from inflammatory chemokines.

The distinction between homeostatic and inflammatory chemokines is less clear for some ligands including CCL17, CCL22 and CCL25. CCL17 and CCL22 are the two ligands specific to CCR4; CCR4 expression is associated with T cell subsets that produce interleukins 4 and 5 (Th2 cells, to be discussed in Section 1.4.4), involved in stimulating the humoral immune response. Whilst these two chemokines are constitutively expressed by secondary lymphoid organs and non-lymphoid tissue, expression can be induced by inflammation and a role in the pathogenesis of allergic airway inflammation, atopic dermatitis, atherosclerosis and septic shock syndrome have been suggested [43-45]. Another example of a chemokine with mixed homeostatic and inflammatory properties is CCL25. CCL25 is the single ligand to CCR9 and is constitutively expressed in the thymus and small intestine. However in both human and animal studies of liver inflammation, CCL25 expression is induced during inflammation and is believed to exacerbate disease by recruiting pro-inflammatory CCR9 expressing cells [46,47]. Furthermore, an inflammatory contribution during intestinal disease is suggested by clinical observations and is demonstrated in some murine studies of intestinal inflammation; these topic will be thoroughly discussed in Sections 1.3.8 & 1.3.9.

1.2.5 Regulation of chemokine receptor expression

Chemokine receptor expression, in combination with adhesion molecules (selectins and integrins) coordinate the movement of leukocytes during cell differentiation, immune surveillance, and tissue specific homing to the source of antigen insult. Therefore the regulation and induction of chemokine receptor expression is one mechanism by which cell movement is synchronized with specific immunological needs.

Homing to and within secondary lymph nodes

Conventional DCs are produced in the bone marrow and are capable of expressing an array of chemokine receptors (including CCR1, CCR2, CCR5, CCR6, CXCR1, CXCR2) which direct them to various peripheral tissues [48]. When foreign antigen is collected, chemokine receptors are down-regulated and CCR7 surface expression is induced, rapidly mobilizing the DC to a lymph node for antigen presentation [49]. CCR7 interacts with cognate ligands CCL19 and CCL21, constitutively expressed in secondary lymph nodes by resident DCs and high endothelial venules (HEV) respectively [48,50,51].

Naive T cells also express CCR7 and L-selectin which direct their circulation between lymph nodes through interactions with HEV [52]. Collectively, CCR7 and cognate ligands position naïve T cells in close proximity to antigen presenting cells, supporting efficient T cell priming (to be discussed in Section 1.4.4) [53]. Following antigenic stimulation, CCR7 expression is down-regulated; some effector $CD4^+$ cells up-regulate expression of CXCR5 (interacting with CXCL13) and CCR4 (interacting with CCL17 and CCL22), directing their migration towards the B cell follicle to help B cells produce antibodies [54,55]. Other effector T cells are programmed to return to the initial site of infection, a process dependent on the antigen and lymph node microenvironment in which the naïve T cell was primed.

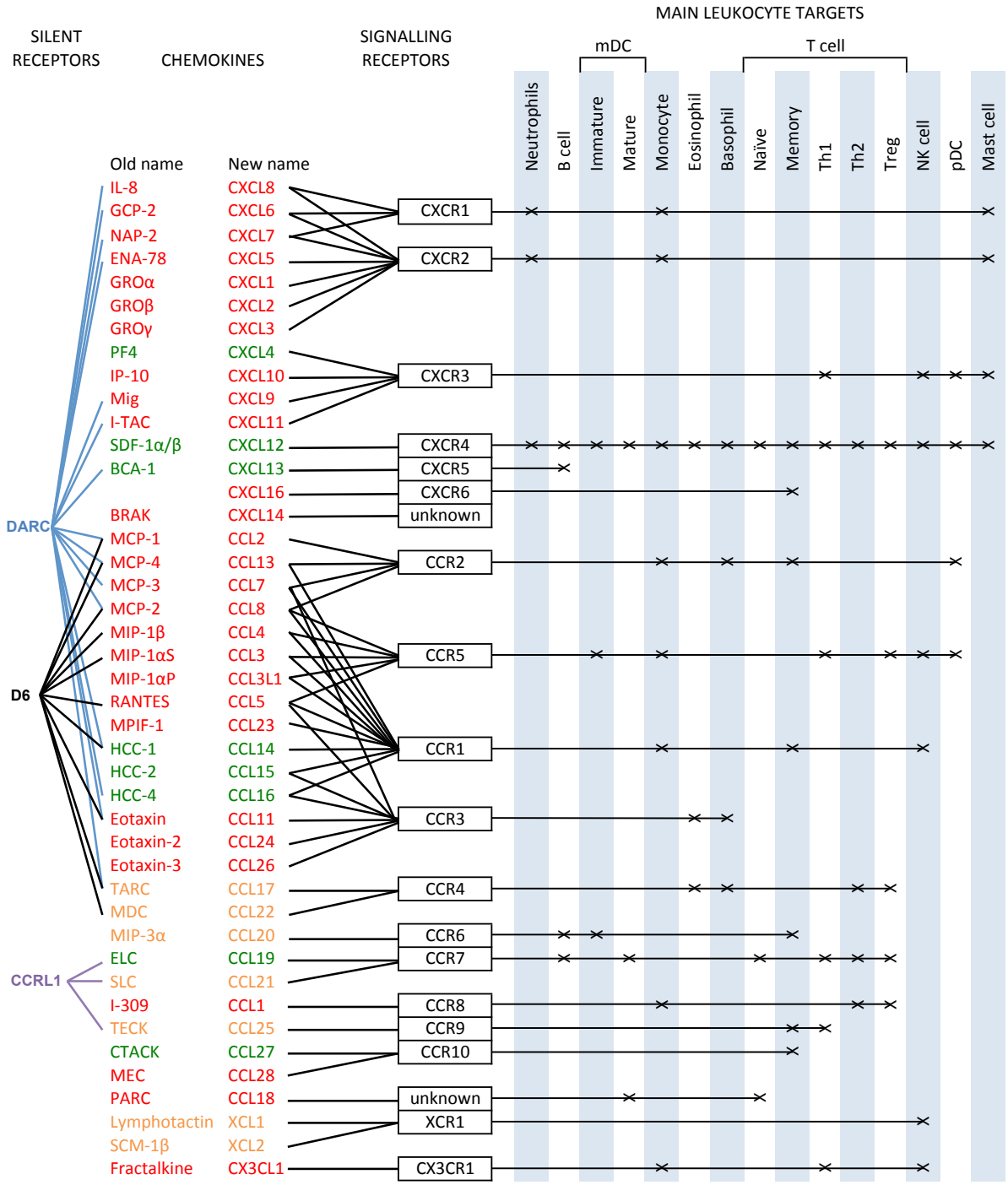


Table 1.1 Human chemokines receptors, their cognate ligand(s) and the cells which express them.

Red = inflammatory chemokines, green = homeostatic chemokines, orange = dual homeostatic/inflammatory chemokines. mDC = myloid dendritic cells, Th1 = T helper type 1, Th2 = T helper type 2, T reg = T regulatory cells. Figure adapted from Luster *et al* (2008) [56]. Data compiled from Mantovani *et al* (2006), Locati *et al* (2005), and Charo & Ransohoff (2006) and Luster *et al* (2008) [35,36,56,57].

Primed effector cells are specialized to act against different classes of pathogens. Type 1 and type 2 helper cells (Th1 and Th2) stimulate cell-mediated and humoral immunity respectively and these cell subsets express different chemokine receptors (CCR5 and CXCR3 versus CCR4 and CCR8 respectively) [58]. Furthermore depending on the tissue draining lymph node where the DC initially encountered antigen, DCs can promote chemokine receptor expression on effector cells to distinguish skin from gut associated pathogens, ensuring that effector cells are equipped to localize to the source of infection [59].

Migration of effector T cells (skin vs gut homing)

CCR4 and CCR10 expression are associated with 'skin homing' effector cells that express cutaneous lymphocyte antigen (CLA), a glycosylated form of PSGL-1 that binds E-selectin on inflamed cutaneous endothelium [60,61]. While E-selectin is expressed at other inflamed tissue sites, cognate CCR4 ligands, CCL17, CCL22 and CCR10 ligand CCR27 are strongly expressed at the epidermis and therefore preferentially direct effector cells to the skin [61]. Induction of skin homing molecules are in part attributed to the Vitamin D3 metabolite, $1,25(OH)_2D_3$. Vitamin D3 is produced in the skin following exposure to sunlight and is converted to $1,25(OH)_2D_3$ by cutaneous-associated DCs which possess p450 enzymes capable of the conversion [62]. *In vitro*, $1,25(OH)_2D_3$, stimulates CCR10 expression on activated T cells while inhibiting the expression of gut homing receptor, CCR9 [62].

Naïve T cells activated in gut draining lymph nodes are preferentially induced to express 'gut homing' molecules, CCR9 and integrin $\alpha_4\beta_7$, directing cells to the intestinal mucosa [59]. CCR9 interacts with cognate ligand CCL25, predominantly expressed in the small intestinal mucosa; $\alpha_4\beta_7$ integrin interacts with adhesion molecules MAdCAM-1 and VCAM-1 present on mucosal endothelium and activated endothelium [63-65]. Consequently, *in vivo* homing experiments show that $CCR9^+\alpha_4\beta_7^+$ effector T cells preferentially migrate to the intestinal tissue [66]. These properties have been attributed to the Vitamin A (mainly from dietary

sources) metabolite retinoic acid, and will be discussed in more detail in Section 1.3.5. Induction of gut homing molecules in turn inhibits the expression of cutaneous associated chemokine receptors, ensuring that an inflammatory response initiated at one mucosal site primes effector cells to return to the initial site of exposure [67].

1.3 CCR9 and CCL25

1.3.1 Identification of CCL25 (TECK)

In 1999, Vicari *et a*l (1997) identified murine CCL25 during the analysis of cDNA isolated from the thymus of recombinase activation gene-1 (RAG-1) deficient mice [68]. CCL25 was categorized as an orphan member of the CC chemokine family based upon the significant homology with previously described CC chemokines and it's chemoattractant properties for murine thymocytes measured *in vitro*. Consequently, CCL25 was originally designated as TECK, short for Thymus Expressed ChemoKine [68]. Human CCL25 is closely related to murine CCL25, sharing 49.3% sequence homology [68]. In agreement with murine data, human CCL25 mRNA was also found in the human thymus [68,69].

1.3.2 Localization of CCL25 expression

Whilst CCL25 was initially cloned from the thymus, abundant CCL25 gene transcripts were also detected in small intestine, with expression absent from the large intestine and other mucosal tissues such as the lung and skin [68]. In the ileum and jejunum, *in situ* hybridization and immunohistochemistry have demonstrated CCL25 production by intestinal epithelial cells with strongest expression in the crypts, decreasing towards the tips of the villi [70-72].

From human tissue, neither CCL25 mRNA nor protein have been isolated from the large intestine, suggesting a regional specificity to CCL25 expression in the gastrointestinal tract [69-71]. While this result has been confirmed by at least three independent laboratories, the number of published sampled tissues is limited to one tissue array (array purchased from

Clontech, published by Kunkel *et al* (2000)), two colonic samples of cDNA (purchased from Clontech, published by Zabel *et al* (1999), and Kunkel *et al* (2000)), and one colonic sample prepared from fresh tissue (Papadakis *et al* (2000)) [69-71]. More importantly, for the majority of 'colonic' samples, there is no indication of the location of sampled colon in relation to the small intestine. It is possible that differences in CCL25 expression exist between the proximal and distal colon and a more detailed analysis of human tissue expression is warranted.

1.3.3 Deorphanization of CCR9

CCL25 is the single identified signalling chemokine ligand for CC chemokine receptor, CCR9. Two years after the identification of CCL25, CCR9 (previously called GRP-9-6) was described by two independent laboratories [69,73]. Zaballos *et al* (1999) initially described the specific interaction between CCR9 and CCL25 by transfecting CCR9 into 293-cells and monitoring calcium flux in response to chemokine stimulation. CCL25 was the only chemokine of 36 recombinant human chemokines tested to elicit a calcium flux response by CCR9-293 cells [73]. These data were supported that same year by Zabel *et al* (1999) who reported CCL25 binding, calcium flux and directed cell migration in human CCR9-transfected cell lines and Molt-4 cells (tumour cell line which constitutively express surface CCR9) [69].

In humans, there are two CCR9 isoforms designated CCR9A and CCR9B expressed at a 10:1 ratio by primary human PBMCs, thymocytes and Molt-4 cells and both encoded on human chromosome 3 [74]. CCR9A has 12 additional amino acids on the N-terminus and is more sensitive to CCL25 stimulated cell migration, measured by Transwell® chemotaxis using CCR9-293 transfectant cell lines [74]. A single publication by Yu *et al* (2007) has investigated differences between CCR9A and CCR9B with no further studies regarding a role in health

and disease owing to a lack of specific antibodies (based on informal communication with Dr Farber, the corresponding last author) [74].

1.3.4 Human CCR9 expression

As summarized in Table 1.2, human CCR9 is expressed on a subset of peripheral blood T and B cells, and on a minority population of natural killer (NK) cells [69,71,75-77]. In agreement with CCL25 expression, $CCR9^+$ cells are enriched in the human thymus and small bowel [69-71]. Analysis by flow cytometry reported by independent research groups demonstrate that the majority of CD4 and CD8 T cell in the small intestine express surface CCR9 and between 10 – 27 % of T cells in the colon are $CCR9^+$ [70,71]. Within the small intestine, Zabel *et al* (1999) reported that all intraepithelial lymphocytes (IEL) express surface CCR9 [69]; this was subsequently supported by the work of Kunkel *et al* (2000) who showed IELs were exclusively $CD8^+$ T cells, 88 - 95% of which expressed CCR9 [70]. However the purity of isolated IELs could be challenged and additional studies of CCR9 expression *in situ* should be performed for confirmation.

cell source	*CD3+*		*CD19 or CD20*	*CD56*	*pDC*	*small IgA B*	*large IgA B*	*References*
	CD4	*CD8*						
PBL	~4	~2	2 - 20	< 2	-	8 - 22	14 - 26	Papadakis 2000, Papadakis 2001, Zabel 1999, Johansson 2005, Kunkel 2003, Berahovich 2006
SB LPL	61 - 97	58 - 96	35	-	-	-	-	Papadakis 2000, Kunkel 2000, Kunkel 2003
SB IEL	-	88 - 95	-	-	-	-	-	Zabel 1999, Kunkel 2000, Papadakis 2000
LB LPL	12 - 25	10 - 27	5	-	-	-	-	Papakis 2000, Kunkel 2000, Kunkel 2003

Table 1.2 Frequency of CCR9 expression by cell type (human).
Summary of published data characterizing the expression of surface CCR9 on primary human cells isolated from the peripheral blood, small or large intestine. Data shows percentage of cells expressing CCR9; references listed. Blank areas (-) indicate no published data. PBL = peripheral blood lymphocyte, SB = small bowel LPL = lamina propria lymphocyte, IEL = intraepithelial lymphocyte, LB = large bowel, pDC = plasmacytoid dendritic cell.

Murine CCR9$^+$ populations not characterized in human

In addition to the population of CCR9 expressing T and B lymphocytes characterized in humans, a population of CCR9$^+$ plasmacytoid dendritic cells (pDC) and macrophages have been described in mice which are currently not described in human. pDC are a small population of cells with a plasmablast morphology, defined in mice as CD11c^{int}B220$^+$Ly6C$^+$ and respond to viral infection with robust IFN production [78]. *In vitro*, CCR9$^+$ pDCs promote regularly T cell induction better than CCR9$^-$ pDCs (measured by FoxP3 and CD25 T cell expression) [79], and *in vivo* homing of pDCs is dependent on CCR9 expression during health and inflammation [77]. Pro-inflammatory murine CCR9$^+$ macrophages have also been indentified in mice but so far not convincingly in humans (to be discussed in Section 1.3.9). Therefore it is possible that there exists a population of pro-inflammatory CCR9$^+$ macrophages and a population of tolerogenic CCR9$^+$ pDCs which have yet to be characterized in humans.

CCR9$^+$ cells express integrin $\alpha_4\beta_7$

Preferential homing of CCR9$^+$ cells to the intestine is enhanced by co-expression of integrin $\alpha_4\beta_7$. Integrin $\alpha_4\beta_7$ interacts with MAdCAM-1 and VCAM-1 expressed by musocal endothelial cells and activated endothelium [80]. The characterization of $\alpha_4\beta_7$ has largely been limited to studies in mice due to restrictions on human specific antibodies; human $\alpha_4\beta_7$ specific antibodies are undergoing clinical trials and are therefore not available for commercial research purposes. The majority of studies on human CCR9 and $\alpha_4\beta_7$ expression have therefore been limited to showing β_7 expression. Indeed primary human CCR9$^+$ cells are exclusively β_7 positive, however this is likely an over estimate of $\alpha_4\beta_7$ heterodimer expression [69]. A single report by Eksteen *et al* (2004) did use human specific $\alpha_4\beta_7$ antibody (ACT-1, Millenium) and demonstrated that CCR9$^+$ T cells are exclusively $\alpha_4\beta_7^+$, with the

caveat that the tested cells were isolated from the inflamed liver during primary sclerosing cholangitis (to be discussed in section 1.3.8) [47].

1.3.5 Induction of CCR9 expression (all *trans* retinoic acid)

In a series of studies conducted in mice, it was discovered that DCs from the gut associated lymphoid tissue (GALT), including the gut draining mesenteric lymph node (MLN) and Peyer's patch (PP), could prime naive T cells to express surface CCR9 and $\alpha_4\beta_7$ [81-83]. This was in contrast to splenic, hepatic and stellate derived DCs which could not induce CCR9 expression [84]. It was Iwata *et al* (2004) who identified that retinoic acid is a potent inducer of gut homing molecules CCR9 and $\alpha_4\beta_7$ *in vitro* and that DCs from the GALT express the enzymes necessary to catalyze the production of retinoic acid [66].

Dietary vitamin A (retinol) undergoes a series of enzymatic oxidation steps to produce RA. Briefly, retinol is oxidized by alcohol dehydrogenase (ADH) to form retinal. Retinal in turn is oxidized by retinal dehydrogenase (RALDH) into retinoic acid (RA) [85]. RA signals through activation of RA receptors (RARs) and retinoid X receptors (RXRs) which belong to the family of nuclear hormone receptors and act as ligand-induced transcription factors [86]. All *trans* retinoic acid (ATRA) is a physiologically active retinol metabolite that binds with high affinity to RAR [86]. *In vitro*, $CD8^+$ T lymphocytes activated (CD3/CD28 stimulation) in the presence of ATRA expand the population of $CCR9^+$ cells from 1% to 63% [84].

In vitro derived $CCR9^+$ cells (both $CD4^+$ and $CD8^+$) migrate to CCL25 in a dose dependent manner *in vitro* [82,87], and in an elegant experiment, Iwata *et al* (2004) demonstrated that ATRA-cultured murine T cells preferentially home to the small intestine *in vivo* [66]. Naïve T cells were activated and expanded in the presence or absence of ATRA (10 nM ATRA) and the two populations (± ATRA) labeled with distinguishing fluorochromes. An equivalent number of the two populations were adoptively transferred into recipient mice and the

frequency of cells within a given tissue was assessed by flow cytometry on disaggregated tissue and by immunohistochemical staining. ATRA-cultured cells preferentially homed to the murine small intestine (Peyer's patches), did not accumulate in the peripheral lymph nodes and were found at an equivalent density to control labeled cells in the spleen [66].

1.3.6 CCR9/CCL25 signalling

Cell migration

Collectively, CCR9/CCL25 mediated cell migration is demonstrated in CCR9 transfected cells, Molt-4 cells, primary thymocytes and lamina propria lymphocytes (T and B cells) [69,73,88]. Primary human thymocytes migration to CCL25 was demonstrated by two independent groups, demonstrating robust migration between 200 - 600 nM CCL25 [69,88]. Kunkel *et al* (2000) measured optimal migration by small bowel lamina propria lymphocyte (SB LPL) migration with 250 nM CCL25 which was comparable to the results by Papadakis *et al* (2000) who showed peak SB LPL migration with 250 - 500 nM CCL25 [70,71].

Effect of pertussis toxin on CCL25 mediated cell migration

With regards to intracellular signalling initiated by CCL25, characterization in primary cells is limited and are at odds with reports using CCR9 transfected cell lines and Molt-4 cells. Similar to most chemokine receptors, CCR9 mediated cell migration by primary thymocytes and SB LPL is sensitive to pertussis toxin, indicating that CCR9 signalling is Gαi-coupled [71,88].

In contrast to the primary cell data, Zaballos *et al* (1999) showed that CCR9 transfected HEK 293 cells had only partially impaired CCL25 mediated calcium flux following pertussis toxin treatment; in contrast, CXCL12 mediated calcium flux was completely ablated, demonstrating sufficient Gαi inhibition [73]. Zaballos and colleagues found the same result in Molt-4 cells, that PTX only partially impaired CCL25 mediated calcium flux and completely

impaired CXCL12 mediated calcium flux [73]. Collectively these data demonstrate that differences in CCR9-coupled signalling exist between primary, transfected and tumor cells lines and therefore using primary or primary derived cells should be the preferred choice.

Intracellular calcium mobilization

With regards to intracellular calcium mobilization, initial characterization of CCL25 demonstrated robust calcium flux by CCR9-transfected cells between 20 – 200 nM CCL25 [73]. Calcium flux in Molt-4 cells was also observed with a similar concentration of CCL25, a result which has subsequently been confirmed by several independent laboratories [69,87,89]. Calcium mobilization by *in vitro* generated ATRA-cultured cells have not been described in the published literature.

Cell adhesion

In addition to directed cell migration, CCL25 is demonstrated to enhance primary $CCR9^+$ cell adhesion to VCAM-1 and MAdCAM-1 measured *in vitro* [47,90]. This is in accordance with the activity of other chemokines which are recognized to increase integrin affinity and/or valency [19,91].

1.3.7 Phenotype and cytokine production by human $CCR9^+$ T cells

The phenotype of $CCR9^+$ cells isolated from the peripheral blood of healthy donors indicates that the majority are memory cells (> 65% $CD45RO^+$) and a proportion are activated, effector cells (25% $CD25^+$ and 17% $CD69^+$) [75]. Roughly 40% of peripheral blood $CD4^+CCR9^+$ cells stimulated *in vitro* (PMA/ionomycin) produced IFN-γ, while IL-10, IL-2 and IL-4 production were limited to roughly 13%, 14% and 4% respectively [75].

The majority of small bowel $CD3^+CCR9^+$ cells stimulated with PMA/ionomycin produced IFN-γ (~79%) [71], which was supported by a separate study reporting 47.8±4% of cells were IFN-γ producing (n=5 [90]). In contrast, IL-10, IL-17, and IL-4 were produced by 7.2±1.8%

10.1±1.7 and 1.9±0.93% of $CCR9^+$ T cells respectively (cells isolated from the small bowel), suggesting a preferential Th1 polarization [90]. Collectively the published data demonstrate that the majority of peripheral blood and intestinal $CCR9^+$ cells are pro-inflammatory, producing IFN-γ upon *in vitro* stimulation while a smaller proportion of $CCR9^+$ cells produce IL-17A and IL-10, and IL-4 production is largely absent.

1.3.8 The role of CCR9 and CCL25 in human inflammation

The tissue specificity of CCR9 and CCL25 expression, and the predominantly Th1 phenotype of $CCR9^+$ T cells have identified this chemokine-chemokine receptor pair as a potential source of inflammation during autoimmune and inflammatory diseases of the intestine. In particular, Crohn's disease (CD) and coeliac disease, two chronic conditions characterized by an accumulation of leukocytes in the small intestine have been investigated. Additionally, inflammation of the liver during PSC, which is highly associated with IBD, has been studied. The data investigating CCR9 during human inflammatory diseases is reviewed.

Elevated frequency of circulating $CD4^+CCR9^+$ cells during Crohn's disease and coeliac disease

Papadakis *et al* (2001) showed that during during active Crohn's disease and Coeliac disease (inflammation largely restricted to the small intestine), the proportion of peripheral blood $CCR9^+CD4^+$ cells were elevated compared to healthy control patients (8.1% and 8.5% compared to 3.5% respectively); in contrast, patients with Colitis (inflammation of the large intestine), had an equivalent proportion of circulating $CCR9^+CD4^+$ T cells. In this study, the frequency of other circulating $CCR9^+$ populations, such as CD8 T cells and B cells were not described [72].

Equivalent effector/memory phenotype between normal and CD $CCR9^+$ cells

Six years later, and as the last author, Papadakis examined the phenotype and cytokine production by $CD3^+CCR9^+$ cells isolated from small bowel lamina propria lymphocytes (SB

LPL), comparing patients with CD to healthy control. By flow cytometry, the proportion of $CCR9^+CD3^+$ cells expressing CD25, CD69, OX40, CTLA4, CD40L, HLA-DR and CD45RO were equivalent between healthy donors and donors with small bowel CD [90]. Furthermore, the proportion of $CCR9^+$ T cells expressing IFN-γ, IL-10, IL-17 and IL-4 were equivalent between cells isolated from the normal SB and CD SB (~52%, ~8%, ~10%, ~2% respectively, analyzed by flow cytometry from 5 normal SB LPL and 5 CD SB LPL samples stimulated with PMA/ionomycin for 5 hours) [90].

$CCR9^+$ LPL from CD produce more IFN-γ and IL-17A compared to normal control

Whilst the proportion of $CCR9^+$ cells producing cytokines (IFN-γ, IL-10, IL-17 and IL-4) was equivalent during health and CD, the amount of IFN-γ and IL-17 protein produced by $CCR9^+CD3^+$ cells was significantly greater for cells isolated from the SB CD than from healthy control SB. For example, anti-CD3 and anti-CD-28 stimulation produced undetectable levels of IFN-γ from normal $CCR9^+$ SB LPL, while $CCR9^+$ CD LPL produced on average ~10 ng/ml (n=4) [90]. The same stimulation on healthy $CCR9^+$ LPL produced ~1 ng/ml IL-17 compared to CD $CCR9^+$ LPL which produced on average ~7 ng/ml (n=4). Analysis of protein concentration for IL-17 and IL-10 production were not reported by Saruta and colleagues (including Papadakis as a last author) although the article by Papadakis *et al* (2003) demonstrated that IL-10 could be detected in the supernatant from $CD4^+CCR9^+$ cells stimulated by anti-CD3 and anti-CD28 for 72 hours (~8 ng/ml IL-10 measured by ELISA) [75].

Abnormal CCL25 expression measured by IHC

Characterization of CCL25 expression during active CD is limited. Papadakis *et a*l (2000) showed human intestinal tissue stained for CCL25 by immunohistochemistry and reported an altered pattern of CCL25 expression in areas of T cell infiltration, analyzed from patients with CD [72]. A significant limitation is the author reported that CCL25 was absent from the colon by IHC and qRT-PCR analysis, but failed to report the CCL25 mRNA expression in

the small bowel comparing CD and healthy control [72]. Elevated expression of CCL25 mRNA and protein during intestinal inflammation is however well documented in several murine models and will be discussed in Section 1.3.9.

The role of CCR9/CCL25 in primary sclerosing cholangitis

Primary sclerosing cholangitis is a chronic inflammatory disease of the liver strongly associated with IBD; approximately 2 – 7.5% of patients with UC have PSC and 75 - 90% of patients with PSC have IBD [92-94]. The precise etiology and pathogenesis of PSC is unknown but disease is characterized by an infiltration of leukocytes (lymphocytes, plasma cells and neutrophils), particularly around the bile ducts, resulting in biliary cirrhosis and potentially hepatic failure [93,95]. In the healthy liver, less than 3% of $CD3^+$ liver infiltrating lymphocytes (LIL) express surface CCR9 and Eksteen *et al* (2004) show that LIL from PSC patients have a significantly increased frequency of $CD3^+CCR9^+$ cells (> 17%, n=8 PSC, n=6 healthy).

In the normal healthy liver, CCL25 mRNA and protein expression are low or undetected [47,70]. Eksteen and colleagues show CCL25 protein detected in the inflamed liver of patients with PSC and not in the inflamed liver of patients with alcoholic liver disease suggesting a unique characteristic to the liver microenvironment induced during PSC. Analysis by IHC of liver tissue from PSC patients showed CCL25 expression by portal dendritic cells/macrophages and hepatic sinusoidal endothelial cells [47]. Eksteen and colleagues propose that long lived memory gut homing cells ($CCR9^+\alpha_4\beta_7^+$) previously activated during episodes of active IBD, exacerbate PSC by binding the hepatic vasculature thorough interactions with CCL25 and MAdCAM-1, ectopically expressed during PSC. The ability of $CCR9^+$ cells to disseminate inflammation is additionally demonstrated in a study of postoperative ileus, where previously activated $CCR9^+$ T cells from one portion of the intestine can re-circulate and initiate inflammation in another previously unaffected area.

CCR9$^+$ cells during postoperative ileus

Manipulation of the small intestine during intestinal surgery or major abdominal trauma frequently leads to postoperative ileus, characterized by inflammation and dysmotility of the bowel for up to 72 hours [96]. Inexplicably, disease frequently propagates to areas of the gastrointestinal tract not initially handled during surgery. In a murine model of disease, Engel *et a*l (2010) identified CCR9$^+$ Th1 cells as the principal contributors to the dissemination of disease along un-manipulated portions of the intestine [97]. These cells exacerbated disease through the secretion of IFN-γ, activating resident macrophages whose nitric oxide production directly inhibited myocyte function, paralyzing intestinal motility [97]. Strikingly, treatment with a drug to sequester lymphocytes in the lymphatics and mucosal tissues (FTY720) prevented both the onset and propagation of disease, suggesting that cell migration was imperative to the initial activation and subsequent translocation of inflammation. Furthermore, in patients who underwent abdominal surgery (but not thoracic or vascular surgery), the number of memory CCR9$^+$CD4$^+$ IFN-γ producing cells in the peripheral blood increased 10 fold one hour after surgery (n=5 abdominal surgery, n=5 control), suggesting a possible role in exacerbating human postoperative ileus through the dissemination of inflammation [97].

1.3.9 CCR9 and CCL25 deficient mice and murine models of intestinal inflammation

Genetically engineered CCR9 deficient mice (CCR9$^{-/-}$) and CCL25 deficient mice (CCL25$^{-/-}$) thrive under steady state conditions and have been used to characterize difference in T cell distribution within the thymus and small intestine where ligand and receptor expressing cells are enriched. In the murine thymus, double positive thymocytes (CD4$^+$CD8$^+$) in the cortex express functional CCR9; as T cells mature from double positive to single positive (CD4$^+$ and CD8$^+$), migrating from the cortex to the medulla, CCR9 surface expression is down-regulated, with a fraction of single positive cells expressing functional CCR9 [98]. In the

thymus, the relative percentages of double negative, double positive and single positive cells is comparable between CCL25$^{-/-}$ mice, CCR9$^{-/-}$ mice and wild type mice indicating a redundant role of CCR9 and CCL25 in thymocytes maturation [99,100].

In the intestine the most significant difference is a 50% reduction in intraepithelial lymphocytes (IEL) in both CCL25$^{-/-}$ and CCR9$^{-/-}$ mice compared to WT mice [99]. In the lamina propria (LP), Wurbel *et al* (2007) reported a slightly lower frequency of CD8 T cells relative to total T cells in both the CCL25$^{-/-}$ and CCR9$^{-/-}$ mice compared to WT although total T cell numbers could not be quantified between the mice stains [99]. Wurbel and colleagues used antigen specific CD8 T cells (T cell receptor specific of ovalbumin), adoptively transferred into CCL25$^{-/-}$ mice and demonstrated a significant reduction in CD8 cells homing to the LP and epithelium following oral ovalbumin challenge, supporting the notion that CCR9-CCL25 interactions are important for the homing of antigen specific T cells to both the epithelium and the LP of the small intestine [99].

SAMP-1/Yit

In a mouse model of spontaneous, chronic ileitis (SAMP-1/Yit) mice develop lesions in a discontinuous pattern along the ileum resembling human Crohn's disease. The cause of inflammation is a non-hematopoietic source, independent of commensal bacteria, and potentially due to increased epithelial cell permeability in the small intestine [101]. In this model, levels of CCL25 mRNA and protein were significantly elevated in the inflamed small intestine and could not be detected in the colon [102]. Treatment with anti-CCL25 or anti-CCR9 antibodies were effective in preventing the induction of small intestinal inflammation but were not effective in healing established disease [102].

TNF$^{\Delta ARE}$

The TNF$^{\Delta ARE}$ model of spontaneous ileitis has a genetic deletion of the TNF-AU rich element (ARE) which normally functions to repress TNF mRNA stability and translation to protein. Consequently this genetic modification results in elevated production and accumulation of TNF and animals develop spontaneous arthritis and ileitis [87,103]. At weeks 4, 8 and 20 disease is minimal, peaks and plateaus respectively, with elevated CCL25 mRNA expression detected in the inflamed ileum [104]. Three independent groups have used the TNF$^{\Delta ARE}$ model (to test CCR9 or CCL25 blocking antibodies, CCR9 small molecule antagonist or to cross the TNF$^{\Delta ARE}$ mice with CCR9$^{-/-}$ or CCL25$^{-/-}$ mice) with conflicting conclusions. The first publication from Apostolaki *et al* (2008) found that CCR9$^{-/-}$ TNF$^{\Delta ARE}$ and CCL25$^{-/-}$TNF$^{\Delta ARE}$ had equivalent progression of ileitis to WT TNF$^{\Delta ARE}$, measured over 16 weeks [105].

The second publication using the TNF$^{\Delta ARE}$ mouse was reported by Walters *et al* (2010). Mice treated with the small molecule CCR9 antagonist, CCX282-B were protected from developing ileitis [87]. At 12 weeks of age, 80% of TNF$^{\Delta ARE}$ mice had moderate to severe intestinal inflammation; mice treated with 50 mg/kg CCX282-B (twice daily by subcutaneous injection) had a 30% incidence of moderate disease and no cases of severe disease [87].

The most recent work using TNF$^{\Delta ARE}$ mice was reported by Wermers *et al* (2011). In contrast to the work from Apostolaki *et al* (2008), Wermers and colleagues reported more severe disease in CCR9$^{-/-}$ TNF$^{\Delta ARE}$ mice compared to WT TNF$^{\Delta ARE}$ [104]. Wermers and colleagues also reported that TNF$^{\Delta ARE}$ mice treated with a CCR9 blocking antibody had more severe intestinal disease than isotype treated mice; 4 week old mice were administered CCR9 blocking antibody every third day for three days bringing the mice to a final age of 5.3 weeks. This is a surprisingly short time point considering the author shows low disease activity at 4 weeks, peak disease at week 8 and chronic disease at week 20 with all other measurements of disease activity focusing on week 20. Furthermore, the levels of disease

activity measured with the addition of a CCR9 blocking antibody were modest (activity score of 1 in isotype treated group and 3 in CCR9 antibody treated group) compared to the levels reported by the author at weeks 8 and 20 (activity score of 4 and 6 respectively) [104]. Therefore while the author concludes that therapeutic blockade of CCR9 exacerbated inflammation in $TNF^{\Delta ARE}$ mice, the results should be interpreted with caution.

Dextran Sulfate Sodium (DSS)

DSS is administered in the drinking water, inducing a reversible form of colitis by disrupting the mucosal integrity [106]. Wurbel *et al* (2011) report that $CCR9^{-/-}$ mice have increased mortality following DSS treatment, reporting 30.65% in $CCR9^{-/-}$ mice (n=78) compared to no mortality in WT mice (n=66) [107]. Furthermore, for the $CCR9^{-/-}$ mice that did survive, disease scores were significantly higher in $CCR9^{-/-}$ compared to WT control mice [107]. The effect of CCR9 or CCL25 blockade using a small molecule inhibitor or blocking antibody have not been reported in the DSS model but would be an interesting comparison as transient CCR9 inhibition might have a different outcome than constitutive CCR9 deficiency.

T cell transfer

In the T cell transfer model of intestinal inflammation originally described by Powrie *et al* (1993), $Rag^{-/-}$ mice (deficient of mature T and B cells [108]) adoptively transferred with $CD4^{+}CD45RB^{high}$ T cells develop severe colitis with inflammation largely absent from the small bowel [109]. The same experiment, conduced in $CCR9^{-/-}$ $Rag^{-/-}$ recipients show severe inflammation in the small and large intestine [110]. Mizuno *et al* (2012) propose that resident and infiltrating $CCR9^{+}$ pDCs in the small intestine are responsible for suppressing the development of ileitis in the original T cell transfer model described by Powie *et al* (1993). However Mizuno and colleagues fail to definitively prove this by not testing the resolution or preventative effect of transferring $CCR9^{+}$ pDCs back into $CCR9^{-/-}Rag^{-/-}$ recipient mice [110].

Concanavalin A (con A) model of acute hepatitis

In a murine model of acute hepatitis, induced by intravenous injection of con A, Nakamoto *et al* (2012) show an accumulation of $CCR9^{+}$ macrophages and a reduction in $CCR9^{+}$ pDCs in the inflamed liver; $CCR9^{-/-}$ mice were resistant to con A induced liver inflammation [46]. Nakamoto and colleagues showed that $CCR9^{+}$ macrophages were in part responsible for con A induced liver inflammation by adoptively transferring $CCR9^{+}$ macrophages isolated from the liver of con A treated mice into $CCR9^{-/-}$ recipient mice. Liver inflammation was induced in mice adoptively transferred with $CCR9^{+}$ macrophages but not $CCR9^{-}$ macrophages nor $CCR9^{+}$ and $CCR9^{-}$ pDCs [46].

1.4 Intestinal anatomy and immunity

The gastrointestinal tract (GI) can be divided into the small and large intestine with the former responsible in chemical digestion and nutrient absorption and the later in re-absorption of water and electrolytes. The small bowel can be divided into three sections: the duodenum, jejunum and ileum (Figure 1.4A). The duodenum starts at the pyloric valve and contains the pancreatic duct by which bile from the gallbladder and pancreatic juice are delivered to the intestine. The jejunum immediately follows the duodenum and is the primary site of digestion and nutrient absorptions; circular folds, villi and micovilli increase the surface area, and a rich blood supply collectively support nutrient absorption [111]. The ileum is the final portion of the small bowel which has less vasculature but is a prominent site of lymphatics. Unique to the ileum are nodular lymphoid aggregations termed Peyer's patches (PP). PP are abundantly distributed in the ileum, visible to the naked eye and become larger as the ileum reaches the large intestine. Section 1.4.2 will discuss the role of Peyer's patches and other lymphoid tissues in antigen sampling from the intestinal lumen and the priming of the adaptive immune response.

The large intestine has a relatively large diameter of 6.5 cm, approximately 1.5 meters in length and is divided into four parts: the caecum, colon, rectum and anal canal (Figure 1.4A). The caecum is a blind pouch which has the appendix attached. The colon is composed of four parts that form right angles to frame the small intestine: ascending, transverse, descending and sigmoid colon. The rectum is the final portion of the large intestine and functions as a temporary storage site for feces until they are expelled [112,113].

1.4.1 Histology

A cross section of the intestine reveals four distinct tissue layers: mucosa, submucosa, muscularis externa and serosa (Figure 1.4B). The mucosa is in direct contact with the luminal content and can be further subdivided into the epithelium, lamina propria and muscularis mucosae. The submucosa is composed of loose connective tissue which contains blood vessels, lymphatics, nerves and mucous secreting glands. Beneath the submucosa is the muscularis externa, which is composed for two layers of muscle responsible for propelling luminal content the length of the gastrointestinal tract. Finally the serosa is a thin layer of connective tissue which blends into the surrounding connective tissue to fix the intestines in position [113,114].

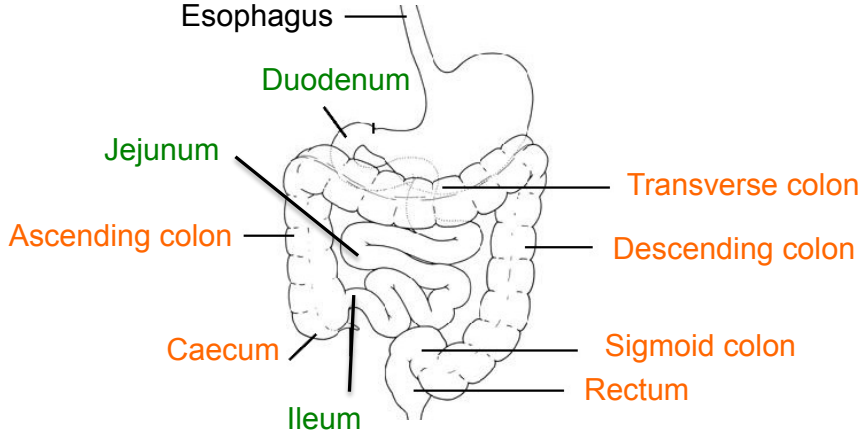
The epithelium is the barrier between host and luminal content. The small bowel has villi covered in columnar enterocytes (with brushed borders) for nutrient absorption, interspersed with mucus secreting goblet cells [114]. The villi continue down into crypts which are composed of stem cells, enteroendocrine cells and Paneth cells. Stem cells regenerate epithelial cells pushing them up along the villi until they reach the tip and are shed into the lumen; epithelial cells are constantly regenerated and have a lifespan of 3 - 6 days [115]. Enteroendocrine cells contain basally oriented secretory granules, delivering hormones into the lamina propria. Paneth cells also contain secretory granules which are oriented apical to the cytoplasm, secreting anti-microbial factors, contributing to the host barrier defense [116].

The large intestine has no villi, a much a greater density of mucus secreting goblet cells and crypts that run deeper than in the small intestine (Paneth cells are largely absent from the large intestine) [113]. The lamina propria of the small and large intestine are similar in appearance, composed of loose connective tissue with capillaries and a central lacteal [114]. The lamina propria is constitutively occupied by leukocytes of the innate and adaptive immune system which enter from the peripheral blood circulation via interactions with post-capillary high endothelial venules [117].

1.4.2 Components of the intestinal immune system

The gastrointestinal tract is the site of nutrient and water absorption, home to 10^{14} bacteria from over 400 different species and continually subjected to benign and pathogenic microorganisms [118]. Therefore the intestine must be equipped to function as both a barrier defense and as an absorptive tissue, distinguishing vital nutrients and commensal bacteria from pathogens. The two branches of the immune system, the innate and adaptive, cooperate to promote immune tolerance to non-pathogenic and self antigens, while stimulating an appropriate immune response to invading pathogens.

A



B Image cannot be reproduced due to copywrite. Please refer to reference for image.

Figure 1.4 Schematic representation of the healthy gastrointestinal tract.
Portions of the small intestine are highlighted in green while portions of the large intestine are highlighted in orange.
A: Schematic summary of the gastrointestinal tract.
B: Cross sectional schematic of the healthy small and large intestine. Image adapted from Lacy *et al* (1991) [113].

1.4.3 Barrier defense and innate immunity

The first line of defense against pathogens consists of 'immune exclusion,' preventing the entrance of microbial pathogens from the outside environment into the host. In the case of the intestine, the epithelium is the first barrier; epithelial tight junctions prevent the passive movement of material and microbes from the lumen into the lamina propria [119]. Goblet cells disbursed in the epithelial layer secrete a layer of mucus (particularly thick in the large intestine where there is a larger bacterial burden) which prevents the adherence of bacteria to the epithelium [120]. Paneth cells in the crypts of the small intestine secrete anti-microbial factors (lysozyme, secretory Phospholipase A2 type IIA, α-defensins) into the gut lumen [116], and secretory IgA antibodies in the intestinal lumen bind viruses, bacteria and toxins, to prevent attachment to the epithelium [121].

Microbes that breach the epithelial barrier are exposed to the second line of defense, the innate immune system. The innate immune system utilizes germ-line encoded pattern recognition receptors (such as toll-like receptors, NOD-like receptors and RIG-I-like receptors) to recognize pathogen-associated molecular patterns (PAMPs), consisting of conserved components of pathogens not found in human (such as components of the bacterial membrane and double stranded RNA) [122,123]. These receptors are expressed by macrophages, dendritic cells, mast cells, epithelial and endothelial cells and activation leads to the production of inflammatory mediators, increases phagocytosis by macrophages, promotes degranulation by mast cells, and recruits leukocytes to the site of infection [124]. If the innate immune response is unable to eliminate the cause of infection, it contains it until the adaptive immune response has developed.

1.4.4 Adaptive immunity

Positioned throughout the gastrointestinal tract are gut-associated lymphoid tissues (GALT), comprised in part, by organized lymphoid structures: Peyer's patches, lymphoid aggregates and cryptopatches in the intestinal mucosa and mesenteric lymph nodes draining the intestine via afferent lymphatic vessels [125,126]. Organized lymphoid tissues are composed of B cell follicles (large germinal centers following antigen stimulation) separated by T cell rich areas and interspersed with antigen presenting cells. These organized structures are the primary site for initiating an adaptive immune response. Also within the GALT are leukocytes dispersed within the lamina propria and between epithelial cells; these cells comprise the effector cells of the local immune response.

Adaptive immunity has a humoral and cellular component. Humoral immunity is mediated by antibodies, secreted by activated B cells with specificity to the initial antigen of exposure. Antibodies bind cognate antigen, preventing further infection of host cells, and additionally label pathogens for destruction through phagocytosis and complement activation [127-129]. The cellular component of the adaptive immune system is mediated by T cells. Unlike innate cells which can be directly activated by antigen, T cells require presentation of antigen on type I or type II major histocompatibility complex (MHC) molecules. It is within organized lymphoid tissue that naïve T cells are primed by APCs, and subsequently where helper T cells provide co-stimulatory signals to B cells to promote antigen specific antibody production[125].

As previously described in Section 1.2.5, the coordinated migration of naive lymphocytes and activated APCs into lymphoid follicles is mediated by homing molecules (CCR7, L-selectin) interacting with post-capillary HEV situated within lymph tissues [130]. Additionally, Peyer's patches in the terminal ileum are covered by specialized microfold cells (M cells) which lack the brush border and instead transport antigens from the intestinal lumen into the follicle to

be collected by naïve APCs [131]. Naïve T cells migrate through peripheral lymphoid tissues, transiently binding peptide-MHC complexes presented by APCs, in search of cognate antigen.

For T cell priming to produce an effector T cell, antigen presentation must be accompanied by co-stimulatory signals, such as CD80 and CD86 (B7.1 and B7.2 respectively). Three cell types are equipped with co-stimulatory molecules necessary for T cell activation: macrophages [132], activated B cells [133,134] and dendritic cells [135]. The co-stimulatory B7 molecules are members of the immunoglobulin superfamily and are exclusively expressed on activated APCs [136]. B7 interacts with CD28 expressed on the surface of T cells; CD28 is essential for optimal clonal expansion [137]. Following activation, T cells undergo clonal expansion by autocrine signalling, expressing both interleukin-2 (refer to Table 1.3) and the high affinity IL-2 receptor, CD25 producing a large population of antigen specific T cells [138].

Naïve T cells can be distinguished into two main types based upon expression of co-receptor molecules CD4 and CD8. Activated CD8 T cells differentiate into cytotoxic T lymphocytes (CTL) which are efficient killers of infected cells. In contrast, activated CD4 T cells can differentiate into distinct lineages, each suited to a particular immune function which exert their functions through the expression of co-stimulatory molecules and the secretion of cytokines, small soluble proteins that act upon target cells through activation of cytokine receptors. Table 1.3 summarizes the key cytokines produced by effector T cells, and the predominant functions on target cells.

CD8 cells differentiate into cytotoxic T lymphocytes (CTL)

Unlike members of the innate immune system, which directly target pathogens, effector T cells act upon the infected host and not the pathogen itself. Cytotoxic T cells are activated

Cytokine	Principal source	Principal cellular targets and effects
IL-2	Naïve, Th1 cells	T cells: proliferation and survival
		B cells: proliferation
		NK cells: proliferation and activation
IFN-γ	Th1, CTL, NK cells	T cells: promotes Th1 differentiation and inhibits Th2 differentiation
		B cells: isotype switching to opsonizing and complement-fixing IgG subclasses
		macrophages: activation (increase microbicidal functions), increased MHC class I and class II
		epithelial cells: activation
		NK cells: proliferation and activation
Lymphotoxin	Th1, some CTL	T cells: kills
		B cells: inhibits
		macrophages: activation, stimulates NO production
		Neutrophils: recruits and activates
IL-4	Th2, mast cells	T cells: promotes Th2 differentiation, T cell proliferation and survival
		B cells: activation, growth, isotype switching to IgE
		macrophages: inhibits IFN-γ activation
		mast cells: proliferation
IL-5	Th2	B cells: proliferation, IgA production
		Eosinophils: activation, growth
IL-10	T reg, some Th1	T cells: inhibits Th1 differentiation
		B cells: increases MHC class II
		macrophages: inhibits cytokine release
		mast cells: proliferation
TNF-α	Th1, some Th2, some CTL, macrophages	macrophages: activation, stimulates NO production
TGF-β	T reg, macrophages, other cell types	T cells: inhibition of proliferation and effector functions
		B cells: inhibition of proliferation, IgA production
		macrophages: inhibition of activation
		neutrophils: chemoattractant, activation
IL-17	Th17, macrophages	neutrophils: recruits and activates
		epithelial cells: increased chemokine and cytokine production
IL-22	Th17, dendritic cells	epithelial cells: β defensin production, cytokine production (pro and anti-inflammatory)

Table 1.3 Cytokines, their sources and activities.
Data from Abbas *et al* (2005) and Murphy *et al* (2008) [124,138].

following presentation of antigen on MHC class I molecules. Only pathogens that have entered the host cell can be presented on MHC class I molecules [139]. The exception to this rule is 'cross presentation,' when APCs process and present extracellular antigens on MHC class I molecules to CD8 T cells [140]. All nucleated cells express class I MHC proteins, enabling cytotoxic T cells to kill any cell infected with an intracellular microbe.

Within 5 minutes of TCR activation, a synapse between the CD8 and target cell is formed, delivering cytotoxic proteins including perforin, granzymes and granulysin to induce cell death [141]. This synapse allows the precise delivery of cytotoxic granules to target cells. Another mechanism by which CTLs induce cell death in target cells is by engaging surface expressed Fas ligand (CD95L) with Fas (CD95/APO-1) expressed by target cells, a mechanism which triggers cell apoptosis without the use of cytotoxic granules [142,143]. This pathway regulates T cell numbers following antigen stimulation [144,145], the significance of which is illustrated *in vivo,* as mice and humans with Fas mutations develop lymphoproliferative disease [146,147]. Additionally, CTLs produce cytokines including IFN-γ, TNF-α, IL-17, IL-22 and lymphotoxin to exert effector functions (refer to Table 1.3 for cytokine activities) [148-150].

CD4 T cells differentiate into helper T cells

CD4 expressing T cells are activated by presentation of cognate antigen on MHC class II molecules. This type of antigen presentation is therefore limited to microorganisms which have been phagocytosed from the extracellular space and is restricted to macrophages, dendritic cells and B cells [151]. Helper T cells, in contrast to their naïve counterpart, express surface CD40 ligand which has a critical role in macrophage and B cell activation through interaction with surface CD40 protein. CD40 ligand provides the necessary co-stimulatory signal to activate B cells, promoting proliferation and differentiation into memory or antibody

producing B cells [152]. Helper T cells also exert effector functions through the secretion of cytokines.

During CD4 T cell priming, the antigen presenting cell and surrounding environment (particularly cytokines produced locally or by the APC) determine the polarization of CD4 T cells towards one of four distinct lineages: Th1, Th2, Th17 and T regulatory. These distinct CD4 subsets are distinguished by expression of specific transcription factors and by their cytokine production profile. Figure 1.5 summarizes the subsets of effector $CD4^+$ T cells and their predominant immune functions. For the topics covered in this thesis a more thorough review of Th1, Th17 and T regulatory cells is provided.

1.4.5 Th1 cells

Th1 cells are characterized by production of the pro-inflammatory cytokines IFN-γ and TNF-α under the transcriptional regulation of T-bet [153]. Th1 cells have a critical role in host defense against intracellular pathogens such as cytosolic bacteria and viruses. Signalling through surface CD40 ligand and via the secretion of IFN-γ, Th1 cells activate infected macrophages, promoting their production of oxygen radicals and nitric oxide and increasing the fusion of lysosomes with phagosomes to collectively eliminate intracellular pathogens [124]. Cytokines produced by activated Th1 cells promote inflammation by inducing the expression of selectin and adhesion molecules on the vascular endothelium and stimulating chemokine production, which ultimately promotes the attachment and extravasation of leukocytes into the affected tissue [16,17].

Th1 differentiation is preferentially induced during TCR stimulation in the presence of IL-12 and IFN-γ, therefore activated Th1 effector cells perpetuate the production of Th1 cells [153]. Furthermore, *in vitro* and *in vivo*, IL-12 can re-polarize Th2 and Th17 cells towards a Th1 phenotype [154]. During T cell polarization, chemokine receptor expression is induced, and in

particular, CXCR3 and CCR5 are preferentially found on Th1 cells [58]. These receptors bind chemokine ligands induced by IFN-γ, synchronizing the accumulation of Th1 effector cells to the appropriate tissue location [58]. While Th1 cells are essential for host protection against intracellular pathogens, a dysregulated Th1 tissue environment can be detrimental to the host and is implicated in the pathophysiology of several autoimmune and inflammatory conditions, including Crohn's disease [155,156].

1.4.6 Th17 cells

Th17 cells were originally characterized for their production of IL-17 (1L-17A and IL-17F) but are also recognized to produce other cytokines including IL-22, IL-6 and TNF-α, with a significant contribution to host defense against extracellular microbes such as bacteria and fungi [157]. In particular, IL-17 stimulates non-myeloid cells (fibroblasts, endothelial cells and epithelial cells) inducing the production of CXCL8 and granulocyte colony stimulating factor (GM-CSF), stimulating the recruitment of neutrophils [158]. Human Th17 cells are characterized by their surface expression of IL-23R, predominant expression of CCR6 (and to a lesser degree CCR4 and CCR5) and expression of transcription factor RORγt which regulates the production of IL-17 [159,160]. Human Th17 cells have also been shown to express Th1 associated cytokines (IFN-γ) under the transcriptional regulation of T-bet, therefore a degree of plasticity between Th1 and Th17 cells exists, dependent on the microenvironment in which they are stimulated [160,161].

A role of Th17 cells in autoimmune and inflammatory disease has been supported by reports of increased IL-17 expression at sites of inflammation in patients with RA [162], psoriasis [163], MS [164,165], uveitis [166,167] and IBD [168,169]. In particular, the relationship with IL-23 have been highlighted by recent studies. In response to PRR stimulation, IL-23 is produced by members of the innate immune system, including DCs and macrophages [170]. IL-23 in turn stimulates IL-17 production in responding cells [157], and in humans the IL-23 receptor and

other members of the Th17 pathway have been identified in genome wide association studies of CD and UC, suggesting a role in the pathogenesis of IBD [171-173].

1.4.7 Regulatory T cells

Regulatory T cells are a division of T helper cells characterized by the expression of transcription factor FoxP3, and production of cytokine IL-10 [174,175]. Secreted IL-10 binds IL-10 receptor on target cells to suppress inflammation by inhibiting cytokine production by macrophages [176], suppressing Th1 cytokine synthesis [177], and the inhibiting of T cell proliferation. [178]. The presence and secretion of IL-10 by regulatory T cells is critical in the maintenance of intestinal immune homeostasis, demonstrated in murine models of IBD and a rare genetic deficiency in human characterized by IBD-like symptoms in the first year of life.

IL-10 deficient mice develop spontaneous colitis [179]. In the T cell transfer model and Helicobacter hepaticus model of colitis, intravenous administration of regulatory T cells can prevent induction and additionally reverse signs of disease [109,180,181]. Furthermore, recombinant IL-10 administered to colitic mice completely abrogates disease [182], while anti-IL-10 treatment exacerbates intestinal inflammation in these model [180,183].

In humans, Immune dysregulation polyendocrinopathy enteropathy X-linked syndrome (IPEX) is a rare but aggressive autoimmune disease, caused by a mutation in the FoxP3 gene resulting in a significant reduction or absence of regulatory T cells [184]. Disease onset is typically in the first month of life and characterized by severe autoimmune enteropathy affecting any part of the gastrointestinal tract but most commonly involving the small bowel [185]. Treatments are limited to immunosuppressive agents and bone marrow transplantation when possible, with a poor long term prognosis.

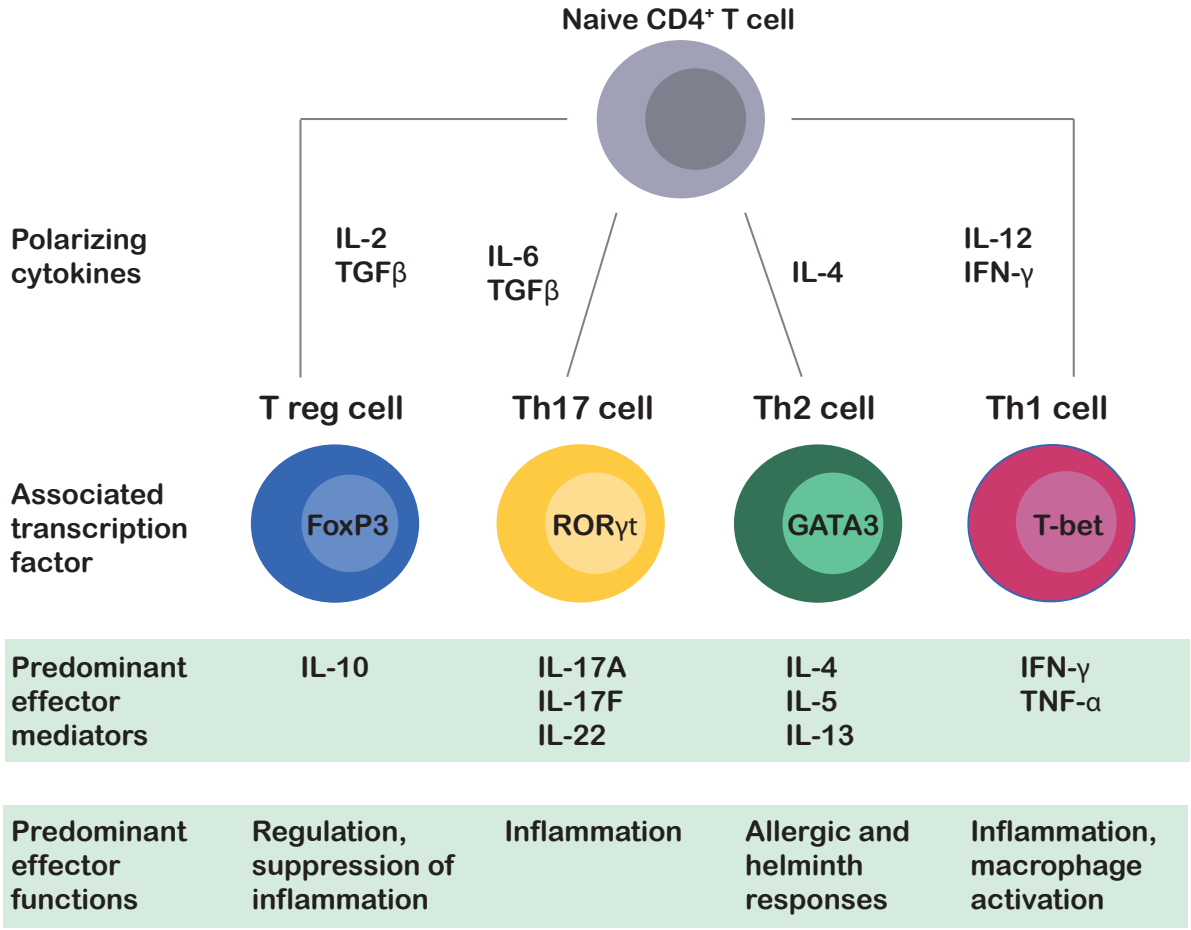


Figure 1.5 CD4$^+$ effector cell subsets distinguished by Th cell polarization.
Upon recognition of cognate antigen in the presence of co-stimulatory signals, such as during antigen presentation by an activated APC, naïve CD4 T cells undergo clonal expansion and differentiation. At least four effector Th subsets have been characterized, with polarization dependent on the microenvironment, antigen, and APC but particularly on soluble cytokines acting on the CD4 T cell during activation. The Th cell subsets are controlled by unique transcription factors and produce unique cytokine repertoires. Figure adapted from Swain *et al* (2012) [153].

1.5 Inflammatory Bowel Disease (IBD)

The two main forms of IBD are Crohn's Disease (CD), which can affect any part of the intestine, and in the majority of cases includes the distal small intestine, and Ulcerative Colitis (UC), in which inflammation is confined to the colon. While the precise etiology of these conditions remains undefined, increasing evidence suggests that disease susceptibility is partly the consequence of genetic predisposition, environmental exposure and interactions with the intestinal microbiota [186]. The severity and presentation of disease varies between individuals but however both conditions are characterized by an exacerbated accumulation of leukocytes in the intestine and therefore studying the mechanisms which mediates tissue specific recruitment is an intense area of research and a potential therapeutic area to target.

1.5.1 Current prevalence and incidence

IBD is associated with the industrialization of nations, with the highest incidence and prevalence in North America and Europe and a rising incidence of disease in developing countries [187-189]. In total it is estimated that 2.2 million people in Europe and 1.4 million North Americans are affected with IBD (estimate from 2004) [190]. In Canada for example, it is estimated that 0.6% of the population has IBD, with an annual incidence of 19.2 CD cases and 20.2 UC cases per 100,000 persons [187]. IBD occurs equally in both sexes, and the incidence is highest in the second to fourth decades of life, affecting people at the prime of their economic and reproductive lives [187,191].

1.5.2 Health costs and economic impact

IBD has no cure, and consequently the medical costs over a life time of chronic disease is significant. The cumulative health care costs of Crohn's disease alone, which comprises half of IBD cases, is estimated at £2.4 billion a year in Europe [192]. During disease remission, health care costs are low, estimated at < £60 annually per patient for the service of primary

care visits (estimates from patients in the UK) [193]. Bassi *et al* (2004) demonstrated that the greatest costs in IBD are incurred by patients requiring secondary care and in particular, inpatient care. On average the cost for secondary care services were £1,256 for patients with UC and £1,652 for patients with Crohn's disease over six months per patient [193]. Therefore one can appreciate that the primary objective to IBD treatment is to maintain patients in a state of disease remission for the health, wellbeing and economic benefits.

1.5.3 Crohn's disease

The symptoms of CD typically include abdominal pain, diarrhoea and weight loss [194]. CD manifests as transmural inflammation of the intestinal wall in a discontinuous pattern along the GI tract. CD can affect any portion of the gastrointestinal tract, from the oesophagus to rectum, and in 80% of cases the distal small intestine and proximal colon are affected. Intestinal granulomas are a distinguishing feature of CD, formed by lymphocytes and macrophages [195]. Also characteristic to CD are strictures and fistulas which arise from chronic inflammation. Strictures restrict the passage of luminal contents and often require surgical resection, whereas fistulas may have associated abscesses, or cause complications arising from connections between abdominal organs e.g. entero-vaginal fistulas. It is estimated that 70 - 80% of patients with CD will require surgery within their lifetime [192,196]. Lymphoid aggregates are more numerous in the submucosa of CD patients and an early sign of disease is the appearance of small ulcers overlaying lymphoid follicles and Peyer's patches [118].

1.5.4 Ulcerative colitis

UC presents as bloody diarrhoea often accompanied by urgency and/or tenesmus, and abdominal pain. Disease typically starts in the rectum and progresses proximally along the large intestine in an uninterrupted pattern and in some cases affecting the entire colon

(pancolitis) [187,196,197]. In the acute phase of UC, there is a depletion of mucin, an infiltration of neutrophils into the surface epithelium and crypts, and the formation of crypt abscesses. Chronically, UC damages the mucosal architecture, distorting crypts and producing scar tissue that can shorten and narrow the colon. Active UC is also characterized by leukocyte infiltration into the lamina propria with a characteristic accumulation of granulocytes. Approximately 20% of patients with UC ultimately require a colectomy [196].

1.5.5 Cytokine environment in IBD

At the active lesions of CD, the lamina propria is expanded with a pronounced accumulation of leukocytes. Although infiltrating cells are a heterogeneous mixture of leukocytes, it is frequently reported that Crohn's disease is a Th1 associated inflammatory condition [191,198-200]. This is on the basis of work since the early 1990's, demonstrating that CD lesions (either extracting LPLs or analyzing the bulk cell material from biopsies) actively produce elevated levels of IFN-γ, IL-12 and TNF-α compared to healthy tissue [200-204].

An elevated Th1 cytokine environment is not a general feature of intestinal inflammation as UC ulcers have either undetectable or low levels of IFN-γ [199,202]. In contrast to CD, inflamed tissue from UC patients is reported to have elevated levels of Th2 associated cytokines, including IL-5 and IL-13 [199,205,206]. More recently it has been shown that both CD and UC lesions have increased IL-17 production [168].

1.5.6 Chemokines implicated in intestinal inflammation

Active IBD is characterized by an accumulation of leukocytes in the intestinal mucosa but perhaps surprisingly, few intestinal T cells are actively proliferating in the human intestine [207]. Fell *et al* (1995) demonstrated by IHC staining for Ki67 (marker of cell proliferation), that less than 1.5% of lamina propria and follicular $CD3^+$ T cells are proliferating during active CD and UC [208]. Therefore the extravasation and retention of LPLs has a critical role in

the accumulation of intestinal leukocytes during IBD. This is in contrast to mice, where models of IBD such as the T cell transfer model rely upon the expansion of T cells for disease induction and resolution and is therefore an important difference between IBD and murine models of disease [209,210].

Within healthy human intestine, several chemokines have been identified by mRNA and protein analysis, and during inflammation the majority of these are found at elevated levels [65,211]. However only a selected few pairs of chemokine and chemokine receptors have been implicated in the pathogenesis or exacerbation IBD, including CCL20/CCR6, CCL28/CCR10, CXCL10/CCXCR3, CX_3CL1/CX_3CR1, and CCL25/CCR9 [65,212-215]. The following section will briefly described these chemokine/chemokine receptor pairs (refer to Sections 1.3.8 & 1.3.9 for discussions of CCL25/CCR9) discussing the extent of human data and the relevant results in murine models of intestinal disease.

CCL20/CCR6

CCR6 expression is found on many cell types but is best described on immature DCs, B cells and memory/effector T cells [216-218]. Within effector cells, CCR6 expression is found on Th17 cells and FoxP3 expressing regulatory T cells [219,220]. CCR6 has a single ligand, CCL20 which is constitutively expressed in the small and large intestine and is also inducible expressed by inflammation in the intestine, lungs and liver [217,221].

Within the healthy intestine, CCL20 production is elevated at gut associated lymphoid follicles including the Peyer's Patches (PP) and isolated lymphoid follicles (ILF), attracting B cells and immature DCs through their surface CCR6 [222]. Indeed CCR6 has a critical role in lymphoneogenesis in the intestine. CCR6 deficient mice have smaller PPs (the result of fewer $CCR6^+$ B cells), fewer ILFs and fail to form cryptopatches. These data demonstrate the non-redundant role for CCR6 in the development of lymphoid tissues within the murine

intestine [222-224]; tissues which have a critical role in stimulating oral tolerance against non-pathogenic antigens and the induction of an adaptive immune response against intestinal pathogens.

Salazar *et al* (2006) show that $CCR6^{-/-}$ mice orally infected with S. typhimurium failed to respond to the invading bacterium as a consequence of fewer $CCR6^{+}$ DCs positioned at the dome region of PPs [224]. Cook *et al* (2000) showed that $CCR6^{-/-}$ mice orally immunized with keyhole limpet hemocyanin (KLH) and adjuvant had fewer antigen specific antibody producing cells than WT mice, and reduced levels of KLH-specific IgA and IgG antibodies (likely the consequence of fewer CCR6 B cells positioned in Peyer's Patches) [225]. These data demonstrate that CCR6 has a non-redundant role in host protection against oral pathogens in mice.

Whilst studies of murine CCR6 suggests a fundamental role in host protection, a role in human IBD has also been hypothesized. Genome wide association studies in CD have identified CCR6 as a disease susceptibility loci, suggesting a possible role in the pathogenesis of intestinal inflammation [171,173]. At active sites of CD and UC elevated expression of CCL20 mRNA is detected [226]. Hovhannisyan *et al* (2010) showed an elevated number of $CCR6^{+}CD4^{+}$ LPLs from patients with active CD (but not active UC), which expressed FoxP3 but displayed phenotypic markers of Th17 cells (CCR6, CD161, RORγt) [227]. Upon *in vitro* stimulation, these cell produced cytokines indicative of Th17 polarization (IL-17, IL-22, IL-21), and additionally produced IFN-γ. While these $CCR6^{+}FoxP3^{+}IL\text{-}17^{+}$ cells displayed suppressive activity in co-cultures with $CD4^{+}$ cells (suppressing cell proliferation), they produced low levels of IL-10 [227]. These data suggest a level of plasticity between Th17 and Treg cells which depending on the tissue environment can polarize FoxP3 expressing cells towards a Th17 effector phenotype.

Murine models to investigate the role of CCR6 in acute models of IBD have generated conflicting results. In the DSS-induced model of colitis, CCL20 is upregulated during inflammation and CCL20-blocking antibody treatment is reported to significantly reduce the infiltration of T and B cells into the colon [228]. This was supported by work from Varona *et al* (2003) who show that $CCR6^{-/-}$ mice had less severe disease following DSS administration compared to WT mice [229]. However in the same article, Varona and colleagues shows that following rectal injection with adjuvant (TNBS), $CCR6^{-/-}$ mice had more severe colitis [229]. The TNBS induced model of colitis was also tested by Katchar and colleages who show that anti-CCL20 antibody ameliorated TNBS induced colitis in WT mice [230]. Collectively these results are conflicting, however DSS and TNBS are acute models of inflammation with significant distinctions from human disease.

In the T cell transfer model, $CCR6^{-/-}$ T cells ($CD4^{+}CD45RB^{high}$) transferred into $Rag2^{-/-}$ mice had more severe colitis compared to mice transferred with WT cells [231]; the consequence of $CCR6^{+}$ Treg cells not efficiently migrating to the intestine to regulate inflammation. Collectively studies of murine CCR6 demonstrate a non-redundant role in initiating host defense against oral pathogens by the positioning of $CCR6^{+}$ DCs in the intestinal lymphoid follicles, and recruiting $CCR6^{+}$ regulatory T cells and B cells which have a critical role in regulating inflammation and providing humoral immunity respectively.

CCL28/CCR10

CCL28 is chemotactic for IgA producing plasma cells through interaction with surface CCR10 [215]. CCR10 has a second chemokine ligand, CCL27 which is highly expressed by keratinocytes of the skin (CCL27 also signals through CCR3 to mediate homing of memory T cells to the skin) [232]. CCL28 expression is found at mucosal surfaces in the intestine (small and large bowel), the bronchi of the lungs and additionally in the salivary and mammary glands [233]. Mice genetically deficient for CCR10 have a normal accumulation of IgA

secreting cells in the intestine, and comparable levels of IgA measured in the serum and fecal content (interestingly there is a dramatic reduction in IgA producing cells in the mammary glands and significantly suppressed transfer of IgA to the nursing neonates) [234,235].

A single report has shown elevated CCL28 mRNA (roughly 3 fold increase) in the ileum of patients with small bowel CD compared to control ileum [65]. Tarlton *et al* (2012) reported an elevated frequency of CCR10 expressing plasmablasts in the peripheral blood of pediatric UC patients [236]. While the CCL28/CCR10 axis has a role in mucosal immunology, a direct role in IBD is not well characterized.

Hu *et al* (2011) studied IgA response following infection with the pathogenic bacterium Citrobacter rodentium, which following oral administration produces inflammation of the colonic mucosa characterized by a Th1 response [237]. Hu and colleagues reported that while the primary response to pathogen was comparable between WT and $CCR10^{-/-}$ mice, a second challenge with pathogen (5 months after primary infection) revealed deficiencies in long-lived, antigen-specific IgA cell response [234]. $CCR10^{-/-}$ mice had a lower frequency of Citrobacter-specific IgA cells in the small and large intestine and lower titers of Citrobacter-specific IgA in the serum and feces [234]. These data suggest that CCR10 may have a non-redundant role in the maintenance of memory IgA producing cells in the intestine.

CXCL10/CXCR3

CXCR3 is expressed by a wide variety of cells but is best characterized on activated T cells, and in particular Th1 cells [238]. CXCR3 has three chemokine ligands: CXCL9, CXCL10 and CXCL11 which are inducibly expressed by IFN-γ [239,240]. CXCR3 and its ligands have been implicated in the pathogenesis and perpetuation of several inflammatory conditions, including atheroscloerosis [240], multiple sclerosis [241], and transplantation rejection [242].

In IBD, increased CXCR3 mRNA levels were detected in intestinal biopsies [243]. Furthermore, independent studies have measured increased mRNA expression of all three CXCR3 specific ligands in the intestinal mucosa from IBD patient [65,244]. Yuan *et al* (2001) show that roughly 40% of intestinal derived $CD4^+$ T cells express CXCR3 and this proportion is consistent between healthy donors and donors with CD and UC [245].

The role of CXCR3 has been examined in two murine models of IBD. In DSS-induced colitis, colitic mice had elevated mRNA expression of both CXCL10 and CXCR3 and CXCL10 blocking antibody treatment significantly reduced damage to the epithelium, measured by increased crypt survival [246]. Mice genetically deficient for IL-10 develop spontaneous colitis [247]; in this murine model, both CXCL10 and CXCR3 mRNA expression were elevated in the colon of colitic mice [248]. Treatment of colitic mice with anti-CXCL10 blocking antibody reduced signs of colitis measured by weight loss, serum amyloid A, and serum IL-6 [248]. Improvements in disease were associated with fewer CXCR3 expressing intestinal $CD4^+$ T cells NKT cells and NK cells [249]. These data suggest that inhibiting CXCR3 mediated cell recruitment could be a good therapeutic target in IBD although this axis is not specific to the intestine and could therefore have the adverse effect of modulating the immune response in other tissues.

CX_3CL1/CX_3CR1

CX_3CL1 (Fractalkine) is expressed in the heart, brain, lung, kidney and pancreas [250] and is produced by endothelial cells, smooth muscle cells and macrophages [251-253]. CX_3CL1 is also inducibly expressed in most tissues by inflammatory mediators such as TNF-α, IFN-γ and LPS [251-253]. Surface CX_3CR1 is found on several different populations of leukocytes (including T cells, NK cells and microglia), but is best described on cytotoxic T cells and monocyte/macrophages [250,254,255].

CX_3CL1 mRNA has been detected at elevated levels in the inflamed intestine during IBD [65,256]. Primary human intestinal microvasular endothelial cells (HIMECs) stimulated *in vitro* (IFN-γ and TNF-α for 48 hours) showed that cells isolated from IBD patients had significantly higher levels of CX_3CL1 mRNA and protein expression compared to healthy control cells [257]. Two independent groups have reported an increased proportion of peripheral blood CX_3CR1^+ T cells during active IBD (CX_3CR1 expression by an average 15% of $CD4^+$ cells in IBD compared to 3% in healthy control) [256,257]. While Sans *et al* (2007) show elevated CX_3CR1 stained by IHC analysis of intestinal biopsies, it is not demonstrated that stained cells were $CD3^+$ cells. Furthermore while CX_3CR1 expressing macrophages could be detected, Kobayashi *et al* (2007) could not detect $CX_3CR1^+CD3^+$ cells from intestinal sections analyzed by flow cytometry (labelling both LPLs and IELs) [256]. Therefore it is unclear if CX_3CR1^+ T cells reach the intestine and what role, if any, they might have in IBD.

In murine models of IBD, CX_3CR1 expression by monocyte/macrophages and myloid cells have been identified as potent suppressor of murine intestinal inflammation. Medina-Contreras *et al* (2011) demonstrated that in mice, the majority of LP macrophages express CX_3CR1, with a reduction in LP macrophages in $CX_3CR1^{-/-}$ and $CX_3CL1^{-/-}$ mice. DSS-induced colitis had greater tissue damage and intestinal cell infiltration in $CX_3CR1^{-/-}$ and $CX_3CR1^{-/-}$ mice compared to WT, and adoptive transfer of macrophages suppressed DSS-induced colitis [258]. Kayama *et al* (2011) identified CX_3CR1^{high} myloid cells in the murine intestinal LP. Co-transfer of these cells during the T cell transfer model of colitis prevented the induction of disease through the inhibition of T cell proliferation [259]. However CX_3CR1 expression by myeloid cells in the human intestine is not well characterized and a role in IBD is not described.

1.6 Corticosteroids in the treatment of IBD

Prior to the 1950s, treatment for IBD was limited to managing the gross symptoms of disease; patients were prescribed agents to control diarrhoea, given vitamin and nutritional supplementation, and treated for symptoms of anaemia. By and far, surgery was the dominant intervention in IBD. Between 1937-1970, in a group of 221 IBD patients monitored at the Radcliffe Infirmary (Oxford, England), 83.5% of patients underwent surgery, many with more than one operation [260].

It was in 1949 that Philip Hench and colleagues described the efficacy of cortisone (compound E) in the treatment of rheumatoid arthritis (RA) [261,262]. In 1952, following the success of cortisone in RA, Dr Sydney Truelove conducted the first clinical trials in Ulcerative Colitis, comparing the effect of intravenous cortisol to placebo. Collectively the trials in UC and later Crohn's disease were an extraordinary success for IBD, demonstrating that cortisol was more effective than placebo at inducing disease remission [263,264]. Today, corticosteroids continue to be a common and effective treatment in IBD and their use is only limited by their side effects, particularly apparent with long-term use [265]. The effect of glucocorticoids on CCR9 expression and function are examined in this thesis, therefore to set the scene for this work, an overview of steroid hormones is briefly reviewed.

1.6.1 Steroid hormones

Five classes of steroid hormones exist based upon the primary receptor they bind and activate: glucocorticoids, mineralocorticoids, androgens (male sex hormones), estrogens (female sex hormones), and progestogens (pregnancy and gestation hormones). Cholesterol is the precursor for all steroid hormones undergoing enzymatic modifications to generate hormone precursors and distinct steroid hormones. Steroid hormones are produced by steroidogenic tissue of the adrenal and gonad tissue; in particular, glucocorticoids and

mineralocorticoids are produced in the adrenal gland and the sex hormones are produced in the testis and ovary [266,267].

Corticosteroids define two families of steroid hormones, the glucocorticoids and the mineralocorticoid (named for their production in the cortex of the adrenal gland). Endogenous glucocorticoid, such as cortisone/hydrocortisone/cortisol are released in response to stress and low blood sugar and are responsible for stimulating gluconeogenesis to increase the blood sugar levels and stimulate the metabolism of fat, protein and carbohydrates. Mineralocorticoids by contrast regulate sodium homeostasis to indirectly influence water retention. Distinct to glucocorticoids are potent and efficacious anti-inflammatory effects [266-268].

1.6.1 Anti-inflammatory effect of glucocorticoids

Glucocorticoids are well documented inhibitors of inflammation and allergic reactions, acting upon both the innate and adaptive immune system [269-271]. The best described mode of anti-inflammatory actions are mediated through activation of the glucocorticoid receptor (GCR). Free glucocorticoids are lipophilic and freely diffuse across the cell membrane to bind and activate cytosolic glucocorticoid receptors [272]. The ligand-receptor complex translocates to the nucleus, modifying gene transcription through mechanisms of trans-activation and trans-repression [269,273]. The GCR-ligand complex can directly bind glucocorticoid response elements (GRE) in the genome or alternatively bind transcription factors, antagonizing gene transcription [269,273]. For example, activated GCR promotes the transcription of anti-inflammatory mediators including annexin-1, secretory leukoprotease inhibitor (SLPI), interleukin-10 (IL-10) and Iκb (the negative regulator of NF-κB) [271,274], and GCs decrease NF-κB activity by physically antagonizing the p65 subunit [275].

Collectively, GCs have broad ranging anti-inflammatory effects. In T cells, GCs suppress pro-inflammatory cytokine production, T cell receptor activation, and cell proliferation [276,277]. During allergic reactions, GCs inhibit mast cell degranulation and suppress production of Th2 associated cytokines [271,278]. With regards to cell extravasation, GCs inhibit neutrophil extravasation and increase neutrophil apoptosis. The effects of GCs on chemokine receptor expression and function are poorly characterized (to be discussed in Section 5.1.2) but could identify novel modes of anti-inflammatory action.

1.7 Coeliac disease

Coeliac disease is an immunological intolerance to gluten protein found in wheat, barley and rye in genetically predisposed individuals [279,280], characterized by symptoms of severe intestinal discomfort, diarrhoea, bloating, weight loss and anaemia [279,281,282]. Coeliac disease can develop at any age, with a peak of onset in early childhood and the fourth decade of life [283], and an estimated prevalence of 1% in Western populations [283,284]. Withdrawal of dietary gluten is an effective treatment for the majority of patients, resolving symptoms and reducing the histological features of active disease [280,285,286]. Diagnosis of coeliac disease is made on the basis of serology, endoscopy, histopathology and genetic tests [279,285].

In the serum, coeliac disease is associated with IgA antibodies against gliadin and autoantibodies specific to tissue transglutaminase (tTg) [287-290]. Active disease primarily affects the small intestine and is characterized by an infiltration of intestinal leukocytes, atrophy of the villi, hyperplasia of the crypts and a characteristic accumulation of intraepithelial lymphocytes [286,291]. The overwhelming majority of patients with Coeliac disease express the heterodimeric HLA class II genes HLA-DQ2 (90 – 95%) or HLA-DQ8 however expression does not confer disease as these HLA alleles are present in the general population at high frequency (30 – 40%) [292]. There is strong evidence that some of the DQ2

and DQ8 susceptibility is mediated by presentation of gluten derived peptides to $CD4^+$ T cells in the small intestine.

1.7.1 Pathophysiology

Ingested gluten is resistant to complete digestion, generating a diverse library of peptides including a family of glycoproteins called gliadins (α, β, and ω gliadins), which are the principal toxin in coeliac disease. Gliadin crosses the epithelium, entering the lamina propria where it undergoes deamination by tTg [293]. Deaminated gliadin peptides bind with high affinity to HLA-DQ2 and HLA-DQ8 [294,295] and gluten specific HLA-DQ-restricted T cells have been isolated from patients with coeliac disease [296,297]. Upon *in vitro* stimulation, these cells predominantly produce IFN-γ [298]. Furthermore the mucosa of coeliac patients have increased expression of active IL-18 and IFN-α, both of which promote Th1 cell differentiation in human T cells [299,300].

Intraepithelial lymphocytes comprise an enriched population of $CD8^+$ T cells whose precise role in coeliac disease remains enigmatic. In contrast to lamina propria $CD4^+$ T cells, specificity of IELs for gluten derived peptides is poorly described; Gianfrai *et al* (2003) identified a gliadin derived peptide (mapping to the 123-123 position of A-gliadin) recognized in the context of HLA-A2 presentation by CD8 T cell isolated from coeliac patients that stimulated IFN-γ production [301] and later in a separate study reported these cells had cytotoxicity against the epithelial cell line Caco-2 [302]. Another nonexclusive hypothesis is that IELs during active coeliac disease have enhanced cytotoxicity against epithelial cells through genetic and phenotypic reprogramming, independent of TCR signalling. Meresse *et al* (2006) report that IELs from coeliac patients have elevated expression of NK cell receptors including NKG2D and NKG2C [303] which *in vitro* are shown to engage ligands (MIC A and HLA-E respectively) expressed by activated enterocytes, promoting their killing [304]. As nonclassical MHC class I molecules, MIC and HLA-E are upregulated on enterocytes during

active coeliac disease and these markers could target enterocytes for cytolytic activity by IELs, exacerbating signs and symptoms of active disease.

1.8 Experimental Aims

CCR9 and CCL25 mediate homing of leukocytes to the small intestine, and the majority of human $CCR9^+$ cells are Th1 effector cells. Therefore CCR9 expressing T cells are a potential therapeutic target in diseases characterized by an exacerbated Th1 response in the small intestine, such as Crohn's disease and coeliac disease. However human data is limited and experiments in murine models of disease have been conflicting. The objective of this thesis was to explore the role of CCR9 and CCL25 during human disease using intestinal tissue and primary derived cells. To achieve this, experiments were performed with the following aims:

- To validate a technique for measuring CCR9 expressing cells *in situ*.
- To measure the effect of CCR9 antagonist treatment on T cell recruitment to the small intestine during active disease (Crohn's disease and coeliac disease).
- To investigate the effect of CCL25 on human T cells analyzed *in vitro.*
- To measure levels of CCL25 mRNA in the human intestine during active IBD.
- To investigate the effects of glucocorticoids on CCR9 expression and function.

CHAPTER 2: Materials and Methods

2.1 Materials

2.1.1 Cells

Molt-4 cells, HEK-293 and CCR9-HEK cells: a gift from ChemoCentryx, Inc. (Mountain View, CA, USA). Molt-4 cells originally supplied by ATCC (Middlesex, UK)

Primary peripheral blood mononuclear cells: Blood Bank (Oxford, UK)

2.1.2 Cell culture materials

All *trans* retinoic acid, Bovine serum albumin (BSA), Dulbecco's phosphate buffered saline (D-PBS), fetal calf serum (FCS), 4-(2-hyroxyethyl)piperazine-1-ethanesulfonic acid (HEPES), Penicillin-Streptomycin, Roswell Park Memorial Institute (RPMI) 1640 with L-glutamine, Trypsin-EDTA 1X solution, Trypan Blue Stain: Sigma Aldrich (Gillingham, UK)

Ultra-LEAF™ Purified anti-human CD3 Antibody (clone OKT3), Ultra-LEAF™ Purified anti-human CD28 Antibody (clone CD28.2): Biolegend, distributed by Cambridge Bioscience (Cambridge, UK)

G418 Geneticin®: Life technologies™ (Paisley, UK)

2.1.3 Immunohistochemistry reagents

Human serum: NHS (Oxford, UK)

Fluorescent anti-mouse IgG Kit, VECTOR® Blue Alkaline Phosphatase Substrate Kit III, ImmEdge™ Pen, VECTOR® Nuclear Fast Red Counterstain, VECTOR® Methyl-green counterstain, VectaMount Mounting Media: Vector Laboratories (Burlingame, CA, USA)

Dako REAL EnVision™ Detection System, Peroxidase/DAB Rabbit/Mouse: Dako (Cambridgeshire, UK)

Aquatex® (aqueous mounting media): BDH (Poole, England, UK)

Microscope Cover Glasses, No. 1 thickness: Marienfeld Laboratory Glassware, distributed by Thermo Scientific (Cramlington, UK)

Shandon cards, Shandon pre-made cuvettes: Shandon Inc., distributed by Thermo Scientific (Cramlington, UK)

2.1.4 Flow cytometry reagents

Sodium azide: Sigma Aldrich (Gillingham, UK)

Live/dead 7AAD stain: eBioscience (Hatfield, UK)

BD Cytofix™ Fixation Buffer: BD Biosciences (Oxford, UK)

DAPI, Live/dead fixable near IR dead stain kit, SYTOX® Green dead cell stain: Invitrogen (Paisley, UK)

2.1.5 Migration assay reagents

Polycarbonate Membrane Transwell-Inserts, HTS Transwell-96 Well Permeable Supports: Corning, Life Sciences (NY, USA)

CellTiter-Glo® Luminescent Cell Viability Assay: Promega (Southampton, UK)

2.1.6 Intracellular calcium flux reagents

Fluo3, AM: Enzo®, Life Sciences (Exeter, UK)

Fura Red, AM, Hanks Buffered salt solution (HBSS): Invitrogen (Paisley, UK)

Pluronic F127: Sigma Aldrich (Gillingham, UK)

Ionomycin: Sigma Aldrich (Gillingham, UK)

2.1.7 Cell isolation and sorting reagents and equipment

Ficoll-Paque™ PLUS: GE Healthcare (Chalfont St. Giles, UK))

Anti-APC MicroBeads, MACS® Separation columns (sizes LS and MS), Pan T cell isolation kit: Miltenyi Biotec (Surrey, UK)

2.1.8 Cytokine quantification by flow cytometry

Phorbol 12-myristate 13-acetate (PMA), Ionomycin: Sigma Aldrich (Gillingham, UK)

BD GolgiStop™ Protein Transport Inhibitor: BD Biosciences (Oxford, UK)

eBioscience Fixation and Permeabilization Kit, Human Basic Kit FlowCytomix™, Human IL-10 FlowCytomix™ Simplex, Human IL-22 FlowCytomix™ Simplex, Human IL-TNF-α FlowCytomix™ Simplex, Human IFN-γ FlowCytomix™ Simplex, Human IL-17A FlowCytomix™ Simplex: eBioscience (Hatfield, UK)

2.1.9 Quantitative real time polymerase chain reaction (qRT-PCR) reagents

Pestle motor, Pestle for 1.5ml Microtube: VWR (Lutterworth, UK)

RNeasy® Mini kit, QuantiTect® SYBR® Green PCR kit: Qiagen (Crawley, UK)

Ambion® TURBO DNA-free™ Kit, Nuclease-free water: Ambion (distributed by Invitrogen, Paisley, UK)

ThermoScript™ RT-PCR System: Invitrogen (Paisley, UK)

Agilent RNA 6000 Pico Reagents Part I: Agilent Technologies (Leeds, UK)

2.1.10 Phospho-kinase array and Western blotting reagents

Human Phospho-kinase Antibody Array: R&D Systems® (Abingdon, UK)

Complete Mini Protease inhibitor cocktail tablets: Roche (Welwyn Garden City, UK)

Pierce® BCA Protein Assay Kit: Thermo Scientific (Cramlington, UK)

NuPAGE® 10% Bis-Tris Gel 10 wells, NuPAGE® MOPS SDS Runner buffer 20x, NuPAGE® LDS sample buffer (4X), NuPAGE® transfer buffer 20x, Blotting filter paper 2.5mm thick: Invitrogen (Paisley, UK)

Full-range Rainbow™ Molecular Weight Markers: VWR (Lutterworth, UK)

Hybond-C Extra Nitrocellulose: GE Healthcare (Chalfont St. Giles, UK)

Supersignal West Pico chemiluminescent substrate: Perbio (Cramlington, UK)

Amersham™ hyperfilm ECL 5x7 inches, Amersham™ ECL Plus Western Blotting Detection System: GE Healthcare Life Sciences (Chalfont St Gile, UK)

2.1.11 Antibodies (flow cytometry, immunohistochemistry, and Western blotting)

Target	Supplier	Conjugate	Clone	Isotype
CD3	Invitrogen	Pacific	UCHT1	Mouse IgG1, κ
	eBio	PE-Cy7	UCHT1	Mouse IgG1, κ
	eBio	APC-	UCHT1	Mouse IgG1, κ
	eBio	Alexa Fluor70	UCHT1	Mouse IgG1, κ
CD4	eBio	eFluor 450	OKT-4	Mouse IgG2B
	eBio	FITC	OKT-4	Mouse IgG2B
CD8α	eBio	eFluor	RPA-T8	Mouse IgG1, κ
	Biolegend	FITC	HIT8a	Mouse IgG1, κ
	eBio	PE	RPA-T8	Mouse IgG1, κ
CD19	eBio	AlexaFluor	HIB19	Mouse IgG1, κ
	eBio	PerCP-Cy5.5	HIB19	Mouse IgG1, κ
CD25	BD	PerCP-Cy5.5	M-A251	Mouse IgG1, κ
CD69	BD	V450	FN50	Mouse IgG1, κ
	R&D	PE	298614	Mouse IgG2a, κ
CX_3CR_1	Biolegend	FITC	2A9-1	Rat IgG2b,κ
CXCR3	BD	PE	1C6	Mouse IgG1, κ
	Biolegend	PerCp-Cy5.5	TG1	Mouse IgG1, κ
CXCR4	eBio	APC	12G5	Mouse IgG2a,
	eBio	PE	12G5	Mouse IgG2a,
	Biolegend	PE-Cy7	12G5	Mouse IgG2a,
CCR5	BD	PE-Cy5	N/A	N/A
	eBio	Purified	T21/8	Mouse IgG1,κ
CCR6	eBio	PE-Cy7	R6H1	Mouse IgG1,κ
	Biolegend	PE	TG7	Mouse IgG2b,
	eBio	Purified	R6H1	Mouse IgG1,κ
	BD	PE	11A9	Mouse IgG1,κ
CCR9	R&D	-	248621	Mouse IgG2A
	R&D	APC	248621	Mouse IgG2A
	R&D	-	112509	Mouse IgG2A
	R&D	APC	112509	Mouse IgG2A
CCR10	R&D	APC	314305	Rat IgG2a,κ
Integrin β7	eBio	PE	FIB504	Rat IgG2a,κ
Secondary antibodies				
anti-mouse IgG	eBio	APC	-	Donkey IgG
anti-mouse IgG	Biolegend	APC	Poly4053	Goat IgG
anti-mouse IgG	Vector	FITC	-	Horse IgG
anti-mouse IgG	Biolegend	PerCP-Cy5.5	Poly4053	Goat IgG
Isotype controls				
mouse IgG2A	R&D	-	133304	Mouse IgG2B
mouse IgG2B	R&D	-	73009	Mouse IgG2A
mouse IgG1, κ	Biolegend	PE	MOPC-21	Mouse, IgG1, κ
Rat IgG2b, κ	BD	FITC		Rat IgG2b, κ

Table 2.1 Antibodies used in this thesis for flow cytometry.
Ig = immunoglubulin; APC = allophycocyanin; FITC = fluorescein isothiocyanate; PE = phycoerythrin. Invitrogen (Paisley, UK); eBioscience (Hatfield, UK); Biolegend, distributed by Cambridge Bioscience (Cambridge, UK); R&D Systems® (Abingdon, UK); BD Biosciences (Oxford, UK); Vector Labs (Peterborough, UK).

Target	Supplier	Clone	Isotype	Format
CD3	Dako	F7.2.38	Mouse IgG1, κ	mono
FoxP3	Gift*	236A/E7	Mouse IgG1, κ	mono
CD8	Gift**	C8/144B	Mouse IgG1	mono
CD4	AbCam	1F6	Mouse IgG1	mono
CCR9	ATCC	LS129-3C3-E3-1 (3C3)	Mouse IgG2b	mono
CCR9	R&D	248601	-	
CCR9	R&D	112509	Mouse IgG2A	mono
CCR9	R&D	248621	Mouse IgG2A	mono
CCR9	AbCam	N/A (AB38564)	Rabbit IgG	poly
CCR9	Imgenex	N/A (IMG-71216)	Rabbit IgG	poly

Table 2.2 Antibodies used in this thesis for immunohistochemistry.
Dako (Cambridgeshire, UK); AbCam (Cambridge, UK); ATCC (Middlesex, UK); R&D Systems® (Abingdon, UK); Imgenex (Upper Heyford, UK). *Gift from Dr Teresa Marafioti (University College London, UK).

Target	Supplier	Clone	MW (kDa)	Isotype	Dilution
Phospho-PLCγ1	Cell Signaling	Tyr783	155	Rabbit IgG	1:1000
PLCγ1	Cell Signaling	D9H10	150	Rabbit IgG	1:2500
β actin-HRP	Cell Signaling	13E5	45	Rabbit IgG	1:2500
Anti-rabbit IgG, HRP-linked	Cell Signaling		-	Goat	1:4000

Table 2.3 Antibodies used in this thesis for Western blotting.
Cell Signaling Technology®, distributed by Cambridge Bioscience (Cambridge, UK).

2.1.12 Cytokines and chemokines

Protein (Cytokine/Chemokine)	Supplier	Use
Recombinant Human Interleukin-2 (IL-2)	R&D	TC
Recombinant murine Interleukin-6 (IL-6)	R&D	TC
Recombinant Human CCL5 (RANTES)	PeproTech	CTX
Recombinant Human CCL25 (TECK)	gift*	CTX
Recombinant Human CXCL11 (I-TAC)	PeproTech	CTX
Recombinant Human CXCL12 (SDF-1α)	PeproTech	CTX

Table 2.4 Recombinant proteins used in this thesis.
TC = Tissue culture; CTX = chemotaxis assay. R&D Systems® (Abingdon, UK); PeproTech, (Rocky Hill, NJ, USA); *gift from ChemoCentryx, Inc. (Mountain View, Ca, USA) originally sourced from PeproTech. All cytokines were reconstituted and stored according to the manufacturer's instructions.

2.1.13 Primers

Target	Reference Sequence	Location	Exons	Product (bp)	Forward primer (5'->3' plus strand)	Tm
β-actin	NM_001101	29-134	1 to 2	106	CACAGAGCCTCGCCTTTGCC	63.34
CCL5	NM_002985	31-155	1 to 2	125	CAGCACGTGGACCTCGCACA	63.45
CCL20	NM_004591.2	118-226	1 to 2	109/112	GCTACTCCACCTCTGCGGC	63.14
CCL25	NM_005624.3	83 - 266	2 to 3	184	GTGCCCAGGGAGGAGGACC	65.3
CXCL8	NM_000584.3	119-294	1 to 2	176	CGTGGCTCTCTTGGCAGCC	63.14
CXCL10	NM_001565.3	44-168	1 to 2	125	GAGGAACCTCCAGTCTCAGCAC	63.98
GAPDH	NM_002046.3	994-1117	8 to 9	143	GGGGCTGGCATTGCCCTCAA	63.5
VIL1	NM_007127	2129-2264	17 to 18	136	GCGTGACCCTGAGACCCC	62.8

Commercially purchased primers

Target	Reference Sequence	Exons	Product size	Qiagen product code
CCRL1	NM_01557	-	75	QT01665951
PLC-γ1	NM_002660	1 to 2	188	QT00048377

Table 2.5 Primers used in this thesis.
GAPDH = glyceraldehyde 3-phosphate dehydrogenase, VIL1 = villin. Synthesized primers made by Eurofins MWG Operon (Oxford, UK). Commercially purchased primers from Qiagen (Crawley, UK).

2.1.14 Steroids

Steroid	Supplier	Diluent
Dexamethasone	Sigma	water
Prednisolone	Sigma	ethanol
Deoxycorticosterone acetate	Sigma	ethanol
Mifepristone	Sigma	ethanol

Table 2.6 Steroids used in this thesis.
Sigma Aldrich (Gillingham, UK). All steroids were reconstituted to the manufacturer's instructions and stored in aliquots at -20°C.

2.2 Cell culture

2.2.1 Molt-4 cell culture

Molt-4 cells are an immortalized suspension human lymphoblastic leukaemia cell line [69]. Molt-4 cells were cultured in RPMI-1640 supplemented with 10% fetal calf serum (FCS), 50 U/ml penicillin and 50 μg/ml streptomycin (Complete growth media) in a 37°C / 5% CO_2 incubator. Cells were maintained at a density between 0.5 – 2 x 10^6 cells/ml.

2.2.2 HEK-293 cell culture

HEK-293 cells are a semi-adherent immortalized embryonic kidney cell line [305]. Wild-type HEK-293 cells and cells transiently expressing CCR9 (CCR9-HEK cells) were a kind gift from ChemoCentryx, Inc., and were maintained in Dulbecco's modified Eagle's media (DMEM) supplemented with 10% FCS, 50 U/ml penicillin, 50 μg/ml streptomycin, 4 mM L-glutamine and 400 μg/ml G418 Geneticin®. When cells reached 90% confluence they were passaged: media was aspirated and the cells washed once with Dulbecco's phosphate buffered saline (D-PBS) before being detached with the addition of 2 – 3 ml Trypsin-EDTA solution. After 3 - 5 minute incubation at 37°C, trypsin was neutralized by the addition of media containing FCS. Cells were pelleted by centrifugation at 300 x g for 10 minutes at room temperature (RT) and resuspended in fresh Complete growth media. Cell viability was assessed by adding an equal volume of cell suspension to Trypan Blue Stain. Viable cells (those excluding Trypan Blue) were counted using a haemocytometer and cells plated at 2 x 10^3 to 6 x 10^3 viable cells/ cm^2 .

2.2.3 CCR9 antibody collected from hybridoma supernatant

LS129-3C3-E3-1 (3C3) cells are a hybridoma mouse lymphoblast suspension B cell line which produce anti-human CCR9 mAbs that can be collected from the cell supernatant [69]. Cells were maintained at a density of 1 - 2 x 10^6 cells/ml in Eagle's DMEM supplemented

with 10% FCS and 50 U/ml penicillin, 50 µg/ml streptomycin, 1.5 g/l sodium bicarbonate, 4.5 g/l glucose and 50 ng/ml recombinant murine IL-6 (as specified by the supplier, ATCC). Prior to collecting cell supernatant, IL-6 was removed from the culture media over the course of several days by centrifuging down the cells and replacing half of the Complete growth media in the absence of IL-6. Cells were resuspended in fresh Complete growth media (in the absence of IL-6) to a density of 5 x 10^6 cells/ml and left until the media was yellow and < 5% cell viability (assessed by Trypan Blue Stain). Cell supernatant was collected by centrifuging the cell suspension at maximum speed for 30 minutes at 4°C, transferring supernatant to a fresh tube and repeating the centrifugation two more times. Aliquots of supernatant were stored at -20°C.

2.2.4 Long term cell storage

For long term storage, cells were pelleted at 300 x g for 10 minutes at RT and resuspended to 5 x 10^6 cells/ml of Freezing media (see Appendix I). Cells were incubated overnight in a Cryo 1°C freezing container at -80°C to ensure the cells froze at a constant -1°C / minute cooling rate that is optimal for cell cryopreservation and cell recovery. Cryovials were stored at -80°C for up to 3 months or in liquid nitrogen for longer periods.

Frozen cells were recovered by rapidly thawing in a 37°C water bath and immediately adding 10 ml Complete growth media (see Appendix I). Trace DMSO was removed by centrifuging the cells at 300 x g for 10 minutes at RT and resuspended to a density of 1 x 10^6 cells/ml in Complete growth media, pre-warmed to 37°C.

2.3 ATRA-cultured cell preparation

2.3.1 Primary cell isolation

Human peripheral blood mononuclear cells (PBMC) were isolated from a buffy coat (National Blood Service, Oxford, UK) by density centrifugation using Ficoll-Paque™ PLUS to the manufacturer's instructions. Red blood cell (RBC) lysis was performed by resuspending the PBMC pellet in Red blood cell lysis buffer (see Appendix I) for 10 minutes at RT. Cells were washed with D-PBS and centrifuged for 10 minutes at 300 x g. Monocytes were depleted by $CD14^+$ positive bead selection conducted to the manufacturer's instructions (Miltenyi Biotec).

2.3.2 All *trans* retinoic acid (ATRA)-culturing conditions

BD Falcon™ 75 cm^2 Cell Culture Flasks (T75) were coated overnight at 4˚C with 3 µg/ml anti-CD3 and 3 µg/ml anti-CD28 in sterile D-PBS (4 mL per flask). Excess D-PBS was removed and monocyte depleted peripheral blood lymphocytes (PBL) were added at 1 x 10^6 cells/ml in Complete growth media (see Appendix I) supplemented with 100 U/ml recombinant human interleukin-2 (IL-2), and 100 nM ATRA. After 72 hours, cells were transferred to a new T75 tissue culture flask and replaced with fresh Complete growth media supplemented with ATRA and IL-2. Cells surface CCR9 expression was monitored by flow cytometry; cells were used for experiments between days 5 and 7 of culturing.

2.4 Immunohistochemistry

2.4.1 Introduction

Detecting antigen by IHC staining is a powerful way to visualize the distribution of cell markers witin intact tissue. For this technique we collaborated with Dr Teresa Marafioti (University College London, UK) who provided expertise during the validation, optimization and interpretation IHC results. For the reagents used in this thesis, a titration of antibody was

performed against positive and negative control tissues to determine the optimal dilution for each antibody and for the particular chromogen used.

During the analysis of clinical trial samples, a primary stock of solutions (including D-PBS, human serum, antigen retrieval buffer, ddH_20) were prepared to ensure that experiments were standardized. Staining and quantification were performed blinded with regard to patient treatment.

2.4.2 Tissue and slide storage

Human tissue was immediately stored in formaldehyde, individually embedded in paraffin and stored in a cool, dark place. Paraffin tissue blocks were cut into 4 µm thick sections and mounted onto glass microscope slides. Commercially available pre-coated slides improved tissue adherence to the glass surface. Cut tissue was dried overnight at RT and stored at 4°C in a microscope slide rack.

2.4.3 Preparing cell cytospins

Cells were resuspended in Complete growth media (see Appendix 1) to a density of 5 x 10^5 cells/ml. Microscope slides were placed face down on a 'Shandon card' and locked onto a 'Shandon cuvette.' An aliquot of cells (between 100 – 200 µl) were dispensed into each cuvette and centrifuged at 800 x RPM for 5 minutes (Shandon Inc., distributed by Thermo Scientific, Cramlington, UK). Cell cytospins were immediately fixed in 4% paraformaldehyde for 30 minutes at RT. Slides were washed twice in D-PBS for 5 minutes and subsequently dehydrated in a series of ethanol bath, each for 5 minutes: 20%, 40%, 60%, 80% and 100% ethanol. Slides were dried at RT (1 hour) and store at 4°C in a microscope slide box.

2.4.4 Slide preparation and antibody staining by IHC

Tissue sections (paraffin embedded) were incubated at 60°C for 1 hour or overnight to promote adherence to the microscope slide. Tissue sections underwent a series of baths to remove the paraffin and rehydrate the tissue (for cell cytospins, experiment began with '*Primary antibody labelling'*):

1. Histoclear 3 incubations for 10 minutes each
2. 100% EtOH 2 incubations for 10 minutes each
3. 70% EtOH 1 incubations for 5 minutes each
4. 50% EtOH 1 incubations for 5 minutes each
5. wash for 10 minutes in ddH_2O

Antigen retrieval

Antigen retrieval often enhances the strength and quality of antigen detection by IHC analysis. Antigen retrieval was performed by submerging the sections in either Citrate buffer (pH 6) or Tris-EDTA buffer (pH 7.5) and heating in a pressure cooker for 4 minutes (see Appendix I). Slides and buffer were cooled to RT before being transferred to RT D-PBS for 10 minutes of washing.

Primary antibody labelling

Tissue sections were covered completely with primary antibody diluted in D-PBS with 10% human serum. Sections were incubated with primary antibody at RT for 30 minutes and washed two times for 5 minutes in D-PBS. As a control for non-specific binding, an equivalent concentration of isotype control was compared for staining distribution and intensity on a representative tissue sample.

Blocking endogenous peroxidase

Endogenous peroxidase was blocked by treating tissue sections with 3% H_2O_2 for 15 minutes at RT followed by two washes in D-PBS.

Secondary antibody labelling

Tissue sections or cell cytospins were covered completely with 'Labelled polymer-HRP' (peroxidase labelled polymer conjugated to goat anti-mouse immunoglobulin, Dako) used neat and incubated for 30 minutes at RT. Slides were washed two times in D-PBS for 5 minutes each.

Development with substrate

Labelled antigen was visualized by incubating the section in 'DAB+ substrate buffer' (Dako) for 5 minutes. Tissue was washed in ddH_20 for 15 minutes, changing the water every 5 minutes.

Counterstaining to visualize cell nuclei

Tissue was counterstained with either haematoxylin or VECTOR® fast red by rapidly dipping the slide into reagent and immediately washing in ddH_20. The intensity of counterstain could be modified by adjusting the exposure time.

Mounting slides

To attach a coverslip to stained tissues, two mounting medias were used, Aquatex® and VectaMount™ depending on chromogen(s) and counterstain and specified by the manufacturer. Mounted tissue was left overnight at RT to dry.

Double staining by IHC

For double staining, the first primary antibody was detected using VECTOR® Grey substrate. Following complete development to the manufacturer's instructions (5 - 20 minutes) slides were washed three times in D-PBS and incubated for 30 minutes with the alternative, primary antibody, prepared as previously described (see '*Primary antibody labelling'*). Slides were washed twice in D-PBS and incubated for 30 minutes with 'Labelled polymer-HRP' (peroxidase labelled polymer conjugated to goat anti-mouse immunoglobulins) used neat (Dako). Slides were washed twice for 5 minutes in D-PBS. The

second antigen was detected using 'DAB+ substrate buffer' (Dako), incubated for 3-5 minutes. Slides were washed two times for 10 minutes in ddH_20 before counterstaining with VECTOR® fast red. Slides were washed and mounted with VectaMount™ to the manufacture's directions.

2.4.5 Quantification of cell population stained by IHC

Each biopsy was photographed at 20X magnification on a Zeiss AxioSkop2 microscope and analyzed using Adobe Photoshop CS4 software (Berkshire, UK). The overlaying 20X images were merged into a single image using the 'merge tool.' Using the 'laso tool,' epithelial cells were separated from lamina propria tissue (Figure 2.1). Using the 'count tool,' each positively stained cell was selected. Using the 'quantification tool', tissue area was calculated relative to a standardized scale set against the 7 μm diameter of a lamina propria lymphocyte. The entire biopsy was analyzed with the exception of lymphoid follicles which were excluded from cell number and tissue area quantification. Quantification was performed blinded with respect to treatment and time point. Biopsies from Chapter 3 were quantified in collaboration with ChemoCentryx, Inc. Biopsies from Chapter 6 were exclusively quantified in Oxford.

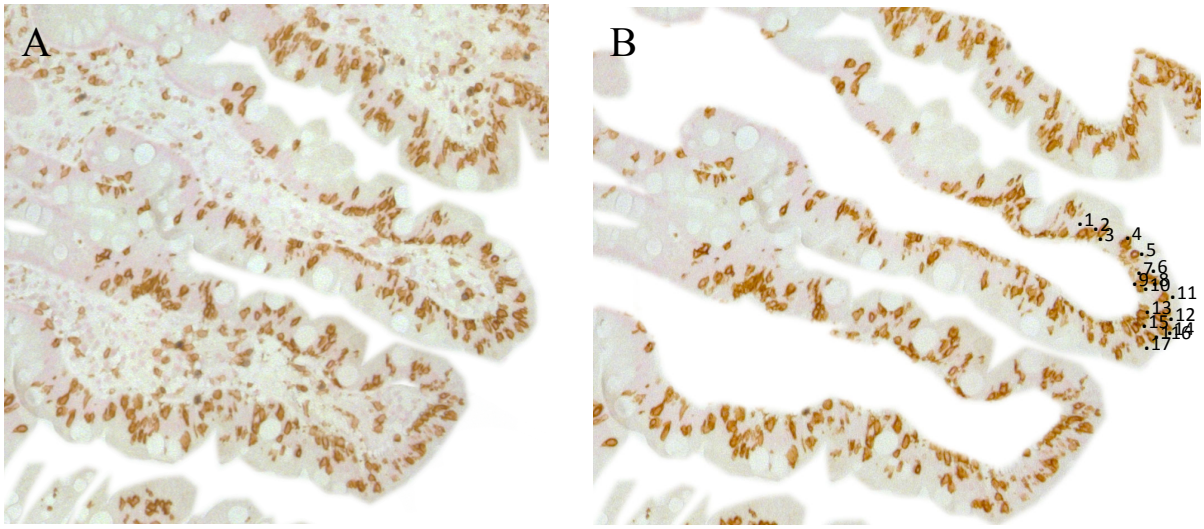


Figure 2.1 Separation of epithelium from lamina propria and subsequent quantification of tissue area and cell number using Photoshop 'laso' and 'count' tool.
Representative example of human duodenum stained for CD3 (brown) and FoxP3 (blue/grey) by IHC. The entire biopsy was captured at 20X magnification, and images stitched together using Photoshop 'Landscape' tool. Tissue area was calculated using a scale set against the 7 µm diameter of a $CD3^+$ lymphocyte identified in the lamina propria (scale standardized between samples). Tissue area and T cell density were quantified separately within the epithelium and lamina propria.
A: Epithelium and lamina propria.
B: Separated epithelium, illustrating the Photoshop 'count' tool used to quantify the number of intraepithelial $CD3^+$ cells.

2.5 Flow cytometry

2.5.1 Measuring surface protein expression

Approximately 1 x 10^6 cells were pelleted at 200 x g for 5 minutes at 4°C. Cell surface antigen labelling was performed in a 100 µl volume of antibody diluted in FACS buffer (PBS + 0.1% BSA + 0.01% sodium azide) and incubated at 4°C for 20 minutes. To detect unconjugated anti-CCR9 (R&D clone 248621 used for all flow cytometry experiments), labeled cells were washed and incubated with fluorochrome-conjugated anti-mouse IgG. All wash steps consisted of resuspending the cell pellet in 200 µl FACS buffer and centrifuging for 5 minutes at 4°C. When appropriate, cells were washed and incubated with fixable live/dead marker diluted in D-PBS and incubated in the dark for 20 minutes at 4°C. Cell

pellets were fixed with the addition of 100 µl Fixation buffer (BD bioscience) incubated for 30 minutes at 4°C, washed and resuspended in FACS buffer. Flow cytometry was performed with an LSRII® or Fortessa® (BD Bioscience, NJ, USA) and data were analyzed using FlowJo software version 9.3.3 (Tree Star Inc., OR, USA). In FlowJo software, cells were gated to exclude non-viable cells (cells which had taken up dye and therefore had a permeable cell membrane) and cell doublets (based upon Forward scatter height (FSC-H) and forward scatter area (FSC-A)).

2.6 Chemotaxis assay

Chemotaxis assays were conducted using Transwell® chemotaxis inserts, separating cells from chemokine by a porous membrane (Figure 2.2). Human T cells have an approximate cell diameter of 7 µm [124], therefore a pore size of 5 µm prevents passive cell diffusion but is large enough to allow active transwell migration into the bottom chamber.

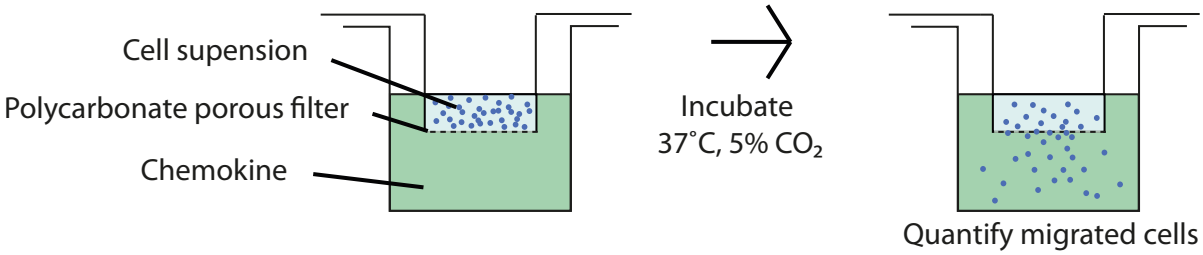


Figure 2.2 Transwell® chemotaxis assay.
Cell suspension is separated from chemokine or buffer by a porous polycarbonate filter. Chemotaxis assays were incubated for 1.5 - 2 hours in a 37°C / 5% CO_2 incubator; cells in the lower chamber are quantified relative to the input cell number.

2.6.1 Chemotaxis protocol

Cells were prepared by centrifuging at 150 x g for 5 minutes and resuspended in RT Chemotaxis buffer (see Appendix 1) to a density of 5 x 10^6 cells/ml. Chemokine was prepared in RT Chemotaxis buffer immediately before the assay was assembled. Chemokine was added to the bottom chamber of the Transwell® migration plate, followed by the cell

suspension added to the top of the Transwell® insert. Volumes varied depending on the size of the wells and were specified by the manufacturer; for example, the 96-well plate is specified to operate with 235 µl chemokine (bottom) and 75 µl cell suspension (top). Chemotaxis assays were incubated in a 37°C / 5% CO_2 incubator for 1.5 – 2 hours. Cell migration to buffer alone was always measured to quantify non-directional cell movement (defined as chemokinesis, and referred to as 'buffer' or 'background signal' in this thesis). A representative sample of cells from the bottom chamber were quantified by Trypan Blue Stain and / or with CellTiter-Glo® reagent as specified in each experiment.

2.6.2 CellTiter-Glo® quantification of live cells

CellTiter-Glo® consists of a cell lysis buffer and a reagent which fluorescently labels intracellular ATP present in metabolically active cells. An equal volume of CellTiter-Glo® and cell suspension were mixed in a white 96-well plate for 5 - 10 minutes at RT on a plate shaker as described according to the manufacturer's instructions. The resulting luminescent signal is proportional to the amount of ATP present, which in turn is proportional to the number of live cells. The luminescent signal was measured using a FLUOstar OPTIMA plate reader (BMG LABTECH, Bucks, UK).

2.6.3 Steroid treated cell chemotaxis

To ensure that an equivalent density of live cells were loaded into Transwell® chemotaxis inserts, cell number was quantified by two independent measures. First live cells were adjusted to equivalent densities based upon Trypan Blue Stain. Secondly, prior to seeding the chemotaxis assays, the CellTiter-Glo® luminescent signal was measured between samples. When cells were adjusted to an equivalent viable cell density by Trypan Blue Stain, ATRA-cultured cells treated with and without 1 µM dexamethasone (DEX) had an equivalent luminescent signal produced by CellTiter-Glo® reagent (Figure 2.3).

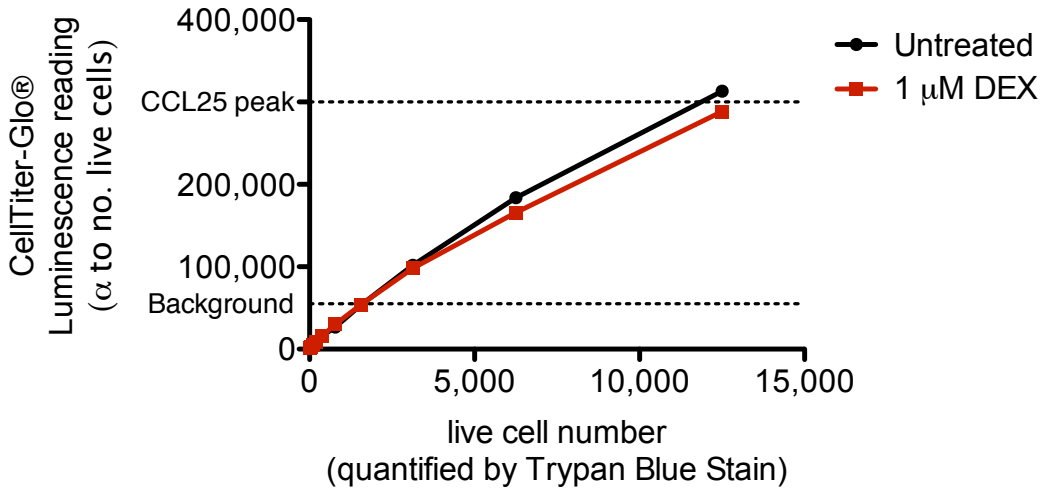


Figure 2.3 CellTiter-Glo® and Trypan Blue Stain are equivalent measures of live cells.
ATRA-cultured cells were treated with 1 μM DEX or vehicle (H_2O) for 16 hours. Cells were adjusted to an equivalent density of live, viable cells by Trypan Blue Stain and then quantified with CellTiter-Glo®. 'CCL25 peak' refers to the maximum signal detected in a Transwell® chemotaxis assay measuring CCL25-mediated migration. 'Background' refers to the signal measured following non-directional migration to buffer alone (chemokinesis).

2.7 Calcium flux assay

2.7.1 Introduction

Increases in the concentration of cytosolic free calcium is a rapid event in lymphocyte activation and one measurement commonly used to detect and quantify chemokine receptor activation [306]. Takahashi *et al* (1999) provides a comprehensive description of commercially available calcium indicator dyes, discussing the strengths and weakness of each [307]. Ratiometric analysis (ratio of increasing signal over decreasing signal) is the preferred method for monitoring calcium flux as it corrects for artifactual changes in fluorescence that result from variations in indicator dye loading, changes in equipment focus, and effects of fluorescent bleaching [308].

Ultraviolet dyes were some of the first calcium indicator dyes available, requiring UV-excitation and generating robust signals (ie Indo-1). Whilst UV-excitable dyes are still used,

dyes which are excited at longer wavelengths are now available, with some clear advantages. Firstly, not all flow cytometry machines are equipped with UV lasers, and UV-irradiation is more cytotoxic than long wavelength irradiation. Using a combination of Fluo-3 and Fura Red (calcium indicator dyes which are excited by longer wavelength irradiation) provides comparable ratiometric results to Indo-1 [309]. Fura Red alone is also compatible with ratiometric analysis, however the signal is weaker than that generated by Fluo-3 and Fura Red combined [307]. The advantage to using Fura Red alone is that an additional channel is then available for detecting cell surface markers.

2.7.2 Cell preparation

Cells were centrifuged at 150 x g for 5 minutes and resuspended to 1 x 10^7 cells/ml in 37°C Hank's buffered saline solution (HBSS). Calcium dye (2 μM Fura Red, AM or 3 μM Fura red with 4 μM Fluo 3, AM) was diluted in HBSS with 0.02% Pluronic F127 (see Appendix I). Cell suspension and calcium indicator dye were mixed in equal parts and incubated in a 37°C water bath for 30 minutes. Cells were washed in excess HEPES Buffered Saline Solution (see Appendix I) and resuspended to 1 x 10^7 cells/ml in HEPES Buffered Saline Solution with SYTOX® Green (diluted 1:1,500). Before analysis by flow cytometry, cells were allowed to equilibrate in a 37°C water bath (~10 minutes).

For experiments where $CCR9^+$ cells were labeled and assessed for calcium flux, CCR9 labelling was performed prior to loading cells with calcium indicator dye. Cell were stained with CCR9 antibody (R&D, clone 248621, antibody diluted 1:150) in Labelling buffer (see Appendix I) at a density of 5 x 10^6 cells per 100 μl and incubated at RT for 15 minutes. Cells were washed twice in RT Labelling buffer and subsequently stained with anti-mouse APC secondary antibody (Biolegend, diluted 1:200) in 100 μl Labelling buffer per 5 x 10^6 cells, incubated at RT for 15 minutes. Cells were washed twic in HBSS and loaded with calcium indicator dye as previously described.

2.7.3 Ratiometric calcium flux measured by flow cytometry

Stimulant was prepared at a 10X concentration in HEPES Buffered Saline Solution (see Appendix I). By flow cytometry using an LSRII®, baseline, non-specific calcium flux was recorded for 25 seconds. The sample was removed, 180 µl of cell suspension was transferred to 20 µl of 10X stimulant and immediately replaced for recording. Recording was continuous at a rate of 8,000 - 10,000 events/second.

For assays with combined Fluo 3 and Fura Red calcium dyes, increasing emission by Fluo-3 were measured by excitation at 506 nm and an emission at 526 nm. Decreasing emission were detected by Fura Red, monitored by excitation at 488 nm and emission at 657 nm. Data were analyzed in FlowJo software as described by the manufacturer (TreeStar, Inc.) and ratiometric analysis was calculated as Fluo3 over Fura Red (AlexFluor488 / PerCP-Cy5.5).

Ratiometric analysis of Fura Red dye was measured by excitation by the violet laser (420 nm) and the green laser (480 nm). Emission was detected by two different filter sets: increases in emission were monitored off the violet laser (630LP and 660/20 BP), while a decrease in emission was detected off the red laser (685LP and 710/50 BP). Figure 2.4A illustrates the gating strategy for analysis in FlowJo software, excluding non-viable cells (SYTOX Green$^-$) and cell doublets (determined by FSC-A versus FSC–H). Fura Red Ratio was calculated as QDot655 / PE-Cy5.5 using the Kinetics application in FlowJo software (Figure 2.4 B & C).

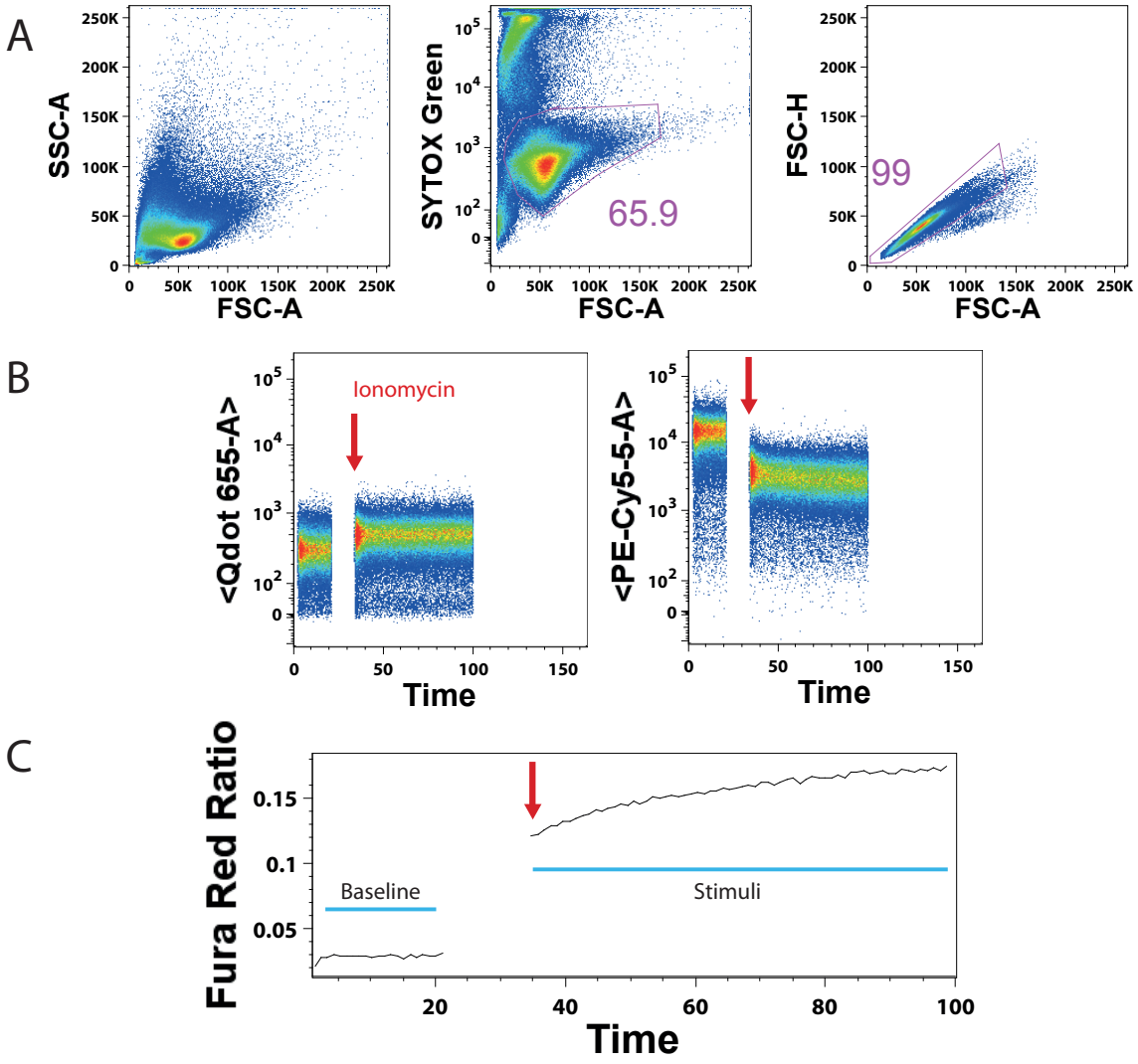


Figure 2.4 Fura Red ratiometric analysis of calcium flux.
ATRA cultured cells were loaded to a final concentration of 1 µM Fura Red/AM for 30 minutes at 37°C. Cells were washed in an excess of HEPES Buffered Saline (see Appendix I) and incubated at 37°C for 10 minutes with SYTOX Green (live/dead marker). Intracellular calcium mobilization in response to ionomycin was monitored by flow cytometry.
A: ATRA-cultured cells were gated on live cells (SYTOX Green-), single staining cells (based upon FSC-H and FSC-A).
B: Mobilization of intracellular calcium was monitored over time by measuring a rise in fluorescence collected in the QDot655 channel and a decrease in fluorescence in the PE-Cy5.5 channel. The arrow indicates when ionomycin was added.
C: Ratiometric analysis of intracellular calcium levels (Fura Red Ratio) was calculated as the MFI of QDot655 over PE-Cy5.5. Baseline fluorescence was measured for 20 seconds. Cells were removed from the flow cytometry machine, a selected volume of cells was transferred to an aliquot of stimulant and immediately replaced for an additional 80 sec of data collection. 8-10K total cell events per second were collected.

2.7.4 Calcium flux assay ± DEX treatment

Vehicle- and DEX-treated cells were centrifuges at 200 x g for 10 minutes. Cell pellets were separately stained with monoclonal anti-CCR9 (R&D Systems, Clone 248621, 1:150 dilution) in Labelling buffer (see Appendix I) and incubated for 15 minutes at RT. Cells were washed by adding 2X excess volume Labelling buffer and centrifuging for 10 minutes at 200 x g. Vehicle- and DEX-treated cell pellets were separately labelled with anti-mouse secondary APC (Biolegend, 1:200 dilution) in Labelling buffer for 15 minutes at RT. Cells were washed two times in Labelling buffer. Vehicle-treated cells were labelled with anti-CD3 APC-eFluor780 and DEX-treated cells were labelled with anti-CD3 AlexaFluor700 diluted in Labelling buffer and incubated for 15 minutes at RT. Cells were washed three times in RT Hank's buffered saline solution (HBSS). An equivalent number (determined by Trypan Blue Stain) of vehicle- and DEX-treated cells were combined to a final density of 2 x 10^6 cells/ml in HBSS with 0.02% Pluronic F-127, 1 μM Fura Red, AM and incubated for 30 minutes at 37°C. Cells were washed and resuspended to 1 x 10^7 cells/ml in HEPES Saline Solution (see Appendix I) with live/dead cell marker, SYTOX® Green (diluted 1:1,500) and incubated in a 37°C water bath until analysis by flow cytometry.

Data was acquired on an LSRII and analysis was performed with FlowJo software. The gating strategy was as follows: live cells (SYTOX Green-), single cells (determined by FSC-A versus FSC–H), CCR9-APC positive cells and finally, vehicle- and DEX-treated cells distinguished by their unique CD3 conjugated fluorochromes. Stimulation with ionomycin (5 μg/ml final concentration) was included in each assay to ensure that vehicle- and DEX-treated cells were evenly loaded with Fura Red dye and changes to calcium flux were readily measurable.

2.8 Internalization assay

2.8.1 Cell treatment

Roughly 1 x 10^6 cells were prepared for each condition, resuspended to a final density of 2 x 10^6 cells/ml in pre-warmed, 37°C Complete growth media (see Appendix I) supplemented with or without chemokine and incubated in a 37°C / 5% CO_2 incubator.

2.8.2 Analysis by flow cytometry

At the appropriate time point, cells were washed three times in 4°C FACS buffer (see Appendix I) and labeled for surface CCR9 and/or CXCR4 as previously described (see Section 2.5.1). Cells were also stained with a live/dead cell marker.

2.8.3 Preparation as cell cytospins

Cells were treated as described in Section 2.8.1, washed three times in 4°C FACS buffer (see Appendix I) and immediately prepared as cell cytospins as previously described (see Section 2.8.3).

2.9 Measuring cytokine production by flow cytometry

2.9.1 Cell treatments

For anti-CD3, anti-CD28 and recombinant MAdCAM-1 stimulation, 96-well flat-bottom sterile plates (Corning) were pre-coated overnight at 4°C with antibody (3 µg/ml) or recombinant protein (2.5 µg/ml) in 100 µl D-PBS. Excess PBS was removed, and washed gently once with sterile D-PBS. To each well, 200K sorted $CCR9^+$ ATRA-cultured cells were seeded in Complete growth media (see Appendix I) to a final volume of 200 µl per well (final cell density of 1 x 10^6 cells/ml) and incubated for 16 hours in a 37ºC / 5% CO_2 incubator. When appropriate, CCL25 was added during the start of each stimulation period.

Anti-CD3, recombinant MAdCAM-1, anti-CD3/anti-CD28 and anti-CD3/anti-CD28/MAdCAM-1 stimulated cells were incubated overnight (12 hours), and the following day BD GolgiStop™ was added to the manufacturer's directions and further incubated for 4 hours (16 hours total stimulation). For PMA/ionomycin stimulation, cell were incubated for 12 hours (± CCL25) and the following day, stimulated for 4 hours with PMA/ionomycin (final concentration 100 ng/ml PMA and 1 µg/ml ionomycin) and BD GolgiStop™ reagent simultaneously.

2.9.2 Staining for intracellular cytokines for analysis by flow cytometry

ATRA-cultured cells were transferred to round bottom 96-well plates and washed 3X in 200 µl FACS buffer (see Appendix I) by centrifuged at 200 x g for 5 minutes at 4°C. Cells were stained for surface CCR9 as previously described (see Section 2.5.1). Cell pellets were subsequently incubated in BD Fixation/Permeabilization buffer (BD Bioscience) for 30 minutes at 4°C. Cells were washed 3X in 200 µl Fixation/Permeabilization buffer and incubated for 30 minutes at 4°C with anti-cytokine antibody diluted in Fixation/Permeabilization buffer. Cells were analyzed on an LSRII® (BD Bioscience, NJ, USA).

2.10 Sorting CCR9$^+$ cells

Buffy coat derived PBMCs were isolated by Ficoll-Paque™ PLUS density centrifugation to the manufacturer's instructions. T cells were isolated by negative selection using the 'Pan T Cell Isolation Kit' to the manufacturer's instructions (Miltenyi Biotec). T cells were stained with monoclonal anti-CCR9 antibody (R&D, clone 248621, antibody diluted 1:150) at a density of 5 x 10^6 cells per 100 µl Labelling buffer (see Appendix I) incubated at RT for 15 minutes. Cells were washed twice in RT Labelling buffer and subsequently stained with anti-mouse APC secondary antibody (Biolegend, diluted 1:200) in 100 µl Labelling buffer per 5 x

10^6 cells, incubated at RT for 15 minutes. Cells were washed and labeled with anti-APC MicroBeads and isolated by positive bead selection according to the manufacturer's instructions (Milteyni Biotec). Figure 2.5 depicts the isolation technique and theoretical number of primary $CCR9^+CD3^+$ cells possible to isolate from a single buffy coat. The majority of ATRA-cultured cells were T cells (>90%, see Figure Figure 4.2) therefore sorting $CCR9^+$ ATRA-cultured cells was performed to the same specification while omitting the 'Pan T cell Isolation Kit' step.

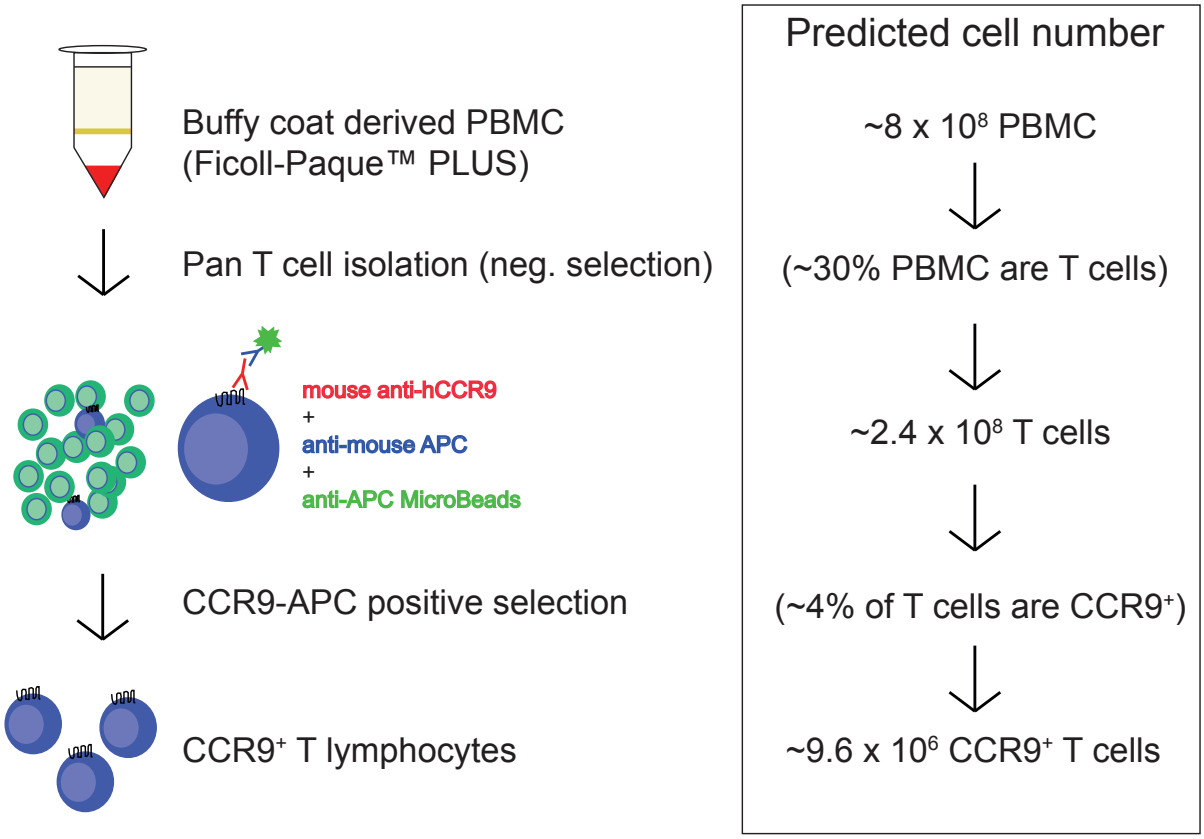


Figure 2.5 Predicted $CCR9^+CD3^+$ cell isolation from buffy coat derived PBMC. Buffy coats were isolated for T cells and sorted for $CCR9^+$ cells by positive MicroBead selection. Estimate that ~ 10^7 primary $CCR9^+CD3^+$ cells can be isolated from one buffy coat.

2.11 Measuring cytokine concentrations in the cell supernatant by FlowCytomix™ Multiplex Technology

2.11.1 Introduction

Classically, the concentration of protein in cell supernatant is measured by enzyme-linked immunosorbent assay (ELISA) whereby the antigen of interest is bound by antigen specific antibody conjugated to an enzyme that in the presence of substrate produces a particular color. The intensity of the color is proportional to the amount of starting antigen and can be quantified relative to a protein control of known concentration. eBioscience has developed a system which utilizes the general principals of ELISA with the distinction of acquiring data by flow cytometry. This system has the particular advantage of detecting up to 20 different antigens simultaneously.

Beads are coated with antigen specific antibodies; the beads come in different sizes for different antigens and can therefore be distinguished during Flow Cytometry based upon forward and side scatter properties. Primary antibody is detected with a biotin-conjugated secondary antibody, followed by Streptavidin-Phycoerythrin. The fluorescent signal is acquired by flow cytometry and analyzed using FlowCytomix Pro Software (eBioscience). Similar to an ELISA, a protein standard run alongside samples enables the quantification of protein concentration in the FlowCytomix™ assay.

2.11.2 Protocol

Cells were stimulated as previously described (see Section 2.9.1) omitting the addition of BD GolgiStop™. Cell suspensions were transferred to a U-bottom 96-well plate and centrifuged at 300 x g for 5 minutes at 4°C. Supernatant was transferred to fresh eppendorf tubes and stored at -20°C; cell pellets were processed for qRT-PCR. Samples (supernatant) and standards were prepared to the manufacturer's description using the 'Human Basic Kit,

FlowCytomix' manual. Flow cytometry was performed using a Fortessa® (BD Bioscience, NJ, USA) and data were analyzed using FlowCytomix Pro Software (eBioscience).

2.12 Human tissue and ethics

All intestinal biopsy samples used in Chapter 5 of this thesis were obtained with patient consent and approval from a Research Ethics Committee. Samples from patients with Inflammatory Bowel Disease were collected under the following ethics:

> Inflammatory Bowel Disease in Oxford: prospective cohort for outcomes, treatment, and predictors. Research Ethics Committee Reference: 09/H1204/30

All samples collected from patients without IBD were collected under the following ethics:

> Oxford Gastrointestinal Illness Biobank. Research Ethics Committee Reference: 11/YH/0020

2.13 Quantitative reverse transcriptase polymerase chain reaction (qRT-PCR)

2.13.1 Tissue collection, storage and handling

To minimize RNA degradation, tissue was collected in a 1.5 ml eppendorf tube, immediate placed on dry ice or liquid nitrogen and stored at -80°C. All molecular biology procedures were performed while wearing gloves and using filter tips on a clean working surface. Molecular biology grade or DEPC-treated water were used to prevent nucleic acid and nuclease contamination.

2.13.2 RNA isolation

Total RNA was isolated using an RNeasy Mini Kit according to manufacturer's instructions (Qiagen). For tissue sections, directions for the 'Purification of Total RNA from Animal Tissues' were followed. For RNA isolation from cultured cells, directions for the

'Purification of Total RNA from Animal Cells using Spin Technology' were followed. Tissue was homogenized in 'RLT' lysis buffer using a motorized pestle and disposable, RNase free pestle inserts.

2.13.3 DNAse treatment

To prevent contamination with genomic DNA, RNA samples were treated by DNase I digestion using the TURBO DNA-free Kit™ according to the manufacturer's instructions.

2.13.4 RNA quantification

Isolated RNA was quantified by measuring the absorbance at 260 nm using a NanoDrop ND-1000 Spectrophotometer (Thermo Fisher Scientific, Cramlington, UK). RNA quantification and purity were assessed by analyzing 1.2 µl of sample. RNA purity was measured by the A260/280 ratio, with a value > 1.95 considered satisfactory for further analysis by qRT-PCR.

2.13.5 RNA quality analysis

The integrity of RNA isolated from human intestinal biopsies was analyzed using an Agilent 2100 Bioanalyzer (Gloucestershire, UK). Samples were prepared to the manufacturer's instructions and analyzed on a 'Pico chip.' Analysis by this method provided information about RNA concentration, the ribosomal RNA ratio (28s / 18s), and the RNA Integrity Number (RIN) (see Section 4.2.4).

2.13.6 Reverse transcription

To reverse transcribe RNA into complementary deoxyribonucleic acid (cDNA), reactions were performed according to the manufacturer's instructions. In summary, RNA sample (1 µg), oligo dT primer (0.5 µg) and dNTP mix (0.6 µl of 100 mM) were combined in a 12 µl reaction and incubated for 5 minutes at 65°C to denature the RNA template. Samples were immediately cooled on ice and the following components were added from a master mix (adding 8 µl of master mix for a final volume of 20 µl): 4 µl 5X cDNA synthesis buffer, 1 µl

0.1M DTT, 1 µl RNase OUT (40 U/µl) 1.8 µl RNase free water and 0.2 µl ThermoScript reverse transcriptase (200 U/µl). Reactions were incubated at 55°C for 60 minutes and the reaction terminated by incubating at 85°C for 5 minutes. Reactions omitting reverse transcriptase (-RT) were used as a negative control to indicate any contamination by genomic DNA. cDNA was diluted 1:5 with molecular grade water and stored at -20°C.

2.13.7 Primer design

Primers were designed using NCBI's Primer-BLAST tool (http://www.ncbi.nlm.nih.gov/tools/primer-blast) with the following criteria to prevent non-specific primer annealing and amplification of genomic DNA:

- Primer length: 18-25 nucleotides
- Primer melting temperature: 55-65°C, maximum difference of 3°C between forward and reverse primers.
- Target PCR length: 60-150 nucleotides.
- Target intron spanning.
- Avoid >3 G's or C's at the 3' end.
- Avoid a T at the 3' end.
- Avoid >3 G's in a row and >5 of any one nucleotide in a row.
- Avoid complementarity within a primer sequence and between primer pairs.
- Target GC content: 40-60%

The specificity of primer pairs against all possible human genes was assessed using the UCSC in-silico PCR tool (http://genome.ucsc.edu/cgi-bin/hgPcr?command=start). Primers were ordered through Eurofin MWG Operon (Oxford, UK) and arrived as lyophilized powders that were resuspended in molecular grade water to a concentration of 10 µM. A master mixe of forward and reverse primer pairs were made and stored at -20°C aliquots to avoid repeated freezing and thawing.

2.13.8 Primer validation

To verify that designed primers were in fact specific to the target gene, produced a single product, and had similar amplification rates, the following tests were performed for each primer pair (Figure 2.6):

1. Melting temperatures were monitored to ensure a single product of the expected size were produced (Figure 2.6B).
2. A titration of cDNA was analyzed to compare amplification rates between target gene and reference gene (Figure 2.6C).
3. PCR products from qRT-PCR reactions were run on an agarose gel to determine the number and size of PCR product(s) (Figure 2.6D).

2.13.9 qRT-PCR

qRT-PCR was performed using SYBR® Green reagent. SYBR Green is a dye which emits a fluorescent signal when double stranded DNA is produced. To ensure equivalent additions of both primer and cDNA between samples, the following master mixes were made on ice and combined in equal parts for a final 25 µl PCR reaction:

Master mix 1	**Master mix 2**
12.5 µl : 2X SYBR® Green master mix	10.5 µl : nuclease free water
0.8 µl : 10 µM Primer mix (Forward + Reverse)	2 µl : cDNA template

Each sample was assayed in triplicate. The following conditions were used on a Rotor-Gene RG-3000 (Qiagen, Crawley, UK):

95°C for 15 min	*(activate HotStarTaq DNA polymersase)*	
94°C for 15 sec	*(denature)*	} *40 cycles*
60°C for 30 sec	*(anneal)*	
72°C for 30 sec	*(extension – data acquisition)*	

A melt curve analysis of PCR products was performed to verify that a single product of the expected size was produced (Figure 2.6B).

2.13.10 Quantification

Gene expression was quantified relative to a reference gene (GAPDH or villin) for each sample using the threshold cycle value (Ct) (Figure 2.6A). Expression was calculated based on a replication rate for 2^n using the following calculation described by Livak *et al* (2001) [310]:

Relative expression = $2^{-\Delta\Delta Ct}$ = (Power 2, Ct Reference gene – Ct Target gene).

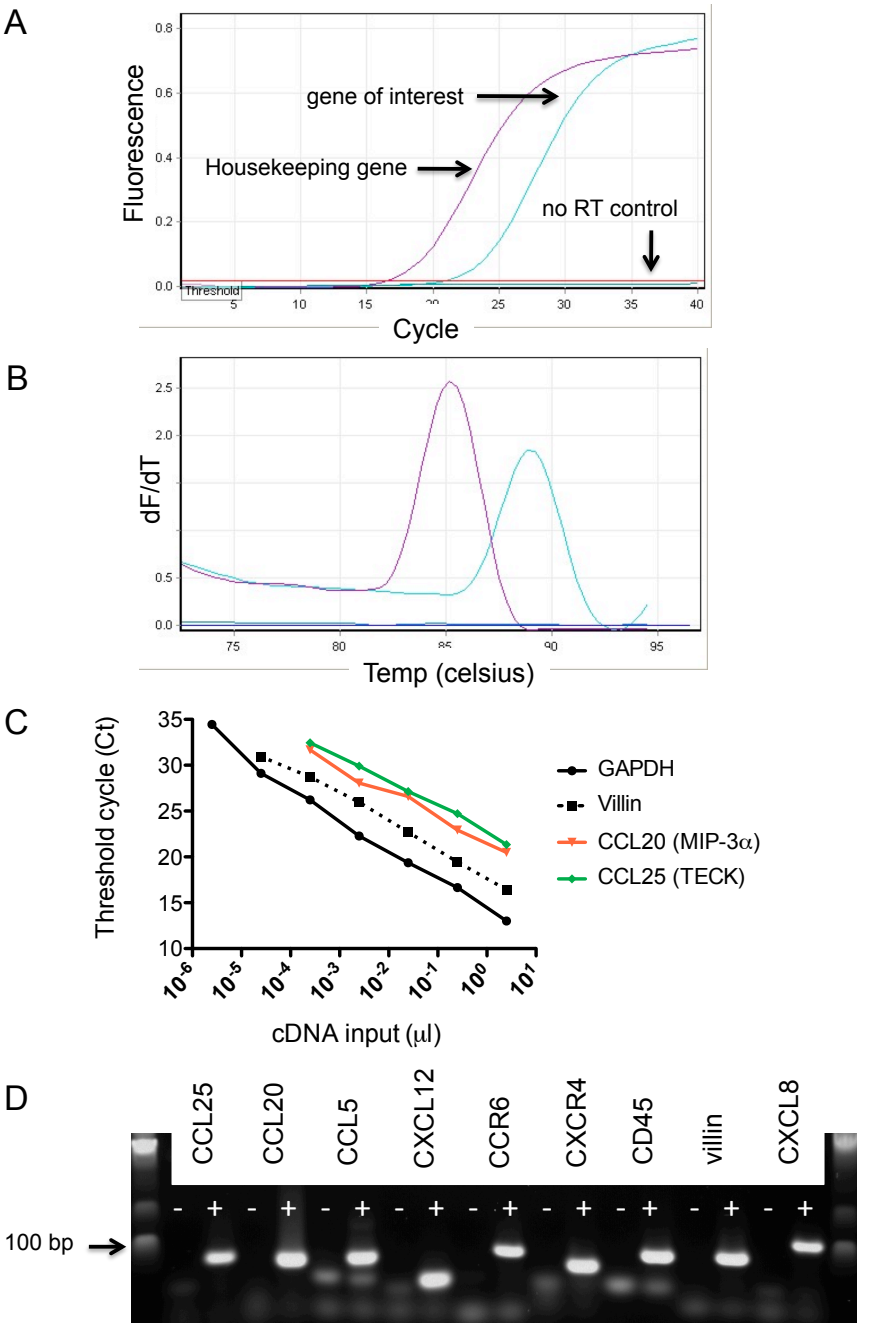


Figure 2.6 Sample output from real time SYBR green PCR experiment and validation of primer pairs.

A: Amplification plots of cDNA sample comparing housekeeping gene, gene of interest and no reverse transcriptase (-RT) control.

B: Melt curves were analyzed to confirm that a single PCR product was produced for each primer pair during an experiment.

C: A standard curve relative to the housekeeping genes was performed for each primer pair to verify that replication rates were comparable.

D: PCR products run on an agarose gel to validate the size of the product and confirm that a single PCR product is made. '+' indicates reaction with reverse transcriptase; '-' indicates reaction without reverse transcriptase. In this example, CCL5 primers did not pass because a product in the –RT control is present.

2.14 Phospho-kinase array and Western blotting

2.14.1 Cell stimulation

Sorted CCR9^{+} ATRA-cultured cells were resuspended to 5 x 10^{6} cells/ml in Serum free Media (see Appendix I) and incubated at 37°C for 4 hours. Serum free media was used to avoid FCS induced phophorylation. To assure that an equivalent number of live cells were stimulated between different conditions, a sample of cells were analyzed by CellTiter-Glo® as previously described (see Section 2.6.2). Aliquots of cells were prepared to avoid cell handling prior to chemokine stimulation. Chemokine was prepared to a 2X concentration in Serum free media pre-warmed to 37ºC. Cells were combined with chemokine or buffer in equal parts, incubated at 37ºC for 5 minutes and immediately pelleted by centrifuging at maximum speed for 30 seconds. Cell pellets were washed by resuspending in RT D-PBS and centrifuging at full speed for 30 seconds.

2.14.2 Lysate preparation

Cell pellets were immediately lysed in 30 µl Lysis buffer (see Appendix I) per 1 x 10^{6} cells. Cell lysates were incubated at 4°C on a shaking unit for 30 minutes. Lysed cells were centrifuged at 13,000 x RPM at 4°C for 30 minutes, and the supernatant transferred to a fresh eppendorf tube. Protein concentration was immediately measured and the sample was stored at -80°C.

2.14.3 Determination of protein concentration

The concentration of protein in each lysate was measured using a BCA Protein Assay according to the manufacturer's instructions alongside BSA protein standards (Pierce). Absorbance readings at 562 nm were taken using a FLUOstar OPTIMA plate reader (BMG LABTECH, Bucks, UK). Figure 2.7 illustrates a typical linear regression analysis from which the sample protein concentrations was calculated.

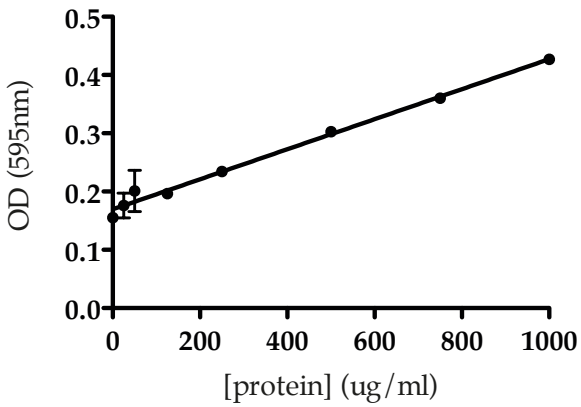


Figure 2.7 Standard curve for BCA Protein Assay.
BCA working reagent was added to duplicates of protein standards prepared according to the manufacturer's instructions. Representative example of BCA standard curve used to determine sample protein concentration.

2.14.4 Phospho-kinase array

An equivalent concentration of protein was added to each array and processed according to the manufacturer's instructions.

2.14.5 SDS-PAGE

Samples were mixed in a 3:1 ration with 4X NuPAGE® LDS Sample Buffer, heated to 100°C for 5 minutes and chilled on ice before loading onto SDS-PAGE gels. SDS-PAGE separates denatured protein according to the molecular weight. Protein (10 - 30 µg/well) was loaded onto a 4% stacking gel on top of a 12% separating gel. On the same gel, a molecular weight rainbow ladder was loaded (5 µl). Gels were run at 150V for 90 minutes in Running buffer (Invitrogen, Paisley, UK) using XCell SureLock™ Mini-Cell Electrophoresis System (Invitrogen).

2.14.6 Western blotting

Nitrocellulose membrane was prepared by washing in 100% methanol for 10 minutes, followed by a 10 minute wash in ddH_20 and a final 10 minute equilibration in Transfer buffer (Invitrogen) all conducted at RT. Samples were transferred from the SDS-PAGE gel onto the

nitrocellulose membrane by wet blotting using the Hoefer TE77X Semi dry transfer unit (Isogen Life Science, distributed by SERVA Electrophoresis, Cambridge, UK) as instructed by the manufacturer, filled with Transfer buffer (Invitrogen) and run at 200 mA for 2 hours. The nitrocellulose membrane was then blocked in 5% non-fat milk / TBS-T (see Appendix I) for 1 hour at RT on a rolling unit. Membrane was washed twice for 5 minute in TBS-T and incubated with primary antibody diluted in 5% non-fat milk / TBS-T overnight at 4°C on a rolling unit. The following day, the membrane was washed for 1 hour in TBS-T, changing the washing buffer every 10 minutes. The membrane was then incubated with HRP-conjugated secondary antibody diluted in 5% non-fat milk / TBS-T, for 1 hour at RT on a rolling unit. Membrane was washed for 1 hour in TBS-T, changing washing buffer every 10 minutes. Membrane was incubated with SuperSignal West Pico Chemiluminescent Substrate for 5 minutes at RT, according to the manufacturer's instructions. Chemiluminescence was detected by exposure to X-ray film. Densitometric analysis of the Western blots were performed using the ImageJ software.

2.14.7 Western blot stripping

To reprobe a Western blot, the nitrocellulose membrane was stripped of the original primary and secondary antibodies by incubating in Stripping buffer (see Appendix I) for 30 minutes at RT. The nitrocellulose membrane was washed at RT in TBS-T for 30 minutes, changing TBS-T every 5 minutes and reprobed by resuming the Western blotting protocol starting with the '5% milk / TBS-T blocking step'.

2.15 Data analysis

With the exception of the Z-test (performed using Microsoft excel version 12.3.4), all statistical analysis was performed using GraphPad Prism software (version 5.0a). Datasets were tested for normality using D'Agostino and Pearson's normality test. In Chapter 3

normality was evaluated using log10 values. For normally distributed data, statistical significance between two groups was assessed with the student's t-test (two-tailed) or by one-way ANOVA with an appropriate post-hoc test when multiple comparisons were made. Dunnett's post-hoc test was used to compare experimental values to a control value, and Bonferonni's post-hoc test was used to compare multiple selected groups. For non-normally distributed data, comparison of a single variable between two groups was analyzed by a nonparametric Mann-Whitney test and by a Kruskal-Wallis test for comparison between multiple groups.

CHAPTER 3: Quantifying changes to lymphocyte populations following CCR9 antagonist treatment during active Crohn's disease

3.1 Introduction

Crohn's disease is characterized by an accumulation of immune cells in the intestinal lamina propria with elevated Th1 and Th17 associated cytokines produced from biopsied intestinal tissue [168,199,201,311-314]. In the intestinal epithelium, a slightly higher frequency of IELs have been reported during active CD, the majority of which are $CD8^+$ T cells [314,315]. Cell extravasation during inflammation is in part mediated by chemokines, and in the context of CD, the CCR9-CCL25 axis is a possible intestinal specific therapeutic target; $CCR9^+$ T cells are predominantly Th1 effector cells and expression of cognate ligand, CCL25, is largely restricted to the small bowel where active CD is predominantly localized [70,75,90,192]. Furthermore, during active CD there is an elevated frequency of circulating $CD4^+CCR9^+$ T cells [72].

3.1.1 CCR9 antagonist, CCX282-B

ChemoCentryx, Inc., has developed an orally bioavailable, small molecule CCR9 antagonist, CCX282-B. *In vitro*, CCX282-B inhibits CCL25 mediated cell migration and calcium mobilization measured in cells which express surface CCR9, including Molt-4 cells and primary human T cells activated and expanded in the presence of all *trans* retinoic acid [87]. Furthermore, tested *in vivo*, CCX282 protected $TNF^{\Delta ARE}$ mice from developing spontaneous ileitis (see Section 1.3.9) [87].

PROTECT-1 was a Phase II, double blind clinical trial, testing the efficacy of CCX282-B in CD, measuring induction and maintenance of disease remission (Figure 3.1A) [316]. 436

patients with active disease (CDAI ≥ 250, C-reactive protein > 7.5 mg/L) were enrolled and randomly assigned to one of four treatment groups [316]:

- Placebo twice daily
- 250 mg CCX282-B once daily
- 250 mg CCX282-B twice daily
- 500 mg CCX282-B once daily

Induction of remission was evaluated over the first 12 weeks, during which, the primary measure of clinical outcome was a decrease in CDAI ≥ 70 points from Baseline levels [316]. Of the three tested doses, 500 mg daily CCX282-B was more efficacious than placebo (Figure 3.1B). Biopsies from the terminal ileum were collected at study enrollment (Baseline) and following 12 weeks of treatment (End of Induction), formalin fixed and paraffin embedded. The work presented in this chapter explores ways of quantifying $CCR9^+$ cells, stained by the immunohistochemical (IHC) technique.

3.1.2 Quantification by IHC

IHC detection has the distinct advantage of visualizing cells within the natural tissue architecture; this is in contrast to studies of disaggregated tissue analyzed by flow cytometry which cannot exclude nor account for lymphoid aggregates, and cannot with complete accuracy, assess difference in the localization of cells, such as IELs versus cells in the lamina propria [317]. In the present study I describe a technique for quantifying cell number relative to tissue area (cells/mm^2 tissue), measuring T cells in the lamina propria and epithelium separately. Alternative methods for measuring immunohistochemical findings have been described, including counting cells within several high powered fields or relative to a set number of epithelial cells, however these techniques are subject to selection bias [311,314]. The method described circumvents this limitation by allowing quantification of the entire biopsy, even when differences in tissue orientation arise. Whilst similar analyzes have been

conducted, to describe the frequency of cell populations between intestinal diseases for example [312,315], to the best of my knowledge, this is the first description using such an analysis to measure the effects of therapeutic treatment.

3.1.3 Aims of this chapter

CCR9 is a potential target in CD, however studies of CCR9 and CCL25 in human disease are limited. The experiments in this chapter were designed to quantify the effects of CCR9 antagonist treatment on T cell density in the small intestine during active Crohn's disease. Biopsies from the terminal ileum collected as part the PROTECT-1 trial, from patients taking placebo or 500 mg daily CCX282-B, were analyzed by IHC. The experiments presented in this chapter will include:

- Evaluation of CCR9 staining by IHC.
- Development of protocol to quantify lymphocyte density within the intestinal lamina propria and epithelium stained by IHC.
- Quantification of cell density to assess:
    - All T cells ($CD3^+$ and $CD8^+$)
    - Cytotoxic T cells ($CD8^+$)
    - Estimate of T helper cells ($CD3^+CD8^-$)
- Comparison of cell density following placebo and CCX282-B treatment.

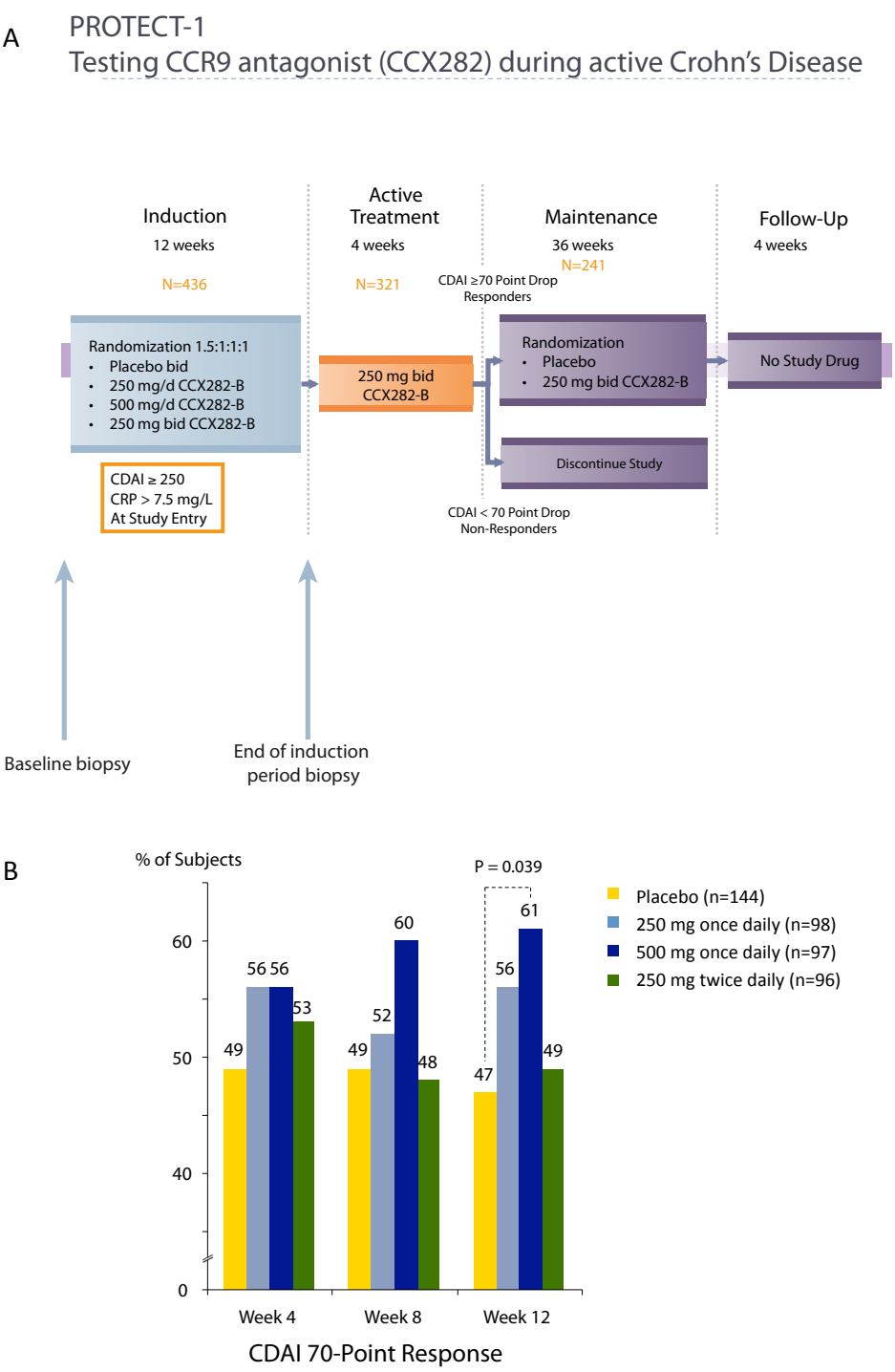


Figure 3.1 PROTECT-1 trial design and clinical response to CCX282-B measured in Crohn's disease.

A: PROTECT-1 clinical trial design. Biopsies from the terminal ileum were collected prior to drug or placebo treatment, and 12 weeks later. Arrows indicate the collection of biopsies used for analysis by IHC staining.

B: Primary clinical endpoint during the 'induction' phase of PROTECT-1. Graph depict the percent of enrolled patients with a CDAI decrease great than 70 points from Baseline. CDAI = Crohn's disease activity index. Adapted from Keshav *et al* (2013) [318].

3.2 Results

3.2.1 Evaluation of CCR9 staining by IHC

To quantify changes to $CCR9^+$ cells in the intestine, a validated antibody for CCR9 staining by IHC was required. While several different commercially available antibodies were tested, the work presented in this chapter were performed with one antibody (3C3 hybridoma supernatant, specific for the NH_2 terminus of CCR9 [69]) which exhibited the strongest staining and the least non-specific binding by IHC. Staining by other tested CCR9 antibodies can be found in the appendix, detailing why there were not pursued (see Appendix 3). CCR9 specific, 3C3 antibody was previously used to characterize expression by flow cytometry and is validated for specificity by Western blotting [69,72,75,319]. For each tissue, antibody was titrated to determine the optimal working dilution.

Cell cytospins

Molt-4 cells are a human acute lymphoblastic leukaemia derived cell line that constitutively express surface CCR9 protein, measured by flow cytometry [69]. Molt-4 cells were prepared as cell cytospins and stained by IHC, comparing isotype control (IgG1,κ), CCR9, and CD3 (positive control) antibodies. Non-specific isotype staining was not detected, while CCR9 and CD3 were detected by the immunoperoxidase technique and shown as brown staining (Figure 3.2A - C). Wild type (WT) HEK-293 cells were mixed with cells stably expressing CCR9 (CCR9-HEK cells), prepared as cell cytospins and stained for CCR9. Strong CCR9 staining was observed on the expected proportion of cells, with minimal non-specific staining on WT HEK-293 cells (Figure 3.2D & E). Collectively, CCR9 detected by IHC demonstrated specific staining with minimal non-specific antibody binding on cell cytospins.

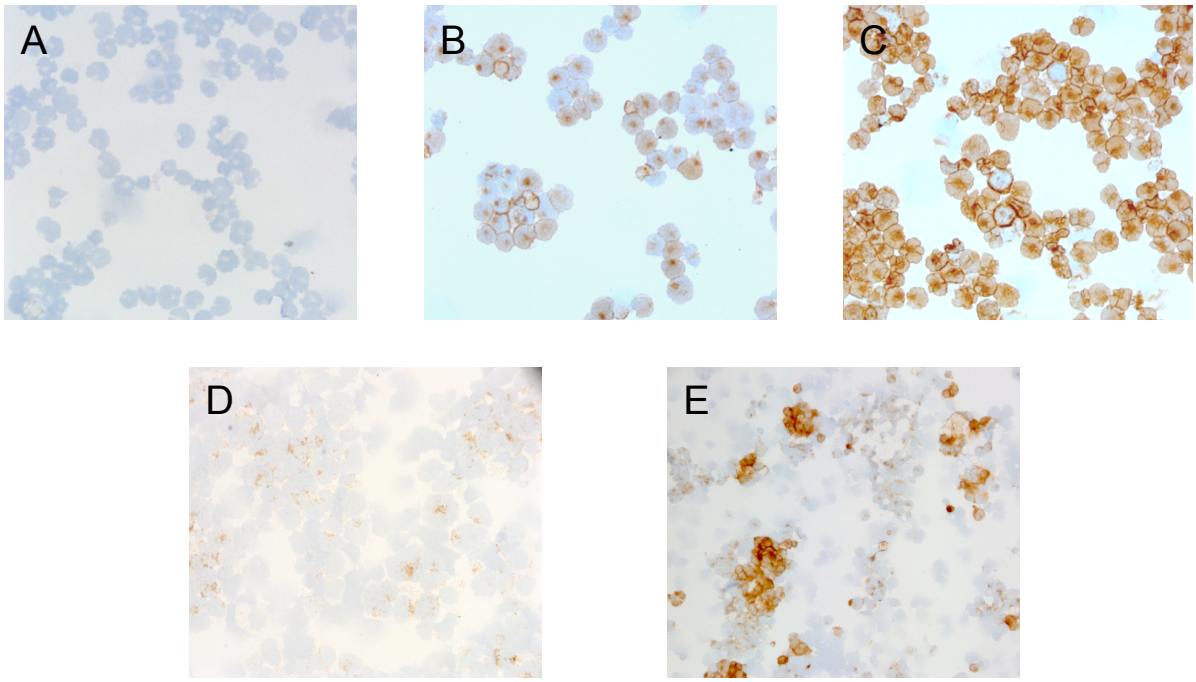


Figure 3.2 Cell cytospins stained by IHC.
Molt-4 cells constitutively express surface CCR9 protein. HEK-293 cells (WT) were combined with HEK-293 cells stably expressing human CCR9 (CCR9-HEK cells). Staining was performed by the immunoperoxidase technique and haematoxylin counterstained to visualize cell nuclei (blue).
A: Molt-4 cells, isotype control (IgG1, κ)
B: Molt-4 cells, anti-CCR9
C: Molt-4 cells, anti-CD3 (positive control)
D: WT HEK-293 cells, anti-CCR9
E: 3:1 mixture of WT HEK-293 cells to CCR9-HEK cells, anti-CCR9

Human tonsil

In human tonsil, surface CCR9 is detected on < 2% of cells, analyzed by flow cytometry [320]. Formalin-fixed, paraffin embedded human tonsil was stained for CCR9 by IHC showing a few scattered cells which were strongly positive, with membrane-associated staining (Figure 3.3A & B). Background, non-specific staining was negligible in the tonsil, providing clear differentiation between stained and unstained cells (Figure 3.3B).

Human thymus

In the human thymus, $CCR9^+$ cells are abundant in whole tissue preparations measured by Northern blotting, flow cytometry and qPCR [69,73,88]. Based upon studies of murine CCR9 expression during T cell maturation in the thymus, CCR9 expression in the cortex was predicted with a lower proportion of cells staining in the medulla (see Section 1.3.9).

Paraffin embedded human thymus was obtained as 8 μm sections (all other tissue analyzed in this thesis were 4 μm thick). To examine tissue quality, CD3 staining was performed. Analysis by phase-contrast microscopy revealed multiply layers of CD3 expressing cells, generating hazy brown staining in areas where cells were layered (Figure 3.3C). Nevertheless, strong membrane-associated CD3 expression was observed with negligible staining by isotype control, demonstrating that the quality of tissue sections were amenable to IHC (Figure 3.3D).

In accordance with murine data, in sections of human thymus the majority of CCR9 expression was localized to the cortex, with a lower proportion of cells stained in the surrounding medulla (Figure 3.3E). In contrast to the strong membranous CD3 staining, CCR9 was diffuse and weak, localized to the cell cytoplasm, with focal points of strong staining (Figure 3.3F). The quality of CCR9 staining in the thymus was poor, however for

the purposes of analyzing PROTECT-1 samples I was most concerned with CCR9 expression in the intestine, therefore I went on to study these tissues.

Human intestinal tissue

Independent studies have demonstrated by disaggregation of tissue and analysis by flow cytometry, that the majority of small intestinal $CD4^+$ and $CD8^+$ T cells express surface CCR9 (58 – 96%; see Section 1.3.4). Cells referred to as IELs (although the purity of isolation could be challenged) are also predominantly $CCR9^+$ (88 – 95%) [69,70]. Therefore detection of CCR9 expressing LPLs and IELs were expected. Paraffin embedded human small intestinal tissue was stained for CCR9 by IHC.

Cells stained by CCR9 antibody were scattered throughout the LP with granular and punctate staining localized to the cell cytoplasm (Figure 3.4). The pattern of expression resembled that observed in the human thymus (see Figure 3.3F) and was in contrast to the well defined, membranous staining in the human tonsil (see Figure 3.3B). Strong membrane-associated CCR9 staining was less frequent in the small intestine, however in some cases could be found within lymphoid aggregates (Figure 3.5).

The CCR9 antibody consistently stained the intestinal epithelium (Figure 3.6). Expression was diffuse and weak, with strong punctate staining on the apical side of enterocytes and goblet cells (Figure 3.6A). At the time of this thesis, no published data indicated CCR9 expression by epithelial cells, therefore this staining was interpreted as non-specific. As predicted, CCR9 stained IELs were also identified (Figure 3.6B).

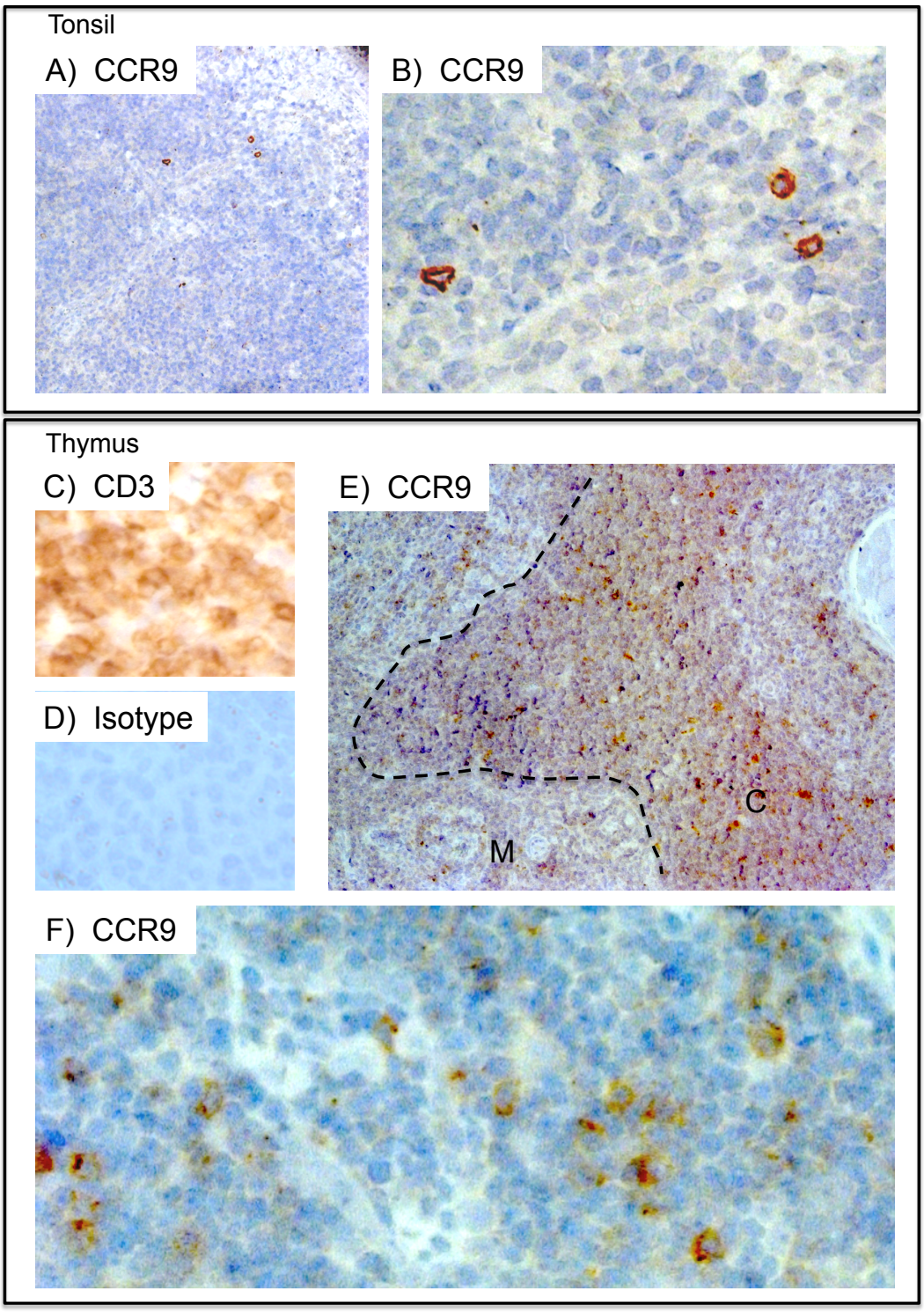


Figure 3.3 Human tonsil and thymus stained by IHC.
Formalin-fixed, paraffin embedded human tissue was stained by IHC (brown) and haematoxylin counterstained (blue).
A - B: Human tonsil, anti-CCR9
C: Human thymus, anti-CD3
D: Human thymus, isotype control (IgG1, κ)
E - F: Human thymus, anti-CCR9.
Images representative of 3 - 8 independent patient samples.

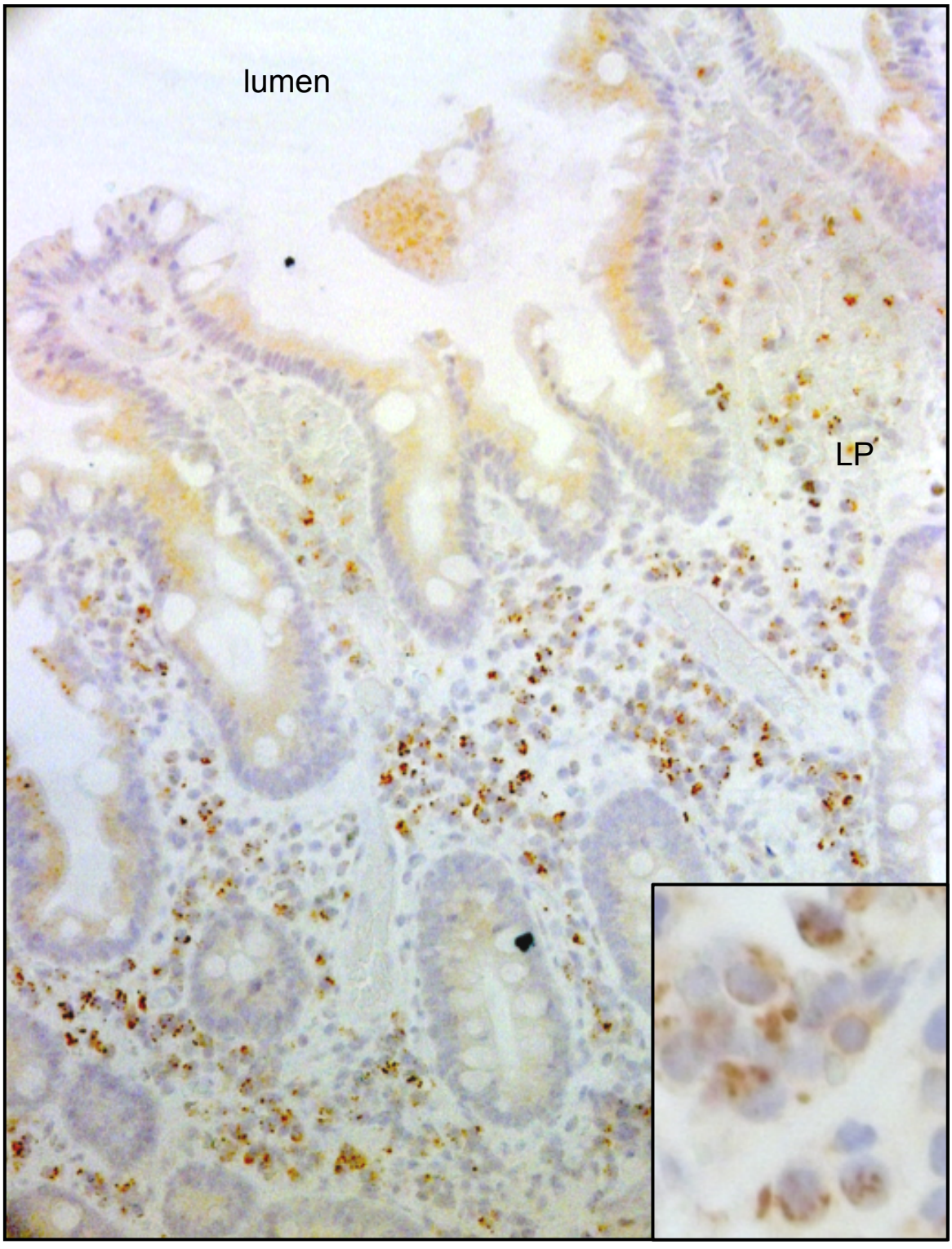


Figure 3.4 Human intestinal tissue stained for CCR9.
Formalin-fixed, paraffin embedded human tissue was stained for CCR9 (brown) by IHC and haematoxylin counterstained (blue nuclei). Image illustrates, at high magnification, cytoplasmic associated, punctate CCR9 staining of LPLs. LP = lamina propria. Image representative of 30 independent patient samples.

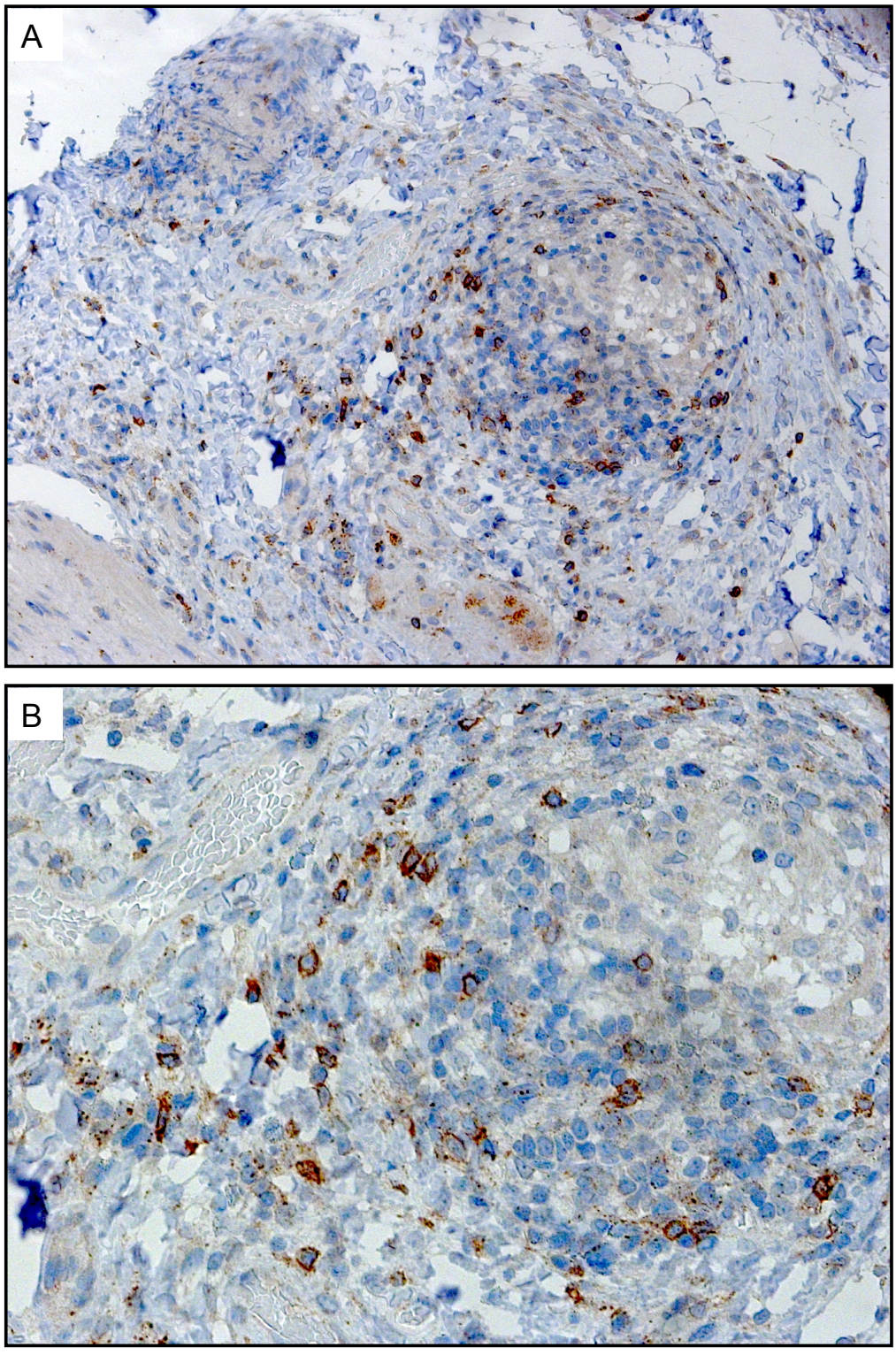


Figure 3.5 Human intestinal lymphoid follicle stained for CCR9.
Formalin-fixed, paraffin embedded human tissue was stained for CCR9 (brown) by IHC and haematoxylin counterstained (blue nuclei). The image illustrates strong membrane-associated CCR9 staining of cells within an intestinal lymphoid follicle. (A) 20X magnification. (B) 40X magnification. Image representative of 3 independent patient samples.

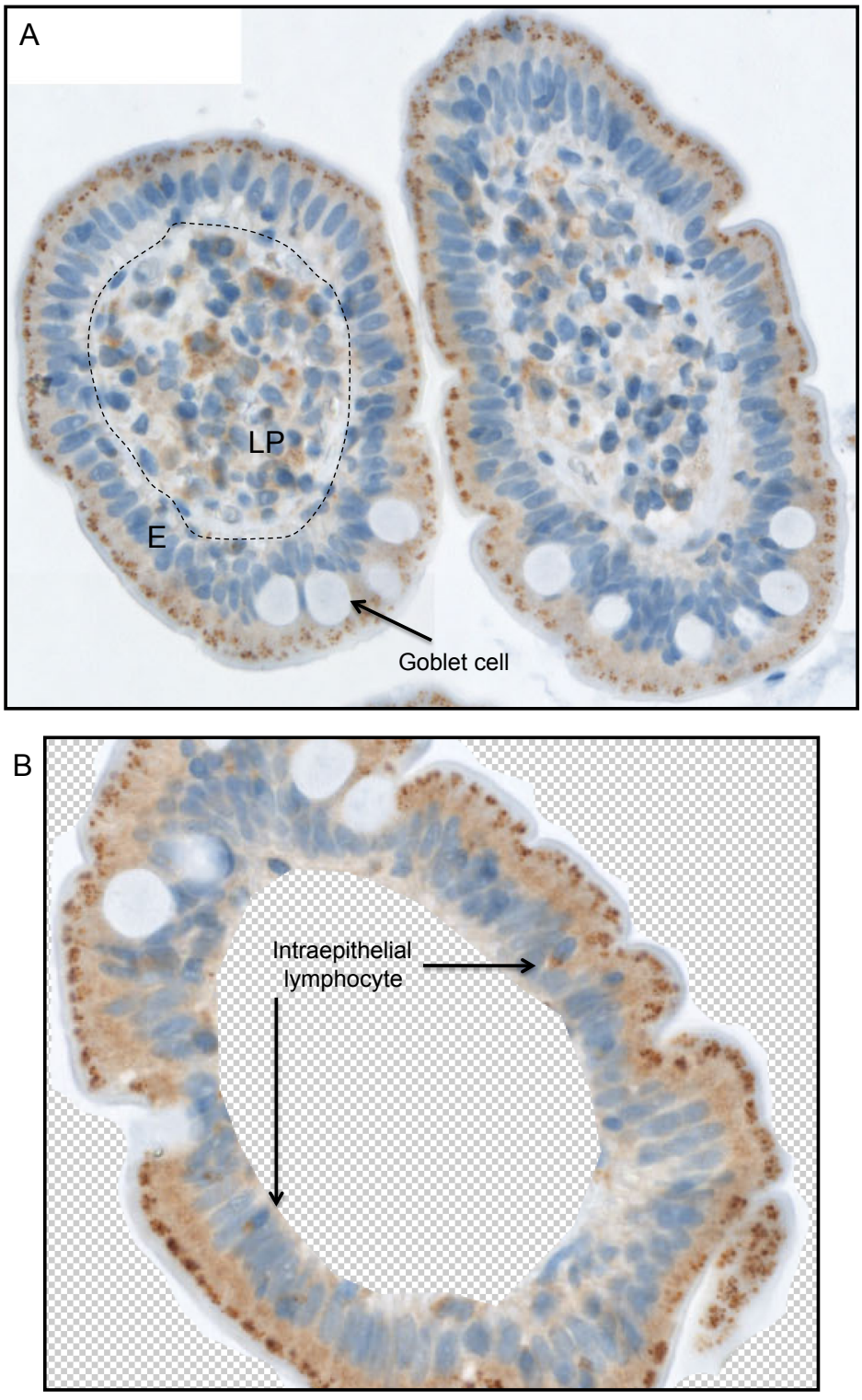


Figure 3.6 CCR9 stained intestinal epithelial cells and intraepithelial lymphocytes. Formalin-fixed, paraffin embedded human tissue was stained for CCR9 (brown) by IHC and haematoxylin counterstained (blue nuclei). Cross section of small intestinal villi are shown. A: Image illustrates weak and diffuse CCR9 staining with punctate granules at the apical edge of small intestinal enterocytes and goblet cells. LP = lamina propria, E = epithelium. B: Cross section of intestinal villi with the lamina propria removed. Arrows highlight intraepithelial lymphocytes stained for CCR9.

Double staining CCR9 with CD3, CD8 or CD68 in human intestinal tissue

To examine the phenotype of cells detected by CCR9 antibody, double staining was performed with T cell markers CD3 and CD8; as a negative control, double staining was performed with anti-CD68, a marker used predominantly to identify macrophages but also expressed by DCs [321,322]. Antibodies specific for human CD4 are excellent for analysis by flow cytometry but do not produce strong staining by IHC (based upon attempts to optimize CD4 staining and conversations with colleagues who experienced similar poor results), therefore CD4 was not pursued for double staining.

In human intestinal tissue, cells co-stained for CCR9 and CD3 were identified in the lamina propria but were a minority population compared to single stained CCR9 cells and single stained CD3 cells (Figure 3.7). Intestinal tissue doubled stained for CCR9 and CD8 illustrated differences in the location of antigen: CD8 staining was membrane-associated, in contrast CCR9 staining was punctate, appearing as granules located in the cell cytoplasm (Figure 3.8). Unexpectedly, in a sample of colonic human tissue, cells positive for CCR9 were co-localized with CD68, suggesting CCR9 expression in macrophages (Figure 3.9).

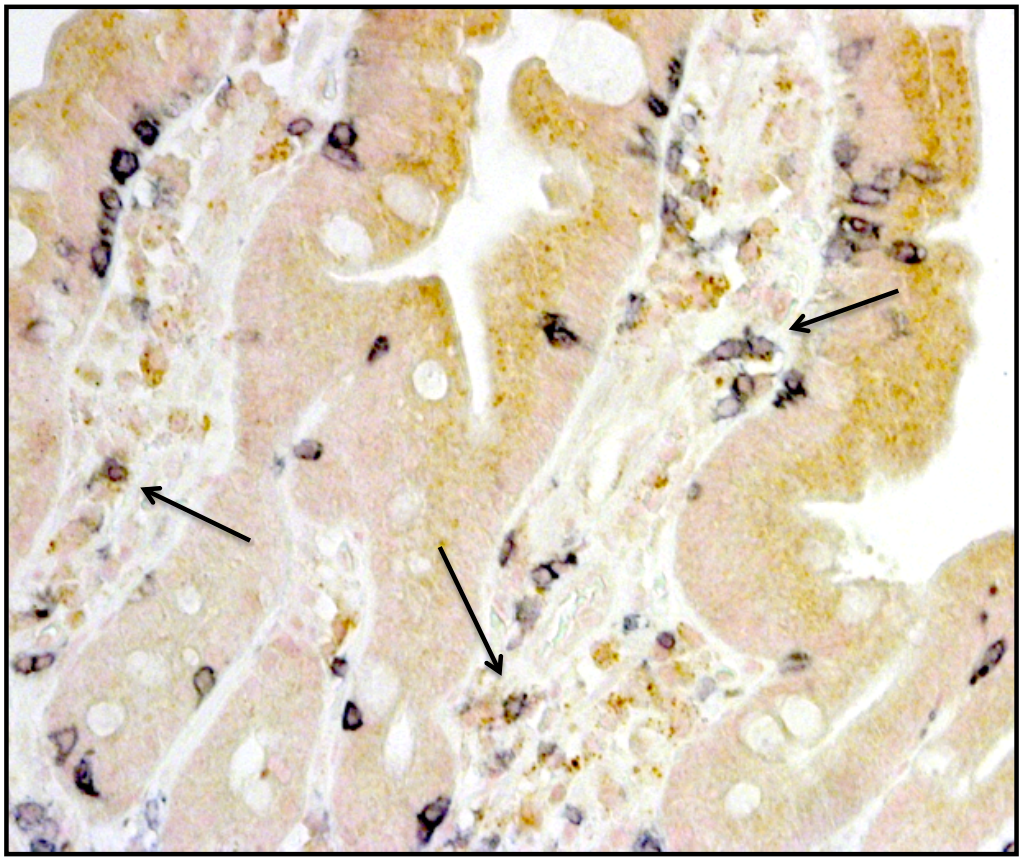


Figure 3.7 CCR9 and CD3 double staining in human small intestinal tissue.
Formalin-fixed, paraffin embedded human tissue was stained for CCR9 (brown) and CD3 (blue/grey) by double immunoenzymatic labelling. Arrows indicate cells co-stained for CCR9 and CD3. Image representative of 4 independent patient samples.

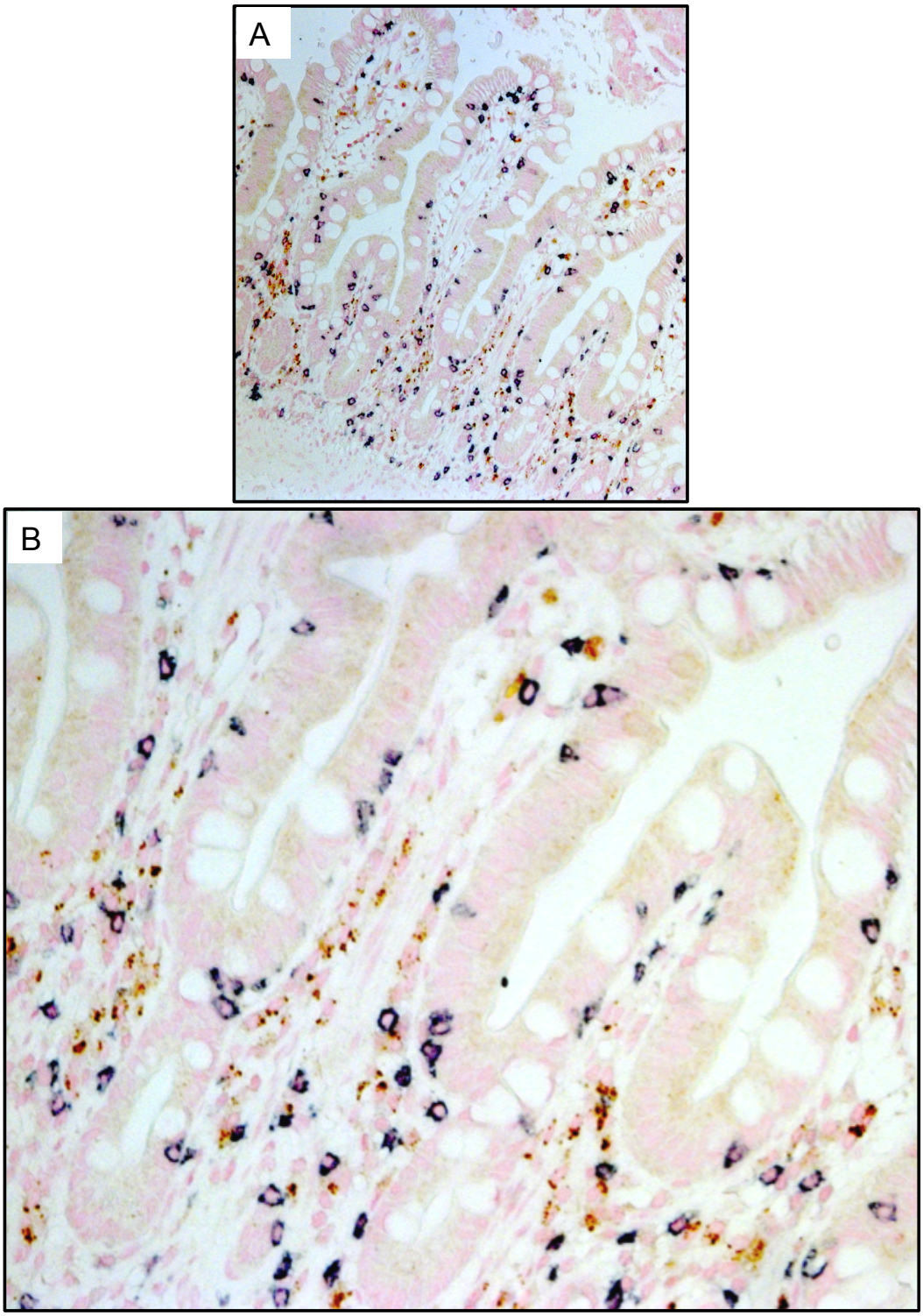


Figure 3.8 CCR9 and CD8 double staining in human small intestinal tissue.
Formalin-fixed, paraffin embedded human tissue was stained for CCR9 (brown) and CD8 (blue/grey) by double immunoenzymatic labelling and counterstained with Vector red (red). Image, at high magnification (B) illustrates cytoplasm-associated, punctate CCR9 staining. In contrast, CD8 stained cells displayed strong membrane-associated staining. Image representative of 3 independent patient samples.

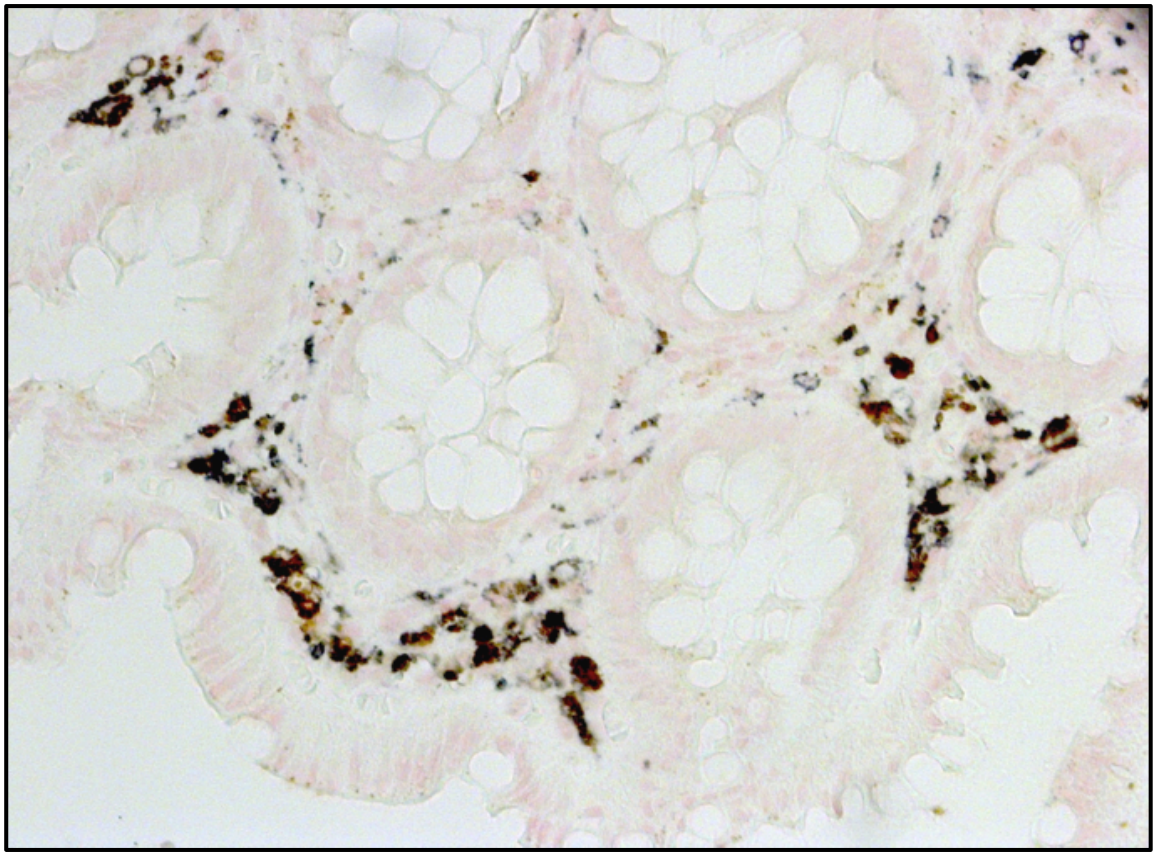


Figure 3.9 CCR9 and CD68 double stained of human large intestine by IHC.
Formalin-fixed, paraffin embedded human colonic tissue was stained for CCR9 (brown) and CD68 (blue/grey) by double immunoenzymatic labelling and counterstained with Vector red (red). CCR9 stained cells were co-stained with CD68, generating a dark purple/black precipitate. Image representative of 3 independent intestinal tissues.

3.2.2 Alternative for estimating CCR9$^+$ cells in the small intestine by IHC (CD3 and CD8 double staining)

Collectively CCR9 expression detected by IHC on cell cytospins, human tonsil and human thymus were in line with the expected frequency and distribution. However in more complex tissues such as the intestine, staining gave results that were at odds with the current literature; fewer T cells were co-localized with CCR9 while macrophages were strongly positive. Furthermore, the quality of staining in human tissues was poor such that accurate quantification would be unattainable. Consequently, staining for CCR9 directly was abandoned and an alternative approach for estimating CCR9$^+$ T cells by IHC was adopted, measuring small intestinal T cells subsets, the majority of which express CCR9 (see Section 1.3.4).

Antibodies against CD3 and CD8 provide clear differentiation between positive and negative cells (Figure 3.10). To estimate the density of cytotoxic T cells, CD8 expressing cells were measured, with the assumption that all CD8 cells were co-stained by CD3. Small intestinal CD4 T cells are also predominantly CCR9 expressing, however CD4 staining by IHC is not robust. Therefore to approximate the density of CD4$^+$ T helper cells, CD3$^+$CD8$^-$ cells were quantified.

In total, 40 ileal biopsies from placebo (17 Baseline and 23 End of Induction) and 30 biopsies from CCX282-B treated patients (16 Baseline and 14 End of Induction) were analysed. Biopsies were double stained for CD3 and CD8 by IHC, and tissue area and cell count measured in Adobe Photoshop relative to a standardized scale set against the 7 μm diameter of a lamina propria lymphocyte [138] (see Section 2.4.5). All T cells (CD3$^+$), cytotoxic T cells (CD8$^+$) and an approximation of T helper cells (CD3$^+$CD8$^-$) cells were counted in the epithelium and lamina propria separately and expressed as cells per mm^2 tissue (Figure 3.10B). Lymphoid aggregates were excluded from the analysis.

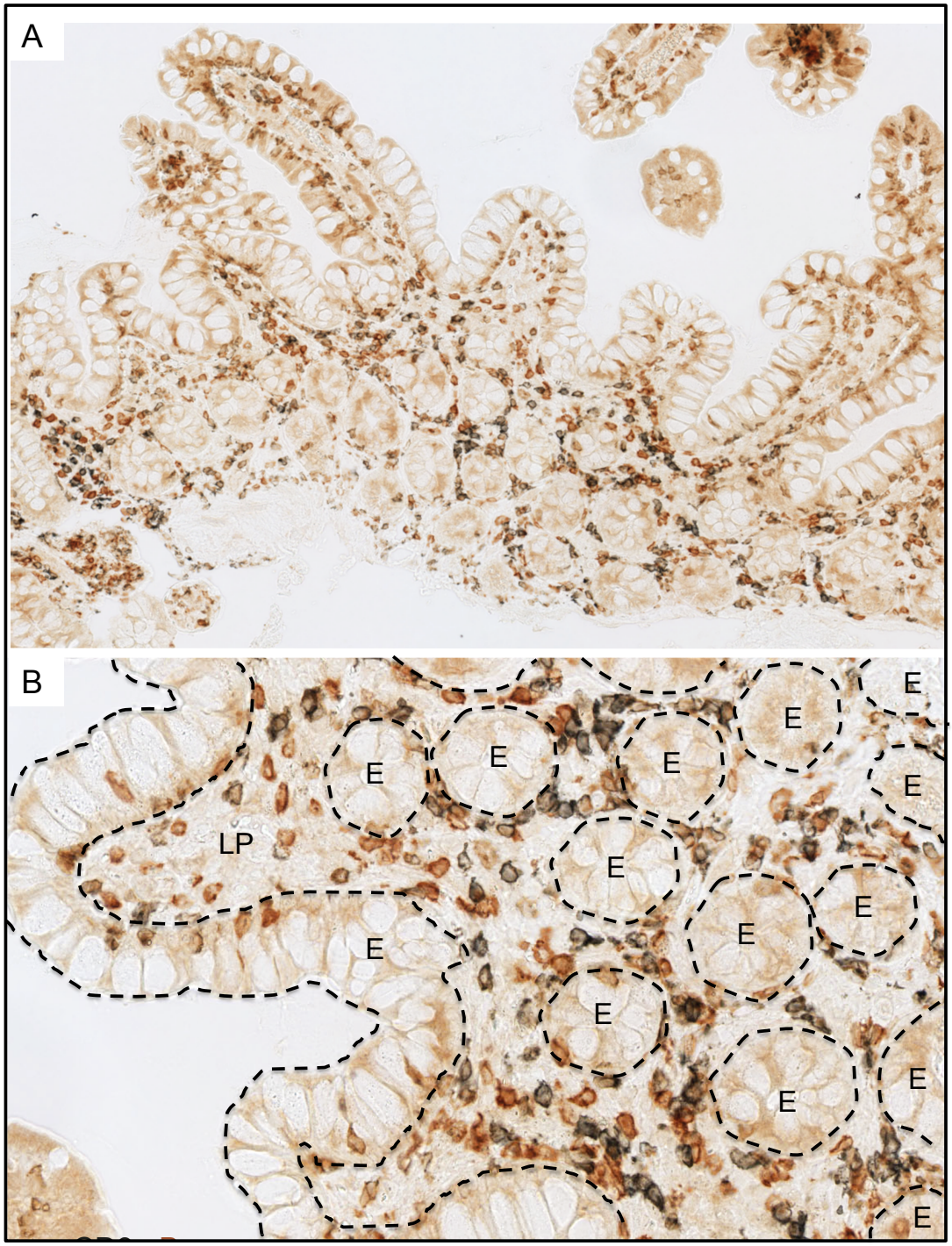


Figure 3.10 CD3 and CD8 double staining and quantification of biopsies from PROTECT-1.

Patient biopsies from the terminal ileum were formalin fixed, paraffin embedded and stained for CD3 (brown) and CD8 (blue/gray) by double immunoenzymatic technique.

A: Representative biopsy from PROTECT-1 stained by IHC.

B: $CD3^+$ and $CD8^+$ cells within the lamina propria and epithelium were separately quantified relative to the tissue area. E = epithelium, LP = lamina propria.

3.2.3 Lamina propria lymphocytes

Cell counts per mm^2 tissue were significantly higher in the lamina propria than in the epithelium for 'all T cells', $CD8^+$ cells and $CD3^+CD8^-$ cells ($p<0.0001$, $p<0.0005$, $p<0.0001$ respectively; Student's t test compared to Baseline placebo values; Figure 3.11A & Figure 3.12A). In accordance with previous reports, there were approximately twice as many T helper cells ($CD3^+CD8^-$) as cytotoxic T cells ($CD8^+$) cells in the lamina propria (Figure 3.11A) [315,323].

From Baseline to End of Induction, placebo treated patients had a 6.3% increase in all T cells, largely contributed by an increase in $CD8^+$ cells (19.7% increase in $CD8^+$ cells compared to 0.5% increase in $CD3^+CD8^-$ cells) however these changes were not statistically significant (Figure 3.11Ai).

In contrast, CCX282-B treated patients had a 16% decrease in all T cells, reflected as a decrease in $CD8^+$ cells (16.3% decrease) and $CD3^+CD8^-$ cells (15.9% decrease), however these changes were also not statistically significant (Figure 3.11Aii).

Although there was a trend that CCX282-B treatment had a greater decrease in cell density (from Baseline to Day 91), an analysis of whether the mean change differed between placebo and CCX282-B treatment found no significant difference in each of the analyzed cell populations (Figure 3.11Aiii). Figure 3.11B depicts the values for each biopsy, illustrating the degree of data scatter.

A

	i				*ii*				*iii*
	Placebo				*CCX282-B*				mean change between Placebo and CCX282-B
	Baseline	*End of Induction*	*% change*	*p-value*	*Baseline*	*End of Indcution*	*% change*	*p-value*	*p-value*
	mean cells/mm²				*mean cells/mm²*				
Lamina propria									
All T cells	2210	2349	6.3	0.43	2389	2007	-16.0	0.69	0.20
CD8+	668	800	19.7	0.37	856	716	-16.3	0.60	0.17
CD3+CD8-	1542	1550	0.5	0.42	1533	1290	-15.9	0.70	0.20

B

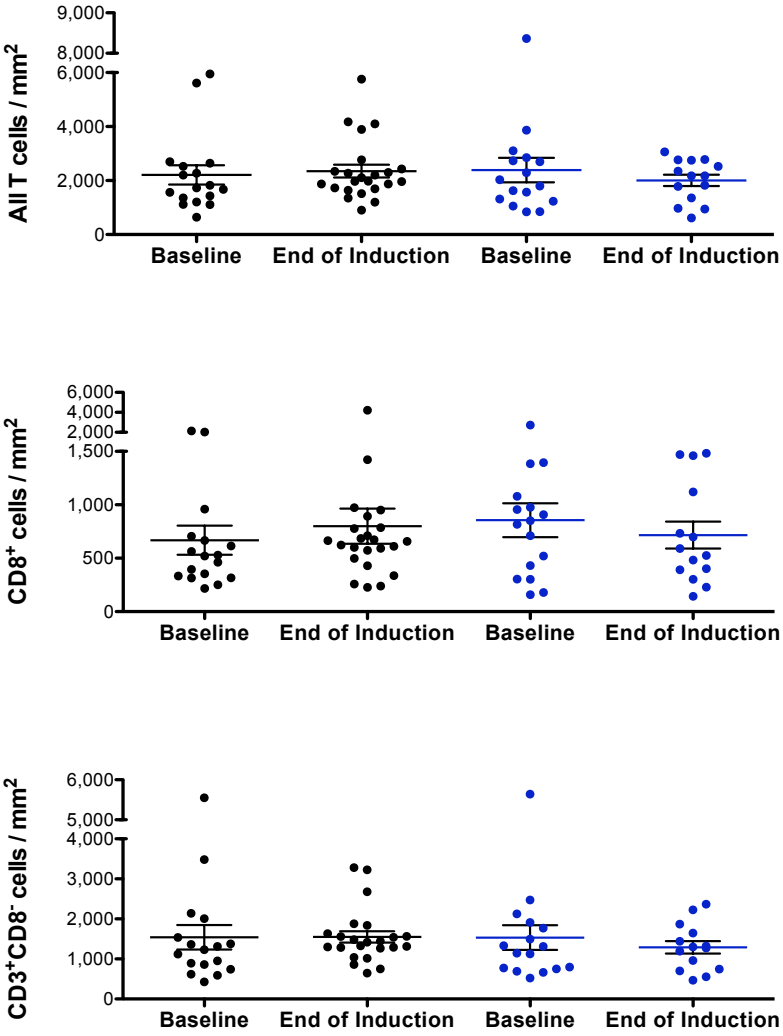


Figure 3.11 Quantification of lamina propria lymphocytes.
A: Summary table of data.
B: Each data point is a single biopsy comparing placebo (black) and CCX282-B treatment (Blue). Data shows mean ± SEM.
Baseline to End of Induction analyzed by Student's t test (Ai and Aii). To test whether the mean change in cell count differed between Placebo and CCX282-B, a one-sided Z-test, assuming unequal variance between groups was performed (Aiii).

3.2.4 Intraepithelial lymphocytes

Analysis of disaggregated tissue measured by flow cytometry reports that the majority of IELs are $CD8^+$, however my analysis found an approximately equivalent number of $CD8^+$ and $CD3^+CD8^-$ IELs (Figure 3.12Ai). Indeed a similar result was reported in an analysis of colonic and rectal biopsies measured by IHC [315]. In the present study, the position of IELs were frequently at the basal membrane, near the border between LP and epithelium (see Figure 3.10). It is possible that analysis by IHC is a more sensitive technique for quantifying IELs, while analysis of disaggregated tissue could inadvertently select for $CD8^+$ cells.

From Baseline to End of Induction, IEL density decreased following placebo and CCX282-B treatment, however these changes were not statistical significant for either treatment (Figure 3.12Ai & Aii). There was a trend that CCX282-B treatment produced a greater decrease in IELs compared to placebo (43% decrease following CCX282-B compared to 13% decrease in placebo in 'all T cells'), however these differences were not statistically significant ($p=0.29$, Figure 3.12Aiii). The greater decrease following CCX282-B treatment was potentially the consequence of a higher Baseline value for that group, however there was no significant difference in Baseline values between placebo and CCX282-B treatment (Kruskal-Wallis test; Figure 3.12B).

3.2.5 Comparison between placebo and CCX282-B treatment in LPLs and IELs

Collectively these data show a trend that CCX282-B treatment reduced T cell density in the lamina propria and epithelium to a greater degree than placebo, however changes from Baseline to End of Induction were not significant (for either placebo or CCX282-B), nor were differences between placebo and CCX282-B treatment significantly different for the cell populations analyzed in this study.

A

	i				*ii*				*iii*
	Placebo				*CCX282-B*				mean change between Placebo and CCX282-B
	Baseline	*End of Induction*	*% change*	*p-value*	*Baseline*	*End of Indcution*	*% change*	*p-value*	*p-value*
	mean cells/mm²				*mean cells/mm²*				
Intraepithelial									
All T cells	448	388	-13	0.25	828	472	-43	0.20	0.29
CD8+	257	168	-34	0.15	449	231	-48	0.08	0.31
CD3+CD8-	258	220	-15	0.24	377	241	-36	0.26	0.31

B

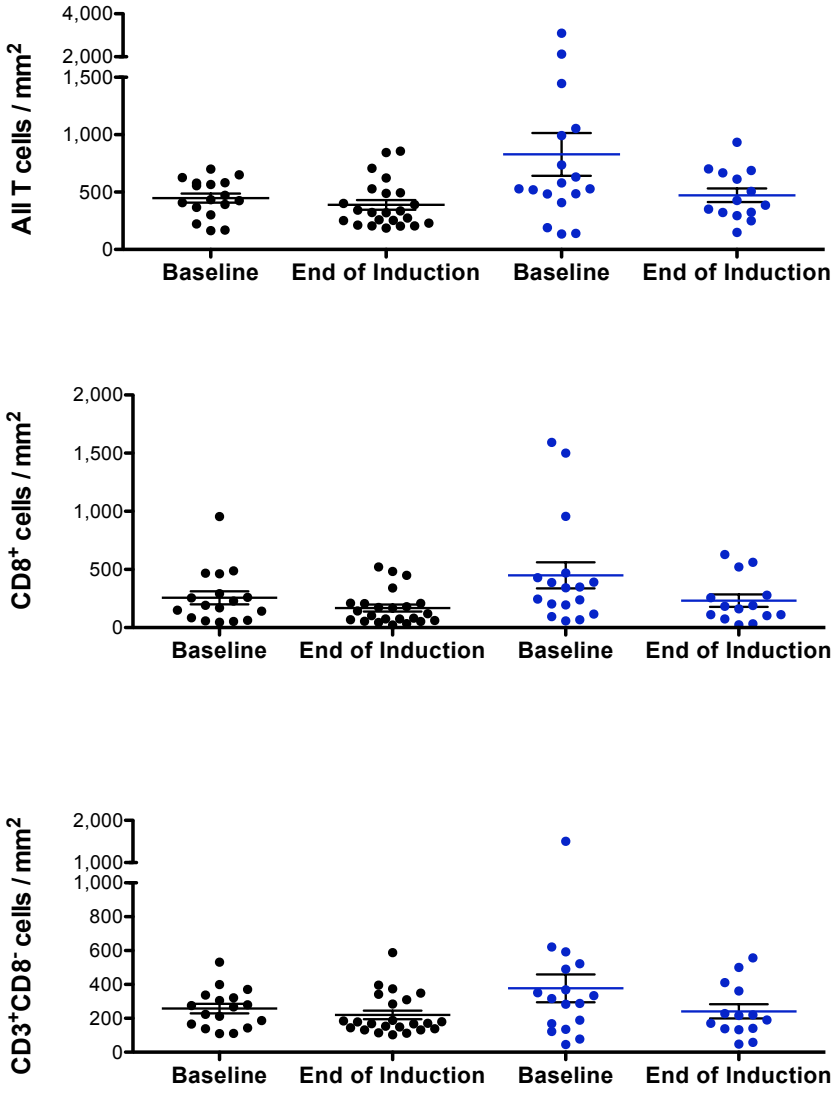


Figure 3.12 Quantification of intraepithelial lymphocytes.
A: Summary table of data.
B: Each data point is a single biopsy comparing placebo (black) and CCX282-B treatment (Blue). Data shows mean ± SEM.
Baseline to End of Induction analyzed by Student's t test (Ai and Aii). To test whether the mean change in cell count differed between Placebo and CCX282-B, a one-sided Z-test, assuming unequal variance between groups was performed (Aiii).

3.3 Discussion

In this chapter I describe attempts to validate CCR9 staining in human tissues, detected by IHC. CCR9 staining was poor in the intestinal tissue but patterns of putative CCR9 expression did stimulate novel hypotheses later addressed in this thesis. As an alternative technique for estimating changes to CCR9 expressing cells, I show an analysis of $CD3^+$, $CD8^+$ and $CD3^+CD8^-$ cells, analysing patient biopsies collected as part of a clinical trial in CD. In this chapter I describe a technique for quantifying cells relative to tissue area, separately analysing LPLs and IELs. Using this approach, I measured changes to T cells, comparing placebo and CCX282-B treatment. The present study shows that clinical measures of efficacy (decrease in CDAI $\geq$ 70 points) were associated with a trend in biological changes, measured as a decrease in T cell density in the lamina propria and epithelium, but which never reached statistical significance.

3.3.1 CCR9 staining by IHC

Efforts to validate CCR9 detection by IHC initially looked promising: cell cytospins showed clear differentiation between $CCR9^+$ and $CCR9^-$ cells and in the human tonsil a few scattered cells had strong, membrane-associated staining. In the human thymus, expression was most abundant in the cortex as predicted, however staining was poor, with patches of strong cytoplasmic associated granular staining. Ultimately, the poor quality of CCR9 staining in the human thymus and intestinal tissue led me to abandon this technique a direct means of CCR9 quantification, however observation made during these studies were hypothesis generating.

In particular, the cytoplasmic, granular staining present in human tissue led me to consider the possibility of CCL25 induced CCR9 internalization. Expression of CCL25 is abundant in the small intestine and absent from the healthy tonsil [70]. Incidentally, CCR9 staining in the

small intestine was punctate and granular, associated with the cell cytoplasm while CCR9 expression in the human tonsil was distinctly membranous. Chemokine induced chemokine receptor internalization is described for some but not all of the 48 chemokine receptors, and at the time of this thesis had not been explored in relation to human CCR9. Indeed indications of CCR9 internalization measured by flow cytometry from disaggregated human tissue may already exist in the published literature.

Eksteen *et al* (2004) show CCR9 stained lymphocytes isolated from the inflamed liver during primary sclerosing cholangitis. CCL25 is not abundant in the healthy liver, however Eksteen and colleagues demonstrate elevated CCL25 mRNA and protein from the liver of patients with PSC [47]. Strikingly, CCR9 surface staining analyzed by flow cytometry showed a higher mean fluorescence intensity (MFI) for cells isolated from the blood compared to cells isolated from the liver of PSC patients; these data might represent the effects of CCL25 mediated CCR9 internalization present in inflamed human liver.

Another potential example of CCR9 internalization from primary human tissue is the analysis by Zabel *et al* (1999) staining IELs from human small intestine. Intriguingly, CCR9 MFI was lower in IELs than in LPLs [69]. CCL25 is expressed by epithelial cells, therefore it's conceivable that IELs undergo a greater degree of CCR9 internalization compared to their lamina propria neighbors. Chapter 4 of this thesis will examine the effect of CCL25 on surface CCR9, to test the hypothesis that CCL25 induces CCR9 internalization. This could explain the punctate CCR9 staining in the human thymus and small intestine; what remains unresolved and difficult to test experimentally, is the striking CCR9 staining of intestinal epithelial cells.

The possibility of CCR9 expression by IELs was expected based upon the work Zabel *et al* (1999) and Kunkel *et al* (2000), however CCR9 stained cells in the epithelium were not

exclusively lymphocytes; rather goblet cells and enterocytes were also stained, particularly on the apical side of the epithelium (see Figure 3.6) [69,70]. These results may be an artifact of non-specific antibody binding or potentially a novel observation reflecting the expression of CCR9 *in situ.* An alternative technique to examine CCR9 expression is by *in situ* hybridization, staining tissue with RNA specific probes. This technique will not be explored in this thesis, although the Keshav laboratory is pursuing this route of CCR9 analysis.

Double staining found CCR9 expression in macrophages ($CD68^+$). Murine CCR9 expressing macrophages have been reported [46,324] although CCR9 expression by human macrophages is not convincingly demonstrated. Although a closer examination of human intestinal tissue by flow cytometry is warranted, one alternative explanation is that CCR9 staining in macrophages was the consequence of macrophages phagocytosing dead or dying CCR9 expressing lymphocytes. Tissue analysis by *in situ* hybridization could also address this question.

3.3.2 Utility in quantifying changes to intestinal lymphocyte density

Clinical trials in IBD are notorious for high levels of placebo response [325] and in the cohort of patients examined in this study, 61% of CCX282-B treated patients and 47% of placebo group had a decrease in CDAI $\geq$ 70 points. High placebo response rates and natural oscillations in disease activity and remission are variations which make CD particularly challenging to conduct well controlled clinical trials in. The technique described in this chapter could be a supplementary measure of treatment efficacy which is less subject to patient and clinician bias and therefore could improve the evaluation of inflammation. Another clinical setting where this analysis could be of utility is the study of agents that inhibit integrins and adhesion molecules. As some of these treatments show clinical efficacy (ie Natalizumab, humanized monoclonal antibody against α_4 is approved for use in the USA)

[326-328]; a quantification of cell density by IHC could further support the mechanism of anti-inflammatory action.

3.3.3 Alternative mechanisms

While the reduction in intestinal cell density following CCX282-B treatment was not statistically significant, it does not discount the possibility that the measured changes could be biologically significant. An analysis conducted by Caballero *et al* (1995) measured the density of several cell populations in the colon of healthy control, active UC and active CD patients [315]. Whilst this is a different segment of the gastrointestinal tract, it does illustrate the degree of differences one might measure during disease activity and quiescence. The mean $CD3^+$ cell density (cells / mm^2 lamina propria) for control, inactive UC and active UC were 918±119, 742±101 and 1166±113 respectively [315]. These data demonstrate the change in $CD3^+$ cell density during active and inactive IBD (~27% decrease between active UC and normal tissue); therefore the 16% reduction measured following CCX282-B treatment, had it been significant, could be biologically and clinically relevant.

In the presented study, there may be alternative explanations for why clinical efficacy did not correlate significantly with changes to intestinal T cells. One possibility is that clinical efficacy was not the result of inhibiting all cell recruitment, but rather the effect of rebalancing the populations of cells which entered the inflamed small intestine. It's conceivable that CCX282-B inhibited the recruitment of $CCR9^+$ Th1 effector cells while the recruitment of regulatory T cells (via CCR6 for example) was unabated; this would not have been captured by the present study but could be explored by the analysis of FoxP3 expression relative to CD3 cells.

Another possibility is that CCL25 influences cytokine production by $CCR9^+$ T cells and antagonising CCR9 inhibits this induction. Recently, Nakamoto *et al* (2012) showed that

CCL25 induced TNF-α and IL-6 production by activated $CCR9^+$ murine macrophages [46]. At the time of this thesis, the effect of CCL25 on T cell cytokine production was not described. In chapter 4 of this thesis, the effects of CCL25 on human $CCR9^+$ T cell cytokine secretion are investigated.

3.3.4 Limitations of this study

CD8 is a marker of T cells and NK T cells

In my analysis I used the CD8 marker as a measure of cytotoxic T cells, however a population of NK T cells also express CD8 [329]. The immunoenzymatic technique for staining antigens, as compared to the immunofluorescence technique, has the advantage of visualizing tissue architecture but has the disadvantage of being difficult to accurately measure single versus double stained cells. Consequence, in this analysis I had to assume that all CD8 expressing cells were also $CD3^+$, although I know this to be an overestimate.

Alternative analysis of the data

In the present analysis of T cell density following treatment, some patients received multiple biopsies at a single time point and all patients analyzed had at least one sample at Baseline and End of Induction. Due to the inexact nature of collecting biopsies, it was assumed that samples could not be matched between donors and all biopsies were therefore an independent data point. However it is likely that differences between individuals exist in the starting density of intestinal cells, and therefore a paired analysis would be an alternative and possibly more powerful way of assessing changes. Under these conditions, the size of the current data set would shrink to 12 placebo treated patients and 9 CCX282-B treated patients.

3.3.5 Future experiments in this thesis

The analyses presented in this chapter stimulated new questions regarding human CCR9. In particular, the following questions will be addressed in subsequent chapters of this thesis:

1) [Chapter 4] The effect of CCL25 on CCR9 surface expression. As a means of elucidating why CCR9 staining in the tonsil was strong and membrane-associated, while staining in tissues where CCL25 is abundant (small intestine and thymus) displayed punctate, cytoplasm-associated staining.
2) [Chapter 4] The effect of CCL25 on $CCR9^{+}$ T cell cytokine production. A potential alternative mechanism by which antagonizing CCR9 could modulate inflammation.
3) [Chapter 5] The effect of corticosteroids on CCR9 expression and function. A significant proportion (~50%) of patients enrolled in PROTECT-1 were on concomitant corticosteroid treatment, the effect of which is unknown on CCR9.
4) [Chapter 6] Quantification of changes to intestinal T cell density following induction of intestinal inflammation in coeliac disease (following dietary gluten). CD is a complex, multifactorial disease with natural oscillations in disease activity; coeliac disease is comparably homogeneous, with a known immunogen and significant but reversible changes to intestinal cell recruitment following gluten consumption. To assess the role of CCR9 in human intestinal inflammation, I measure the effect of CCX282-B on T cell recruitment to the duodenum following 12 weeks of gluten consumption in patients with coeliac disease.

CHAPTER 4: Analysis of CCR9 signalling in human T cells and CCL25 mRNA expression from intestinal biopsies

4.1 Introduction

4.1.1 All *trans* retinoic acid induces CCR9 expression on T cells

Prior to the discovery in 2004 that all *trans* retinoic acid, a metabolite of vitamin A, induced the expression of CCR9 in T cells [66], the study of CCR9 function was mainly restricted to CCR9 transfected cells lines and the Molt-4 tumor cell line. To a lesser degree, primary human thymocytes and lamina propria lymphocytes were also studied [70,71,73,88]. The use of ATRA *in vitro* has enabled the study of CCR9 function on primary derived cells. Indeed Walters *et al* (2010) used human ATRA-cultured cells to quantify the potency of CCR9-selective small molecule antagonists, measuring CCL25 mediated cell migration [87]. Iwata *et al* (2004) demonstrated that *in vitro* derived murine ATRA-cultured cells preferentially home to the murine small intestine *in vivo* [66].

Collectively these experiments demonstrate that *in vitro* generated ATRA-cultured cells respond to CCL25 both *in vitro* and *in vivo,* yet a thorough characterization of these cells has not been described and would increase their value as a tool for studying CCR9 function on human T cells. In this chapter I characterize the effector phenotype and functional responses by human ATRA-cultured cells in response to CCL25: chemokine-mediated cell migration, intracellular calcium flux, chemokine receptor internalization and cytokine production. As these cells were to be the basis of future work in this thesis, these were critical experiments for informing the design of subsequent assays.

4.1.2 Chemokine receptor internalization

The process of homeostatic and ligand induced chemokine receptor internalization is described for some but not all of the 48 chemokine receptors and is speculated to act as a mechanism for modulating cell sensitivity to ligand. This process also underlies the phenomenon of homologous G-protein coupled receptor desensitization [330]. In primary human Th2 cells, Mariana *et al* (2004) reported CCR4 internalization with increasing concentrations of CCR4 ligand, CCL22 [331]. Meiser *et al* (2008) demonstrated in primary T cells and CXCR3-transfectants that CXCR3 surface internalization is dose and time dependent, showing complete receptor internalization following 100 nM CXCL11 incubated for 60 minutes [332]. Human CCL25-mediated, CCR9 internalization is not described in the published literature but could explain the punctate pattern of expression observed in human tissues where CCL25 is abundantly expressed (see section 3.2.1). In this chapter I study the effect of CCL25 on surface CCR9, measuring expression by flow cytometry and IHC analysis.

4.1.3 Calcium flux

Intracellular calcium flux is a rapid and transient response to chemokine stimulation, commonly used to measure chemokine receptor activation [333]. While calcium flux can be readily monitored in transfected cell lines and tumor cell lines that constitutively express the receptor of interest, measuring activity from a heterogeneous population of cells has proven challenging. Indeed, CCR9-mediated calcium flux in response to CCL25 has not been demonstrated in ATRA-cultured $CCR9^+$ T cells owing to the low frequency of receptor expressing cells; in unpublished data discussed among colleagues it was believed ATRA-cultured cells did not respond to CCL25 by intracellular calcium flux, a potential indication that cells were an inferior tool for studying CCR9 function. In this chapter I use a sensitive technique for measuring calcium flux in single cells to demonstrate that $CCR9^+$ ATRA-

cultured cells calcium flux in response to CCL25, expanding their use experimentally as a source of primary derived $CCR9^+$ cells.

4.1.4 Cytokine secretion stimulated by integrins and chemokines

Chemokines are best characterized for their chemotactic effect on responding cells, however for some chemokines additional functions have been identified including the ability to promote cell survival, cell proliferation, and T cell polarization [334-336]. In $CD3^+$ T cells, Karpus *et al* (1997) used ovalbumin (OVA)-specific TCR transgenic mice to demonstrate the differential effect of two chemokines in polarizing cytokine production towards Th1 or Th2 cytokines. $CD3^+$ cells stimulated *in vitro* with OVA (to activate the TCR) in the presence of CCL3 (MIP-1α) had enhanced IFN-γ production. In contrast, $CD3^+$ cells stimulated with OVA and CCL2 (MCP-1) had enhanced IL-4 production [335].

Recently, Nakamoto *et al* (2012) reported that CCL25 administered *in vitro* to $CCR9^+$ murine macrophages or $CCR9^+$ pDCs promoted cytokine production. In response to CCL25 (35.7 nM CCL25), activated macrophages produced TNF-α (~300 pg/ml) and IL-6 (~200 pg/ml) while resting pDCs were stimulated to produce IL-10 (~20 pg/ml) [46]. The effect of CCL25 on human $CCR9^+$ T cell cytokine production have not been described in the published literature and are studied in this chapter.

4.1.5 Characterization of CCL25 expression during intestinal inflammation

The most thorough characterization of CCL25 expression during intestinal inflammation is described for murine models of IBD. In the $TNF^{\Delta ARE}$ model of spontaneous ileitis, and the SAMP1/YitFc model of intestinal inflammation, CCL25 expression is significantly elevated during active disease [102,104]. In humans however, characterization of CCL25 production during intestinal inflammation is limited. Indeed only one report by Papadakis *et al* (2001) has reported an "altered expression" of CCL25 at sites of intestinal inflammation, measured

by qualitative analysis of IHC staining in human intestinal tissue [72]. In this chapter I show that a single intestinal biopsy can yield enough RNA to allow qRT-PCR; using this technique I studied the expression of CCL25 along the gastrointestinal tract, comparing un-inflamed and inflamed tissue from the small and large intestine to address the question of whether CCL25 expression is modulated during intestinal inflammation.

4.1.6 Aims of this chapter

The experiments in this chapter were influenced by the observations made in Chapter 3 while studying CCR9 expression by IHC and measuring the effect of CCR9 antagonist treatment on T cells in the intestine. CCR9 staining by IHC appeared granular and localized to the cell cytoplasm in tissues where cognate ligand, CCL25 is abundant, leading me to speculate that ligand induced CCR9-internalization could account for the pattern of staining. Furthermore, having found in the previous chapter that clinical efficacy following CCX282-B treatment did not correlate with changes to T cell density in the intestine, I was interested to investigate alternative mechanisms by which antagonizing CCR9 could suppress inflammation. Finally, to expand upon the limited characterization of CCL25 expression during intestinal inflammation, I measured CCL25 mRNA, comparing relative levels of expression between the small and large intestine in the presence and absence of inflammation. The results in this chapter will include the following:

- Characterization of cells used to study CCR9 cell function.
- Development of flow cytometry based calcium flux assay.
- Assessment of CCL25-mediated CCR9 internalization by flow cytometry and IHC.
- Assessment of cytokines produced by $CCR9^+$ cells under various stimulation conditions.
- Investigation of the effect of CCL25 on $CCR9^+$ T cell cytokine production.

- Validation of qRT-PCR analysis of human intestinal biopsies.
- Assessment of CCL25 mRNA expression along the gastrointestinal tract in the presence and absence of inflammation.

4.2 Results

4.2.1 Characterization of human ATRA-cultured T cells used in this thesis

As previously described, activating T cells in the presence of IL-2 and ATRA increases the proportion of $CCR9^+$ T cells from a baseline of approximately 2 - 5% to 25 - 70% of the total population, measured by flow cytometry (Figure 4.1) [171]. ATRA-cultured cells were predominantly $CD3^+$ (> 90%) and a mixture of $CD4^+$ and $CD8^+$ T cells, the majority of which were single positive (Figure 4.2A). In ATRA-cultured cells, the proportion of CD4 to CD8 T cells was roughly equivalent (Figure 4.2A). As anticipated from the culture conditions, ATRA-cultured cells expressed surface markers indicating an activated phenotype: $CD25^+$, $CD45RO^+$, $CD69^+$ (Figure 4.2B); this is in accordance with characterization of primary peripheral blood $CD4^+$ $CCR9^+$ T cells and primary $CCR9^+$ LPLs which are reported to be almost exclusively $CD45RO^+$ (68% and >89% respectively) and high for CD69 and CD25 expression compared to equivalent $CCR9^-$ cells [75,90].

In addition to CCR9, ATRA-cultured cells uniformly expressed CXCR3 and CXCR4 (Figure 4.3). A minority population ATRA-cultured cells expressed CCR5 and CCR6 and cells were uniformly negative for CCR10 and CX_3CR_1 (Figure 4.3). Integrin-$\alpha_4\beta_7$ is co-expressed by CCR9 expressing cells [66,82], however at the time of this thesis, antibodies specific to human $\alpha_4\beta_7$ were not available for commercial laboratory use; ATRA-cultured cell were uniformly β_7^+ (Figure 4.3).

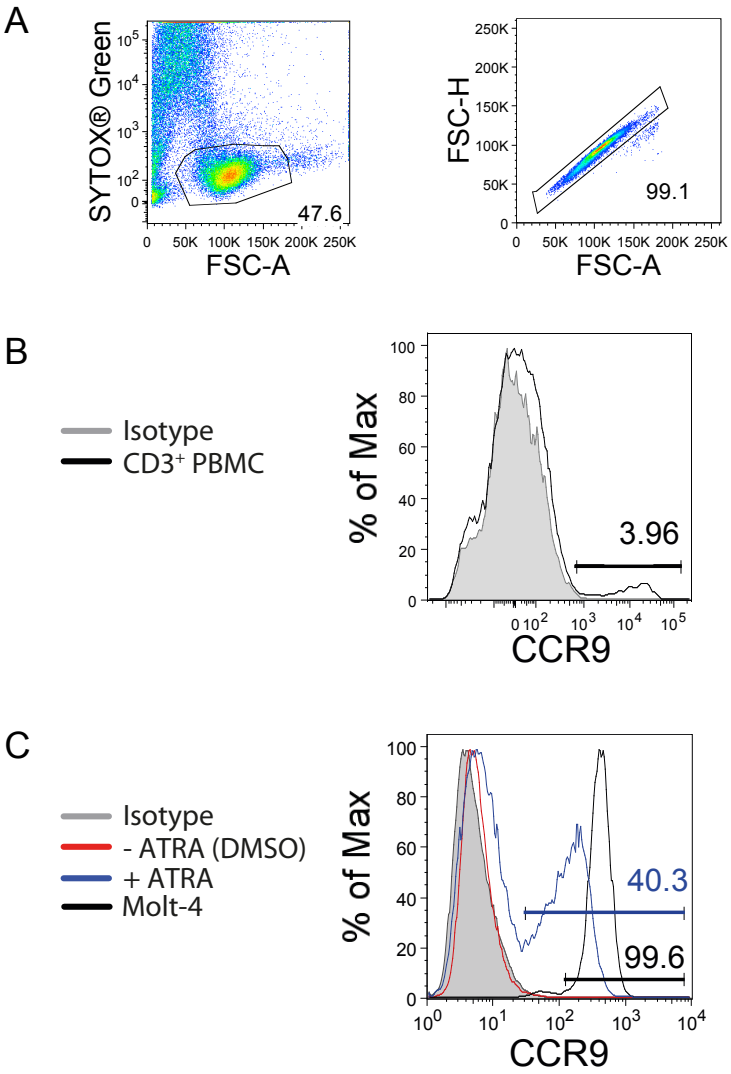


Figure 4.1 All *trans* retinoic acid (ATRA) induces CCR9 surface expression in human T cells.

$CD14^-$ PBMCs were cultured on plate bound anti-CD3 and anti-CD28 with IL-2 and ATRA for three days. On day 4, cells were removed from CD3/CD28 stimulation and cultured with IL-2 and ATRA. On day 7 post initial isolation, cells were stained for surface receptor expression and analyzed by flow cytometry. In FlowJo analysis software, cells were gated to exclude non-viable cells and cell doublets.

A: Gating in FlowJo software: live cells (SYTOX® $Green^-$), excluding cell doublets.

B: Primary human $CD3^+$ PBMC. The number depicts the proportion of $CCR9^+$ cells.

C: Representative histogram illustrating the proportion of $CCR9^+$ cells comparing Molt-4 cells (black) and primary lymphocytes cultured in the presence of ATRA (blue) or absence of ATRA (red).

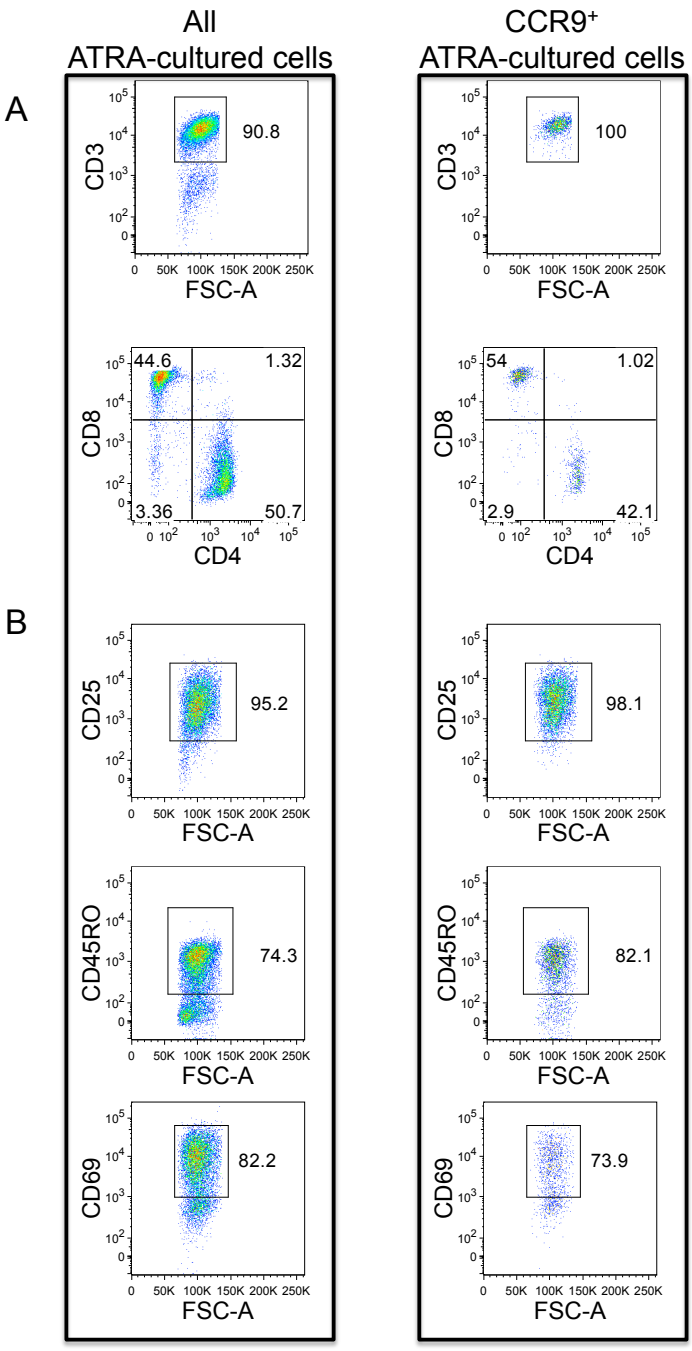


Figure 4.2 Characterization of ATRA-cultured cells used in this thesis.
ATRA-cultured cells were stained for surface receptor expression and analyzed by flow cytometry. In FlowJo analysis software, cells were gated to exclude non-viable cells and cell doublets. Gates set against isotype or unstained control. The number depicts the percentage of cells expressing the marker of interest in the selected population.
A: Representative T cell characterization of ATRA-cultured cells comparing the total cell population (left side) and CCR9$^+$ cells (right side).
B: Representative phenotyping for activation markers on ATRA-cultured cells comparing the total cell population (left side) and CCR9$^+$ cells (right side).
Graphs representative of three independent experiments.

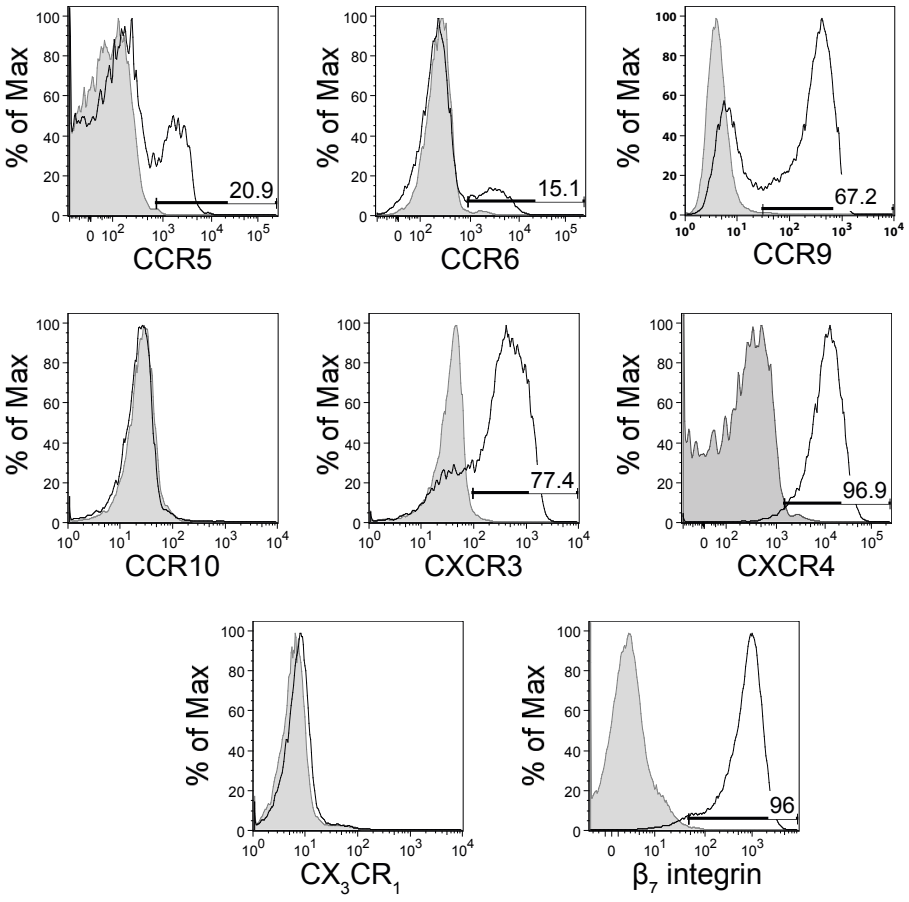


Figure 4.3 Chemokine receptor expression by ATRA-cultured cells.
ATRA-cultured cells were analyzed for chemokine surface receptor expression by flow cytometry. In FlowJo software, cells were gated on live cells, excluding cell doublets. Data shows isotype control (gray filled) and chemokine receptor (black line) expression. The number depicts the percentage of chemokine receptor expressing cells. Graphs representative of three independent cell preparations.

4.2.2 Chemokine-mediated migration by ATRA-cultured cells

To test if surface chemokine receptors expressed by ATRA-cultured cells could mediate directed cell migration, cell migration to increasing concentrations of chemokine were quantified using Transwell® chemotaxis inserts that separate cells (loaded in the top chamber) from chemokine (bottom chamber) by a porous membrane (see Section 2.6). CCL25 stimulated ATRA-cultured cell migration, giving the characteristic bell-shaped dose-response curve, with peak migration observed between 350 - 450 nM CCL25 (Figure 4.4A). This is in accordance with the data from Walters *et al* (2010) who used similar cells to test the effects of CCR9-antagonists on CCR9-mediated chemotaxis [87]. This is also in accordance with data from human LPLs which are reported to have peak migration with 250 - 500 nM CCL25 [70,71]. As a control, PBLs were cultured with an equivalent concentration of DMSO, the vehicle for ATRA. PBLs activated and expanded in the presence of DMSO did not express surface CCR9 (see Figure 4.1C) and did not migrate to CCL25 (Figure 4.4B). However, migration to CXCL12 (via CXCR4) was equivalent between ATRA- and DMSO-cultured cells, demonstrating that the cells were capable of chemokine mediated migration (Figure 4.4B).

ATRA-cultured cells uniformly express CXCR3 that has three identified signalling ligands: CXCL9, CXCL10, CXCL11. By measures of directed cell migration, calcium mobilization and ligand induced internalization, CXCL11 is the most potent of the three ligands [239,332,337]. Increasing concentrations of CXCL11 induced ATRA-cell Transwell® chemotaxis with peak migration measured with 100 nM CXCL11 (Figure 4.5A). CXCL12 is the single chemokine ligand for CXCR4, inducing peak migration of ATRA-cultured cells at 50 nM CXCL12 (Figure 4.5B). Although a proportion of ATRA-cultured cells expressed surface CCR5, migration to CCL5 was not observed (Figure 4.5C).

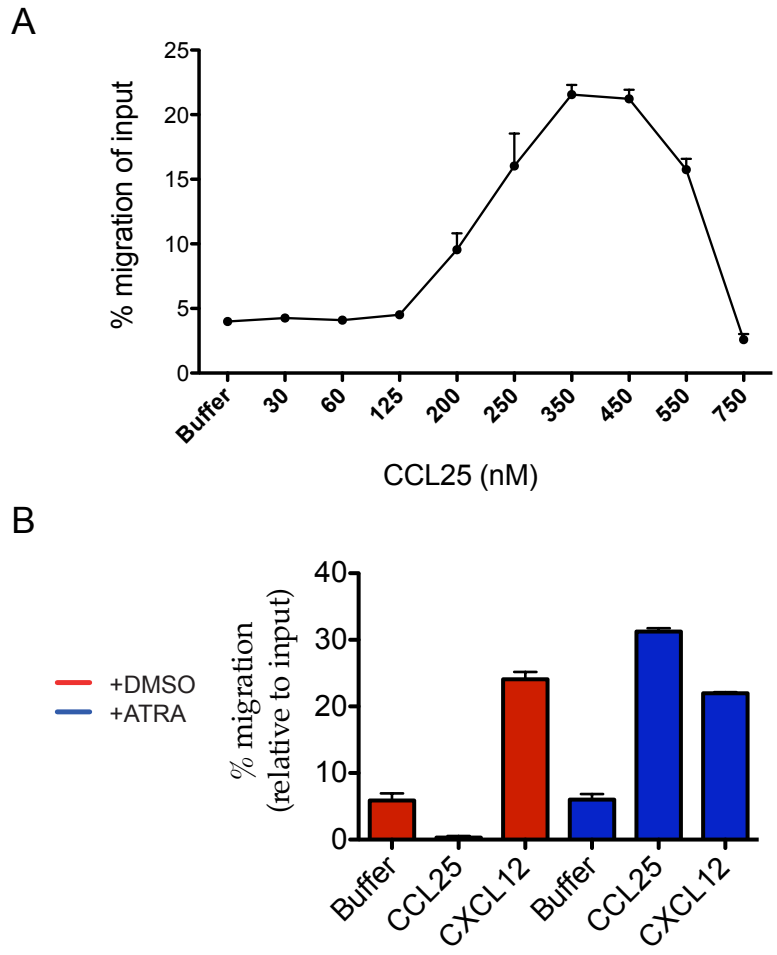


Figure 4.4 CCL25 stimulates a dose-dependent increase in ATRA-cultured cell chemotaxis.
ATRA-cultured cell migration to CCL25 was measured using 96-well, Transwell® chemotaxis inserts which separate cells (top chamber) from buffer or chemokine (bottom chamber). ATRA-cultured cells were allowed to migrate to CCL25 in the bottom chamber for 2 hours while incubated at 37°C. The migrated cell in the bottom chamber were quantified by CellTiter-Glo® and verified by Trypan Blue Stain. The number of migrated cells were quantified relative to the total live input cell number.
A: ATRA-cultured cell migration.
B: ATRA-cultured cell migration to buffer, 250 nM CCL25 or 10 nM CXCL12.
Graphs show mean values ± standard error of the mean (SEM) of three technical replicates. Graphs representative of n≥3 independent experiments.

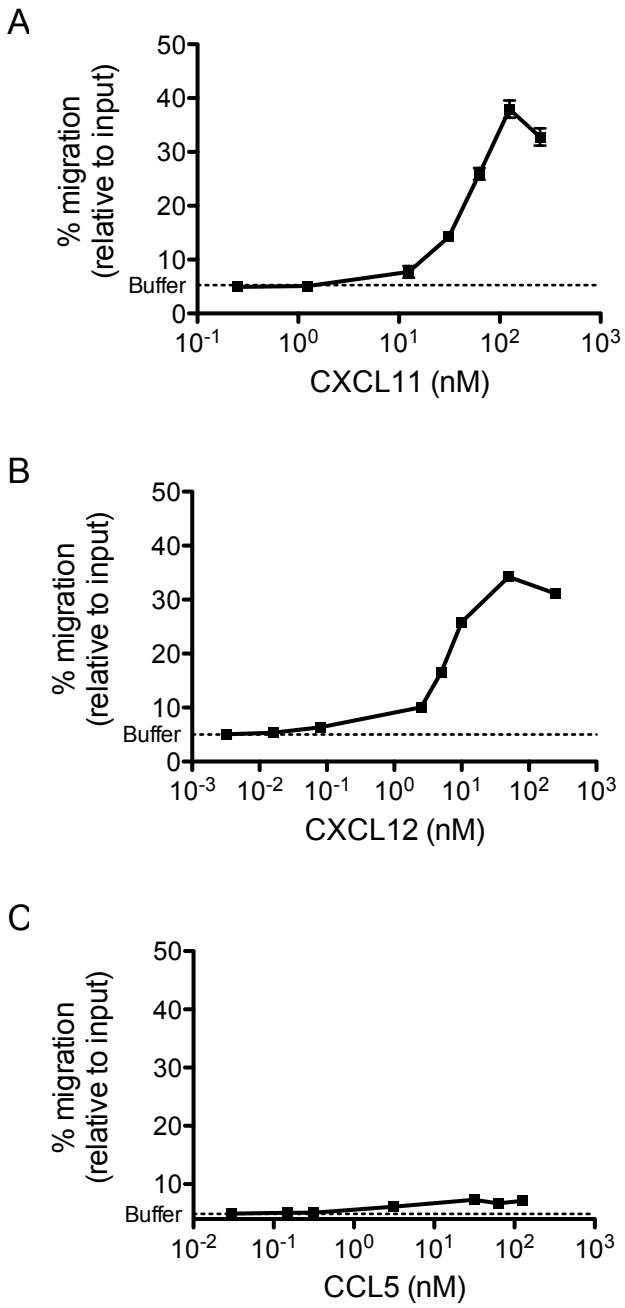


Figure 4.5 ATRA-cultured cells migrate to increasing concentrations of CXCL11 and CXCL12 and do not migrate to CCL5.

ATRA-cultured cells were assessed for chemokine mediated cell migration. Cell migration was measured using 96-well, Transwell® chemotaxis inserts. ATRA-cultured cells were allowed to migrate to chemokine in the bottom chamber for 2 hours while incubated at 37°C. The migrated cell in the bottom chamber were quantified by CellTiter-Glo® and verified by Trypan Blue Stain. The number of migrated cells was quantified relative to the total live input cell number.

A: Chemotaxis to CXCL11 (via CXCR3).

B: Chemotaxis to CXCL12 (via CXCR4).

C: Chemotaxis to CCL5 (via CCR5).

Graphs show mean values ± SEM from triplicate wells. Graphs representative of n≥2 independent experiments.

4.2.3 Characterizing chemokine receptor expression by Molt-4 cells

In common with ATRA-cultured cells, Molt-4 cells express surface CXCR4 (Figure 4.6) [69]. In contrast to ATRA-cultured cells, Molt-4 cells do not express surface CXCR3 nor integrin-β_7. Molt-4 cells are also negative for CCR5, CCR6, CCR7, and CCR10 surface expression (Figure 4.6)

4.2.4 Surface CCR9 internalization with CCL25 treatment

Chemokine receptor internalization following interaction with cognate ligand is described for some chemokine receptors including CCR5 and CXCR3, however no such description is published for human CCR9. To examine the effect of CCL25 on CCR9 surface expression, ATRA-cultured cells were treated with increasing concentrations of CCL25 at 37°C, washed and analyzed for surface CCR9 by flow cytometry. As a negative control, cells were treated with CXCL12 (250 nM) which interacts with co-expressed CXCR4 but does not signal through CCR9. Increasing concentrations of CCL25 between 4 – 250 nM, reduced the proportion of $CCR9^+$ cells and CCR9 MFI, proportional to the amount of surface receptor (Figure 4.7). CCR9 internalization was specific to CCL25 as cells treated with CXCL12 displayed equivalent CCR9 surface staining to untreated cells (Figure 4.7B). Cells treated with CCL25 at 37°C had undetectable levels of surface CCR9; the same treatment conducted at 4°C had a modest reduction in CCR9 MFI (Figure 4.7C), demonstrating that CCL25 stimulated CCR9 internalization was an active process, and bound CCL25 minimally inhibited CCR9 antibody binding.

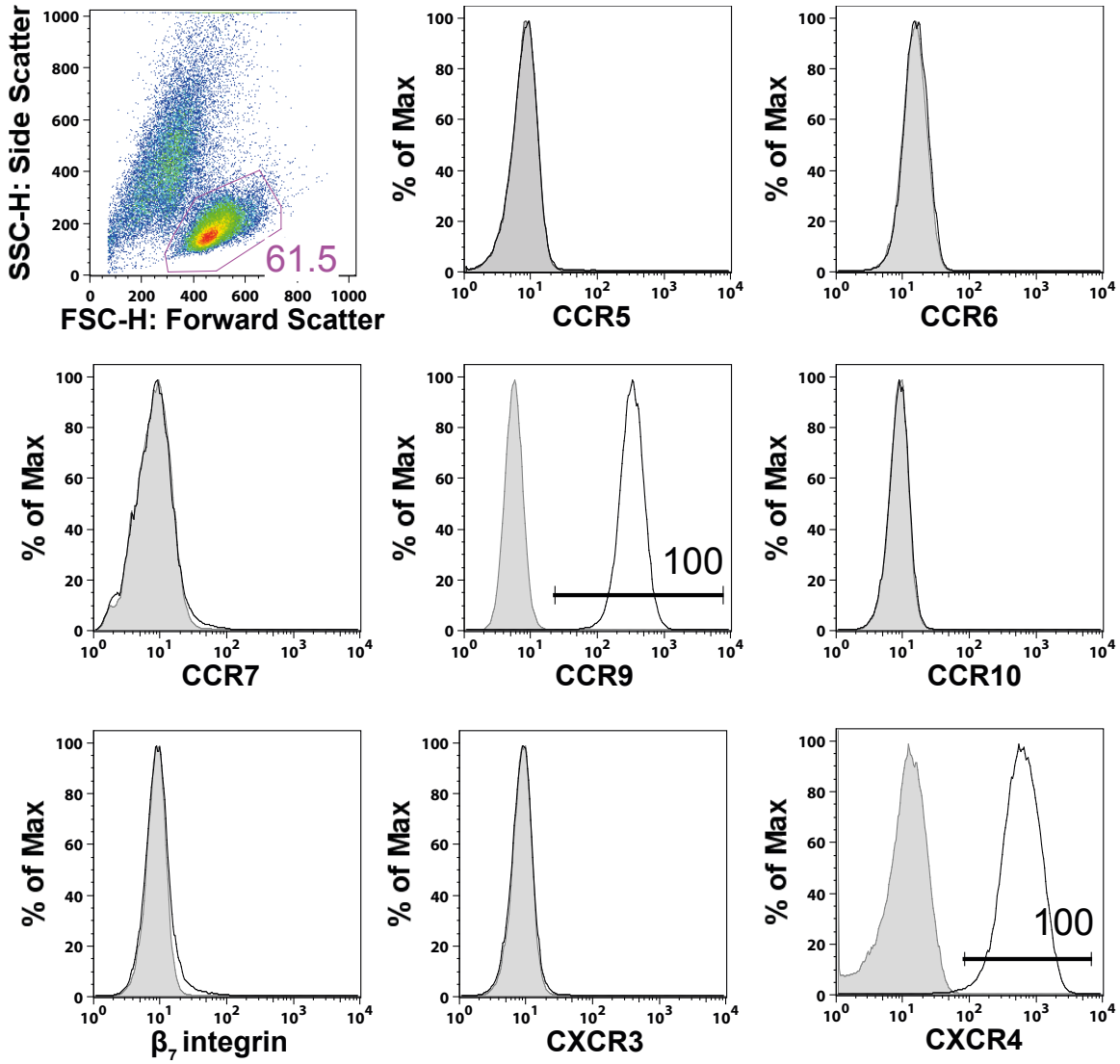


Figure 4.6 Chemokine receptor expression by Molt-4 cells.
Molt-4 cells are a human lymphoblastic leukemia cell line. Cells were stained for surface chemokine receptor expression and analyzed by flow cytometry. Cells were gated on lymphocytes based upon the forward and side scatter plot. Histograms show isotype control (gray fill) and chemokine receptor expression (black line). The number depicts the proportion of cells expressing the marker of interest. Data representative of three independent experiments.

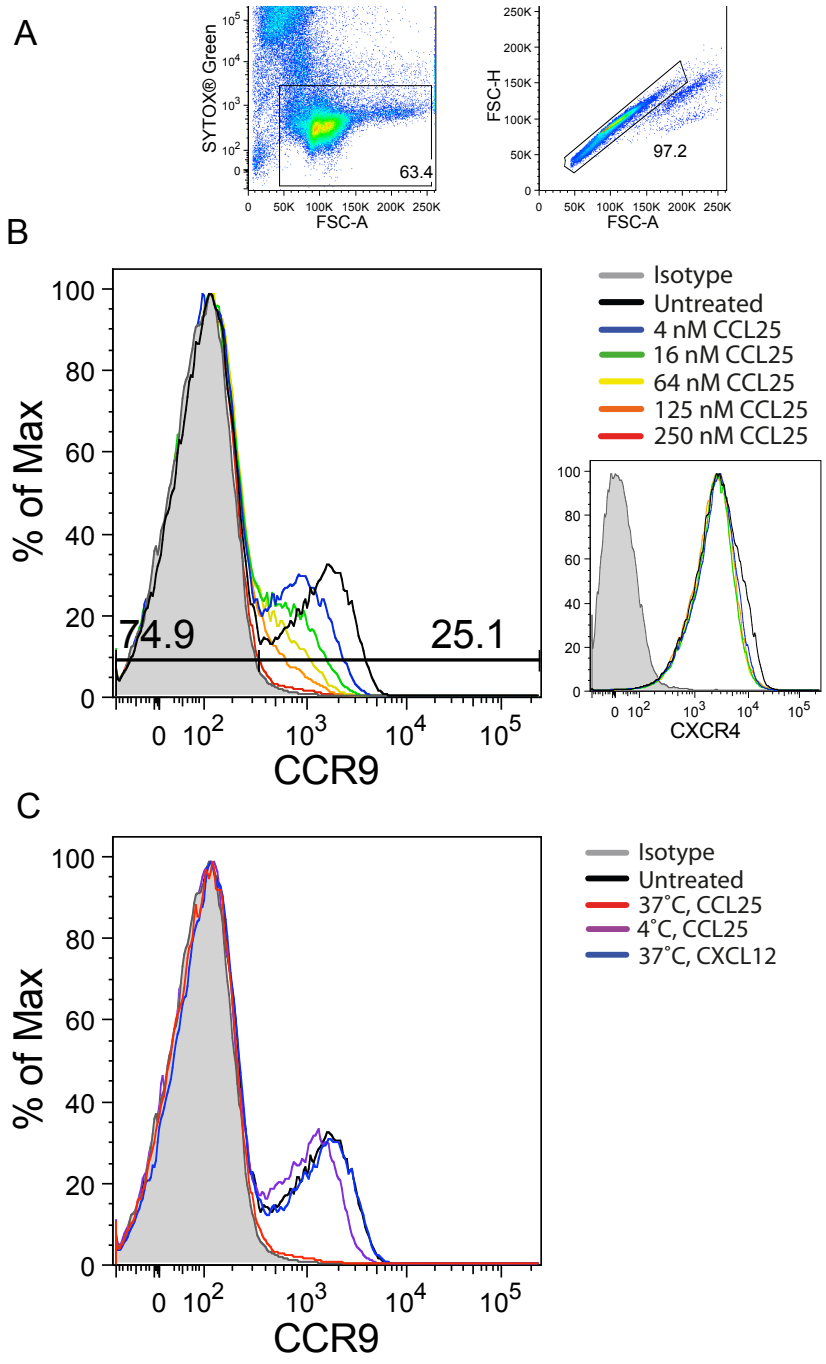


Figure 4.7 Surface CCR9 is internalized upon treatment with CCL25 in a dose dependent manner.

ATRA-cultured cells were incubated with chemokine for 60 minutes at 37°C (unless stated otherwise). Cells were immediately washed 3X in D-PBS with 0.1% BSA and 0.01% sodium azide. Cells were stained for surface CCR9, CXCR4 and live/dead marker SYTOX® Green and analyzed by flow cytometry.

A: Gating in FlowJo software: live cells (SYTOX® Green$^-$), excluding cell doublets.

B: ATRA-cultured cells treated with increasing concentrations of CCL25 at 37°C.

C: ATRA-cultured cells treated with 250 nM CCL25 or 250 nM CXCL12 at the indicated temperature.

Data representative of three independent experiments.

internalization time course measured by flow cytometry

To characterize the kinetics of CCR9 internalization, ATRA-cultured cells were treated with 250 nM CCL25 (concentration which induced complete CCR9 internalization) and surface CCR9 analyzed by flow cytometry over 30 minutes. CCL25-mediated internalization was time dependent, with a modest decrease in CCR9 MFI after 1 minute, and complete CCR9 internalization after 30 minutes (Figure 4.8). This time course is in accordance with work on CCR4 by Mariani *et al* (2004), which showed complete receptor internalization 30 minutes after treatment with CCR4 ligand, CCL22 [331].

internalization measured by IHC on cell cytospins

CCR9 internalization was visualized by IHC on two different cell types, staining cell prepared as cytospins (see Section 2.4.3). In Molt-4 cells, two hour treatment with CCL25 completely diminished surface CCR9, with staining similar to that of isotype control (Figure 4.9A, B & D). Surface CCR9 was unaffected by incubation with CXCL12, supporting the previous observation by flow cytometry that CCR9 internalization is CCL25 specific (Figure 4.9C).

CCR9 internalization was also observed in ATRA-cultured cell cytospins (Figure 4.9E - H). Treatment with 500 nM CCL25 showed CCR9 staining comparable to isotype control while cells treated with 500 nM CXCL12 displayed CCR9 staining comparable to untreated cells (Figure 4.9E - H). Collectively these results demonstrate that surface CCR9, similar to other chemokine receptors, is internalized following interaction with its cognate ligand which affects the staining of surface CCR9 visualized by flow cytometry and IHC and could explain the punctate CCR9 staining observed in primary tissue where CCL25 is abundant.

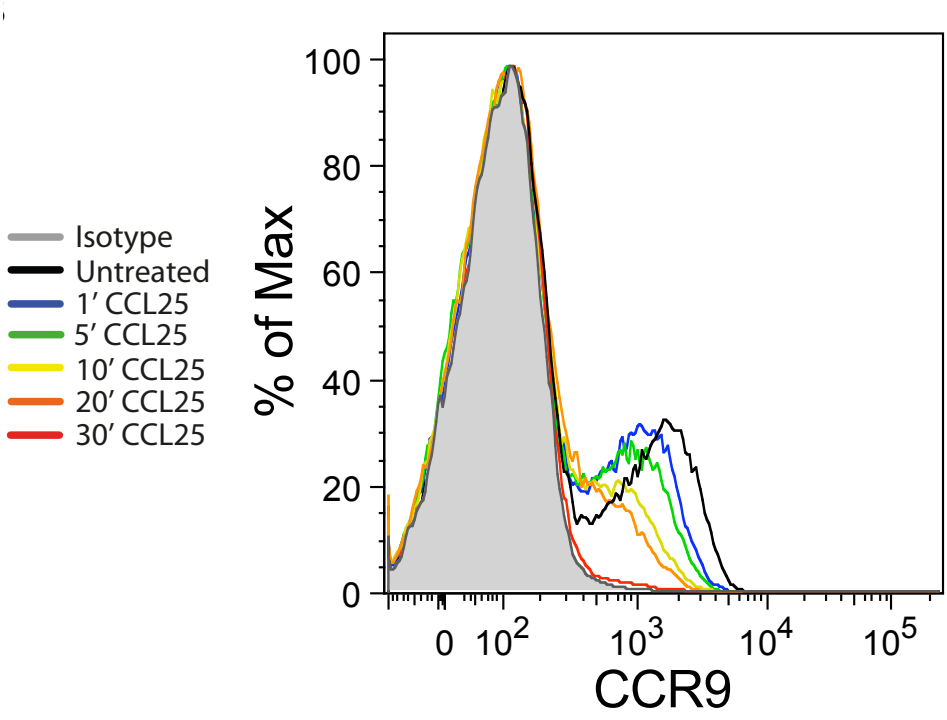


Figure 4.8 CCL25-mediated CCR9 internalization is time dependent.
ATRA cells were incubated with 250 nM CCL25 for the indicated amount of time at 37°C and washed 3X at 4°C in D-PBS with 0.1% BSA and 0.01% sodium azide. Cells were stained for surface CCR9 and live/dead marker SYTOX® Green and analyzed by flow cytometry. Non-viable cells and cell doublets were excluded in FlowJo analysis. Data representative of two independent experiments.

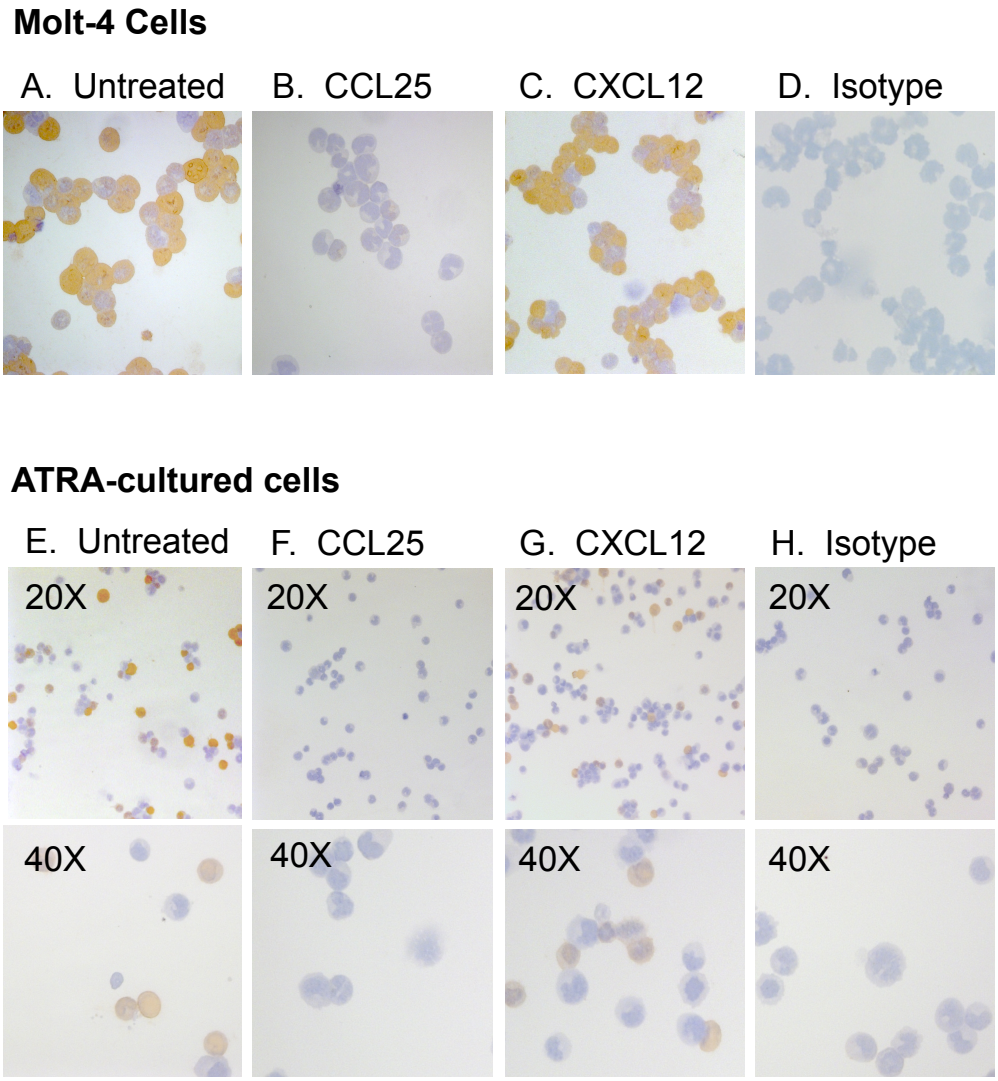


Figure 4.9 CCR9 internalization on Molt-4 and ATRA-cultured cells visualized by IHC on cell cytospins.

Cells were treated with 500 nM CCL25 or 500 nM CXCL12 for 2 hours at 37°C. Cells were washed 3X in 4°C D-PBS supplemented with 10% FCS and 0.1% sodium azide and immediately centrifuged as cell cytospins onto pre-coated slides. Cell cytospins were stained with anti-CCR9 or isotype control followed by HRP-conjugated anti-mouse secondary antibody. CCR9 was visualized with DAB substrate (brown) and cells were counterstained with haematoxylin (blue) to visualize the cell nuclei.

A-D: Molt-4 cells ± CCL25 or CXCL12.

E-H: ATRA-cultured cells ± CCL25 or CXCL12.

4.2.1 CCL25-mediated calcium flux in ATRA-cultured cells

To test for additional functional coupling of CCR9 in ATRA-cultured cells, I followed calcium mobilization, measured by flow cytometry. CCL25 is demonstrated to stimulate intracellular calcium flux in stably transfected CCR9 HEK/293 cells, MOLT-4 cells, primary isolated intestinal T cells and human thymocytes but is not demonstrated in ATRA-cultured cells [69,73,88]. To study this, a technique for monitoring calcium flux in single cells was necessary. By flow cytometry and data acquisition with an LSR II (18 channel capacity) a sufficient number of channels were available to stain cells with calcium specific dye, a live/dead cell marker (SYTOX® Green) and CCR9 specific antibody (Figure 4.10A). Dye and antibodies were titrated to determine the optimal concentrations for this assay.

Indeed, $CCR9^+$ and not $CCR9^-$ cells calcium fluxed in response to 125 nM CCL25 (Figure 4.10B). Analysis of the entire population ($CCR9^+$ and $CCR9^-$) demonstrated a modest calcium response that could account for the previous and inaccurate observation, that ATRA-cultured cells do not response to CCL25 by calcium flux. In accordance with the observation that all ATRA-cultured cells express surface CXCR4 (see Figure 4.3), both $CCR9^+$ and $CCR9^-$ cells mobilized calcium in response to CXCL12 (Figure 4.10C). As a positive control, to demonstrate that cells were loaded with the calcium dye and a calcium response could be measured, ionomycin stimulation was assessed (Figure 4.10D).

CCL25-mediated calcium flux by $CCR9^+$ ATRA-cultured cells was dose dependent, displaying a characteristic bell-shaped dose-response and peak calcium flux with 125 nM CCL25 (Figure 4.11A & B). This is in accordance with characterization of calcium flux in Molt-4 cells and CCR9-transfected 293 cells where optimal calcium flux was measured at concentrations between 60 - 200 nM CCL25 [69,73].

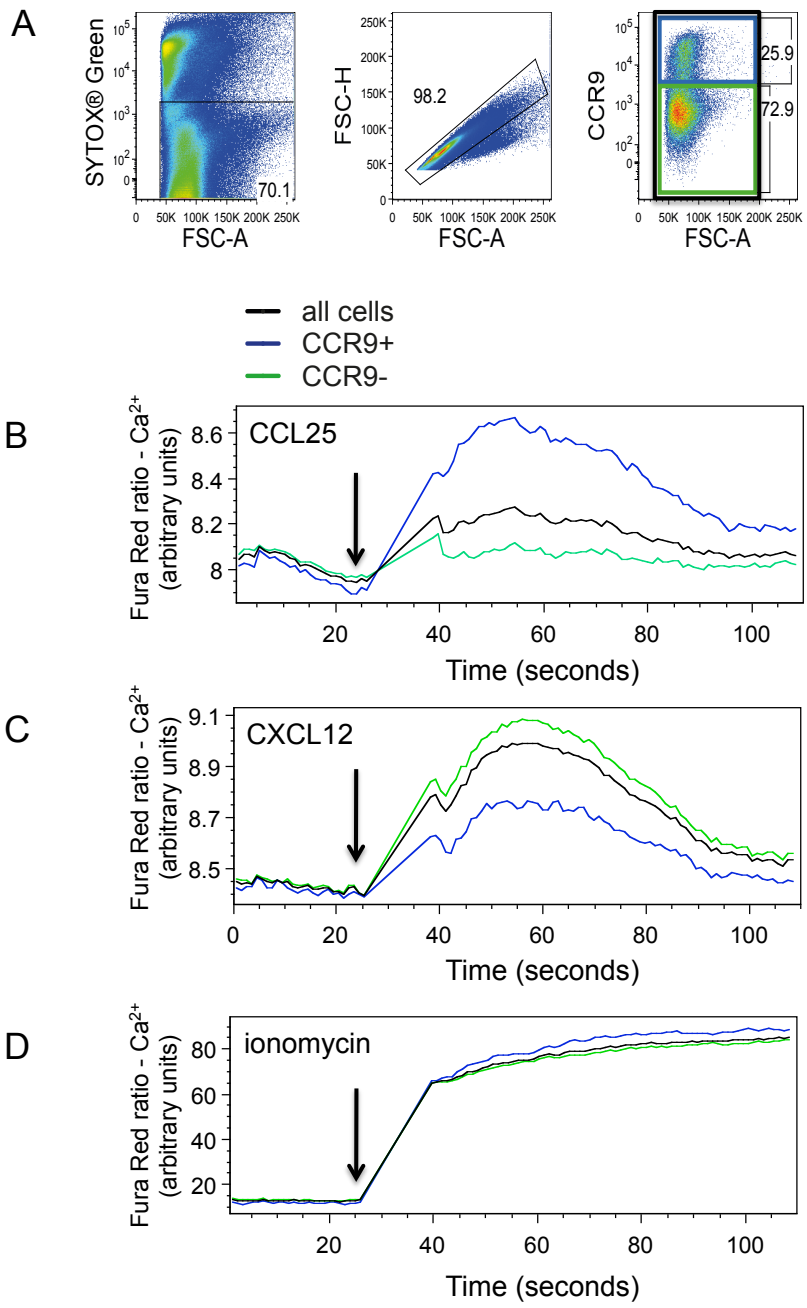


Figure 4.10 CCR9$^+$ ATRA-cultured cells calcium flux in response to CCL25.
ATRA-cultured cells were stained for surface CCR9 followed by anti-mouse secondary conjugated to allophycocyanin (APC). Cells were incubated with Fura Red/AM dye for 30 minutes at 37°C, followed by the addition of lived/dead cell marker, SYTOX® Green. Calcium flux was measured by flow cytometry, measuring Fura Red by ratiometric analysis (QDot655/PE-Cy5.5).
A: Gating in FlowJo analysis: live cells (SYTOX® Green$^-$), excluding cell doublets, CCR9$^+$ or CCR9$^-$.
B: Calcium flux in response to 125 nM CCL25.
C: Calcium flux in response to 10 nM CXCL12.
D: Calcium flux in response to 5 µg/ml ionomycin.
Data representative of five independent experiments.

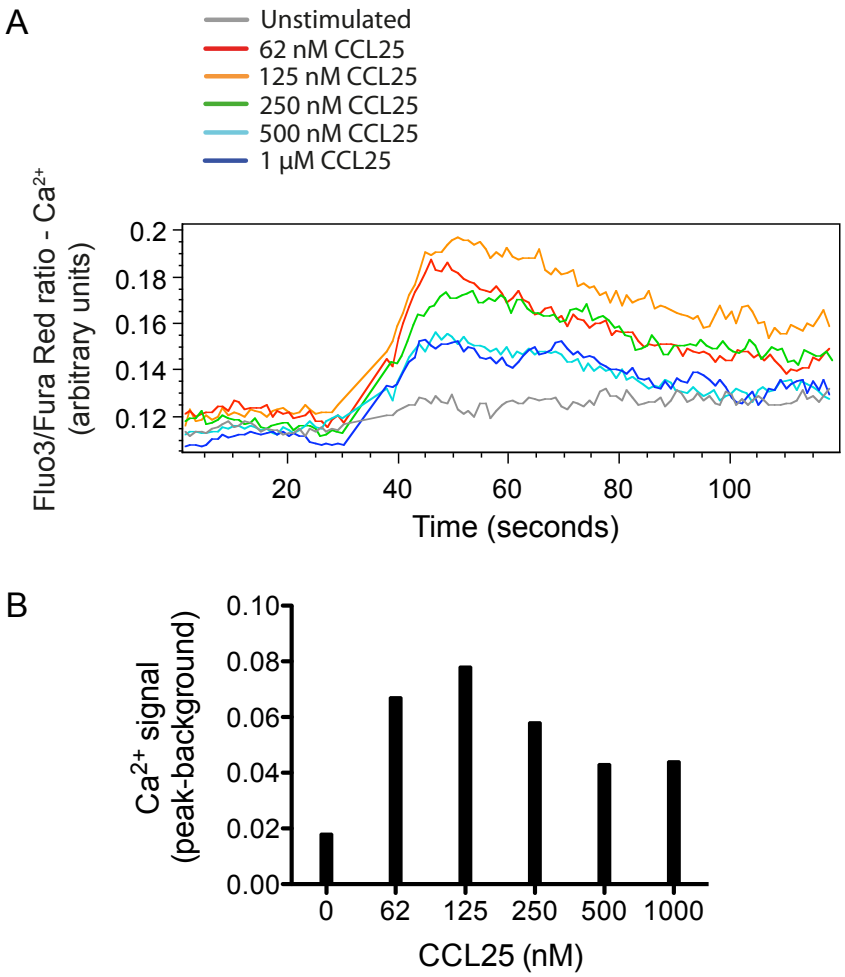


Figure 4.11 CCL25 stimulates a dose-dependent increase in calcium flux in CCR9$^+$ ATRA cultured cells.

ATRA-cultured cells were labeled for surface CCR9 followed by anti-mouse secondary conjugated to allophycocyanin (APC). Cells were incubated with Fluo3 and Fura Red/AM dye for 30 minutes at 37°C, followed by the addition of lived/dead cell marker, SYTOX® Green. Calcium flux was measured by flow cytometry, measuring Fluo3/Fura Red by ratiometric analysis (QDot655/PE-Cy5.5). In FlowJo software, cell were gated to exclude non-viable cells, exclude cell doublets and monitor calcium flux in CCR9$^+$ ATRA-cultured cells.

A: Real time calcium data.

B: Data from A were analyzed as peak signal minus mean background.

Data representative of two independent experiments.

4.2.2 Cytokines produced by ATRA-cultured cells and measured by flow cytometry

To characterize the effector function of ATRA-cultured cells, cytokine production following cell activation was measured. At the time of this thesis, two publications had characterized cytokine production by primary human $CCR9^+$ cells to demonstrate IFN-γ, IL-17A and IL-10 production [75,90]. Therefore these cytokine were included for analysis, along with IL-22 and TNF-α which are elevated in the intestine during active IBD and are produced by subsets of effector T cells [338].

In an initial pilot study I examined cytokine production following 4 hours of PMA/ionomycin stimulation (activation which bypasses the TCR and stimulates robust cell cytokine production[339]), measuring cytokine production by flow cytometry (Figure 4.12). The proportion of IFN-γ producing $CCR9^+$ cells was less than 1.5% of the cell population; 27% of $CCR9^-$ cells produced IFN-γ (Figure 4.12B). TNF-α producing $CCR9^+$ cells comprised 4.8% of the population; $CCR9^-$ TNF-α producing cells were 55% of the population (Figure 4.12C). Less than 2% of all ATRA-cultured cells produced IL-17A (Figure 4.12D). These pilot data showed that a minority population of $CCR9^+$ ATRA-cultured cells produced cytokines following PMA/ionomycin stimulation, consequently quantification of cytokine concentrations in the cell supernatant would largely be the contribution of $CCR9^-$ cells. To more accurately measure cytokine production by $CCR9^+$ ATRA-cultured cells, $CCR9^+$ cells were sorted by magnetic bead separation (see Section 2.10).

$CCR9^+$ ATRA-cultured cells were sorted by magnetic bead separation and added to flat bottom 96-well plates, pre-coated with combinations of recombinant human MAdCAM-1, anti-CD3 and anti-CD28. PMA/ionomycin stimulation was also included as a positive

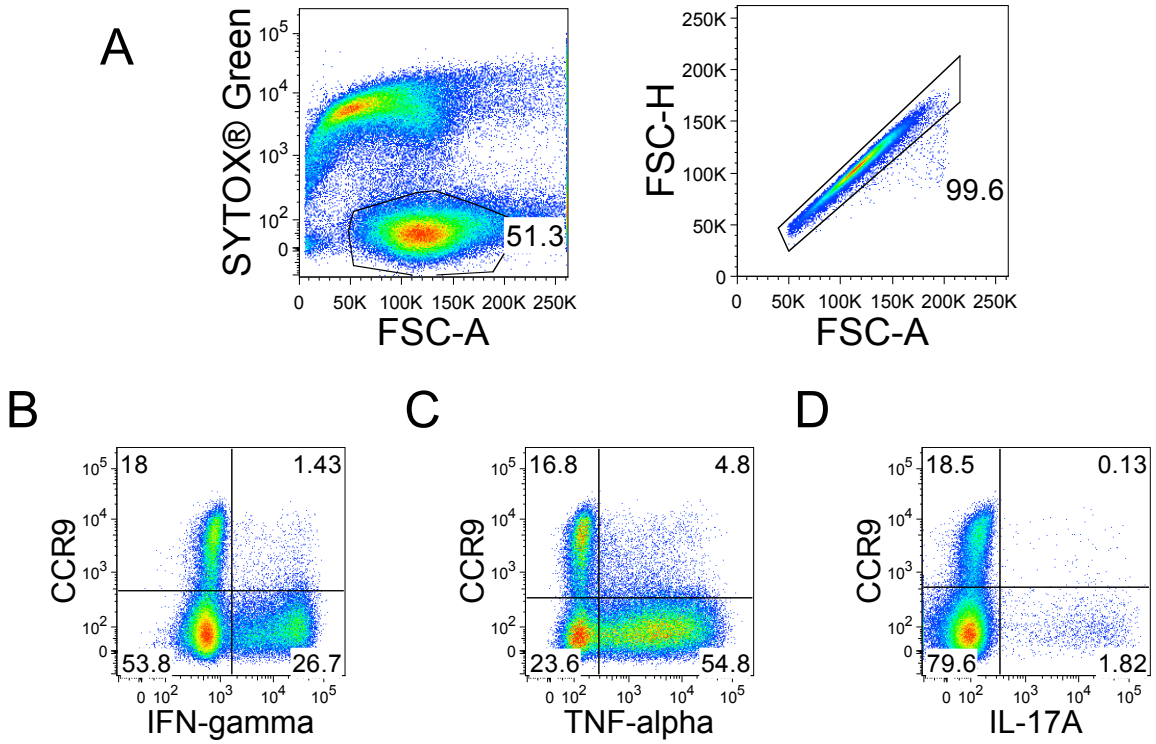


Figure 4.12 Cytokine production by ATRA-cultured cells following PMA/ionomycin activation.

Pilot experiment to measure the proportion of $CCR9^+$ ATRA-cultured cells producing the cytokines of interest. ATRA-cultured cells were stimulated with PMA and ionomycin for 4 hours. Cells were washed and stained for cytokines, measured by flow cytometry.

A: Gating in FlowJo software: live cells (SYTOX® $Green^-$), excluding cell doublets (by FSC-A vs FSC-H).

B: IFN-γ

C: TNF-α

D: IL-17A

Numbers depict the proportion of cells expressing the marker(s) of interest.

control. Following 16 hours of stimulation (4 hours for PMA/ionomycin), cell supernatants were collected and analyzed for cytokine concentration in a flow cytometry based ELISA assay (see Section 2.11).

Following cell sorting, 90 - 95% of the cell population was $CCR9^+$ (Figure 4.13A). Resting $CCR9^+$ T cells (no stimulation) and cells stimulated with MAdCAM-1 alone did not produce any of the measured cytokines. TCR stimulation with co-stimulation (anti-CD3 and anti-CD28) showed a trend towards increasing production of all measured cytokines compared to cells with no stimulation. Strikingly, stimulation with anti-CD3 and anti-CD28 in the presence of MAdCAM-1 significantly increased cytokine production of IFN-γ (4 fold increase, $p<0.01$) and IL-10 (9.8 fold increase, $p<0.05$) compared to no stimulation (Figure 4.13B & E). This stimulation appeared to also increase TNF-α (14 fold increase), IL-17A (2.7 fold increase) and IL-22 (5.4 fold increase), however these data never reached statistical significance (Figure 4.13C - E). For all of the measured cytokines except IL-10, PMA/ionomycin stimulation induced the greatest production of cytokine, significantly increasing IFN-γ (3.8±0.6 ng/ml, $p<0.001$), TNF-α (8.5±1.1 ng/ml, $p<0.001$), IL-17A (1.2±0.3 ng/ml $p<0.01$) and IL-22 (2.2±0.9 ng/ml, $p<0.05$) compared to cells with no stimulation (Figure 4.13B - E).

These data demonstrate two novel observations, the first that $CCR9^+$ cells are capable of secreting TNF-α and IL-22. Secondly, that plate bound MAdCAM-1 in combination with anti-CD3 and anti-CD28 stimulation enhances cytokine production by $CCR9^+$ cells; most notably, production of IL-10 was greatest following MAdCAM-1/CD3/CD28 stimulation (Figure 4.13F).

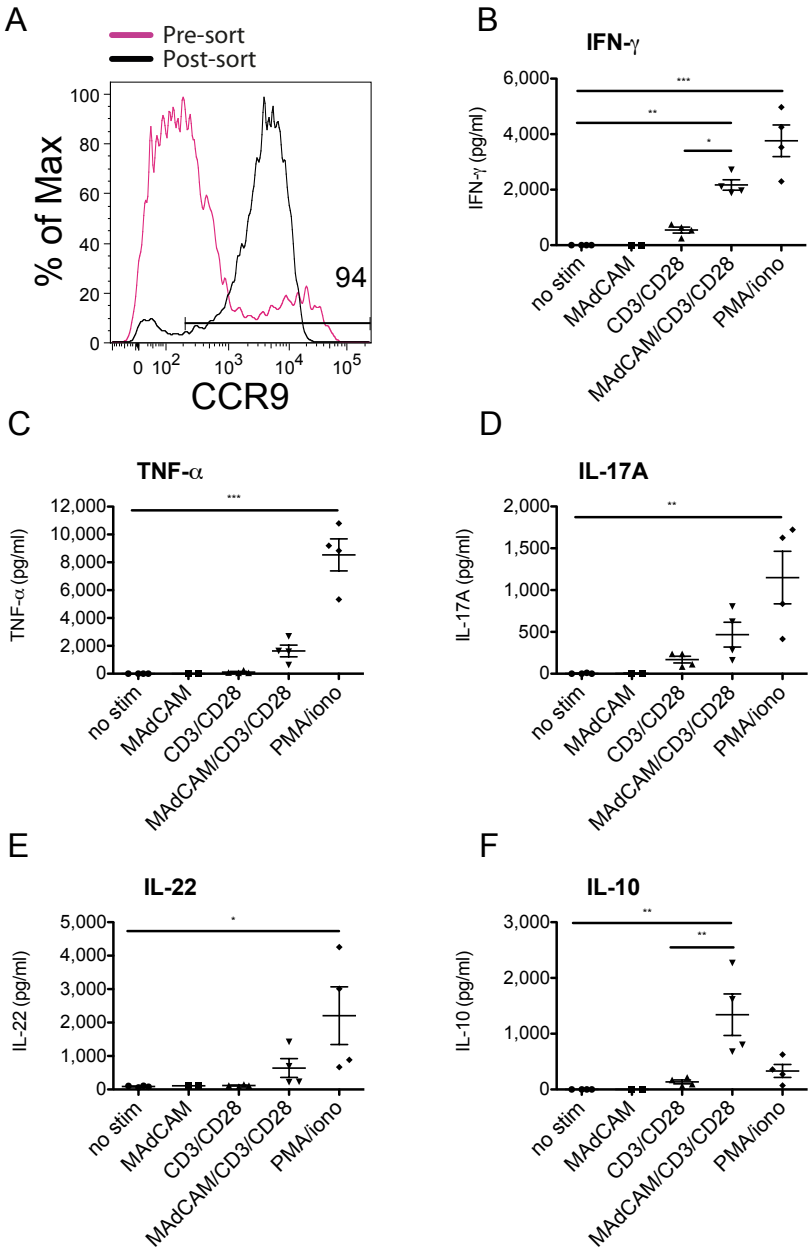


Figure 4.13 CCR9$^+$ T cell cytokine production.
200K CCR9$^+$ ATRA-cultured cells were added to flat bottom 96-well plates, pre-coated with combinations of recombinant human MAdCAM-1, anti-CD3, and anti-CD28 or PMA with ionomycin. After 16 hours (4 hours for PMA/iono), cell supernatants were collected and analyzed for cytokine concentration by a flow cytometry based ELISA.
A: ATRA-cultured cells pre and post magnetic bead separation.
B: IFN-γ
C: TNF-α
D: IL-17A
E: IL-22
F: IL-10
Graphs show mean value ± SEM from four independent experiments. *p<0.05, **p<0.01, ***p<0.001 Repeated measures ANOVA with Bonferroni's post hoc test.

4.2.3 Effect of CCL25 on cytokine production

Having shown that ATRA-cultured cells signal by migration and calcium flux in response to CCL25, I next studied cytokine production by ATRA-cultured cells in response to CCL25. $CCR9^+$ cells were sorted from ATRA-cultured cells and activated in the presence or absence of CCL25 for 16 hours. Two doses of CCL25 were tested, 125 nM and 500 nM which are on either side of the chemotaxis and calcium flux bell-shaped dose-response curves (see Figure 4.4A and Figure 4.11). To test the potential for CCL25 to act as a co-stimulatory molecule, anti-CD3 stimulation alone was included in the analysis.

CCL25 had no effect on cytokine production from resting $CCR9^+$ cells (no stimulation), cells stimulated with anti-CD3 alone or cells stimulated with CD3/CD28 (Figure 4.14). Concentrations of IFN-γ significantly increased with the addition of 500 nM CCL25 following PMA/ionomycin stimulation but was not observed with MAdCAM-1/CD3/CD28 stimulation (increased from 2.3 ng/ml to 3.6 ng/ml, $p<0.05$; Figure 4.14A). Similarly, TNF-α production was significantly greater following 500 nM CCL25 in the presence of PMA/ionomycin (increased from 5.3 ng/ml to 7.5 ng/ml, $p<0.05$; Figure 4.14B).

Production of IL-17A upon MAdCAM-1/CD3/CD28 stimulation was significantly increased by 125 nM CCL25 and not with 500 nM CCL25 (increased from 162 pg/ml to 200 pg/ml, $p<0.05$; Figure 4.14C). While IL-22 appeared to increase at both concentrations of CCL25 following PMA/ionomycin stimulation, this trend failed to be statistically significant (Figure 4.14D). CCL25 had no effect on IL-10 production although ample IL-10 was measured following MAdCAM-1/CD3/CD28 stimulation (Figure 4.14E). Collectively these data suggest that CCL25 can enhanced IFN-γ, TNF-α and IL-17A production in $CCR9^+$ ATRA-cultured cells, albeit to a modest degree and dependent on the form of cell activation.

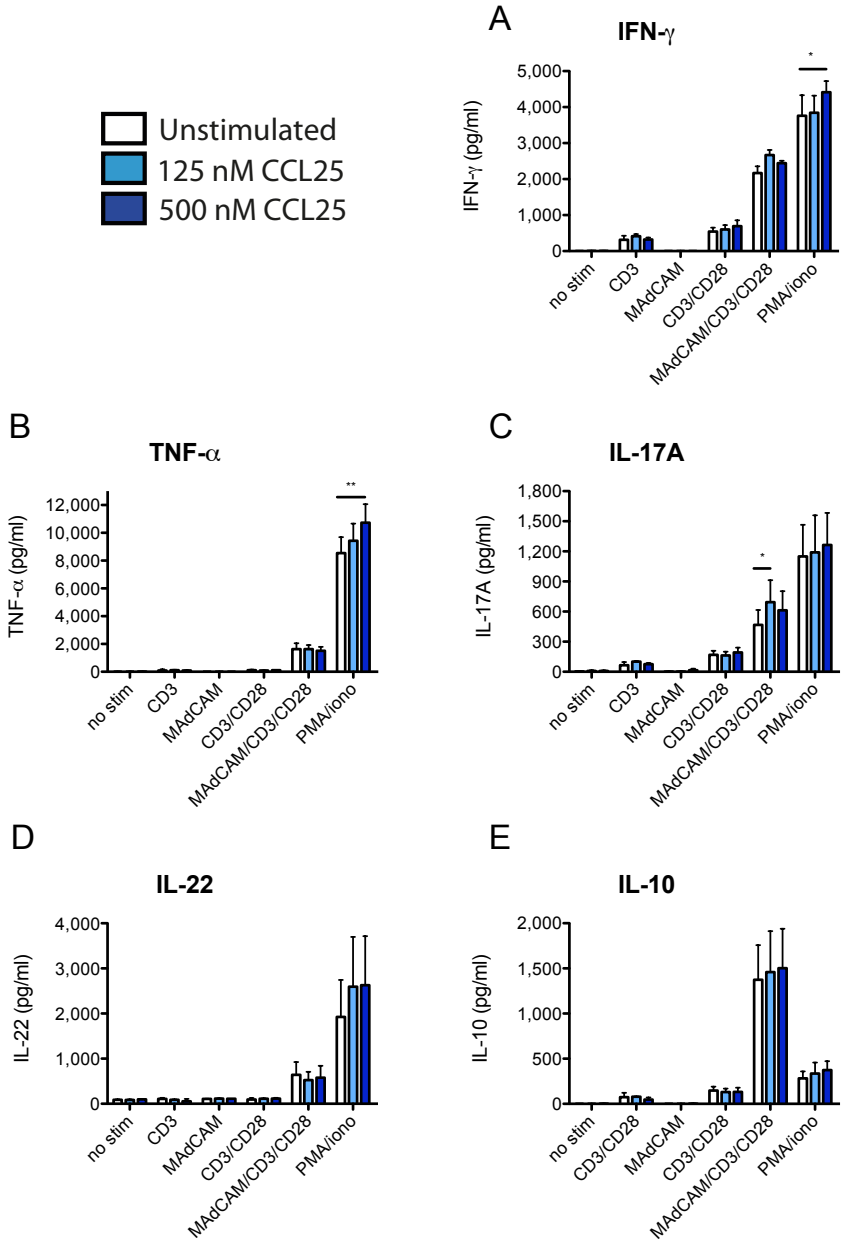


Figure 4.14 The effect of CCL25 on CCR9$^+$ T cell cytokine production.
200K CCR9$^+$ ATRA-cultured cells were added to flat bottom 96-well plates, pre-coated with combinations of recombinant human MAdCAM-1, anti-CD3, and anti-CD28 or PMA with ionomycin. All conditions were incubated for 16 hours. For PMA/ionomycin stimulation, cells were incubated with CCL25 for 16 hours and the last 4 hours were in the presence of PMA/ionomycin. Cell supernatants were analyzed for cytokine concentration a by flow cytometry based ELISA.
A: IFN-γ
B: TNF-α
C: IL-17A
D: IL-22
E: IL-10
Graphs show mean value ± SEM from four independent experiments.
*p<0.05, **p<0.01 Repeated measures ANOVA with Dunnett's post hoc test compared to 'no stimulation'.

4.2.4 Measuring RNA quantity and quality isolated from human intestinal biopsies

One of the greatest obstacles to studying human mucosal immunology is obtaining primary tissue. In the case of the gastrointestinal tract, surgical resection material is one potential resource, however this inherently restricts access to areas of severe inflammation, fibrosis or cancerous tissue (which is often used as 'control' material). Intestinal biopsies collected during endoscopy are more frequently collected and allow tissue isolation from a more diverse selection of diseased and non-diseased areas. To determine if intestinal biopsies could be used for qRT-PCR analysis, the quantity and quality of RNA extracted from a single biopsy were measured.

Intestinal biopsies collected from uninvolved and inflamed tissue were processed for RNA extraction. Figure 4.15A illustrates the small size of an intestinal biopsy, which is generally no larger than 25 μm^2. Figure 4.15B illustrates the motorized pestle used for tissue homogenization. From uninvolved intestinal tissue, an average of 2.7 μg RNA per biopsy was recovered (Figure 4.15C). From inflamed tissue, more RNA was generally extracted (average of 8 μg per biopsy), likely owing to the infiltration of leukocytes and hyperplasia of the epithelium. The quality of extracted RNA was assessed with a Bioanalyzer®.

Analysis with the Bioanalyzer® runs a small sample of extracted RNA along a gel relative to a ladder control (Figure 4.15D). The data is expressed as the intensity of RNA bands relative to size (Figure 4.15E). The relative ratio of ribosomal RNA subunits (18S and 28S) is quantified as an RNA Integrity Number (RIN) which is a reflection of RNA quality and potential degradation. The RIN scale ranges for 10 (totally intact) to 1 (completely degraded) [340]. A RIN greater than 6 is correlated with high quality qPCR data [340]. Figure 4.15E depicts one representative Bioanalyzer® result from an intestinal biopsy (RIN = 7.1). Based upon results from several intestinal biopsies, enough RNA for qRT-PCR (> 1 μg) of high quality

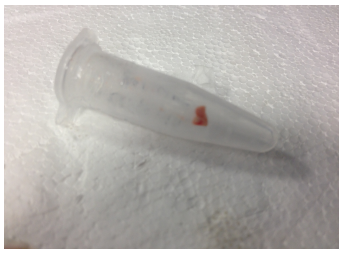
(RIN > 6) could be extracted from a single uninvolved or inflamed intestinal biopsy to allow qRT-PCR analysis.

This was an important resource, allowing the analysis of chemokine mRNA expression along different areas of the gastrointestinal tract from a single patient. It also enabled the comparison of chemokine expression between uninvolved and inflamed intestinal tissue collected from a single patient. Characterization of human CCL25 expression in the published literature is limited to a crude discrimination of small intestine versus large intestine. I was interested to characterize CCL25 mRNA more thoroughly, measuring expression along different regions of the large intestine and small bowel in the absence of inflammation and during active IBD.

4.2.5 Chemokine mRNA expression along the gastrointestinal tract

During routine endoscopy, intestinal biopsies were collected from a single patient along different portions of the small and large intestine from un-inflamed tissue (Figure 4.16A). Analysis of CCL20, CCL25, CXCL8 and CXCL10 mRNA expression were analyzed by qRT-PCR. To control for variations in the proportions of epithelial cells to lamina propria leukocytes between biopsies, gene expression was compared to the housekeeping gene, villin. Villin is a marker of epithelial cells, the predominant producer of CCL25 in the intestine [70,71]. In accordance with previous reports, CCL25 mRNA was detected in the TI (Figure 4.16B). CCL25 was not detected in other areas of the gastrointestinal tract, including the rectum, caecum and different portions of the colon (splenic flexure, hepatic flexure, distal colon). The restricted expression of CCL25 was in contrast to CCL20, CXCL8 and CXCL10 which were detected in all of the examined regions of the intestine (Figure 4.16B). This pattern of expression was observed in three unique donors.

A



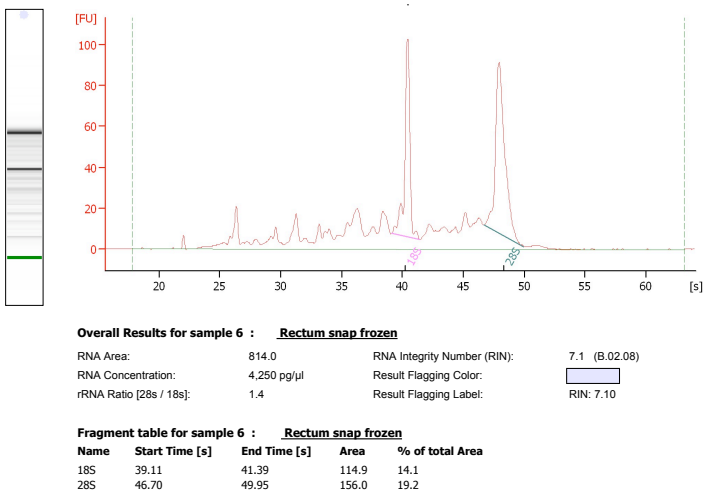
B



C

Location	Status	no. biopsies	A260/280	Total RNA collected (µg)
Splenic flexure (colon)	uninflamed	1	1.99	1.9
Terminal ileum	uninvolved	1	1.99	2.2
Sigmoid colon	uninvolved	1	1.95	3.4
Ascending colon	uninvolved	1	1.99	3.7
Rectum	uninvolved	1	1.97	2.5
Splenic flexure (colon)	inflamed	1	1.98	9.7
Caecum	inflamed	1	1.98	10.7
Rectum	inflamed	1	2.01	7.1
Distal colon	inflamed	2	2	4.4

D E



Overall Results for sample 6 : Rectum snap frozen

RNA Area:	814.0	RNA Integrity Number (RIN):	7.1 (B.02.08)
RNA Concentration:	4,250 pg/µl	Result Flagging Color:	
rRNA Ratio [28s / 18s]:	1.4	Result Flagging Label:	RIN: 7.10

Fragment table for sample 6 : Rectum snap frozen

Name	Start Time [s]	End Time [s]	Area	% of total Area
18S	39.11	41.39	114.9	14.1
28S	46.70	49.95	156.0	19.2

Figure 4.15 Validating RNA isolation from intestinal biopsies.
Intestinal biopsies were collected during clinical endoscopy. RNA isolation was performed with Qiagen RNeasy Mini Kit. Tissue was homogenized in lysis buffer using a motorized pestle and sterile disposable tips. Sample was treated with DNase I to remove genomic DNA and analyzed with a NanoDrop to assess RNA purity (A260/A280) and quantity. To test the integrity of isolated RNA, samples were analyzed with a Bioanalyzer®.
A: Image to illustrate the size of an intestinal biopsy relative to a 1.5 ml eppendorf tube.
B: Motorized pestle used to homogenize tissue.
C: Representative examples of the amount of RNA isolated from intestinal biopsies.
D: RNA analyzed by Bioanalyzer gel.
E: Gel from D quantified as band intensity relative to time (seconds). Representative results from the Bioanalyzer, quantifying RNA integrity from an intestinal biopsy sample.

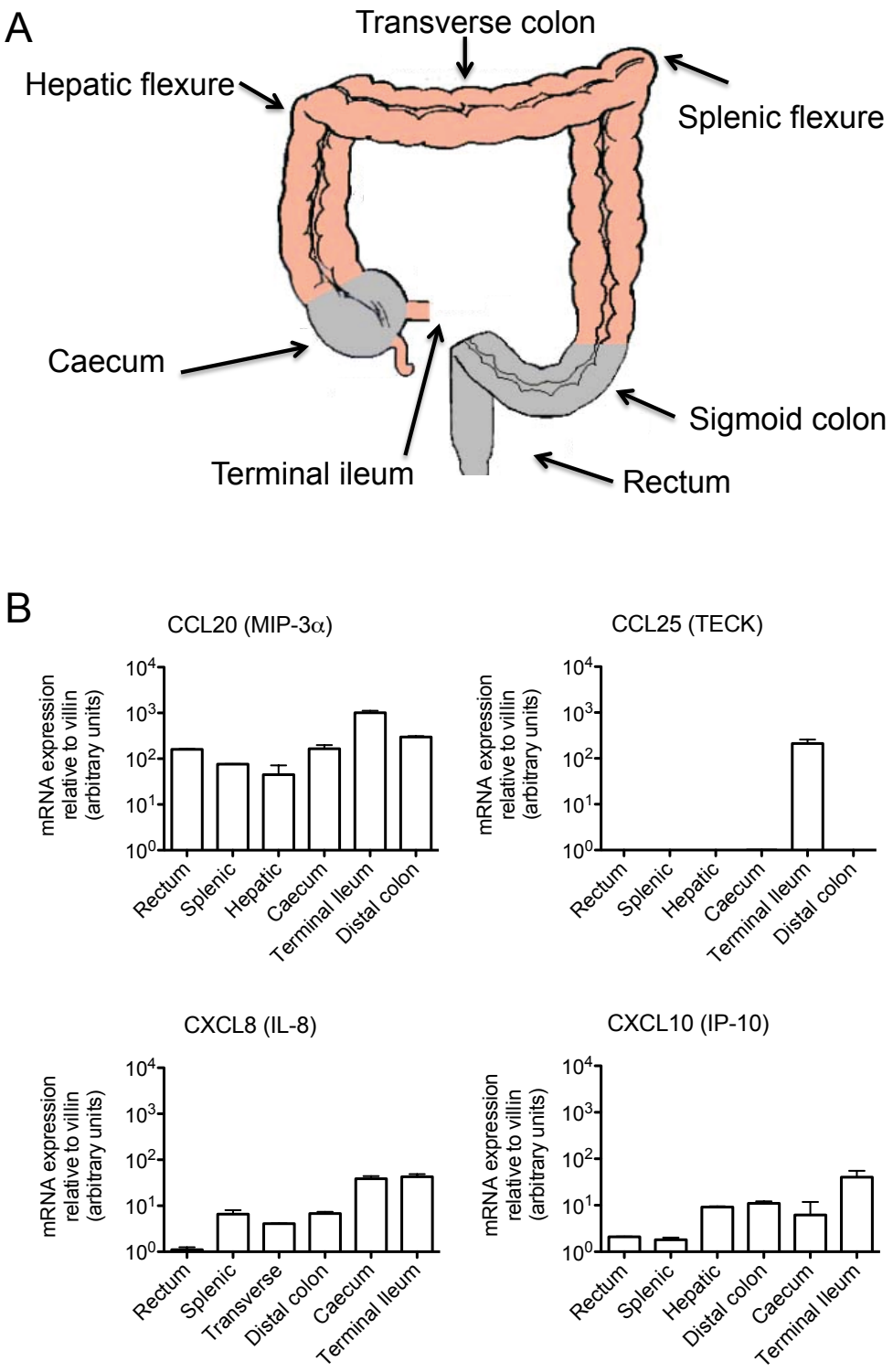


Figure 4.16 Chemokine expression along the gastrointestinal tract from a single patient.

Intestinal biopsies from different areas of the gastrointestinal tract were collected from a single patient during routine endoscopy (un-inflamed). Tissue was analyzed by qRT-PCR comparing chemokine expression relative to the keeping gene, villin. Villin is a marker for epithelial cells, a major contributor to chemokine production. Graphs show mean value ± SEM from three technical replicates.

Representative of three independent donors.

4.2.6 CCL25 mRNA expression in the small intestine with and without inflammation

In murine models that share aspects of IBD pathology, CCL25 expression increases with disease severity, measured by analysis of mRNA and protein expression [102,104]. To further characterize CCL25 mRNA expression during CD, biopsies from the TI during active disease were analyzed by qRT-PCR. As a comparison, biopsies from un-inflamed TI were analyzed, collected from patients during routine endoscopy or from patients with colonic UC. In total 5 un-inflamed donors and 4 inflamed donors were analyzed by qRT-PCR. These data demonstrate a trend that inflamed TI had 1.47 fold more CCL25 mRNA than un-involved tissue, although the difference did not reach statistical significance ($p=0.17$, Figure 4.17). Additional samples will be necessary to ascertain if CCL25 mRNA is elevated in the TI during active CD.

4.2.7 CCL25 mRNA expression during intestinal inflammation comparing colonic and small intestinal tissue

To examine the possibility that colonic CCL25 expression might be induced during active IBD, biopsies were assessed by qRT-PCR, measuring CCL25 expression relative to villin. As a control, small intestinal tissue was also analyzed to ensure that CCL25 mRNA could be detected. Consistent with previous reports, CCL25 mRNA expression was significantly enriched in the small intestine compared to the colon (Figure 4.18). CCL25 mRNA was detected in 2 out of 23 analyzed inflamed colonic biopsies. In these two samples, the relative level of CCL25 expression was 56 fold lower than levels detected in terminal ileum samples. These data demonstrate that CCL25 expression is predominantly restricted to the small intestine but in selected cases can be induced in the colon during active IBD, albeit to lower levels of transcript than the terminal ileum.

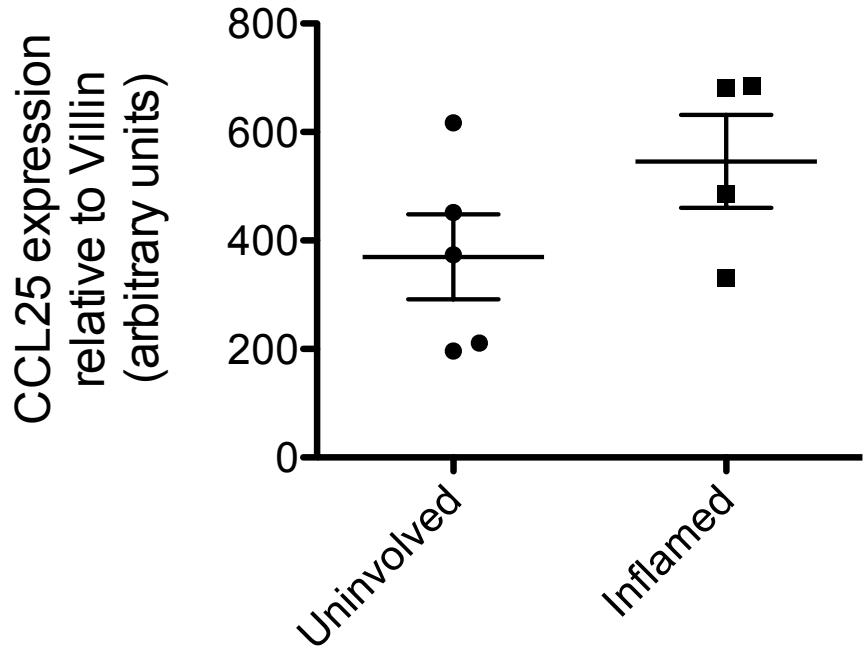


Figure 4.17 CCL25 mRNA expression in the terminal ileum during active Crohn's disease.
Human biopsies were collected from the TI of patient without inflammation (uninvolved, from routine endoscopy or colonic UC) and with active CD (inflamed). Tissue was analyzed by qRT-PCR comparing CCL25 mRNA expression relative to the housekeeping gene, villin. Graphs show mean value ± SEM, each data point is a unique tissue biopsy ($p=0.17$, Student's t test).

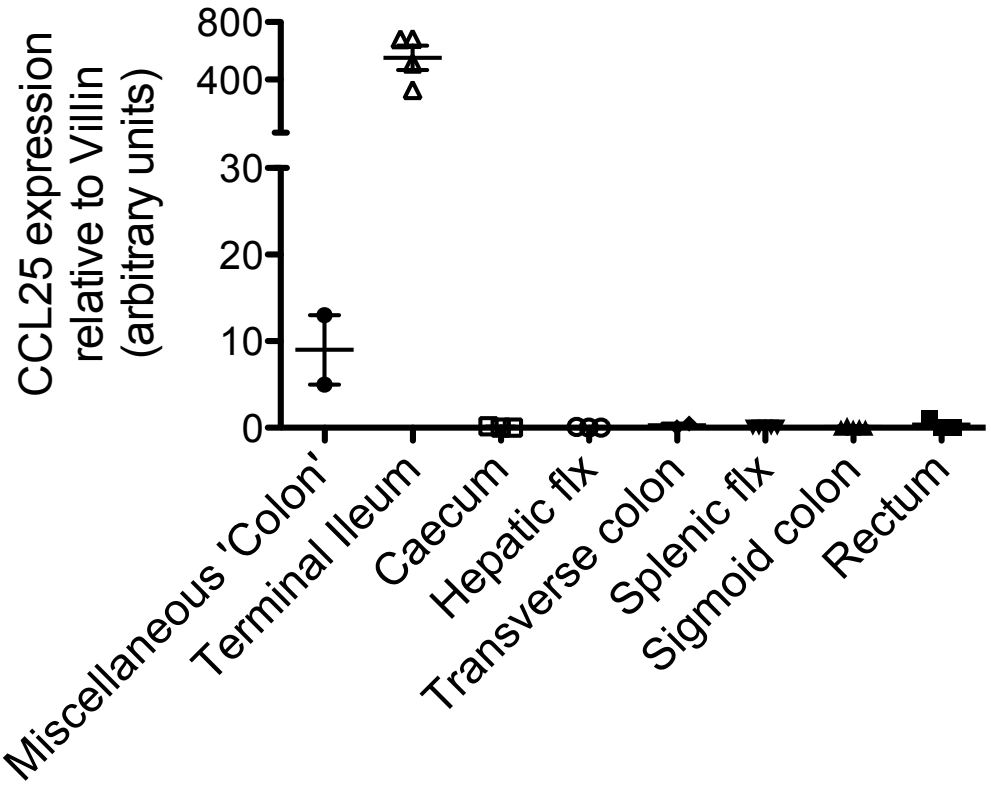


Figure 4.18 CCL25 mRNA expression during active IBD.
Biopsies were collected from patients with active IBD (a mixture of Crohn's and Colitis) from inflamed tissue as assessed during endoscopy. Samples were analyzed by qRT-PCR, quantifying CCL25 mRNA relative to the housekeeping gene, villin. Each data point represents a unique intestinal biopsy. Data shown as mean value ± SEM.

4.3 Discussion

In this chapter I have shown a characterization of ATRA-cultured cells, as they were to be the basis of further experiments in this thesis. As a functional characterization, I have shown for the first time that these cells respond to CCL25 by calcium flux, measured in a flow cytometry based assay which follows the calcium response by single cells. In response to the pattern of CCR9 staining detected by IHC (Chapter 3), I show that CCL25 induces CCR9 internalization, the first such description in human T cells, measured on two different cell types by flow cytometry and IHC staining. CCL25 significantly enhanced the production of IFN-γ, TNF-α and IL-17A although levels of induction were modest and dependent on the form of T cell activation. During an analysis of cytokines stimulated by CCL25, I made an unexpected but highly relevant observation that MAdCAM-1 significantly increased cytokine secretion from $CCR9^+$ T cells. Lastly, using primary human tissue analyzed by qRT-PCR I present a more complete analysis of CCL25 mRNA expression along the GI tract, and show data suggesting a trend that CCL25 mRNA expression is elevated in the small intestinal during active CD. I also show that in a small proportion of UC patients, CCL25 mRNA is detected in the inflamed colon, the first description of colonic CCL25 expression.

4.3.1 ATRA-cultured cell characterization compared to primary $CCR9^+$ T lymphocytes

At the time of this work, ATRA-cultured cells were known to express CCR9 mRNA, have cell surface CCR9 and migrate to CCL25 *in vitro* [66,87]. The composition of human ATRA-cultured cells with regards to T cell phenotype (CD4 versus CD8) and markers of activation was not represented in the published literature. Furthermore, how these ATRA-cultured cells compared to primary human $CCR9^+$ T cells was also unknown.

In the peripheral blood of healthy individuals, the T cell CD4:CD8 ratio is approximately 2:1 [341]; among $CCR9^+CD3^+$ cells, the CD4:CD8 ratio is approximately 1.5:1 [75]. In this chapter I demonstrate that the ATRA-culturing system favors the expansion of CD8 single positive $CCR9^+$ T cells (approximately 1:1 ratio, see Figure 4.2A). Therefore the ATRA-culture system, which favors the expansion of $CD8^+CCR9^+$ cells is not exactly representative of the $CCR9^+$ T cell composition in the healthy peripheral blood.

As discussed in Section 1.4.4, CTLs maintain immune homeostasis by inducing activated T cell apoptosis through Fas-Fas ligand interactions. Activation, expansion and time in culture could trigger CTL to induce CD4 cell apoptosis as a means of regulating 'inflammation.' Conversations with peers suggest that a disproportionate frequency of $CD8^+$ cells in T cell culture systems is a common observation. It is therefore unlikely that something specific to ATRA or CCR9 induction is the principal cause, however this has not been explicitly tested.

The basis of ATRA-culturing conditions is the activation of T cells by anti-CD3 and anti-CD28 in the presence of IL-2 to promote cell survival and T cell proliferation, therefore it was expected that ATRA-cultured cells would have an activated phenotype. In this chapter I show that the majority (>70%) of ATRA-cultured cells (both $CCR9^+$ and $CCR9^-$) express CD69, CD45RO and CD25, markers indicative of an activated, effector/memory T cell phenotype.

Papadakis, *et al* (2003) reported from peripheral blood of healthy donors, $CCR9^+$ cells are 17% $CD69^+$, 68% $CD45RO^+$ and 26% $CD25^+$ [75]. Saruta, *et al* (2007) characterized the phenotype of primary $CCR9^+$ T cells from healthy and inflamed (Crohn's Disease) small bowel and reported that regardless of disease, $CCR9^+$ cells had an activated, memory phenotype: ~98% $CD69^+$, 26-31% $CD25^+$ and 89-98% $CD45RO^+$ [90]. Therefore the ATRA-culturing conditions produce $CCR9^+$ cells that were highly activated and resemble aspects of

primary $CCR9^+$ cells from the small bowel and peripheral blood. Moreover, I show that similar to primary cells, $CCR9^+$ ATRA-cultured cells produce IFN-γ, IL-17 and IL-10, in addition to of TNF-α, and IL-22 that have not been previously described; these data can serve as a reference for future work studying the cytokine secretion of $CCR9^+$ T cells.

4.3.2 CCL25-mediated calcium flux in ATRA-cultured cells

In this chapter I have shown for the first time that CCL25 stimulates CCR9-mediated calcium flux in ATRA-cultured cells. This is an important contribution to the field because it confirms that, similar to most chemokine receptors, these cells mobilize calcium in response to CCL25 and further validates their experimental use as a primary derived source of $CCR9^+$ T cells. This observation was only possible by optimizing a method for measuring calcium flux within CCR9 expressing cells, selectively gated by flow cytometry.

Measuring calcium flux by flow cytometry has the significant advantage of allowing distinct cell populations to be distinguished, in this case, $CCR9^+$ from $CCR9^-$. In the future this technique could be used to validate the specificity of chemokine receptor specific antibodies. This technique has further applications, for example staining distinct populations with unique fluorochromes to simultaneously stimulate and measure calcium flux. This would circumvent the technical problem of 'dye leakage' [307] (the observation that over time, calcium dye is exported from the cell, decreasing the calcium signal) and allow direct comparison between cell populations in response to the same stimuli; I explore this approach in more detail in Chapter 5 of this thesis.

4.3.3 CCL25-mediated CCR9 internalization

Another aim of this chapter was to measure the effect of CCL25 on CCR9 cell surface expression. My data demonstrate that CCL25 mediates CCR9 internalization in both Molt-4 cells and ATRA-cultured cells, measured by both flow cytometry and IHC analysis. These

data are similar to published studies of CCR4 and CXCR3, where receptor internalization is both chemokine concentration and time dependent [331,332]. It is reasonable to believe that the punctate staining observed in the intestine and thymus, where CCL25 is abundant, was the consequence of CCL25 mediated CCR9 internalization. One way to test this *in vivo*, albeit in a different species, is a comparison of CCR9 IHC staining in the intestine of wild type and CCL25 deficient mice.

4.3.4 The effect of MAdCAM-1 on CCR9$^+$ cell cytokine production

A striking result was the effect of MAdCAM-1 on cytokine production. Plate bound MAdCAM-1 enhanced CD3/CD28 stimulated cytokine production for all of the measured cytokines, and was significantly greater for induction of IFN-γ and IL-10 (see Figure 4.13). I originally included MAdCAM-1 in this analysis with the rational that 'outside-in' signalling could alert the T cell once it had reached the relevant destination, thereby enhancing effector cytokine production. However to substantiate this explanation, a more thorough characterization would be required, specifically measuring the kinetics of induction, comparisons with other addressins to determine the specificity of the effect (VCAM-1, ICAM-1) and comparisons with other forms of T cell activation (ie PMA/ionomycin) to see if the effect is specific to co-activation by CD3/CD28.

Another potential explanation is that immobilized MAdCAM-1 is promoting TCR activation by enhancing the immunological synapse, a process described for other integrin-adhesion molecule interactions, particularly during contact between APC and T cell (ie $\alpha_L\beta_2$-ICAM-1 and $\alpha_4\beta_1$-ICAM-1) [20,342-344]. To the best of my knowledge, this effect is not described for MAdCAM-1 likely owing to it's relatively restricted expression on vascular endothelial cells. To address this experimentally, the effects of plate bound MAdCAM-1 compared to soluble MAdCAM-1 could be studied; an immunological synapse requires directional polarization

such as when MAdCAM-1 is plate bound alongside TCR activation. Furthermore, experiments similar to those performed by Contento *et at* (2010), using con-focal experiments could visualize a synapse if one were present [20].

This result is particularly interesting considering the role of MAdCAM-1 in IBD and PSC. Patients with active IBD and PSC have elevated MAdCAM-1 expression, quantified by qPCR and IHC [63,65,345,346]. MAdCAM-1 expression by vascular endothelial cells is well documented [18,347], but expression has also been found on stromal cells and DCs, particularly within lymphoid aggregates identified in the spleen, liver and intestine [63,348-350]. Therefore it is reasonable to speculate that MAdCAM-1 expression within the lamina propria could enhance cell activation *in situ*. Moreover, my data shows that MAdCAM-1 (with CD3/CD28 stimulation) significantly increased IL-10 production, producing greater levels of protein than PMA/ionomycin stimulation; in contrast, all of the other cytokines were most strongly produced by PMA/ionomycin stimulation. Supposing MAdCAM-1 enhances cytokine secretion by LPLs, the balance of Th1 and regulatory T cells *in situ* could determine the effect of MAdCAM-1 on the development or resolution of inflammation in the intestine. A more thorough characterization of MAdCAM-1 expression in the lamina propria during IBD is warranted.

4.3.5 Cytokine production following CCL25 treatment

In a selected few cases, chemokines have been demonstrated to modulate cytokine production (see section 4.1.4). Given the restricted expression of CCL25 and enriched population of $CCR9^+$ cells in the small intestine (and in the liver during PSC), I was interested to know if this receptor-ligand pair could modulate cytokine production in human T cells. Furthermore, given the therapeutic efficacy of blocking CCR9 (by either antibody blockade or small

molecule antagonist treatment), modulating cytokine production could identify an alternative mechanism of action.

The data presented in this chapter suggest that CCL25, when combined with a second stimulus (ie PMA/ionomycin or MAdCAM-1/CD3/CD28) modestly increases IFN-γ, TNF-α and IL-17A production from $CCR9^+$ ATRA-cultured cells (see Figure 4.14). Importantly, CCL25 stimulation alone did not induce the any of the measured cytokines. It is unlikely that the modest effect of CCL25 measured here *in vitro* would have a biologically significant effect *in vivo.*

4.3.6 CCL25 production in the gastrointestinal tract ± inflammation

At the time of this thesis, the characterization of CCL25 expression in the human intestine was limited to seven total intestinal samples, described as either small or large intestine: in the original cloning and characterization of CCL25, Vicari *et al* (1997) show data for CCL25 Southern blotting on a human cDNA tissue library (purchased from Clonetech, Palo Alto, CA, USA) which includes a single sample of small intestine (no colon tissue) [68]; Zabel *et al* (1999) showed CCL25 RNA by Northern blotting, on a commercially available tissue array (also purchased from Clonetech) which included a single sample of small intestine and a single sample of colon; Zabel and colleagues also showed PCR products from commercially available cDNA (purchased from Clonetech), comparing a single colon and small intestine sample [69]; Papadakis *et al* (2000) showed data from a single healthy patient sample, comparing CCL25 mRNA from the whole intestinal mucosa isolated from the colon and the small bowel [71]. In summary, published studies of human CCL25 expression are limited to four independent reports, three of which utilize samples from the same commercial source.

The data presented in this chapter analyzed CCL25 mRNA across different regions of the GI tract, using biopsies collected in the John Radcliffe hospital (Oxford, UK) as part of the IBD

clinic and GI Biobank (see Section 2.12). These data demonstrate that, in accordance with previous reports, under non-inflamed conditions, CCL25 mRNA expression is restricted to the small intestine. This was in contrast to other chemokines (CCL20, CXCL8 and CXCL10) that were detected throughout the colon and in the TI (see Figure 4.16) [69,71]. While my data are in line with previously published reports, they are also an important contribution to the characterization of human CCL25 expression that is under-represented in the literature.

My data also demonstrate that in a small proportion of IBD patients, CCL25 is detected in the inflamed colon. The current dogma is that CCL25 expression is specific to the small intestine and thymus, however the data from this chapter and the previous report of CCL25 in the liver during PSC [47] do not support this. These data support the idea that IBD is a heterogeneous disease and CCL25 expression in the inflamed colon may represent a subset of patients with unique disease etiology; if this were the case, CCL25 expression could serve as a biomarker of disease activity.

4.3.7 Limitations to these studies

Visualizing CCR9 internalization

Whilst surface CCR9 is rapidly internalized, I have not explored the fate of internalized CCR9. By ImageStream (Amnis Corporation, Seattle, WA, USA) which combines flow cytometry with con-focal microscopy, it would be possible to visualize CCR9 in relation to lysosomes (organelle containing hydrolyzic enzymes, which upon fusion degrades material within endosomes [124]) and compare surface CCR9 to the distribution of internalized CCR9. Alternatively, an analysis similar to that performed by Mueller *et al* (2002) using con-focal microscopy could be applied, comparing the distribution of CCR9 protein in untreated and CCL25 treated cells.

CCR9$^+$ ATRA-cultured cell cytokine production

The pilot data presented in Figure 4.12 demonstrate that within the bulk population of ATRA-cultured cells, a greater proportion of CCR9$^-$ cells are producing IFN-γ, TNF-α and IL-17A. It is therefore possible that some of the cytokines measured in the cell supernatants were contributed by the CCR9$^-$ cells, which comprise ~6% of the CCR9$^+$ sorted population (see Figure 4.12A). Between four unique ATRA-cultured cell donors the concentrations of measured cytokines was remarkably reproducible, particularly considering that each donor has variations in the proportion of CD4 to CD8 cells. By Flow Cytometry it would be possible to monitor the contribution of cytokine production by the various CD4, CD8 and FoxP3 CCR9$^+$ ATRA-cultured cells.

Characterization of chemokine production in the intestine

Although I analyzed several patient samples for CCL25 production along the gastrointestinal tract, the analysis does not include such variables as age, length of disease, gender nor concomitant therapeutics. Each of these factors, particularly the use of therapeutic interventions may effect the production of chemokines.

4.3.8 Future experiments in this thesis

The ATRA-cell characterization described in this chapter was critical for informing subsequent experiments performed during my DPhil. In the next chapter I study the effect of corticosteroids on CCR9 surface expression and function, using ATRA-cultured cells and many of the techniques optimized in the current chapter. These experiments were stimulated by the observation that approximately half of the patients in the PROTECT-1 trial were on concomitant steroid treatment, the effect of which was unknown on CCR9 expression and function.

CHAPTER 5: The effect of corticosteroids on CCR9-mediated cell signalling and chemotaxis

5.1 Introduction

Glucocorticoids are among of the most effective immunosuppressants agents, used to treat a large number of immune-mediated disorders including Inflammatory Bowel Disease [265]. Active IBD is routinely and successfully treated with corticosteroids to induce remission in mild to severe cases: on a high dose of prednisolone (potent glucocorticoid with limited mineralocorticoid activity), patients displayed up to 92% remission within 7 weeks [351]. Despite the extensive use of steroids clinically since the 1950s, identifying mechanisms of anti-inflammatory action still remains an active area of research. Indeed it was only in 1985 that the glucocorticoid receptor was discovered (see Section 1.6.1).

5.1.1 The effects of glucocorticoids on T cells

In T cells, GCs inhibit TCR activation, impairing early signalling events and the activation of downstream transcription factors NF-κB, STAT-3 and AP-1 [352], inhibiting the production of pro-inflammatory cytokines including IFN-γ, IL-12, IL-6, IL-5, IL-3, TNF-α, IL-1β, and IL-2 [353-355]. Additionally, GCs suppress T cell activity by inducing cell apoptosis and reducing T cell proliferation [11]. Despite the critical role chemokine receptors play in initiating and exacerbating inflammation, only a limited literature has explored the effect of GCs on chemokine receptor expression and function.

5.1.2 The effect of steroids on chemokine receptor expression

Two independent groups have reported that GCs enhance CCR2 expression and CCL2 mediated migration in primary human monocytes. The first study by Penton-Rol *et al* (1999), showed that *in vitro* treatment with 100 nM dexamethasone (DEX), a potent and

specific glucocorticoid, increased CCR2 mRNA, and enhanced migration to CCL2. In the same cells, DEX-treatment had no effect on CCR1, CCR4 nor CCR5 mRNA expression [356]. This article reported that elevated CCR2 enhanced HIV entry.

Okutsu *et al* (2008) reported that primary human monocytes ($CD14^+$) treated *in vitro* with cortisol, had increased CCR2 expression which was dose (> 100 nM) and time dependent (> 6 hrs treatment), enhanced CCL2 mediated migration, and was abrogated by the GCR antagonist, mifepristone [357]. Okutsu and colleagues collected human serum immediately following intense exercise (when levels of endogenous cortisol are elevated); when primary human monocytes were treated with the post exercise serum, CCR2 expression increased and CCL2 mediated cell migration was elevated [357]. Okutsu *et al* (2008) conclude that elevated CCR2 expression on monocytes following exercise might enhance monocyte recruitment to tissue areas which undergo damage and inflammation as a consequence of exercise or stress [357].

The best documented effect of GCs on a chemokine receptor expression and function are changes to CXCR4, measured in human T cells and eosinophils. I*n vitro,* GC treatment is shown to increase CXCR4 surface expression and CXCL12-mediated intracellular signalling, calcium mobilization and cell migration measured in Jurkat T cells, primary resting T cells, primary activated T cells and primary human eosinophils [358-362]. Enhanced CXCR4 signalling following GC treatment is described to correlate with increased expression of CXCR4 mRNA, and surface protein and was inhibited by the GCR antagonist, mifepristone. Studies have drawn an array of conclusions, most notably that increased CXCR4 surface protein can enhance HIV infection [358,360], account for lymphopenia following stress or exercise [359], redistribute T cells to the bone marrow as a consequence of circadian changes in

circulating cortisol [363], and have anti-allergic effects by sequestering eosinophils to extravascular tissues [362].

5.1.3 Rationale for the experiments

Glucocorticoids are frequently used to treat IBD yet, their broad range of anti-inflammatory action remains only partially understood. This chapter examines the effect of glucocorticoids on CCR9 surface expression, and cell function using ATRA-cultured T cells and primary $CCR9^+$ sorted T cells.

5.1.4 Aims of this chapter

The experiments in this chapter aim to investigate the effect of synthetic glucocorticoids on CCR9 – CCL25 signalling in human T cells and will include:

- Analysis of chemokine receptor expression following GC treatment.
- Comparison of chemokine mediated cell migration following GC treatment.
- Assessment of the effect of GC treatment on surface CCR9 expression and function in primary human $CCR9^+$ T cells.
- Assessment of the effect of GC treatment on CCR9-mediated calcium mobilization.
- Examination of potential mechanisms responsible for GC-mediated inhibition of CCR9 function:
    - Investigating the role of the glucocorticoid receptor
    - Analysis of CCL25-mediated, CCR9 internalization
    - Analysis of CCL25-mediated, Phospho-PLCγ1
    - Analysis of CCRL1 mRNA expression

5.2 Results

5.2.1 *In vitro* glucocorticoid treatment and controls

Dexamethasone is the preferred synthetic steroid for *in vitro* and *in vivo* studies because it specifically activates the glucocorticoid receptor with minimal mineralocorticoid activity [364]. *In vitro* the majority of studies use between 100 nM – 1 μM DEX [356,360,361,365]. The experiments in this chapter use a single, physiologically relevant concentration for each steroid, calculated on the basis of recommended dosing relative to blood volume [366]. As described in Section 5.1.2, GCs are described to increase CXCR4 mediated signalling and function in human T cells. All ATRA-cultured cell express surface CXCR4 (see Figure 4.3), therefore CXCR4 was an appropriate positive control for GC activity.

5.2.2 The effect of dexamethasone on chemokine receptor expression in ATRA-cultured cell

ATRA-cultured cells were treated with 250 nM DEX or vehicle (H_20) for 16 hours and surface chemokine receptor expression was measured by flow cytometry. DEX-treatment had no effect on the proportion of cells expressing the chemokine receptors of interest (Figure 5.1A). CCR9 MFI was equivalent between vehicle- and DEX-treated cells; in contrast, CXCR3 surface expression was significantly reduced following DEX-treatment (1.42±0.07 fold decrease, $p<0.05$) and as previously reported, surface CXCR4 expression was significantly increased following DEX-treatment (3.5±0.45 fold increase, $p<0.01$) (Figure 5.1B).

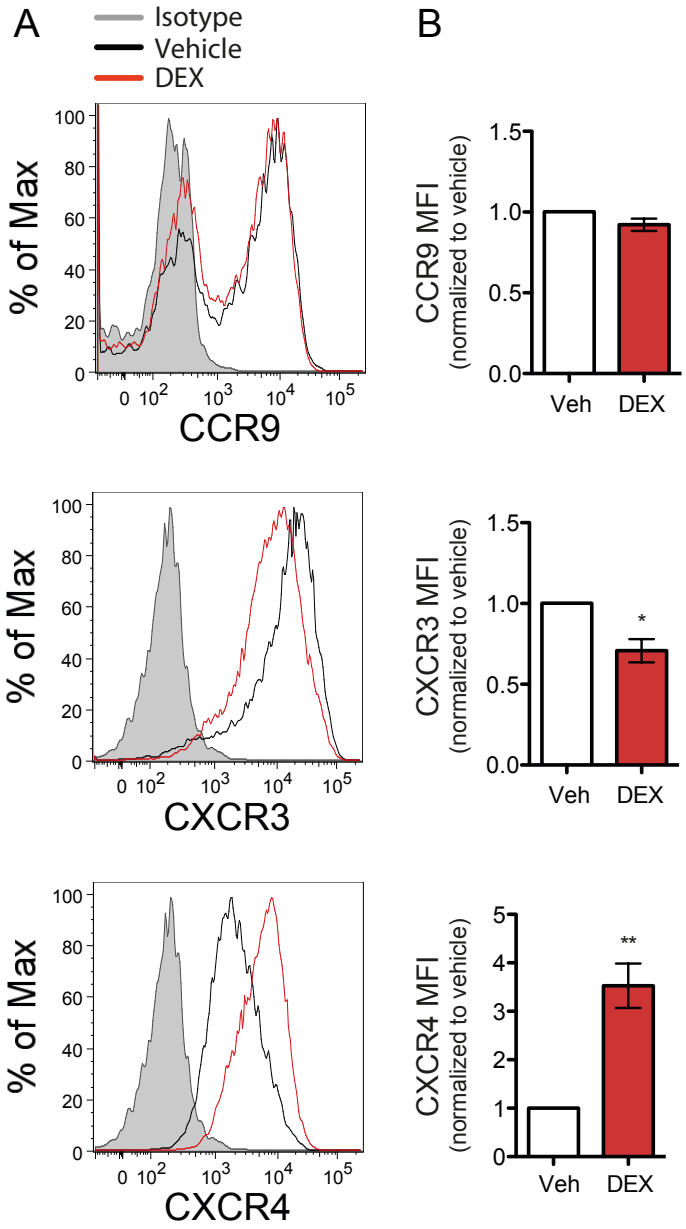


Figure 5.1 Chemokine receptor expression following dexamethasone treatment in ATRA-cultured cells.

ATRA-cultured cells were treated with vehicle (H_20) or 250 nM DEX for 16 hours. Cells were washed and stained for surface chemokine receptor expression, excluding non-viable cells and cell doublets in FlowJo analysis.

A: Histograms are one representative experiment comparing isotype (gray fill), vehicle-treated (black line), and DEX-treated cells (red line).

B: Chemokine receptor surface expression quantified as mean fluorescence intensity (MFI), normalized to vehicle-treated cells.

Graphs show mean values ± SEM from n≥5. *p<0.05, **p<0.01 One-sample t test compared to vehicle.

5.2.3 The effect of dexamethasone on ATRA-cultured cell migration

To measure the effect of GC-treatment on chemokine mediated cell migration, ATRA-cultured cells were treated with 250 nM DEX or vehicle for 16 hours and directed cell migration to buffer, CCL25 (via CCR9), CXCL11 (via CXCR3) or CXCL12 (via CXCR4) were measured by Transwell® chemotaxis. A consistent chemokine concentration to induce cell migration between 75 - 90% of the maximal signal was used: 250 nM CCL25 and 90 nM CXCL11 and 10 nM CXCL12 (see Figure 4.4 & Figure 4.5). DEX-treatment reduced the proportion of viable cells, as measured by Trypan Blue Stain and CellTiter-Glo®, and this was corrected for by adjusting the chemotaxis assay so that equal numbers of live cells were assayed for each condition (see Section 2.6.3).

The proportion of migrated cells was variable between donors (Figure 5.2A), however DEX-treatment consistently reduced CCL25-mediated chemotaxis (48±8% reduction, $p<0.01$), reduced CXCL11-mediated chemotaxis (24±6% reduction, $p<0.05$) and increased CXCL12-mediated chemotaxis (53±21% increase, $p<0.05$) (Figure 5.2B).

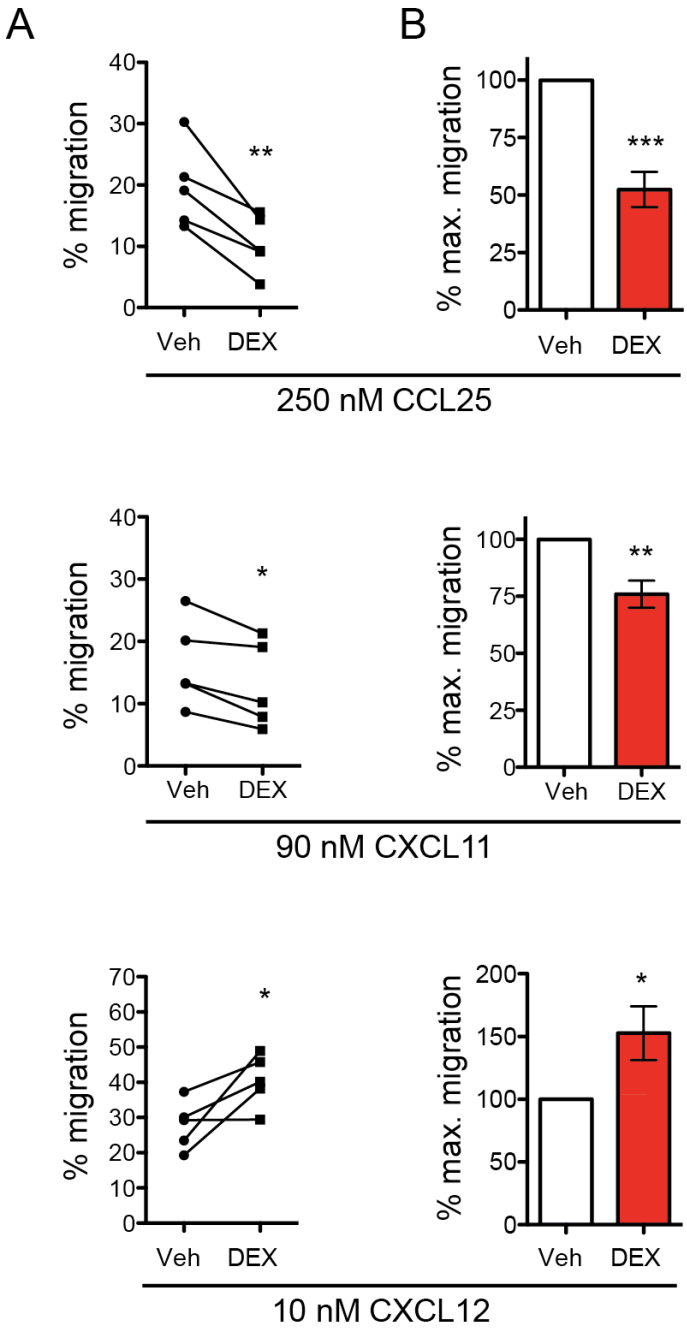


Figure 5.2 Chemokine-mediated cell migration following dexamethasone treatment in ATRA-cultured cells.

ATRA-cultured cells were treated with vehicle (H_20) or 250 nM DEX for 16 hours. Cell migration to buffer, 250 nM CCL25, 90 nM CXCL11 or 10 nM CXCL12 was measured with 96-well, 5 µm pore Transwell® inserts. Following a 2 hour incubation at 37°C, cells in the bottom transwell chamber were quantified by CellTiter-Glo® and verified by Trypan Blue stain.

A: Transwell® chemotaxis shown as % migration (chemokine signal-background/input). Each line depicts a unique experiment.

B: Data from panel A were normalized to vehicle and expressed as % maximum migration, relative to vehicle-treated sample. Graphs shows mean value ± SEM.

*p< 0.05, **p < 0.01, ***p< 0.001 paired t test (A) or One-sample t test compared to vehicle (B).

5.2.4 The effect of dexamethasone on Molt-4 cells

As described in Chapter 4, ATRA-cultured cell are a heterogeneous population of T cells. Elucidating a mechanism by which GCs reduce CCR9-mediated migration while increasing CXCR4-mediated signalling would be less prone to variations if studied in a homogenous population of cells. Therefore the effect of DEX on Molt-4 cells was assessed as a potential for studying CCR9 in a homogenous cell line.

Molt-4 cells were treated with vehicle or 250 nM DEX for 16 hours. CCR9 surface expression was equivalent between vehicle and DEX-treated cells; CXCR4 surface expression was greater in DEX-treated Molt-4 cells, measured by flow cytometry (Figure 5.3A). By comparison with ATRA-cultured cells, DEX-treatment only modestly increased CXCR4 surface expression in Molt-4 cells (3.5 fold increase in ATRA-cultured cells compared to 1.55 fold increase in Molt-4 cells). Vehicle- and DEX-treated cells displayed equivalent migration to CCL25, measured at concentrations ranging from 50–300 nM CCL25 (Figure 5.3B). Despite increased levels of surface CXCR4, CXCL12-mediated chemotaxis was equivalent between vehicle- and DEX-treated cells, measured at 10 nM CXCL12 (Figure 5.3B). From three independent experiments, DEX-treatment had no effect on CCR9- and CXCR4-mediated chemotaxis in Molt-4 cells and therefore could not be used to study the inhibitory effect of GCs on CCR9-mediated signalling and function.

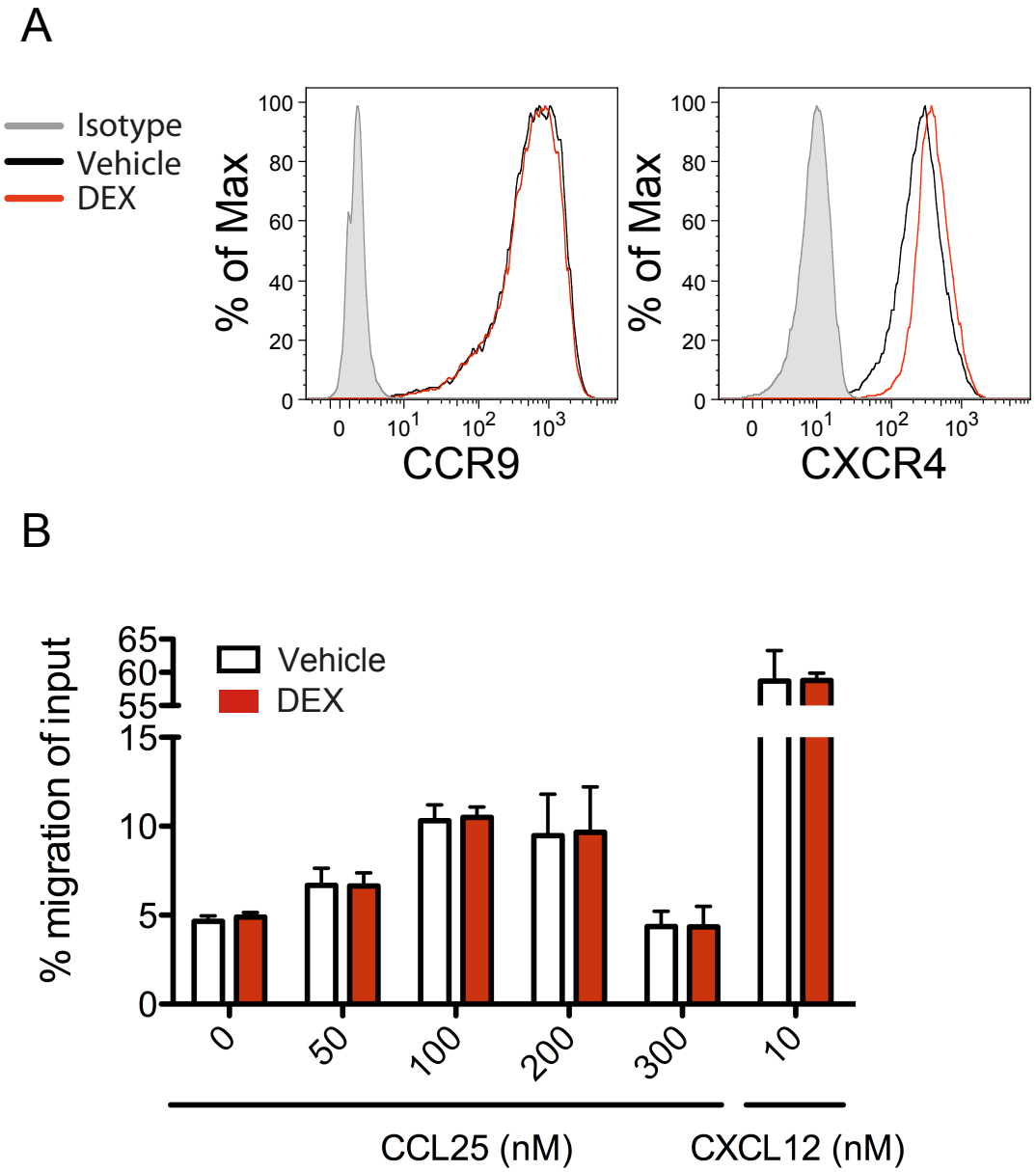


Figure 5.3 Dexamethasone does not affect CCR9- nor CXCR4-mediated cell migration in Molt-4 cells.
Molt-4 cells were treated with vehicle (H_20) or 250 nM DEX for 16 hours. Cell migration to increasing concentrations of CCL25 and 10 nM CXCL12 was measured with 96-well, 5 µm pore Transwell® inserts. Following a 2 hour incubation at 37°C, cells in the bottom transwell chamber were quantified by CellTiter-Glo® and verified by Trypan Blue Stain.
A: Representative histograms comparing the surface receptor expression between isotype (gray fill), vehicle-treated (black line), and DEX-treated cells (red line).
B: Transwell® chemotaxis. Graph shows mean ± SEM of triplicate wells.
Data representative of 3 independent experiments.

5.2.5 Isolation of primary CCR9$^+$ T cells

Having tested two different cell types, there were conflicting results: DEX-treatment reduced CCR9-mediated cell migration in ATRA-cultured cells but had no affect on when measured on Molt-4 cells. To test the effects of DEX on primary human CCR9$^+$ T cells, a protocol for isolating cells by magnetic bead separation was optimized.

From a healthy blood donor, 3 - 5% of circulating T cells express surface CCR9 (Figure 5.4A). From a buffy coat ~8 x 10^8 PBMC were recovered following Ficoll-paque™ PLUS density centrifugation, ~30% of which were CD3$^+$ T cells. Following T-cell isolation and CCR9$^+$ cell magnetic bead selection, 8 – 12 x 10^6 CCR9$^+$CD3$^+$ cells were recovered. From the isolated cells, CD3$^+$ cell purity was greater than 95%, and greater than 70% of CD3$^+$ cells were CCR9$^+$; the sorted population was uniformly CXCR4$^+$ (Figure 5.4B).

5.2.6 Optimizing sorted CCR9$^+$ T cell migration conditions

To test the migratory capacity of isolated CCR9$^+$ T cells, migration to increasing concentrations of CCL25 was measured by Transwell® chemotaxis. Additionally, to optimize the density of cells required to produce a robust migration response, increasing cell densities were loaded, ranging from 12,000 - 400,000 cells per well.

Primary CCR9$^+$ T cells migrated to increasing concentrations of CCL25 with a characteristic bell-shaped dose-response curve, and maximum migration to 250 nM CCL25 (Figure 5.4C). Due to the limited number of cells that could be isolated, a full dose response to CXCL12 was not performed; rather a fixed concentration of 10 nM CXCL12 was used as a positive control. At 10 nM CXCL12, sorted CCR9$^+$ T cells had a robust migration signal (2-3 fold induction over migration to buffer) (Figure 5.4D). Comparison between cell loading densities showed the greatest Transwell® migration response with 400,000 cells per well,

therefore this density of cells was used for subsequent chemotaxis experiments (Figure 5.4C & D).

5.2.7 The effect of dexamethasone on chemokine receptor expression in primary CCR9$^+$ T cells

Sorted CCR9$^+$ cells were treated with vehicle or 250 nM DEX for 16 hours and surface CCR9 and CXCR4 expression were analyzed by flow cytometry. DEX-treatment had no effect on surface expression of CCR9 (measured by MFI) nor the proportion of CCR9$^+$ T cells relative to the total population (Figure 5.5A & B). In contrast, DEX significantly increased surface expression of CXCR4 in all donors, as measured by MFI (2.3±0.36 fold increase, $p<0.05$) (Figure 5.5A & B).

5.2.8 The effect of dexamethasone on chemokine mediated cell migration in primary CCR9$^+$ T cells

Despite equivalent CCR9 surface expression between vehicle and DEX-treated CCR9$^+$ T cells, CCR9-mediated chemotaxis to 250 nM CCL25 was significantly reduced by DEX-treatment (Figure 5.5C). By comparison, CXCR4-mediated migration to 10 nM CXCL12 was either unaffected or increased following DEX-treatment in sorted CCR9$^+$ cells (Figure 5.5C). When independent donors were adjusted for background migration to buffer alone and normalized to vehicle-treatment, DEX treatment reduced CCR9 mediated chemotaxis by 37±4% ($p<0.01$) and increased CXCR4 mediated chemotaxis by 35±20% ($p<0.05$) (Figure 5.5D). These data demonstrate that in primary CCR9$^+$ T cells, a physiologically relevant dose of DEX reduced CCL25-mediated cell migration but these same cells were viable and capable of migrating as demonstrated by the enhanced migration response through co-expressed CXCR4.

5.2.9 The effect of dexamethasone on CD4 and CD8 T cell migration

To determine if the effect of DEX on CCR9- and CXCR4-mediated chemotaxis was preferentially affecting either CD4 or CD8 T cells, the proportion of both populations was examined prior to and following migration to CCL25 or CXCL12. $CCR9^+$ sorted T cells were exclusively single positive CD4 and CD8 T cells, with an average CD4:CD8 ratio of approximately 1.3:1 (see Figure 5.4B). The proportion of CD4 and CD8 positive cells was equivalent between vehicle- and DEX-treated cells (Figure 5.5E). After migration to either CCL25 or CXCL12, the proportions of CD4 and CD8 T cells was similar to the starting population, indicating that the effect of DEX-treatment on CCR9- and CXCR4-mediated migration was equivalent for CD4 and CD8 T cells (Figure 5.5E).

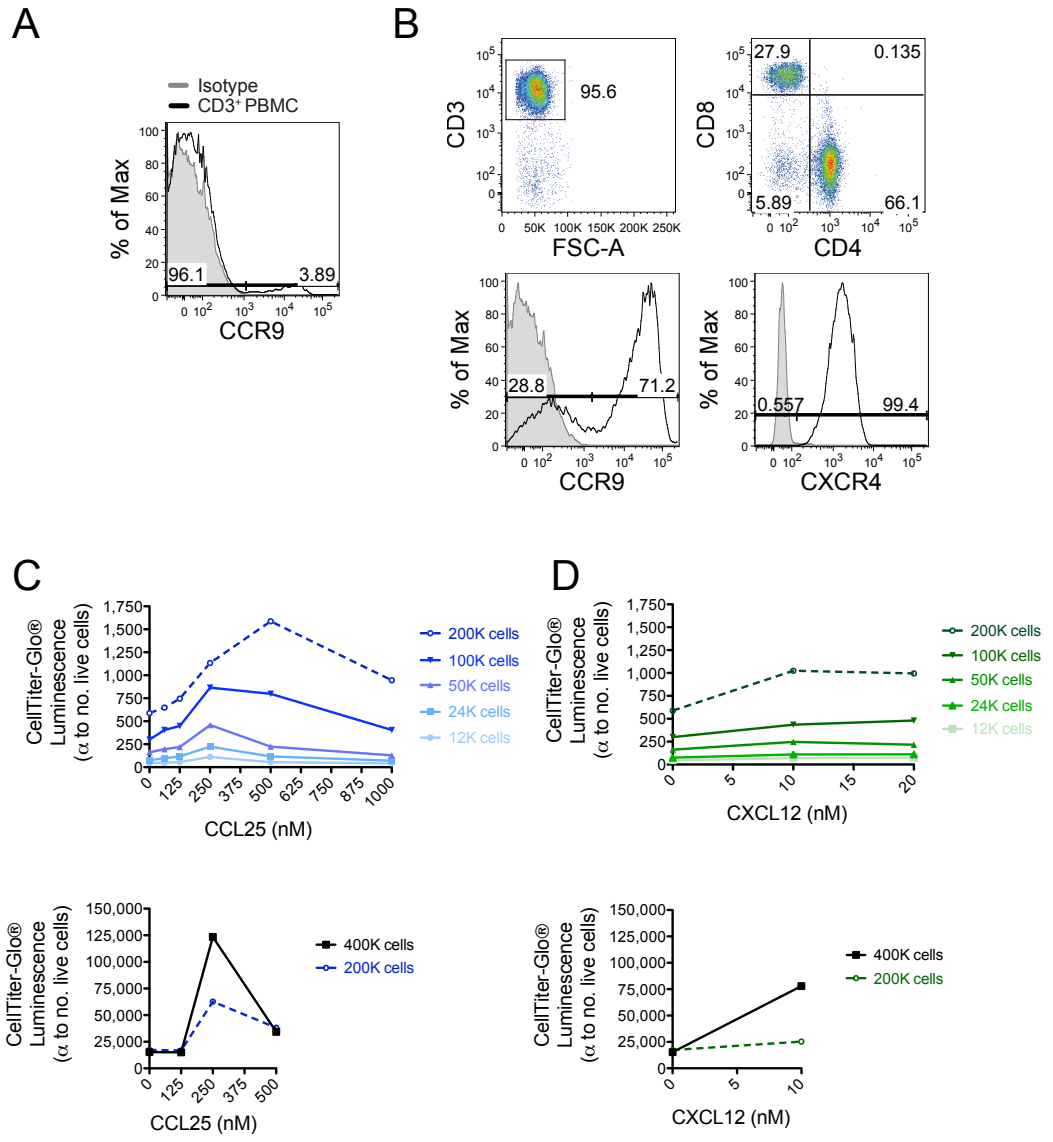


Figure 5.4 Optimizing chemotaxis conditions for primary human CD3$^+$CCR9$^+$ cells. Pilot experiments to determine the optimal number of cells to add per Transwell® insert and the optimal concentration of chemokine ligand to measure cell migration. Primary CD3$^+$CCR9$^+$ cells were isolated by magnetic bead separation. CD3$^+$ cell purity, CD4, CD8 and chemokine receptors expression were analyzed by flow cytometry. Using Transwell® 96-well plate inserts (5 µm pore size), directed cell migration to buffer, increasing concentrations of CCL25 or CXCL12 was assessed following incubation at 37°C for 2 hours.
A: One representative histogram of CCR9 expression in total CD3$^+$ PBMC from a buffy coat blood donor.
B: Surface receptor characterization following CD3$^+$CCR9$^+$ enrichment by magnetic bead separation. Numbers depict the proportion of cells expressing the surface marker of interest. Histograms show one representative example of chemokine receptor expression comparing isotype (gray fill) and CD3$^+$ cells (black line).
C-D: Graphs depict the number of live cells quantified in the bottom chemotaxis chamber by CellTiter-Glo®. Graphs show single data points, due to a restriction on cell number for each assay.

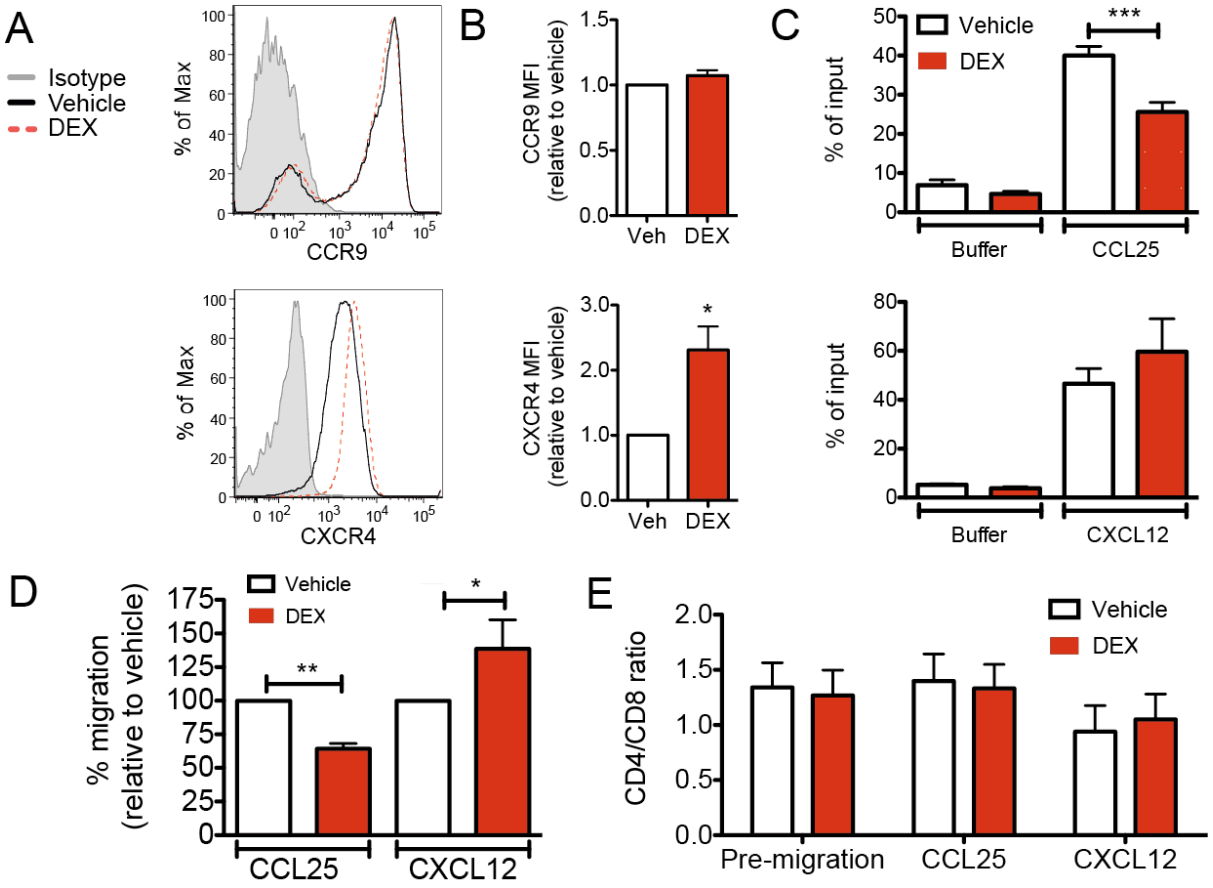


Figure 5.5 The effect of dexamethasone on CCR9 and CXCR4 surface expression and CCR9- and CXCR4-mediated chemotaxis in primary human CCR9$^+$ T cells.
Primary sorted CCR9$^+$ T cells were treated with vehicle (H_20) or 250 nM DEX for 16 hours and surface CCR9 and CXCR4 expression assessed by flow cytometry. Cell migration to buffer, 250 nM CCL25 and 10 nM CXCL12 was measured with 96-well, 5 µm pore Transwell® inserts. Following a 2 hour incubation at 37°C, cells in the bottom transwell chamber were quantified by CellTiter-Glo® and verified by Trypan Blue Stain. The proportion of CD4 and CD8 T cells were quantified by flow cytometry.
A: Surface chemokine receptor expression assessed by flow cytometry. One representative experiment shown.
B: Chemokine receptor mean fluorescence intensity (MFI), normalized to vehicle-treated cells.
C: Chemotaxis to 250 nM CCL25 (upper panel) or 10 nM CXCL12 (lower panel) was measured comparing vehicle- and DEX-treated cells. Data shown as the percent of cells which migrated relative to the input cell number.
D: Data from panel C were adjusted for background (chemokine signal-buffer background) and normalized to the vehicle-treated sample.
E: The proportion of CD4 to CD8 T cells before and after cell migration.
All data shown as mean ± SEM from n ≥ 3 independent experiments.
*p<0.05, **p<0.01, ***p<0.001 One-sample t-test (B), or One-way ANOVA with Bonferroni's post hoc test (C-E).

5.2.10 Calcium assay

Chemokine stimulated intracellular calcium mobilization is a sensitive measurement of chemokine receptor activation [306]. As described in Chapter 4, only $CCR9^+$ cells mount a calcium response to CCL25 while both $CCR9^+$ and $CCR9^-$ cells mobilize intracellular calcium in response to CXCL12 (see Figure 4.10B & C). To examine the effect of DEX on calcium mobilization, a flow cytometry-based assay that allows simultaneous stimulation and monitoring of vehicle- and DEX-treated $CCR9^+$ T cells was designed (Figure 5.6). The yield of primary $CCR9^+$ T cells from peripheral blood was too low to conduct these experiments, therefore ATRA-cultured cells were utilized.

ATRA-cultured cells were treated for with vehicle or 250 nM DEX 16 hours. Cells were separately stained with CCR9 specific murine antibody followed by anti-mouse antibody conjugated to fluorochrome allophycocyanin (APC). To distinguish vehicle- from DEX-treated cells, cells were separately stained with anti-CD3 conjugated to either AlexaFluor700 or APC-Cy7. The CD3 antibodies were of the same clone and could be interchanged without affecting the result. The two populations of cells (vehicle- and DEX-treated) were mixed in a one to one ratio and loaded with Fura Red calcium dye, followed by the live dead cell marker, SYTOX® green (Figure 5.6).

5.2.11 The effect of dexamethasone calcium flux

Analysis of real time calcium mobilization by flow cytometry was performed with FlowJo software. Cells were gated on live cells, excluding cell doublets, gated on $CCR9^+$ cells and vehicle- and DEX-treated cells were distinguished by their distinct CD3 marker (Figure 5.7A). Cell stimulation was performed in a minimum of duplicate samples, monitoring the response to 125 nM CCL25, 10 nM CXCL12 and 5 µg/ml ionomycin (CCL25 concentration optimized in Figure 4.11). Stimulation with ionomycin was included to demonstrate that

vehicle- and DEX-treated cells were evenly loaded with Fura Red dye, and the cells were capable of generating a calcium response.

Figure 5.7B depicts representative real time calcium traces, comparing vehicle- and DEX-treated cells. Figure 5.7C is data pooled from 3 independent experiments, normalized to vehicle-treated cells. In $CCR9^+$ cells, DEX-treatment significantly reduced the total amount of calcium mobilized in response to CCL25-stimulation (28±6% reduction, $p<0.05$). In the same $CCR9^+$ cells, in response to CXCL12, more calcium was mobilized in DEX-treated cells compared to vehicle-treated cells (24±10% increase, $p<0.05$). Ionomycin stimulation confirmed that vehicle and DEX-treated cells were evenly loaded with Fura Red dye and capable of mediating an equivalent calcium response (Figure 5.7C). These data demonstrate that live, $CCR9^+$ T cells treated with DEX have an impaired response to CCL25 while the same cells have an enhanced calcium response when stimulated through co-expressed CXCR4.

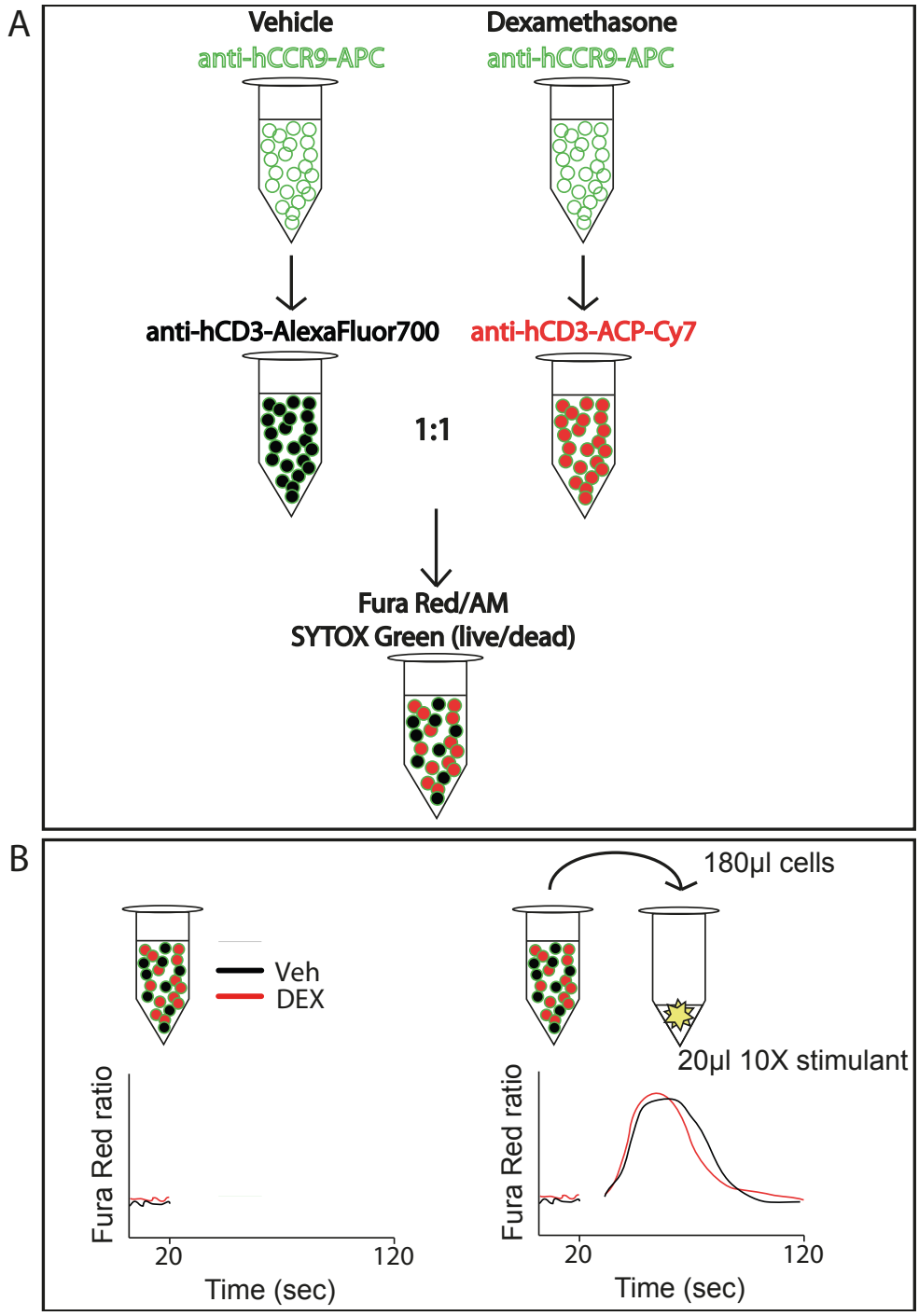


Figure 5.6 Calcium assay design to simultaneously monitor vehicle- and dexamethasone-treated T cells.
ATRA-cultured cells were treated with vehicle (H_20) or 250 nM DEX for 16 hours. To simultaneously measure the calcium flux in vehicle- and DEX-treated cells, the following and flow cytometry protocol was designed.
A: Staining protocol (see Section 2.7.4).
B: Real time calcium data acquisition protocol. Baseline calcium flux was recorded for 25 seconds before cells were transferred to an aliquot of stimulant (chemokine or ionomycin). Recording by flow cytometry was continuous for 120 seconds in total.

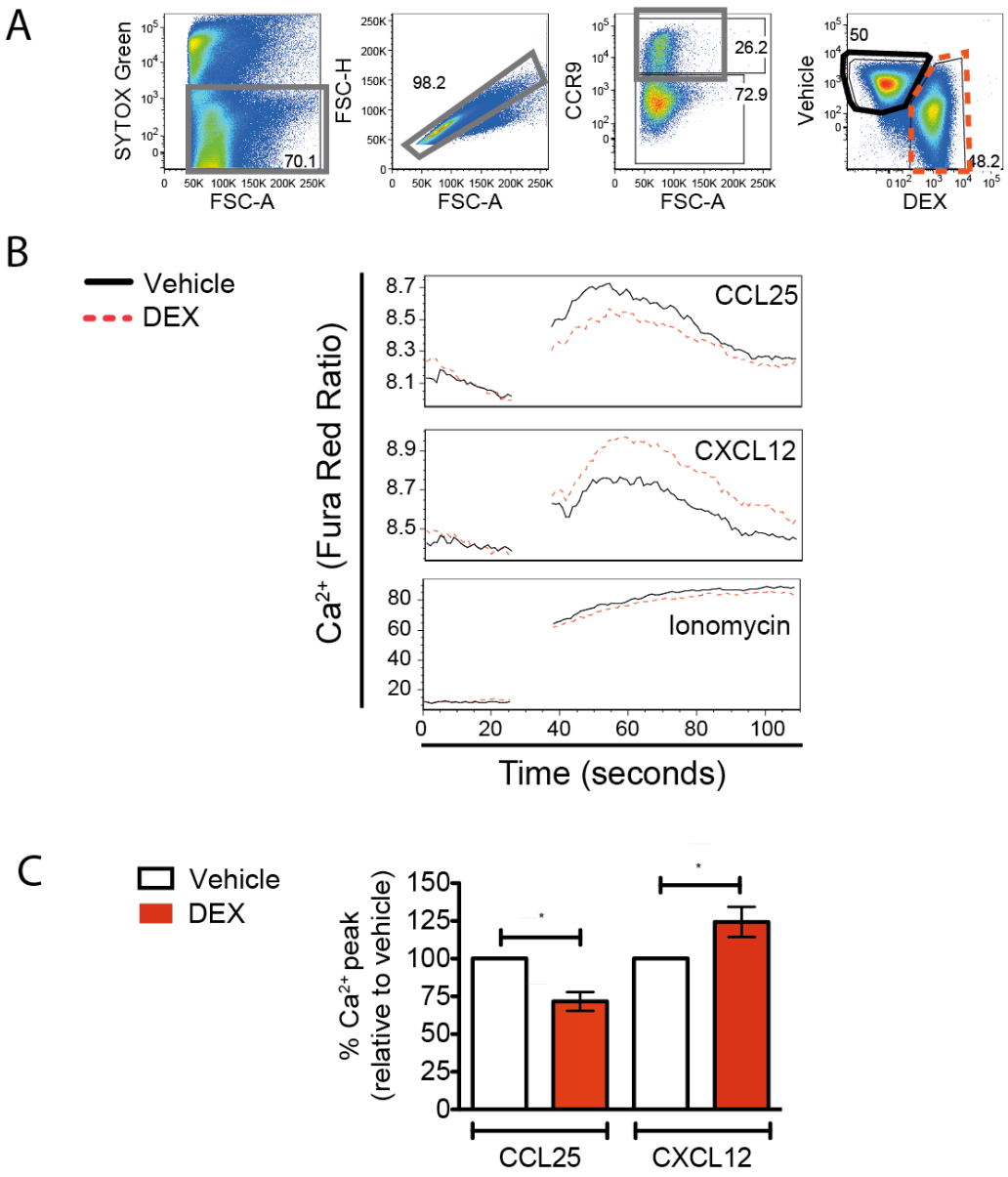


Figure 5.7 Dexamethasone reduces CCL25-mediated calcium flux in CCR9$^+$ T cells.
ATRA-cultured cells were treated with vehicle (H_20) or 250 nM DEX for 16 hours. Cells were stained for surface antigens and loaded with Fura Red calcium dye. Real time calcium mobilization was measured by flow cytometry in CCR9$^+$ cells in response to 125 nM CCL25, 10 nM CXCL12 or 5 ug/ml ionomycin as a positive control.
A: Gating strategy for flow cytometry analysis: live cells (SYTOX® Green$^-$), single stained cells (FSC-H vs FSC-A), CCR9$^+$. Vehicle and DEX-treated cells were selectively gated based upon CD3 antibodies conjugated to distinct fluorochromes.
B: Representative examples of real time calcium flux data. Fura red ratio was calculated as a ratio of QDot655/PE-Cy5.5. Units are arbitrary. Background, non-specific calcium flux was recorded for 25 seconds before the addition of stimulant.
C: Calcium data was quantified as (peak-mean background) and normalized to vehicle-treated sample. Graph shows mean values ± SEM from three independent experiments, run in a minimum of two technical replicates.
*p<0.05 One-way ANOVA with Bonferroni's post hoc test.

5.2.12 The effect of corticosteroids on CCR9-mediated chemotaxis

To test if the effect of DEX on CCR9-mediated migration was shared by another clinically relevant GC, the effects of prednisolone, a corticosteroid with GC activity and minimal mineralocorticoid activity was assessed [364]. As a comparison, the effect of deoxycorticosterone, a corticosteroid with pure mineralocorticoid activity was also assessed [364]. The majority of described effects by GCs require gene modification (requiring >6 hours of steroid treatment) however non-genomic, rapid effects have also been described [367]. To test if the effect of DEX on CCR9-mediated migration was the result of rapid, non-genomic effects, ATRA-cultured cells were treated with DEX for 1 hour and compared to 16 hours of DEX treatment.

The proportion of CCR9 expressing cells and CCR9 MFI were equivalent between all conditions (Figure 5.8A). CXCR4 MFI increased following DEX and PRED treatment (16 hours) but was unaffected by deoxycorticosterone (16 hours) or 1 hour DEX-treatment (Figure 5.8A). The effect of DEX on CCR9-mediated chemotaxis in ATRA-treated cells was reproduced by 16 hours of treatment with prednisolone (35±11% reduction, $p<0.05$), while 1 hour DEX-treatment and deoxycorticosterone had no effect (Figure 5.8B). These results indicate that steroids with glucocorticoid activity but not mineralocorticoid activity inhibit CCR9-mediated cell migration. To substantiate this observation, the effect of glucocorticoid receptor antagonist treatment was examined.

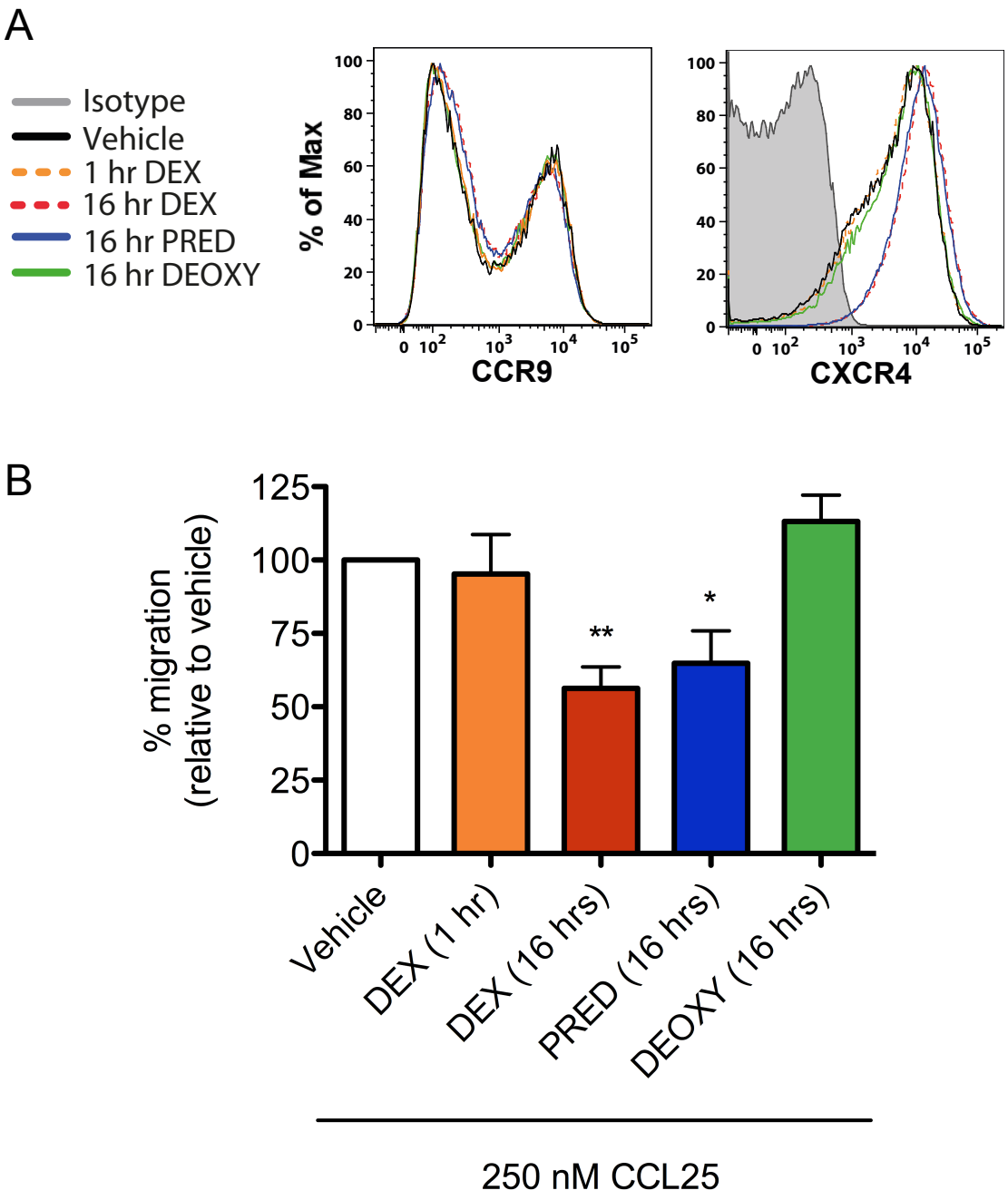


Figure 5.8 Corticosteroids with glucocorticoid and not mineralocorticoid activity reduce CCR9-mediated cell migration.
ATRA-cultured cells were treated with steroid for the indicated amount of time: 250 nM dexamethasone (DEX), 1 µM prednisolone (PRED) or 1 µM deoxycorticosterone (DEOXY). DEX is a pure glucocorticoid. PRED has mixed glucocorticoid and mineralocorticoid activity. DEOXY is a pure mineralocorticoid.
A: Surface chemokine receptor expression by flow cytometry. One representative experiment shown.
B: Chemotaxis to 250 nM CCL25. Graphs show mean ± SEM from n≥3. *p<0.05, **p<0.01 One-way ANOVA with Dunnett's post hoc test compared to vehicle-treated cells.

5.2.13 The effect of mifepristone on chemokine receptor expression

Mifepristone (MIF) is a competitive glucocorticoid receptor and progesterone receptor antagonist [364]. MIF treatment is demonstrated to inhibit GC mediated changes to CXCR4 surface expression and function [361,359]. A titration of mifepristone was performed, measuring cell viability and CXCR4 surface expression to determine the minimum concentration necessary to inhibit GC activity in ATRA-cultured cells.

ATRA-treated cells were pre-treated for 1 hour with increasing concentrations of MIF, followed by 16 hours of 250 nM DEX-treatment. Concentration of MIF from 250 nM – 10 μM had no effect on cell viability (Figure 5.9A). 250 nM DEX reduced cell viability by 29% but was inhibited by concentrations of MIF ≥ 500 nM (Figure 5.9A). MIF inhibited DEX-induced increases to CXCR4 MFI in a dose dependent manner, with maximum inhibition observed with ≥5 μM mifepristone (Figure 5.9B), therefore 5 μM MIF was used in all subsequent assays.

To determine if the effects of DEX on CCR9 function were mediated by activation of the GCR, ATRA-cultured cells were treated with vehicle or 250 nM DEX in the presence or absence of MIF (added 1 hour prior to DEX). Surface CCR9 and CXCR4 protein were quantified by flow cytometry and CCL25- or CXCL12-mediated chemotaxis assessed by Transwell® chemotaxis.

Figure 5.10A shows one representative example of CCR9 and CXCR4 surface expression following steroid treatment, demonstrating that the proportion of $CCR9^+$ and $CXCR4^+$ cells were equivalent between all steroid treatments. By itself, MIF had no effect on surface expression of CCR9 nor CXCR4 (Figure 5.10B). Vehicle- and DEX-treated cells had equivalent CCR9 surface expression. DEX-treatment significantly increased CXCR4 surface protein (3±0.5 fold increase, $p<0.001$; Figure 5.10B). Cells co-incubated with DEX and MIF

had CCR9 and CXCR4 surface expression comparable to vehicle-treated sample (Figure 5.10B). These results demonstrate that 5 μM mifepristone was effective at inhibiting GC-mediated induction of CXCR4 surface expression without affecting levels of CCR9 surface protein.

5.2.14 The effect of mifepristone on chemokine mediated cell migration

MIF-treatment alone did not affect on ATRA-cultured cell chemotaxis to neither CCL25 nor CXCL12 (Figure 5.10C). DEX-treated cells had reduced migration to CCL25 as compared to vehicle-treated cells (43±14% reduction, $p<0.05$). In contrast, DEX-treated cells had enhanced migration to CXCL12 compared to vehicle-treated cells (69±23% increase, $p<0.05$). MIF in combination with DEX, completely reversed the effect of DEX on CCR9- and CXCR4-mediated chemotaxis in ATRA-cultured cells (Figure 5.10C). These results are in accordance with previous work indicating that mifepristone inhibits GC induced increases to CXCR4 surface expression and CXCL12-mediated cell migration [361,359]. These data also demonstrate that CCR9-mediated cell migration is reduced by DEX-treatment and this effect is mediated through activation of the glucocorticoid receptor.

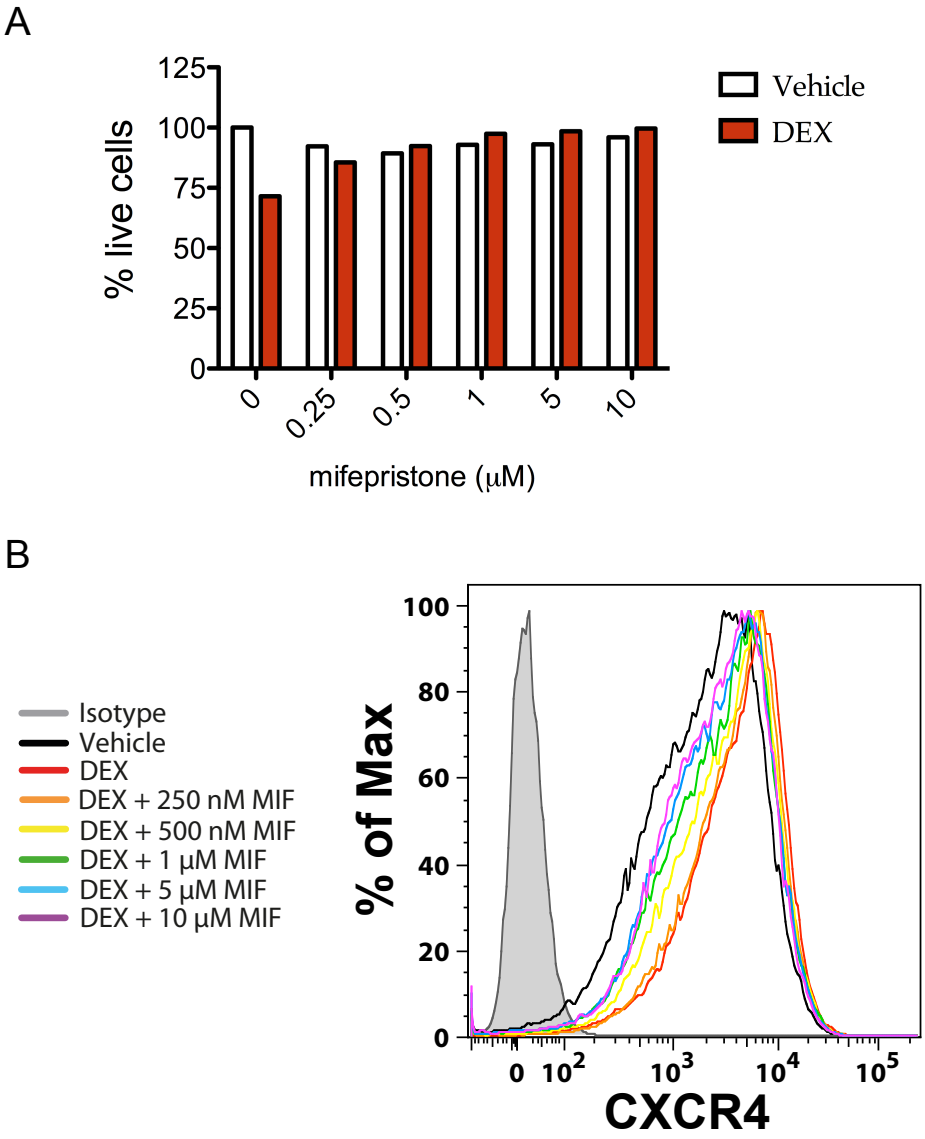


Figure 5.9 Titrating mifepristone (MIF) on ATRA-cultured cells.
Pilot experiment to determine optimal MIF dosing. ATRA-cultured cells were pretreated with MIF for 1 hour followed by the addition of 250 nM DEX for an additional 16 hours of treatment. Cell viability was measured by CellTiter-Glo® and surface CXCR4 expression measured by flow cytometry.
A: Cell viability. Data normalized to vehicle-treated cells.
B: CXCR4 surface expression comparing vehicle-treated cells (black line), DEX-treated cells (red line) with increasing concentrations of mifepristone.

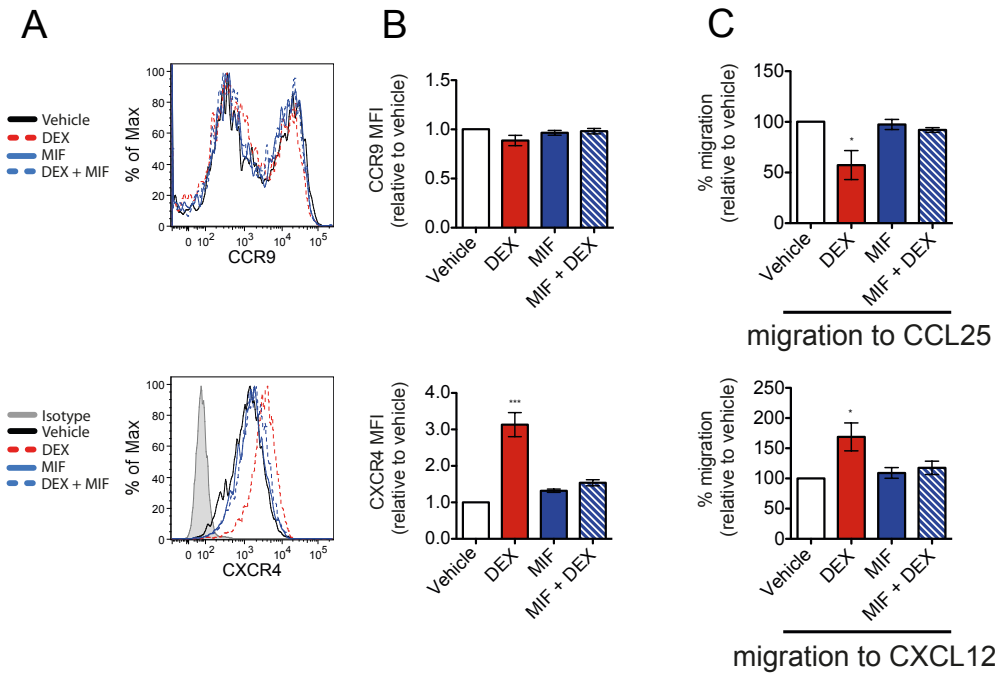


Figure 5.10 The effect of mifepristone on CCR9 and CXCR4 receptor expression and receptor-mediated chemotaxis.

ATRA-cultured cells were treated with vehicle (H_20) or 250 nM dexamethasone (DEX) for 16 hours, in the presence or absence of 5 μM mifepristone (MIF), a GC receptor antagonist. CCR9 and CXCR4 surface expression were measured by flow cytometry. Cell migration to buffer, 250 nM CCL25 or 10 nM CXCL12 was measured with 96-well, 5 μm pore Transwell® inserts. Following a 2 hour incubation at 37°C, cells in the bottom transwell chamber were quantified by CellTiter-Glo® and verified by Trypan Blue Stain.

A: Representative flow cytometry histograms show the proportion of CCR9 and CXCR4 positive cells.

B: Effect of DEX and MIF on cell surface expression (mean fluorescence intensity) of CCR9 and CXCR4 by flow cytometry. Data normalized to vehicle-treated cells.

C: Pooled data from 3 independent experiments analyzing migration towards CCL25 (upper panel) or CXCL12 (lower panel). Data shown as percent migration relative to vehicle-treated cells. All data shown as mean value ± SEM.

*p<0.05, ***p<0.001 One-way ANOVA with Dunnett's post hoc test (B&C) compared to vehicle-treated cells.

5.2.15 The effect of dexamethasone on CCL25-mediated CCR9 internalization

To test if DEX-treatment affected CCL25-mediated CCR9 internalization, ATRA-cultured cells were treated with vehicle or 250 nM DEX for 16 hours and CCR9 surface expression measured following one hour incubation with increasing concentrations of CCL25. As previously described (see Figure 4.7), CCL25 induced CCR9 surface internalization in a dose dependent manner with complete receptor internalization following 1 hour incubation with 250 nM CCL25 (Figure 5.11A). Internalization was prevented when cells were treated with the same dose of CCL25 at 4°C (Figure 5.11B).

DEX-treatment increased expression of surface CXCR4 (Figure 5.11C). CCL25-mediated CCR9 internalization was equivalent between vehicle- and DEX-treated cells measured by the proportion of cells expressing CCR9 (Figure 5.11D) and CCR9 MFI (Figure 5.11E). Collectively these results show that although CCL25-mediated intracellular calcium flux and chemotaxis are impaired by DEX, cells are still able to interact with CCL25 and undergo ligand induced CCR9 internalization.

5.2.16 Phospho-kinase array of $CCR9^+$ ATRA cultured cells ± CCL25

Intracellular signalling downstream of CCR9 in ATRA-cultured cells is not described. To identify phosphorylated kinases downstream of CCR9 activation, $CCR9^+$ ATRA-cultured cells were sorted by magnetic bead separation and stimulated with CCL25 for five minutes (Figure 5.12A). Cell lysates were prepared and an equivalent amount of protein analyzed on a commercially available phospho-kinase array (Figure 5.12B). In a single experiment, phosphorylation of 46 targets were analyzed, 12 targets were phosphorylated, one of which was PLC-γ1 (Figure 5.12C).

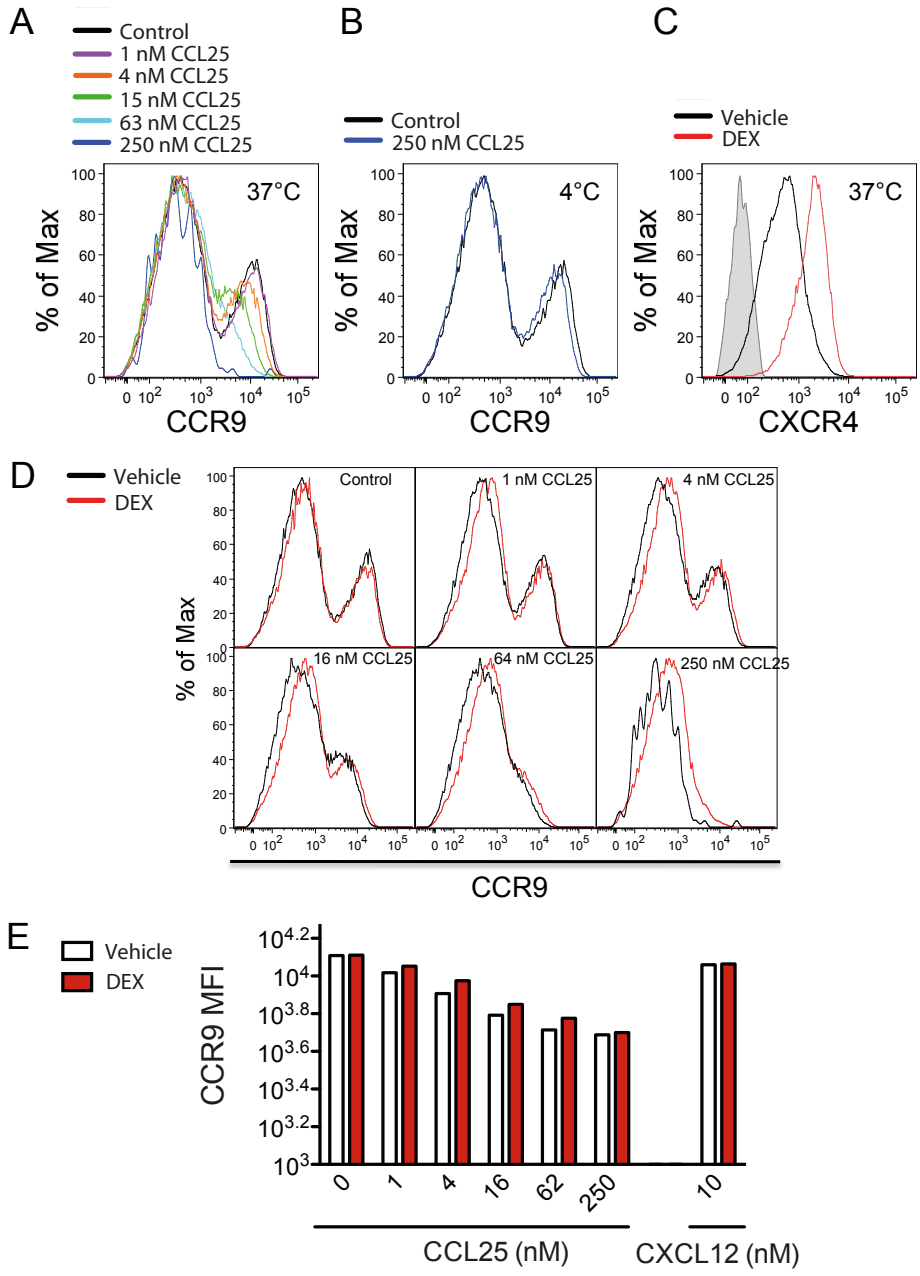


Figure 5.11 Dexamethasone has no effect on CCL25-mediated CCR9 internalization.
A: ATRA-cultured cells incubated for 1 hour at 37°C
B: ATRA-cultured cells incubated for 1 hour at 4°C.
C-E: ATRA-cultured cells were treated with vehicle (H_20) or 250 nM DEX for 16 hours. Cells were washed 3X and an equivalent number of live (as determined by Trypan Blue stain) vehicle- and DEX-treated cells were incubated with chemokine for 1 hour. Cells were washed 3X and surface chemokine receptor expression measured by flow cytometry. Dead cells (SYTOX® Green$^+$) and cell doublets were excluded from analysis.
D: Flow cytometry histograms show the proportion of CCR9 positive cells.
E: Data from D depicted as CCR9 mean fluorescence intensity (MFI).
One representative example from 2 independent experiments shown.

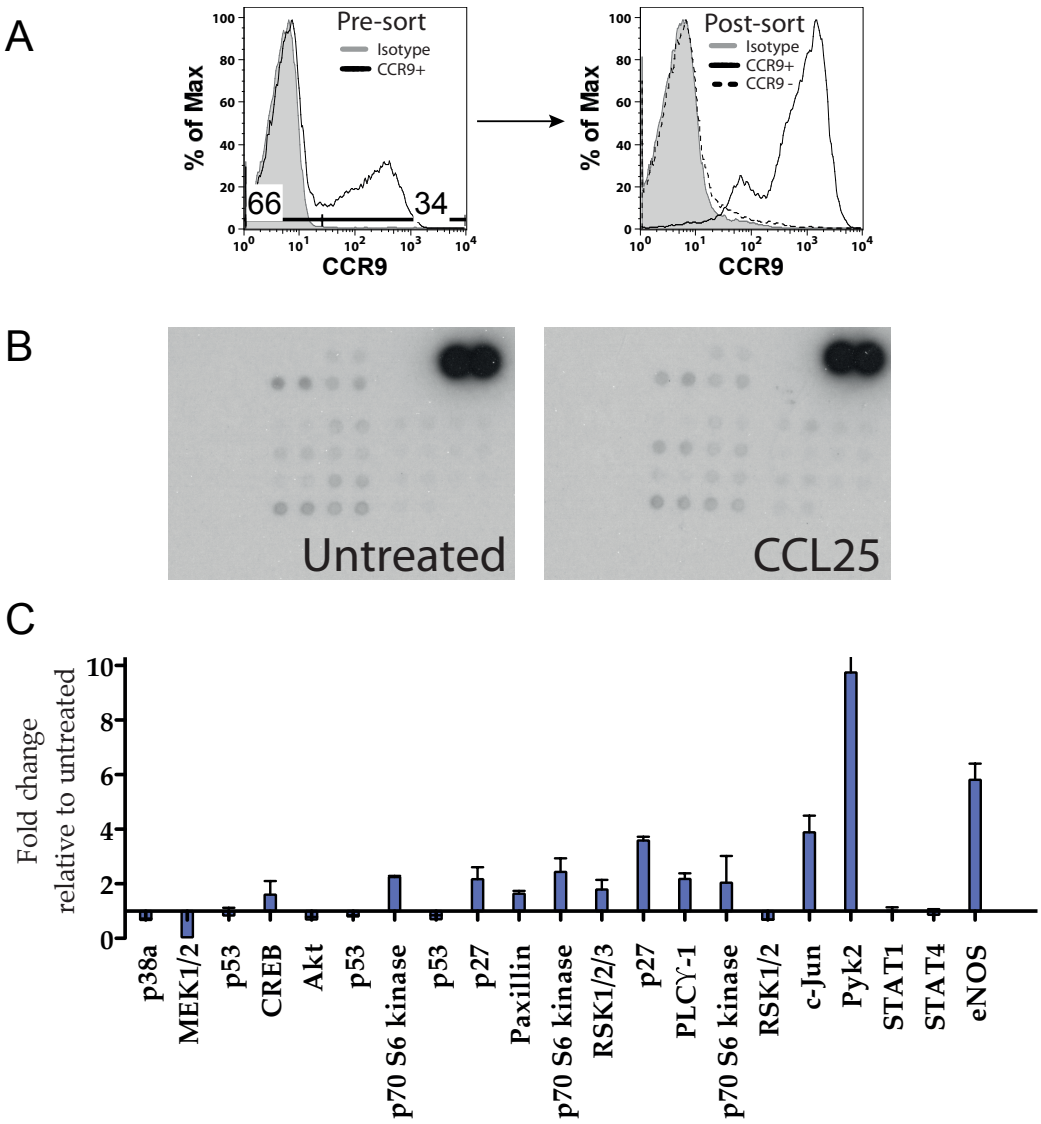


Figure 5.12 Phospho-kinase array of CCR9$^+$ T cells ± CCL25.
CCR9$^+$ ATRA-cultured cells were sorted by magnetic bead separation. Cells were stimulated with 250 nM CCL25 for 5 minutes, washed and prepared as protein lysates for analysis. Antibodies specific to phosphorylated kinase proteins are arranged in duplicates on a nitrocellulose membrane. Cell lysates are incubated on the membrane and visualized by chemiluminescence to detect the levels of target protein.
A: ATRA-cultured cells prior to and following CCR9$^+$ separation by magnetic bead selection.
B: Phospho-kinase blots. Spots in the top right corner are loading controls to ensure an equivalent amount of protein were analyzed between samples.
C: Quantification of phospho-kinase array by densitometry. Graph shows the phophorylation of kinase proteins following CCL25 stimulation relative to untreated cells.

5.2.17 The effect of dexamethasone on total PLCγ1 and phospho-PLC-γ1

To examine the effect of DEX on a signalling element downstream of chemokine stimulation and upstream of calcium mobilization and cell chemotaxis (see Section 1.2.3), the effect of DEX on phosphorylation of PLC-γ1 (P-PLCγ1) was assessed by Western blotting. As a positive control, CD3/CD28 stimulation was included; TCR-stimulation induces transient P-PLCγ1 and this is inhibited by GC treatment [277]. It has been previously demonstrated that CXCL12 does not stimulate phosphorylation of PLC-γ1, measured in Jurkat T cells and was therefore not included in the present analysis [368].

$CCR9^+$ ATRA-treated cells were sorted by magnetic bead separation and treated with vehicle or 250 nM DEX for 16 hours. An equivalent number of live cells were treated with buffer, 250 nM CCL25, or anti-CD3/anti-CD28 for the indicated amount of time. Cells were washed and processed for analysis by Western blotting, taking care to analyze equivalent amounts of protein (see Section 2.14).

In two preliminary experiments, CCL25 induced P-PLCγ1 at 5 minutes but was undetected by 10 minutes (Figure 5.13A). In accordance with previous reports, anti-CD3/anti-CD28 stimulated P-PLCγ1 and was inhibited by DEX-treated (Figure 5.13A) [277]. Although levels of β-actin were consistent between samples, following DEX-treatment total PLC-γ1 was reduced relative to β-actin (Figure 5.13B). Following CCL25 treatment, P-PLCγ1 was detected in untreated cells but was absent in DEX-treated cells (Figure 5.13C). Collectively these preliminary results (n=2) showed that DEX reduced total PLCγ1 protein and additionally reduced levels of CCL25 stimulated P-PLCγ1 in $CCR9^+$ ATRA-cultured cells.

5.2.18 The effect of dexamethasone on PLCγ1 mRNA

To substantiate the observation that DEX reduced total PLCγ1, levels of PLC-γ1 mRNA were assessed. As a control, CXCR4 mRNA was quantified, which is demonstrated to

increase following DEX-treatment [360]. Sorted CCR9$^+$ ATRA-cultured cells were treated with vehicle or DEX for 16 hours, and cell lysates were measured by qRT-PCR relative to GAPDH.

CCR9 mRNA levels were comparable between vehicle and DEX-treated cells (Figure 5.14A) and in accordance with previous reports, DEX increased CXCR4 mRNA expression ($p<0.05$, Figure 5.14B) [360]. In contrast to CCR9 and CXCR4 mRNA, PLC-γ1 was detected at very low levels; in two of four samples, PLC-γ1 mRNA could not be detected. In two remaining samples, results were split: one donor had decreased PLC-γ1 following DEX treatment while the other had increased levels (Figure 5.14C). Further experiments are necessary to study the effect of DEX on total PLC-γ1 protein and activation downstream of CCL25 stimulation.

5.2.19 CCRL1 expression by CCR9$^+$ T cells

CCR9 is the single identified signalling receptor for CCL25. CCL25 also binds the atypical, non-signalling receptor, CC receptor like 1 (CCRL1). CCRL1 is described as a decoy, scavenging receptor which specifically binds CCL19, CCL21 and CCL25 [369]. Human CCRL1 specific antibody is not available, limiting characterization to detection of mRNA. CCRL1 mRNA is found in the human heart, colon, small intestine and lung [370]. In mice, CCRL1 expression is described on non-hematopoietic cells including stromal cells and epithelial cells [371], and Gosling *et al* (2000) showed CCRL1 RNA in one of two human T cell donors and one T cell donor activated by PHA [369]. To explore a potential mechanism by which GCs impair CCL25 mediated signalling, I was interested to test if CCR9$^+$ T cells expressed CCRL1, and if DEX could modulate expression.

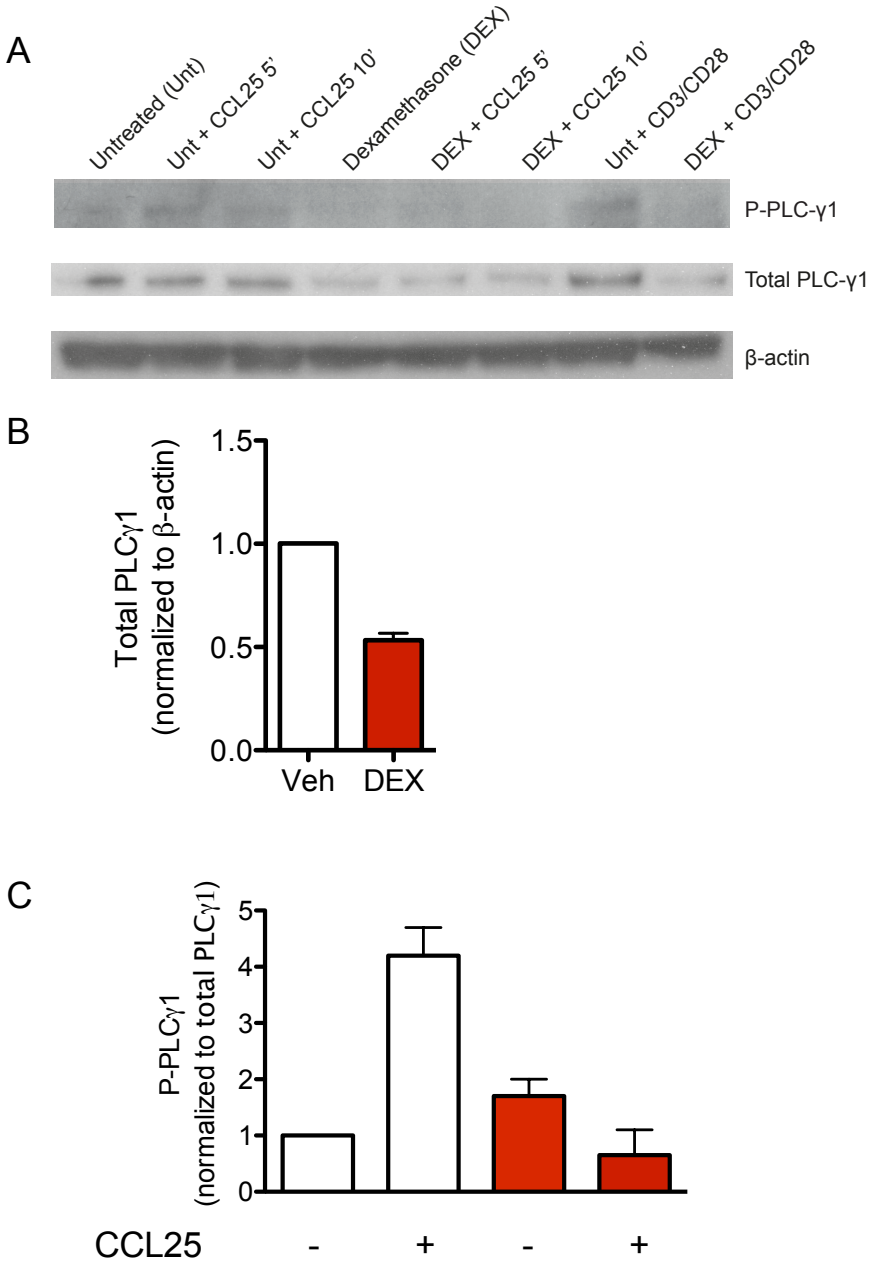


Figure 5.13 Dexamethasone reduces total PLCγ1 and CCL25-stimulated P-PLCγ1 in CCR9$^+$ T cells

CCR9$^+$ ATRA-cultured cells were sorted by magnetic bead separation. Cells were treated with vehicle (H_20) or 250 nM DEX for 16 hours. Cells were washed and stimulated with 250 nM CCL25 or 5 μg/mL CD3/CD28 for the indicated duration of time. Cells were washed and immediately made into cell lysates for quantification by Western blot. Analysis of P-PLCγ1, total PLC and β-actin were quantified by densitometry.

A: Representative Western blot.

B: Total PLCγ1 normalized to β-actin (samples in the absence of stimulation).

C: CCL25-stimulated PLCγ1 phosphorylation in the presence and absence of DEX-treatment normalized to total PLCγ1.

Data pooled from 3 independent experiments (B - C).

*p<0.05, **p<0.01 One-sample t test (B) or One-way ANOVA with Dunnet's post hoc test (C).

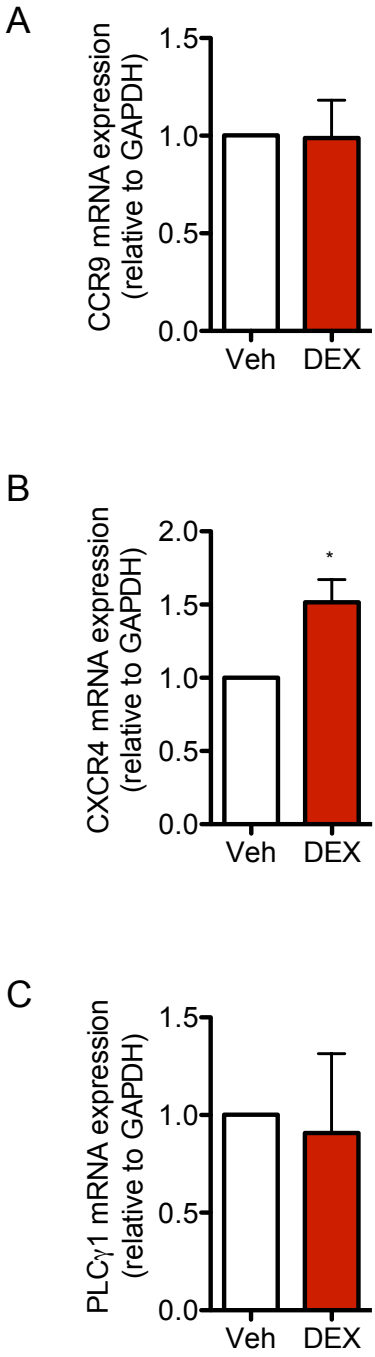


Figure 5.14 Effect of dexamethasone on PLCγ1 mRNA in CCR9$^+$ T cells.
CCR9$^+$ ATRA-cultured cells were sorted by magnetic bead separation. Cells were treated with vehicle (H_20) or 250 nM DEX for 16 hours. Cells were washed, RNA isolated and cDNA made by reverse transcription using 1 µg RNA. Quantitative real time PCR was performed using SYBR Green reagent measuring gene expression relative to the housekeeping gene, GAPDH. Data normalized to vehicle-treatment.
A: CCR9 mRNA *(n=4)*
B: CXCR4 mRNA *(n=4)*
C: PLCγ1 mRNA *(n=2)*
Graphs show mean ± SEM from specified number of independent experiments. *p<0.05 One sample t test.

$CCR9^+$ cells were sorted from ATRA-cultured cells by magnetic bead separation and CCRL1 mRNA expression measured in $CCR9^+$ and $CCR9^-$ ATRA-cultured cells relative to GAPDH. As a positive control for CCRL1 expression, human intestinal tissue (from tissue biopsies) was analyzed [372].

By qRT-PCR, $CCR9^+$ ATRA-cultured cells expressed CCRL1 mRNA and $CCR9^-$ cells did not ($p<0.001$; Figure 5.15). The relative amount of CCRL1 from $CCR9^+$ T cells was significantly greater than small intestinal biopsies (46 fold increase, $p<0.01$, Figure 5.15). Colonic biopsy tissue (three independent samples) did not have detectable levels of CCRL1 mRNA. These results are a novel observation that $CCR9^+$ T cells express the non-signalling, scavenger receptor, CCRL1, assessed by mRNA.

5.2.20 The effect of dexamethasone on CCRL1 expression in human $CCR9^+$ T cells

Having identified that $CCR9^+$ T cells express CCRL1 mRNA, the effect of DEX-treatment on CCRL1 expression was assessed. $CCR9^+$ ATRA-cultured cells were sorted by magnetic bead separation and treated with vehicle or 250 nM DEX for 16 hours. Cell lysates were measured for CCRL1 mRNA levels relative to GAPDH. As a control for GC treatment, CXCR4 mRNA was measured. In four independent cell preparations, vehicle- and DEX-treated cells had equivalent CCRL1 mRNA expression while CXCR4 mRNA was significantly increased ($p<0.05$, Figure 5.16A & B). Therefore the reduced CCR9 signalling following DEX-treatment could not be attributed to elevated expression of the CCL25 scavenging receptor, CCRL1 measured by mRNA expression.

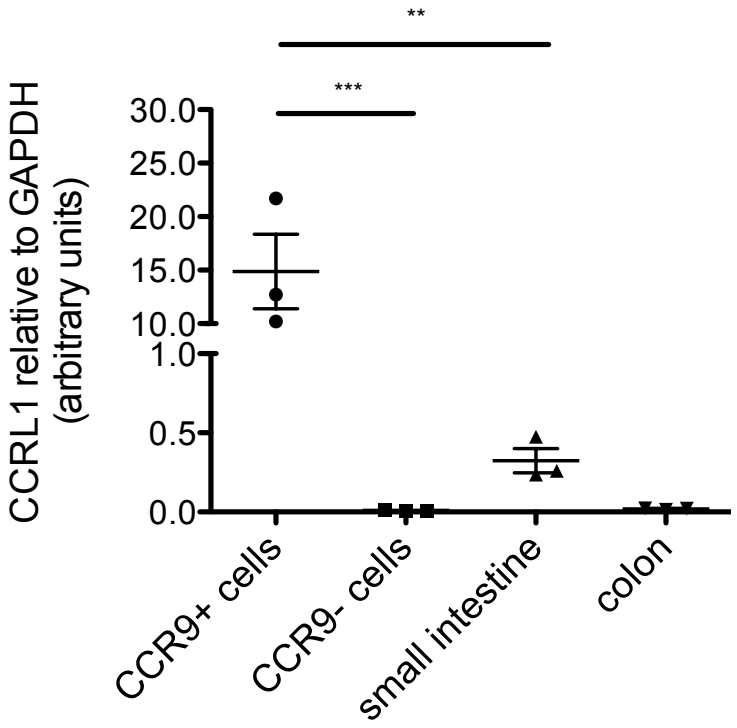


Figure 5.15 CCR9$^+$ ATRA-cultured cells express CCRL1 mRNA.
CCR9$^+$ ATRA-cultured cells were sorted by magnetic bead separation. Cell lysates were analyzed by qRT-PCR, measuring CCRL1 transcripts relative to the housekeeping gene, GAPDH. Intestinal tissue from inflamed samples. Intestinal tissue was used as a positive control and obtained from whole biopsy material. Data shows mean ± SEM. **p<0.01, ***p<0.001 One-way ANOVA with Bonferroni's post hoc test.

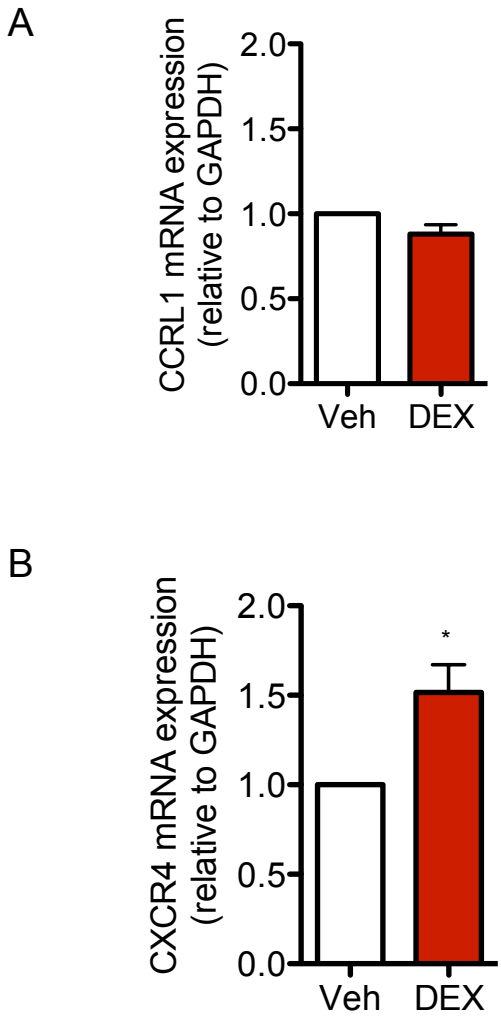


Figure 5.16 The effect of dexamethasone on CCRL1 mRNA expression.
$CCR9^+$ ATRA-cultured cells were sorted by magnetic bead separation. Cells were treated with vehicle (H_20) or 250 nM DEX for 16 hours. Cells were washed, RNA isolated and cDNA made by reverse transcription using 1 µg RNA. Quantitative real time PCR was performed using SYBR Green reagent measuring gene expression relative to the housekeeping gene, GAPDH. Data normalized to vehicle-treatment.
A: CCRL1 mRNA.
B: CXCR4 mRNA (positive control for DEX-treatment)
Graphs show mean value ± SEM from data normalized to vehicle sample (n=4). *$p<0.05$ One sample t test.

5.3 Discussion

The results from this chapter show that glucocorticoids differentially modulate chemokine receptor expression and function, demonstrated in ATRA-cultured cells and primary sorted $CCR9^+$ T cells. Using assays to measure chemokine mediated cell migration, intracellular calcium mobilization and phophorylation of PLCγ1, I demonstrate that DEX significantly inhibits CCL25 mediated CCR9 signalling. These effects were not associated with changes in CCR9 mRNA expression, surface protein presentation nor the ability of CCL25 to stimulate CCR9 internalization. This is the first report of such activity on CCR9 function; *in vivo* this effect could impair intestinal homing of T cells, and provide a further mechanistic basis for the therapeutic activity of GC in IBD.

My data confirms previous reports that GCs increase CXCR4 surface expression and CXCL12 mediated calcium flux and chemotaxis [358-361,363]; effects which were in stark contrast to the reduction in CCR9-mediated signalling. Therefore, although CCR9 mediated signalling was impaired, the cells were viable and capable of functioning through co-expressed chemokine receptor, CXCR4. The effects of DEX on CCR9 and CXCR4 were reproduced by prednisolone and abrogated by the GC receptor antagonist, mifepristone, while the pure mineralocorticoid agonist deoxycorticosterone did not affect CCR9-mediated chemotaxis. Collectively these results demonstrate that steroids with glucocorticoid activity interfere with the function of CCR9 on human T cells and this effect is not a general consequence of all corticosteroid activity. Figure 5.17 is a schematic compiling the experimental observations from this chapter.

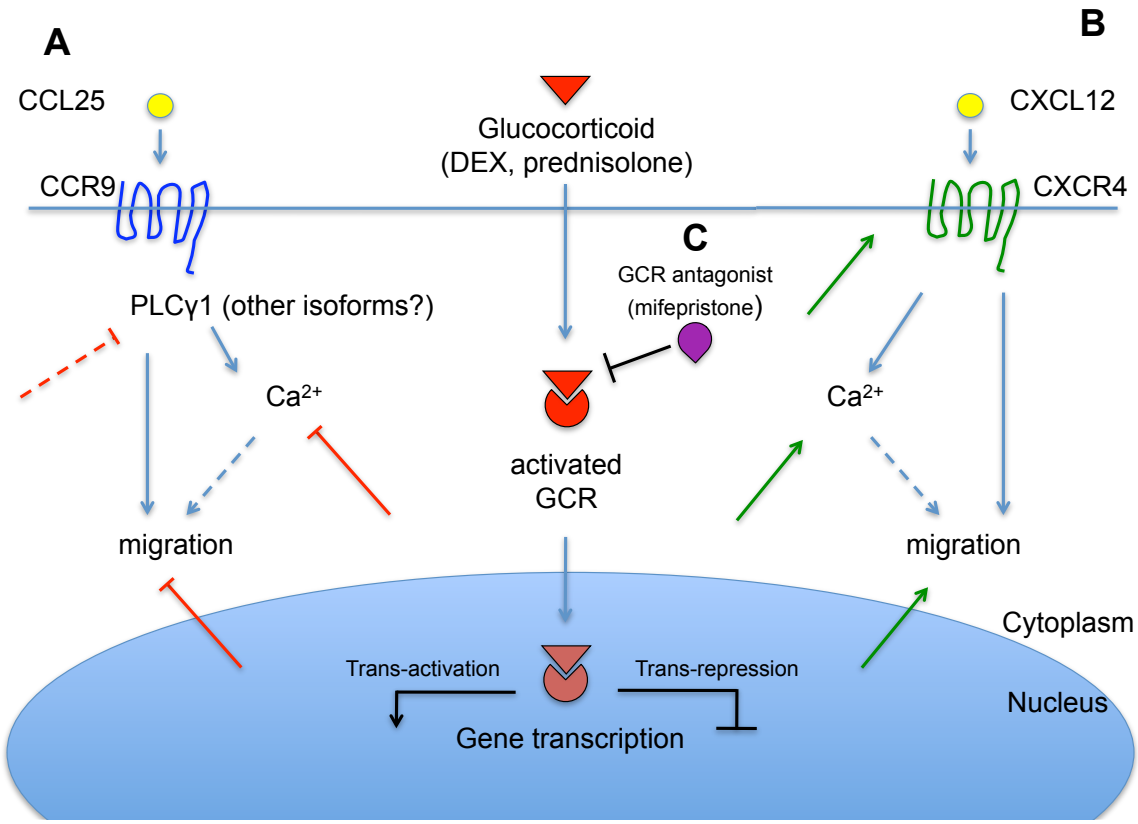


Figure 5.17 Suggested model of GC mediated effects on human CCR9$^+$ T cells.
Glucocorticoids enter the cell cytoplasm, binding constitutively expressed glucocorticoid receptors. The GCR-ligand complex translocates to the nucleus, modifying gene transcription by trans-activation and trans-repression.
A: GCs have no effect on CCR9 mRNA nor surface protein expression but impair CCL25 stimulated intracellular calcium mobilization and directed cell migration. These effects are potentially mediated through reductions in total PLCγ1 protein expression and/or reductions in P-PLCγ1 following CCL25 stimulation. However other PLC isoforms could be involved in the CCR9 signalling cascade.
B: GCs increase CXCR4 mRNA expression, surface protein expression and CXCL12 stimulated intracellular calcium flux and directed cell migration.
C: The effects of GCs on CCR9 and CXCR4 expression and signalling are inhibited by the GCR antagonist, mifepristone.
GCR = glucocorticoid receptor, PLC = Phospholipase C, DEX = dexamethasone. Solid lines indicate direct effect while dotted lines indicate possible effect.

5.3.1 Divergent effect of DEX on CCR9, CXCR4 and CXCR3

An additional novel observation from these experiments was the affect of DEX on CXCR3 surface expression and CXCL11 mediated migration. CXCR3 is expressed on activated T cells (with a predominantly Th1 profile [58,373,374]) and has a role in recruiting cells to sites of inflammation by interacting with three chemokine ligands: CXCL9, CXCL10 and CXCL11 each of which are inducibly expressed by IFN-γ and are frequently observed at peripheral sites of inflammation [239,375,376]. DEX reduced surface CXCR3 expression and also reduced CXCL11 mediated cell migration (24±6% reduction, see Figure 5.1). These *in vitro* results suggest GC treatment could reduce Th1 cell recruitment mediated by CXCR3 *in vivo*. Moreover GCs inhibit IFN-γ production [377], which in turn could reduce the production of CXCR3 ligands at the source of inflammation.

Collectively my data show that within the same population of T cells, GCs differentially modulate chemokine receptor expression and function, generating distinct effects on CCR9, CXCR4 and CXCR3. Certain chemokine receptors are preferentially associated with T cell polarization: CCR5 and CXCR3 are associated with a Th1 response while CCR4 and CCR8 are associated with Th2 polarization [373,374,378]. It would be interesting to study whether CCR5 function is also modulated by GC treatment, to test if GCs preferentially inhibit Th1 associated chemokine receptor function. This particular experiment was not possible on ATRA-treated cells as only a proportion expressed surface CCR5, and CCL5 mediated migration was not observed (see Figure 4.3 and Figure 4.5). As a comparison, Th2 cells could be studied; GCs are a highly effective treatment in Th2 associated diseases (ie asthma and atopic dermatitis) and modulations to chemokine receptor function might identify a novel mechanism of action. Furthermore, a comparison to CCR6 expressing regulatory T cells would be an interesting area of investigation to examine if the migratory capacity of T regs are modulated by GCs.

GCs have broad ranging anti-inflammatory effects and in T cells studied *in vitro*, GCs suppress pro-inflammatory cytokine production (ie IFN-γ, TNF-α, IL-12) [274,379], in some circumstances enhance Th2 cytokine secretion (ie IL-4) [380,381] and either have no effect or enhance IL-10 production [379-382]. Therefore it's reasonable to speculate that regulation of chemokine receptor functionality might also be under a similar dynamic regulation, affecting the movement and retention of effector T cell subsets.

5.3.2 The role of PLCγ1 in CCR9 signalling

The divergent effect of DEX on CCR9 and CXCR4 suggest there exists a unique pathway for CCR9 signalling. In a pilot study looking for phosphorylated kinase proteins following CCL25 stimulation, PLCγ1 was detected. This was a relevant protein target; reduced P-PLCγ1 by DEX was reported in other experimental systems. In mast cells for example, DEX reduced phophorylation of both PLCγ1 and PLCγ2, inhibiting antigen stimulated cell degranulation [278]. Baus *et al* (1996) demonstrated in murine T cell hybrids that DEX (1 μM for 16 hours) reduced signalling downstream of TCR activation, reducing total tyrosine phophorylation including phophorylation of PLCγ1 [383].

In preliminary experiments, I found that CCL25 stimulated phosphorylation of PLCγ1. Activation of PLC is an early signalling component of chemokine receptor activation (see Section 1.2.3) and therefore regulation of this family of proteins (of which there are 13 isoforms) may account for the divergent effect of DEX on CCR9 and CXCR4 mediated signalling. In two pilot experiments, DEX reduced CCL25 stimulated P-PLCγ1 relative to total protein, however the results also showed less total PLCγ1 protein (despite equivalent protein concentrations detected by the loading control, β-actin). The results by Andrade *et al* (2004) in mast cells and work by Baus *et al* (1996) in murine T cell hybrids did not find a change in total PLCγ1 protein following DEX treatment, however these are different cell

types and from a different species. Consequently, further work is necessary to elucidate the effect of DEX on total PLCγ1 and P-PLCγ1 downstream of CCL25 stimulation.

5.3.3 Potential clinical relevance

Whilst CCR9 signalling was inhibited by DEX-treatment *in vitro*, it's unknown if such a reduction (30 - 50%) would translate to a physiological effects *in vivo*. It's tempting to speculate that therapeutic use of GCs inhibit intestinal homing of T cells during active IBD, reducing the inflammation imposed by recruiting pro-inflammatory $CCR9^+$ T cells. This would be a novel mechanistic basis for the therapeutic activity of steroids in IBD and is perhaps supported by the clinical observation that intestinal specific steroid Budesonide, is less effective than systemic corticosteroids such as prednisolone [384].

Budesonide is an orally bio-available GC which upon entering the liver, is rapidly metabolized by cytochrome P-450 enzymes, limiting activity to the GI tract and reducing systemic bio-availability [385]. At the discretion of the clinician, Budesonide is prescribed for IBD treatment, however for unknown reasons, clinical trials show that GCs with high systemic bio-availability are more effective than those with limited bio-availability [384]. Its plausable that the systemic effects of GCs enhance IBD treatment by inhibiting the recruitment of gut homing $CCR9^+$ T cells, however further studies *in vivo* would be necessary to prove this.

5.3.4 Translating in vitro results in vivo

Studying the effects of GC treatment *in vivo* could be performed using a competitive homing experiment in mice similar to that published by Iwata *et al* (2004) [66]. Iwata and colleagues generated murine ATRA-cultured cells *in vitro* using naïve T cells activated and expanded in the presence or absence of ATRA (10 nM) over 4 days. Cells were differentially labeled with CFSE or TRITC and 1×10^7 of each cell population combined and injected intravenously into

recipient mice. While the author shows preferential homing of ATRA-cultured cells (compared to cells cultured in the absences of ATRA) to the small intestine 16 hours post transfer, they do not provide precise quantification of their flow cytometry results, therefore it's difficult to say how robust the migration to the small intestine was precisely. They do quantify histological scores, reporting between 0.1 – 5.8 ATRA-cultured cells per section. None the less, it could be possible to generate ATRA-cultured murine cells, treat them in the presence or absence of DEX and perform a competitive homing experiment with the caveat that the number of recovered cells might be extremely low. However this experiment would not account for other potential effects that could suppress cell extravasation, such as ligand induced integrin activation.

5.3.5 Effects of GCs on CCL25 stimulated adhesion

In the multiple step paradigm of cell extravasation (rolling, adherence and transmigration) chemokines serve to stimulate both directed migration and the initial cell adhesion via activation of integrins (see Section 1.1). $CCR9^+$ cells express integrin $\alpha_4\beta_7$ however the *in vitro* Transwell® chemotaxis and calcium flux experiments described in this chapter have not measured $\alpha_4\beta_7$ activity. It would be possible however to quantify the effect of DEX on CCL25 stimulated $\alpha_4\beta_7$ adhesion using assays which measure static cell adhesion or adhesion under flow, as previously described [91,386]. Miles *et al* (2008) showed that CCL25 promotes $\alpha_4\beta_7$ dependent adhesion of lymphocytes to MAdCAM-1 under flow conditions [387]; a similar experiment could be conducted, staining untreated and DEX-treated cells with distinct fluorochromes and measuring CCL25 stimulated adhesion under shear flow. An effect of DEX on CCL25 stimulated cell adhesion would support to the hypothesis that GCs suppress intestinal inflammation by impairing $CCR9^+$ $\alpha_4\beta_7^+$ cell extravasation.

5.3.6 CCRL1 expression by CCR9$^+$ T cells

My results demonstrate for the first time that CCRL1 mRNA is expressed by CCR9$^+$ T cells, the same cells which signal and migrate in response to CCL25. CCRL1 is a non-signalling, scavenging receptor (see Section 5.2.1) cloned in 2000, and regulation of CCRL1 mRNA by GCs has not been described in the published literature. I hypothesized that DEX could induce CCRL1 expression in CCR9$^+$ T cells, scavenging CCL25 or acting by CCR9-CCRL1 interaction to reduce CCR9 signalling. However by analysis of mRNA expression, CCRL1 was not affected by 16 hours of DEX treatment. At the time of this thesis, no commercially available human CCRL1 antibodies were available therefore further exploration of this hypothesis was not possible. However it is conceivable that the distribution of surface CCRL1 or the activity of the receptor is modulated by DEX.

5.3.7 Limitation to these studies and potential future considerations

Role of PLCγ1 in CCR9 signalling

While my data show a reduction in phosphorylation of PLCγ1, I have not demonstrated that this particular isoform is essential for CCL25-CCR9 mediated migration. There are however commercially available PLC-γ1 inhibitors that will be assessed in the future but as discussed in Section 1.2.3, over 13 PLC isoforms exist; the possibility that other isoforms contribute to CCR9 signalling cannot be excluded.

Clinical trials targeting CCR9

Approximately 50% of patients enrolled in PROTECT-1 were on concomitant steroid treatment, however my data suggest that GCs influence the activity of CCR9, the target of CCX282-B. Patients in PROTECT-1 were randomly assigned CCX282-B or placebo, and therefore the effect of steroids would be evenly distributed between treatment groups. However, the results from this chapter suggest that controlled clinical trials testing agents

which target CCR9 should not include patients on GC treatment and could warrant a retrospective analysis of the clinical data, excluding patients on concomitant steroid treatment.

5.3.8 Future experiments in this thesis

CD is a heterogeneous disease, with significant placebo response, natural cycles of disease relapse and remission and differences in the severity of inflammation between individuals. In the next chapter I study the effect of CCR9 antagonist treatment in patients with coeliac disease. Coeliac disease has a known immune immunogen, gluten, and therefore inflammation of the small bowel can be controllably induced. Furthermore, patients with coeliac disease are not routinely prescribed corticosteroid treatment. Using the IHC technique described in Chapter 3, I measure lamina propria lymphocyte and intraepithelial cell recruitment to the duodenum, comparing CCX282-B and placebo during gluten induced inflammation in patients with coeliac disease.

CHAPTER 6: Quantifying changes to lymphocyte populations following CCR9 antagonist treatment (CCX282-B) during active Coeliac disease

6.1 Introduction

Coeliac disease is an inflammatory condition of the small intestine, triggered by dietary gluten in genetically predisposed individuals. Active disease is associated with histological changes in the proximal small intestine, including increased number of intraepithelial lymphocytes, reduced height and increased width of villi, and lengthened crypts [280,286,388]. The majority of patients express MHC class II isoforms HLA-DQ2 and HLA-DQ8, which bind gliadin (gluten derived peptide) with high affinity, activating gliadin-specific $CD4^+$ T cells [291]. Intraepithelial cells are predominantly CD8 T cells, with accumulating evidence of cytotoxic activity against epithelial cells (see Section 1.7.1) [389].

The expression of CCR9 by the majority of IELs and lamina propria T cells (CD4 and CD8) in the small bowel have identified CCR9 as a potential therapeutic target in coeliac disease. Furthermore, Papadakis *et al* (2001) showed an elevated proportion of peripheral blood $CCR9^+CD4^+$ T cells during active coeliac disease compared to healthy control and active UC patients [72]. A Phase II study in coeliac disease, testing the efficacy of CCR9 antagonist, CCX282-B was initiated by ChemoCentryx, Inc in 2007 and completed in 2008 [390].

Patients who received CCX282-B received no clinical benefit compared to placebo in preventing the onset of adverse clinical symptoms associated with active coeliac disease (unpublished data). Although drug alone was well tolerated [316,391], several patients taking CCX282-B and placebo terminated enrolment early voluntarily or by the instruction of a physician. Whilst there was no clinical advantage of CCX282-B in preventing the symptoms of active coeliac disease, measuring the effects of CCR9 antagonist treatment on cell

recruitment to the small bowel was still of great interest. Initially, a quantification of intestinal $CCR9^+$ cells from patient biopsies was desired, comparing cell density before and after gluten challenge. However, as described in Chapter 3, a validated antibody for staining CCR9 by IHC not available. Therefore an alternative staining design was adopted, quantifying changes to all T cells ($CD3^+$) and regulatory T cells ($FoxP3^+CD3^+$).

Clinical trial design

Approximately 90 patients were enrolled in the double blind Phase II study of CCX282-B in patients with coeliac disease. The key inclusion criteria stipulated that patients had an established diagnosis of coeliac disease and were on a strict gluten free diet for at least 2 years [390]. Enrolled patients were randomly assigned drug (250 mg CCX282-B) or placebo consumed as a capsule twice daily for 7 days in the absence of gluten. Subsequently twice daily dietary gluten (8 grams of gluten in the form of a prescribed biscuit) was introduced with continued drug administration. In total, patients were administered treatment for 91 days (Figure 6.1). From a subset of patient, biopsies were collected from the duodenum prior to treatment (Baseline) and again at the end of the study (Day 91). In total, 19 patents on placebo, and 22 patients on CCX282 treatment had matched biopsies suitable for analysis by IHC.

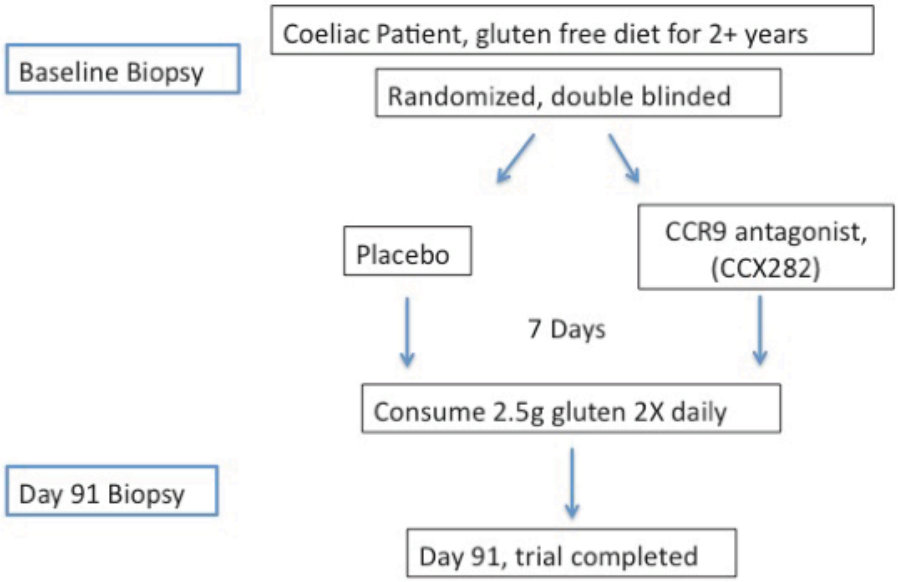


Figure 6.1 Double blind Phase II study of CCX282-B in patients with coeliac disease. Patients were randomly assigned drug taken twice daily for seven days prior to the introduction of gluten. Twice daily drug and gluten were taken for an additional 84 days. Biopsies from the duodenum were collected at Baseline (prior to drug treatment) and again at Day 91.

6.1.1 Aims of this chapter

The experiments in this chapter aim to quantify the effects of CCX282-B on T cell density in the duodenum, comparing the lamina propria and epithelium separately. Biopsies collected as part of a clinical trial in coeliac disease were used and results will include:

- Quantification of cell density before and after gluten challenge, assessing differences between placebo and CCX282-B treatment, assessing the following cell populations:
    - Total T cells ($CD3^+$)
    - Regulatory T cells ($FoxP3^+CD3^+$)

6.2 Results

6.2.1 CD3 and FoxP3 double labelling by immunohistochemistry

Biopsies were stained for CD3 and FoxP3 by IHC as described (see Section 2.4.4). These antibodies are well validated cell markers that provided clear differentiation between positive and negative cells; CD3 is a membranous antigen while FoxP3 is a cytoplasmic transcription factor (Figure 6.2). Comparisons of matched patient biopsies demonstrate the dramatic accumulation of intestinal T cells, particularly within the epithelial compartment (Figure 6.3). To quantify these changes, the density of total T cells ($CD3^+$) and regulatory T cells ($CD3^+FoxP3^+$) were quantified separately within the lamina propria and epithelial compartments (see Section 2.4.5).

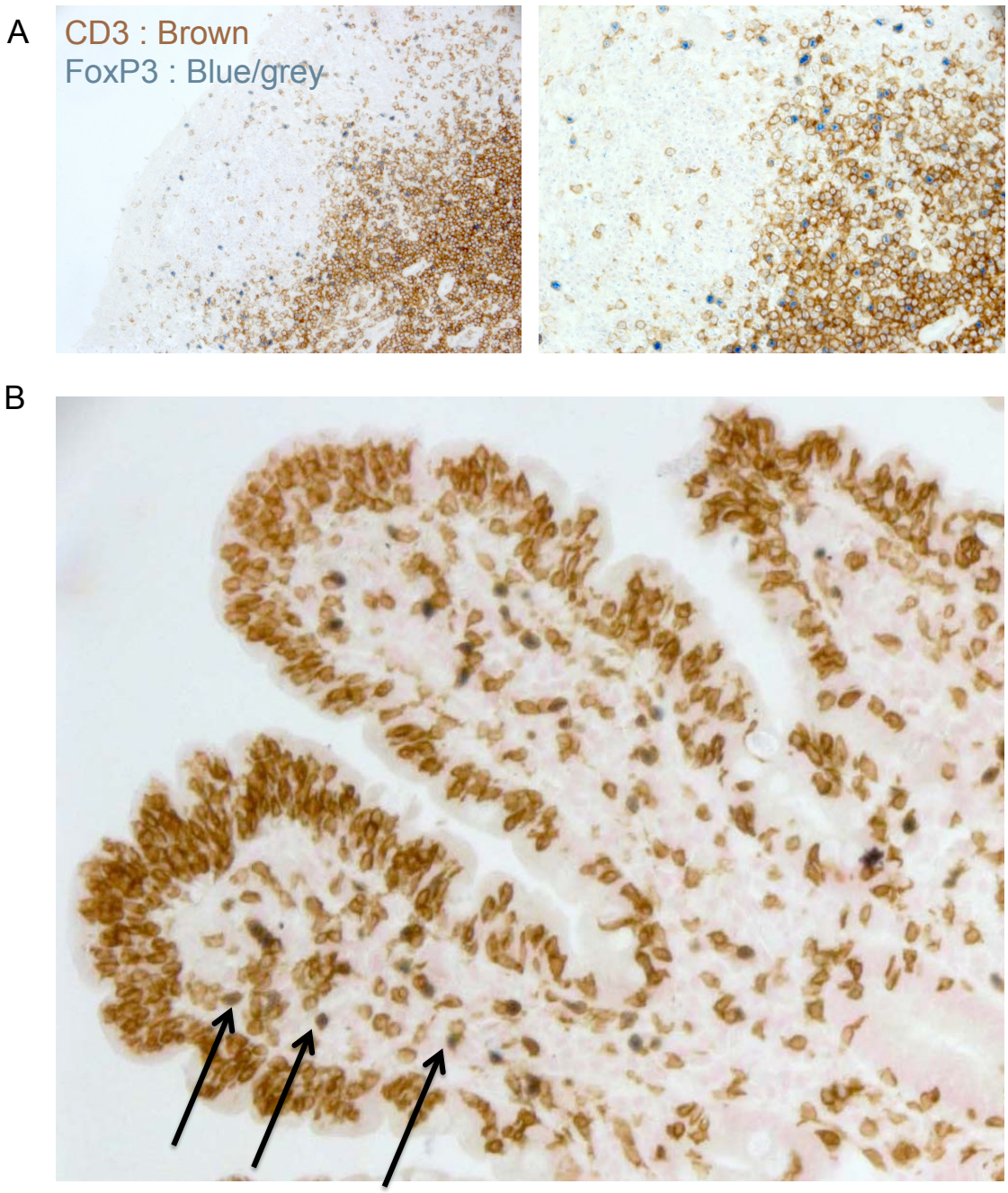


Figure 6.2 Human tissue double stained for CD3 and FoxP3 by IHC.
Human tissue was stained for CD3 (brown) and FoxP3 (blue/gray) by IHC and counterstained with VECTOR® red (red nuclei). CD3 is a membranous receptor and FoxP3 is a cytoplasmic transcription factor.
A: Human tonsil.
B: Human duodenum from a patient with active coeliac disease. Arrows indicated $FoxP3^{+}$ cells in the intestinal lamina propria.

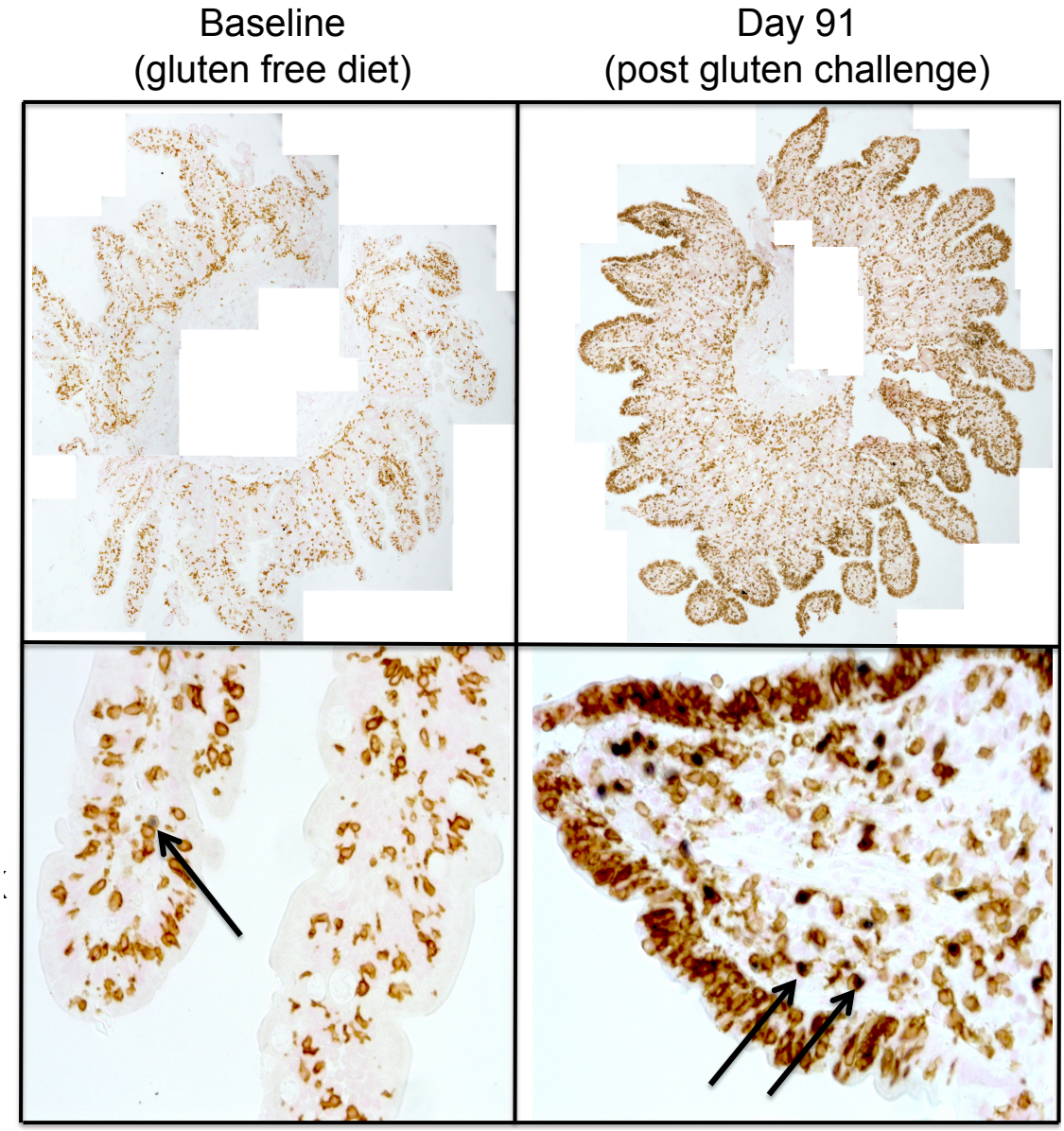


Figure 6.3 Matched coeliac patient biopsies at Baseline and Day 91 stained for CD3 and FoxP3 by IHC.
Biopsies from the duodenum were taken prior to gluten challenge (Baseline) and again following 91 days of gluten challenge (Day 91). Biopsies were formalin fixed, paraffin embedded and stained for CD3 (brown) and FoxP3 (blue/gray) by IHC and counterstained with VECTOR® red (red nuclei). Representative example of intraepithelial $CD3^{+}$ cell infiltration following gluten challenge. Arrows indicate examples of FoxP3 stained cells exclusively concentrated in the lamina propria.

6.2.2 Lamina propria $CD3^+$ cells

The mean density of $CD3^+$ cells per mm^2 lamina propria remained constant from Baseline to Day 91 in both the placebo and CCX282-B treatment groups (Figure 6.4A - B). Both treatment groups had an average change in lamina propria $CD3^+$ cell density from Baseline to Day 91 close to zero, indicating no significant change in lamina propria $CD3^+$ cell density following 91 days of gluten challenge (Figure 6.4C).

Patients on placebo had an increase in the density of lamina propria $CD3^+$ cell density by 11±7% compared to 15±16% for CCX282-B treated patients Figure 6.4D. There was no significant difference between placebo and CCX282-B treated patients with regards to the change in $CD3^+$ cell density from Baseline to Day 91 ($p=0.327$, Mann-Whitney test; Figure 6.4C) and with regards to the percent change in $CD3^+$ cell density from Baseline to Day 91 ($p=0.353$, Mann-Whitney test; Figure 6.4D). These data show a small but not statistically significant increase in the density of lamina propria $CD3^+$ T cells in the duodenum during active coeliac disease which was equivalent between placebo and CCX282-B treatment.

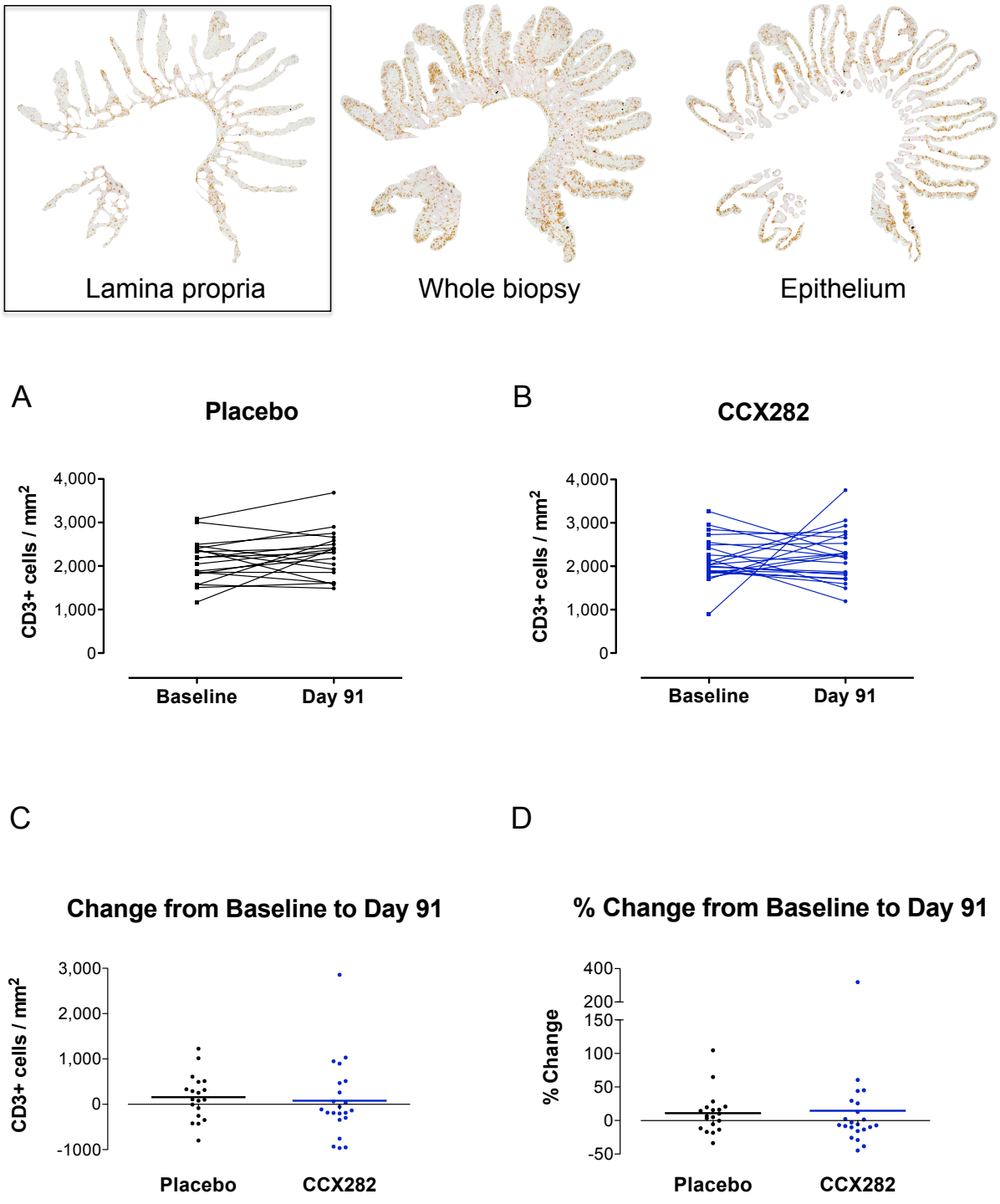


Figure 6.4 Lamina propria CD3$^+$ cells.
The density of CD3$^+$ cells per mm^2 lamina propria tissue.
A: Placebo treatment at Baseline and Day 91.
B: CCX282-B treatment at Baseline and Day 91.
C: Change in CD3$^+$ cells density from Baseline to Day 91 for each patient. The line depicts the mean of the data.
D: Percent change in CD3$^+$ cell density from Baseline to Day 91 for each patient. The line depicts the mean of the data.

6.2.3 Lamina propria FoxP3$^+$ T cells

FoxP3$^+$ cells were exclusively concentrated in the lamina propria but were few in numbers; on average 37 FoxP3$^+$ T cells were counted in an entire biopsy compared to approximately 800 CD3$^+$ cells in the lamina propria. The proportion of regulatory T cells relative to all lamina propria CD3$^+$ cells was quantified (FoxP3$^+$ per 10^3 CD3$^+$).

In agreement with previous reports [392,393], the frequency of FoxP3$^+$ cells increased in the lamina propria during active coeliac disease; in both treatment groups the frequency of regulatory T cells rose significantly from Baseline to Day 91 ($p<0.001$ & $p<0.01$ placebo and CCX282-B respectively, Figure 6.5A – B). For placebo treated patients, FoxP3$^+$ cells per 10^3 CD3$^+$ cells increased on average by 32±8 cells compared to a rise of 31±7 cells for CCX282-B treated patients (Figure 6.5C). The percentage increase in FoxP3$^+$ cells was 249±87% for placebo and 109±27% for CCX282-B treated patients, with no significant difference between the treatment groups ($p=0.213$, Mann-Whitney; Figure 6.5D). Collectively these data show a significant increase in the frequency of lamina propria FoxP3$^+$ T cells during active coeliac disease which was equivalent between patients administered CCX282-B and placebo.

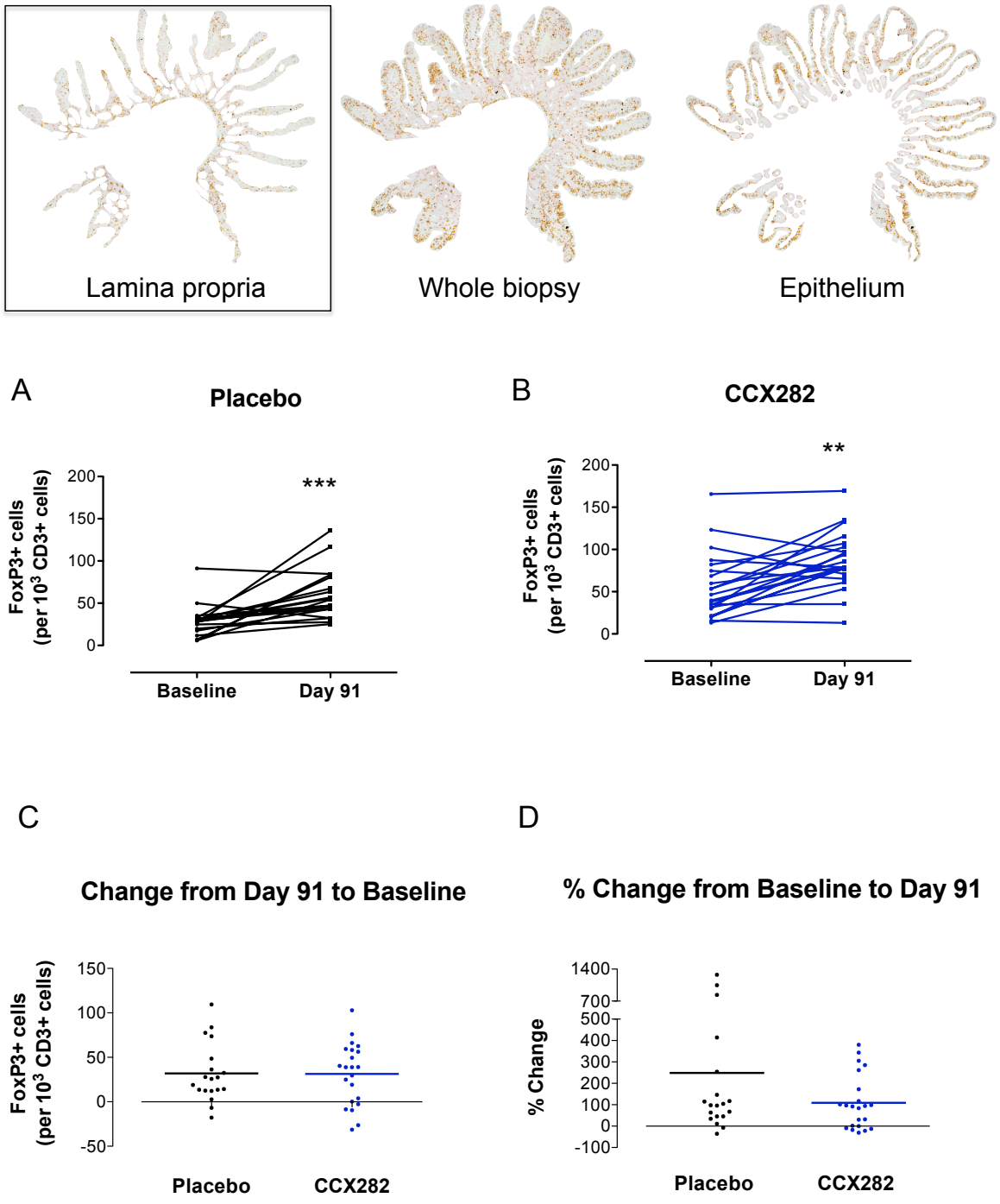


Figure 6.5 FoxP3$^+$ cells within the lamina propria.
The frequency of FoxP3$^+$ cells per 10^3 CD3$^+$ cells was quantified within the lamina propria.
A: Placebo treatment at Baseline and Day 91.
B: CCX282-B treatment at Baseline and Day 91.
C: Change in FoxP3$^+$ cells frequency from Baseline to Day 91 for each patient. The line depicts the mean of the data.
D: Percent change in FoxP3$^+$ cell frequency from Baseline to Day 91 for each patient. The line depicts the mean of the data. **p<0.01; ***p<0.001 Wilcoxon matched pairs test.

6.2.4 Intraepithelial $CD3^+$ cell

To examine the effect of CCX282-B on IEL infiltration, the number of $CD3^+$ cells per mm^2 epithelial tissue was quantified. In agreement with the histological features of active coeliac disease, 91 days of gluten challenge significantly increased IEL density, measured in the placebo treatment group ($p<0.001$, Figure 6.6A), and in patients treated with CCX282-B ($p<0.01$, Figure 6.6B).

On average patients on CCX282-B had a smaller increase in the density of IELs from Baseline to Day 91 compared to the placebo treatment group ($p=0.03$, Figure 6.6C). However when the data is analysed as the percentage change from Baseline to Day 91, the differences between placebo and CCX282-B are not longer statistically significant ($p=0.078$, Fisher's exact test; Figure 6.6D). These data show a significant increase in IELs following gluten challenge and are highly suggestive of an inhibitory effect by CCX282-B on this recruitment although statistical significance is dependent on the presentation of the data.

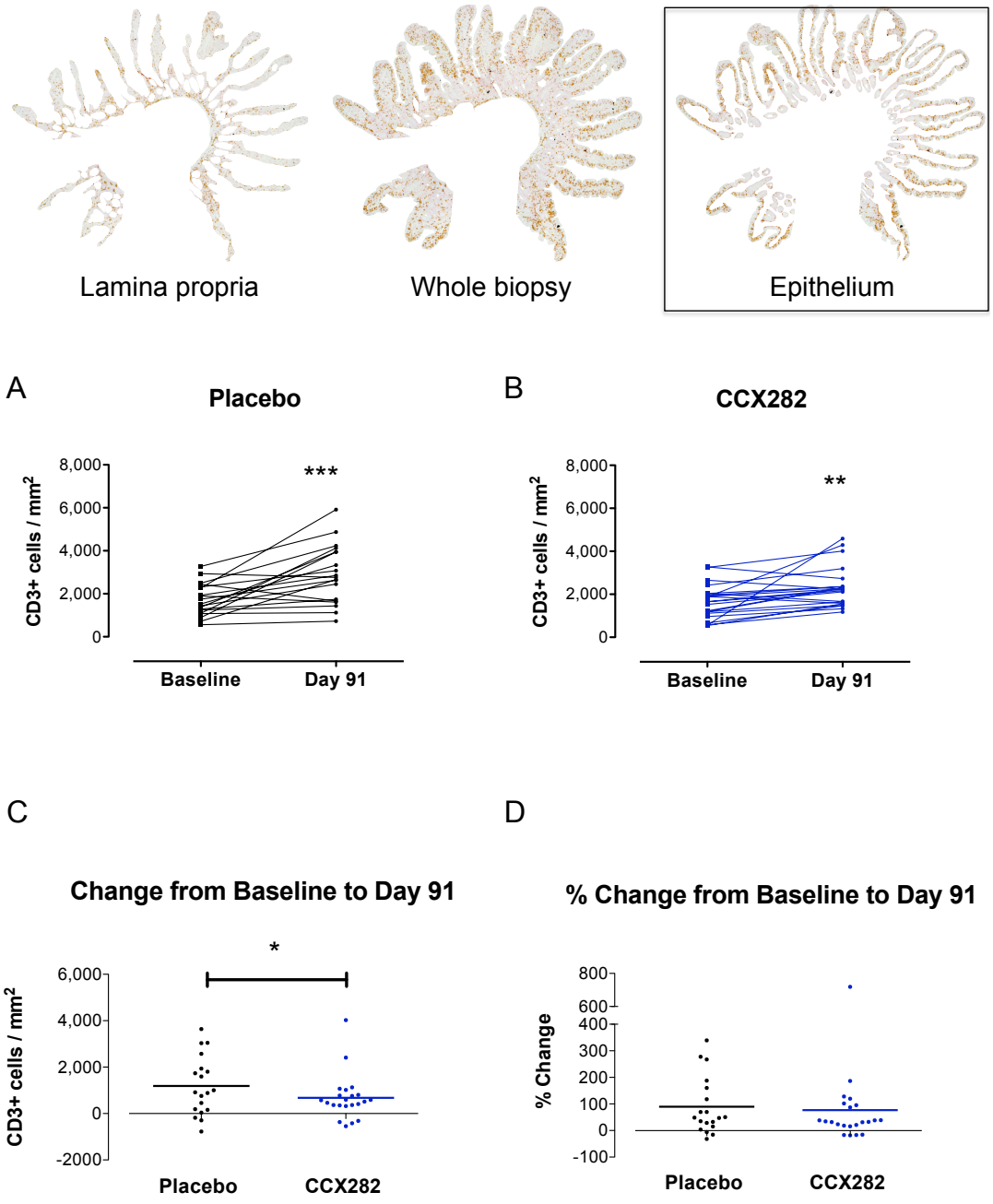


Figure 6.6 Intraepithelial CD3$^+$.
The density of CD3$^+$ cells was quantified within the epithelium per mm^2 of tissue.
A: Placebo treatment at Baseline and Day 91.
B: CCX282-B treatment at Baseline and Day 91.
C: Change in intraepithelial CD3$^+$ cells density from Baseline to Day 91 for each patient. The line depicts the mean of the data.
D: Percent change in CD3$^+$ cell density from Baseline to Day 91 for each patient. The line depicts the mean of the data.
Statistical significance analyzed by paired t-test (A&B) or two-sided Fisher's exact test (C&D); *p<0.05, **p<0.01, ***p<0.001.

6.3 Discussion

In this chapter I show that in accordance with previous reports, gluten consumption by individuals with coeliac disease stimulates recruitment of T cells into the small intestinal mucosa, and in particular, an elevated density of IELs and increased frequency of $FoxP3^{+}$ regulatory T cells in the lamina propria [207,389,394,395]. On average patients treated with CCX282-B had a lower degree of IEL infiltration, suggesting that CCR9 inhibition suppresses the accumulation of IELs during active disease. These are some of the first studies in human measuring the effects of CCR9 antagonist treatment and are highly suggestive of a biological effect on the recruitment of T cells to the inflamed duodenum. The combination of small sample size, patient variability, inadequate receptor coverage (see dosing discussion) and IEL proliferation could have collectively underpowered this study.

6.3.1 Effect on IELs

The data presented in this chapter suggest CCR9 is responsible, at least in part, for the recruitment of IELs in the small intestine during active coeliac disease. Patients on CCX282-B treatment had fewer accumulating IELs compared to placebo, although statistical significance was dependent on the presentation of data (change in density versus percentage change). An a-priori power analysis with the present mean and standard deviation of the data calculates 62 samples per group would be required to reach statistical significance (calculated for a two-tailed t test with a statistical power of 0.8 and a probability of <5%, [396]). Reductions in IEL recruitment following CCR9 blockade is perhaps supported by studies in mice genetically deficient for either CCL25 or CCR9.

Wurbel *et al* (2007) showed by adoptive transfer of antigen specific cells, that cells transferred into $CCL25^{-/-}$ hosts failed to re-populate the intestinal epithelium [99]. In a separate study, Wurbel *et al* (2001) showed that while $CCR9^{-/-}$ mice thrive, there is a 50% reduction in

IELs under homeostatic conditions [100]. This is the first study in human measuring the role of CCR9 in IEL trafficking.

One consideration when measuring the accumulation of IELs is the proliferative capacity during inflammation. Under homeostatic, non-inflamed conditions the majority of IELs are not proliferating and are resistant to proliferation following conventional stimulation techniques performed *in vitro* (including PMA, and anti-CD3 activation) [207,397]. This has been demonstrated in human jujunal sections, measuring Ki67 expression (cellular marker of cell proliferation) by immunofluorescence [207], and by stimulating disaggregated IELs *in vitro* with anti-CD3 antibody and quantifying proliferation by the uptake of [3H] thymidine [394]. However, Halstensen *et al* (1993) showed by immunofluorescence staining, that while healthy control and coeliac patients on a gluten free diet have a low frequency of Ki67 expressing IELs, the frequency increased significantly in patients with active coeliac disease (0% and 4.6% increased to 12.8% respectively) [207]. Therefore the increased frequency of IELs following gluten challenge is at least in part the consequence of cell proliferation. With this in mind, the effect of CCR9 antagonist treatment might be overshadowed by *in vivo* proliferation, and therefore the presence of any inhibitory effect is all the more striking.

With regards to IELs, it should be mentioned that the functional relevance remains poorly understood in coeliac disease. Gliadin specific $CD4^+$ cells in the lamina propria have a well characterized role in disease, recognizing gliadin-MHC class II complexes on the surface of APCs and exacerbating disease by the production of pro-inflammatory cytokines, including IFN-γ [398,399]. IELs are enriched for CD8 expressing TCRαβ and TCRγδ however the specificity of IELs for gluten is not well described [286]; there is accumulating evidence for cytolytic activity of CTLs in coeliac disease, killing epithelial cells and potentially damaging the epithelium (see Section 1.7.1).

6.3.2 FoxP3 expressing cell accumulation

In accordance with previous reports, I show a significant increase in the frequency of LP FoxP3$^+$ T cells during active coeliac disease [392,393]. Furthermore the proportion of FoxP3$^+$ T cells relative to all T cells is in line with previous reports: in this analysis, on average 4.4% of all T cells expressed FoxP3; Vorobjova et al (2009) reported that approximately 10% of CD4 T cells expressed FoxP3 in the intestinal mucosa of children with coeliac disease [393] and Hminda *et al* (2012) reported ~4% FoxP3 expression from CD4$^+$ LPL from the mucosa of patients with active coeliac disease [394]. These data also indicate that antagonizing CCR9 does not preferentially impair the accumulation of regulatory T cells to the intestine, an important contribution to the study of CCR9 during intestinal inflammation.

6.3.3 Limitations of this study

One particular limitation was the dosing of CCX282-B, 250 mg twice daily in this study. At the time of this clinical trial, the results of the PROTECT-1 study were not available. It was only after the present study was completed that the PROTECT-1 trial in Crohn's disease showed efficacy at 500 mg daily CCX282-B but not with 250 mg twice daily (see Figure Figure 3.1). Consequently incomplete receptor antagonist coverage in this study could have compromised the current analysis.

CHAPTER 7: Final Discussion

7.1 Summary of key advances in this thesis

The experiments in this thesis have focused on expanding our knowledge of human CCR9 and CCL25, studying changes *in situ* following CCR9 antagonist treatment, describing techniques for measuring effects of CCL25 on $CCR9^+$ T cells and measuring CCL25 expression in human tissue. The role of CCR9 in human intestinal inflammation and the effects of CCR9 antagonist treatment are summarized in Figure 7.1. In the course of this work, I describe a novel effect of glucocorticoids on the function of CCR9, which may be relevant in understanding intestinal inflammation. To summarize, my key findings are outlined below:

1) [Chapter 3] I describe a technique for quantifying cell density within intestinal tissue analyzed by IHC which can distinguish changes in the lamina propria and epithelial tissues. This technique could be applied to intestinal biopsies collected prior to and following therapeutic treatment in IBD to measure changes in distinct cell subsets, thereby elucidating or substantiating mechanisms of action.
2) [Chapter 3] In a clinical trial that examined the effects of CCR9 antagonist treatment, CCX282-B in patients with active Crohn's disease, I show a trend that CCX282-B reduced T cell density in the intestinal mucosa. These data drew attention to particular challenges of conducting clinical trials in IBD, such as concomitant treatments, variability in disease between individuals and the potential discrepancy between clinical efficacy and biological effects.
3) [Chapter 4] As predicted, although not previously demonstrated, CCL25 stimulates calcium mobilization in ATRA-cultured cells, measured using a flow cytometry based

assay that follows calcium flux in individual cells. These data increase the utility of ATRA-cultured cells in the study of primary human CCR9 function.

4) [Chapter 4] CCR9, similar to other chemokine receptors, undergoes ligand induced internalization. This is an important observation which I show affects the intensity (MFI) and localization (membrane versus cytoplasm-associated) of receptor expression measured by flow cytometry and immunohistochemistry respectively. These data suggest that measuring CCR9 protein *in situ* will be challenging in tissue where cognate ligand is present. Therefore alternative techniques may be required (ie *in situ* hybridization probing for CCR9 mRNA).
5) [Chapter 4] MAdCAM-1 in combination with anti-CD3/anti-CD28 enhances the production of several cytokines (IFN-γ, TNF-α, IL-17A, IL-22), and in particular IL-10 from $CCR9^+$ ATRA-cultured cells. This is a novel observation with clinical relevance as MAdCAM-1 is a therapeutic target in IBD.
6) [Chapter 4] Confirmation of the previous but limited reports that CCL25 mRNA expression in the un-inflamed intestine is restricted to the small bowel and not detected in the colon. In particular I show samples from different regions of the large intestine, demonstrating that CCL25 is absent from un-inflamed tissue spanning the caecum to the rectum.
7) [Chapter 4] Data that CCL25 mRNA is detected in a subset (2 out of 23 samples) of biopsies collected from the inflamed colon of IBD patients; although levels of transcript were significantly lower than levels detected in the terminal ileum where CCL25 is constitutively expressed.
8) [Chapter 5] Glucocorticoids inhibit CCR9-CCL25 mediated signalling in human T cells measured by changes in calcium flux, cell migration and phosphorylation of PLC-γ. These effects were in contrast to co-expressed CXCR4, where GCs increased

surface CXCR4 expression and CXCL12 mediated cell migration and calcium flux in $CCR9^+$ T cells. These data could identify a novel mechanism by which GCs inhibit intestinal cell recruitment during CD.

9) [Chapter 5] I describe a technique for stimulating and measuring calcium mobilization simultaneously in two cells populations, analyzed by flow cytometry. This technique circumvents problems of 'dye leakage' and technical errors and therefore has utility in more precisely comparing cell populations by calcium flux.

10) [Chapter 6] I describe a second clinical trial that examined the effects of CCR9 antagonist CCX282-B in patients with active coeliac disease. I showed through quantification of T cell subsets that there was a decrease in IEL infiltrations, suggesting that while treatment was not clinically efficacious there was a measurable biological effect.

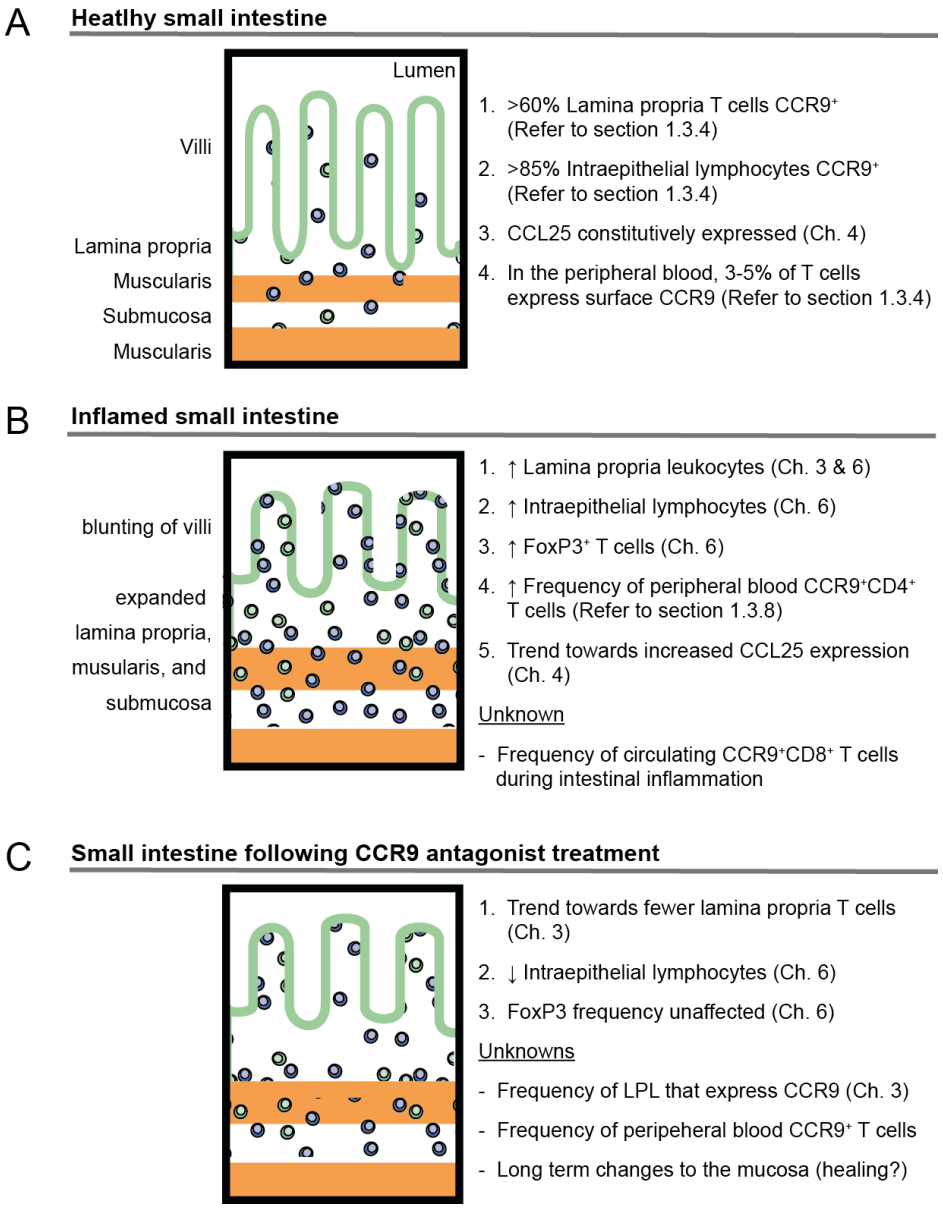


Figure 7.1 The role of CCL25 and CCR9 in human small intestinal inflammation based on published data and novel data presented in this thesis.
A: CCL25 is constitutively expressed in the healthy small intestine. CCR9 expressing T cells are enriched in the small intestine relative to the peripheral blood and other tissues.
B: During small intestinal inflammation, including Coeliac disease and Crohn's disease, there is a recruitment of intestinal leukocytes, an increased proportion of circulating $CCR9^{+}CD4^{+}$ T cells, and possibly a rise in CCL25 mRNA at inflamed lesions. Elevated levels of Th1 and Th17 associated cytokines suggest that T cells exacerbate inflammation or have a role in disease pathogenesis.
C: Conclusions based upon analyses presented in this thesis, studying the effects of CCR9 antagonist treatment (CCX282-B) in Coeliac disease and Crohn's disease using small intestinal biopsies analyzed by immunohistochemistry. During active Coeliac disease, CCR9 contributes to IEL homing but does not contribute to FoxP3 cell recruitment (found exclusively in the lamina propria). During active Crohn's disease, CCR9 may contribute to T cell homing to the lamina propria, however other chemokine receptors may also contribute to leukocyte infiltration.

7.2 Future directions and outstanding issues

7.2.1 Quantifying the effect of CCX282-B (or other therapies) on lymphocyte density in the intestine

GlaxoSmithKline has purchased the rights to CCX282-B and is conducing clinical trials in IBD (listed on clinical trials.gov: NCT01318993 and NCT01316939) [400,401]. Based upon the clinical results of PROTECT-1, the current trials are testing higher doses of CCX282-B (500 mg once daily and 500 mg twice daily) [400,401]. The analysis of intestinal biopsies described in Chapter 3 is not a trivial process: there are challenges to collecting appropriate biopsies (some of the samples were colonic tissue rather than terminal ileum), and staining and quantifying samples is a time consuming process. However, were it possible to collect biopsies from patients with demonstrated efficacy, this analysis could support a proof of concept by demonstrating a reduction in intestinal T cell density, or a change in the composition of effector cells (regulatory T cells to all T cells).

Furthermore clinical trials testing other therapies in IBD might benefit from the analysis described in Chapter 3 of this thesis. In particular, therapies targeting member of the integrin family which have been approved for the treatment of CD in the United States (Natalizumab, humanized monoclonal antibody against α_4)[326-328] and at the time of this thesis are undergoing clinical trials (Danese reviews the current pipeline of therapies in IBD) [402]. Assessing the density of different target populations might provide additional mechanistic insight into these specific therapies that could strengthen our understanding of factors contributing to the resolution of IBD.

7.2.2 *in situ* Hybridization

The IHC results from Chapter 3 suggest CCR9 expression is present on human macrophages and epithelial cells. This was an unexpected finding, and requires analysis by alternative

techniques. In our laboratory we have recently found that disaggregation of intestinal tissue by Ficoll-paque™ PLUS density centrifugation can separate viable epithelial cells from PBMCs (gated on $CD45^-$ $EpCAM^+$). Preliminary data staining these cells for CCR9 with analysis by flow cytometry have not detected CCR9 surface expression by viable epithelial cells (data not shown). It is more likely that epithelial cells non-specifically bind antibodies during analysis by IHC. An alternative approach to measuring CCR9 expression is by *in situ* hybridization, using probes to detect mRNA within intact tissue. Analysis of CCR9 by *in situ* hybridization would be a significant contribution to the study of CCR9; it could substantiate or contest expression by epithelial cells and macrophages and additionally expose the distribution of these cells relative to lymphoid follicles, intestinal villi and crypts. The only caveat is that *in situ* hybridization, while sensitive, can be technically challenging.

7.2.3 Investigating the effect of MAdCAM-1 on cytokine production

To the best of my knowledge, the stimulatory effect of MAdCAM-1 on T cell cytokine secretion is not well recognized. In this thesis I show that plate bound MAdCAM-1 significantly enhanced the production of pro-inflammatory cytokine, IFN-γ but interestingly also enhanced the production of IL-10 by $CCR9^+$ ATRA-cultured cells (see Figure 5.17). This suggests that elevated expression of MAdCAM-1 during IBD and PSC could modify inflammation by enhancing the activation of gut homing cells following their recruitment and extravasation.

Pfizer Inc., has developed a fully humanized anti-MAdCAM-1 blocking antibody (PF-00547,659) and in 2011 reported favorable safety results and preliminary signs of efficacy in UC [403]. It is postulated that efficacy is through reducing inflammatory cell extravasation, however my data suggest blocking antibodies could limit induction of cytokine secretion by $CCR9^+$ cells. A recent review on anti-adhesion molecule therapies in IBD, made no mention

of MAdCAM-1 modulating cell effector function [28] however this could be a highly relevant mechanism of action and warrants further exploration.

7.2.4 Studying the effect of glucocorticoids on CCR9 function *in vivo*

In understanding how the results presented in Chapter 5 have physiological or pathophysiological relevance, *in vivo* experiments investigating the effects of DEX on CCR9-CCL25 mediated migration are necessary. This could be achieved by performing a competitive homing experiment as described in Section 5.3.3. These experiments may require different conditions to be tested, such as constitutive homing, homing under inflammatory conditions, and correcting for other in vivo effects of corticosteroids, and therefore constitute potentially a large body of further work.

7.2.5 Examining the effect of glucocorticoids on CCL25 expression

An additional route for examining the effect of glucocorticoids on the CCR9-CCL25 axis is to study the effect on CCL25 expression. Although not explored experimentally in this thesis, steroids reduce inflammation by inhibiting the production of pro-inflammatory cytokines and by reducing the expression of pro-inflammatory chemokines (including but not limited to CXCL8, CCL2) [404,405]. It is therefore possible that GCs suppress the expression of CCL25, particularly at sites of active inflammation, where elevated expression of CCL25 is detected (such as the liver during PSC) and potentially in the colon, where CCL25 expression is sometimes induced but not constitutive (see Figures 4.16 & 4.18). If it were possible to identify a cell line which constitutively expressed CCL25, or expressed CCL25 under pro-inflammatory cytokine stimulation, one could measure the effect of DEX on CCL25 production.

7.2.6 Studying the mechanism of CCR9 inhibition by glucocorticoids

A significant unanswered question arising from the work in Chapter 5 is how DEX-treatment can inhibit CCR9 function while enhancing the function of co-expressed CXCR4. The preliminary work characterizing phosphorylation of PLC-γ1 was in the effort of elucidating the unique mechanism and further work is necessary. However there are other experimental options to consider, including the use of microarray and proteomic analyses. As demonstrated in Sections 5.2.6 and 5.2.2, DEX-treatment reduced CCR9-mediated migration in sorted $CCR9^+$ T cells and ATRA-cultured cells but was unaffected in Molt-4 cells. It would therefore be possible to compare changes to gene transcription and protein activation, in the presence and absence of DEX, with and without CCL25 stimulation, comparing ATRA-cultured cells to Molt-4 cells. This would constitute a large body of work but could clarify differences in CCR9 signaling between primary derived cells and the Molt-4 cell line and potentially identify targets for studying the effect of DEX on CCR9 signalling.

7.2.7 Designing intestinal specific glucocorticoids

GCs are effective in many inflammatory conditions including IBD, and their clinical use is limited mainly because of the risk of adverse side effects, particularly with chronic administration. However, if it were possible to harness the intestine-specific action of GCs, whilst limiting other systemic effects, by for instance, targeting GCs to $CCR9^+$ cells, their therapeutic benefit and utility might be greatly enhanced. Utilizing the internalization of CCR9 upon ligand binding for example might be one approach to deliver steroids specifically to $CCR9^+$ cells.

REFERENCES

1. Robbins, S.L., Kumar, V. & Cotran, R.S. *Robbins and Cotran pathologic basis of disease*, (Saunders/Elsevier, Philadelphia, PA, 2010).
2. Majno, G. & Joris, I. *Cells, Tissues, and Disease*, (John Wiley & Sons, 1996).
3. Cohnheim, J. Ueber Entzundung and Eiterung. *Virchows Arch Pathol Anat Physiol Klin Med* **40**, 1-79 (1867).
4. Cohnheim, J. *Untersuchungen ueber die embolischen Processe*, (Verlag von August Hirschwald, Berlin, 1872).
5. Metchnikoff, O. & Lankester, E.R. *Life of Elie Metchnikoff, 1845-1916*, (Houghton Mifflin Company, Boston, 1921).
6. Springer, T.A. Traffic signals for lymphocyte recirculation and leukocyte emigration: the multistep paradigm. *Cell* **76**, 301-314 (1994).
7. Butcher, E.C. Leukocyte-endothelial cell recognition: three (or more) steps to specificity and diversity. *Cell* **67**, 1033-1036 (1991).
8. Ley, K., Laudanna, C., Cybulsky, M.I. & Nourshargh, S. Getting to the site of inflammation: the leukocyte adhesion cascade updated. *Nat Rev Immunol* **7**, 678-689 (2007).
9. Ley, K. & Kansas, G.S. Selectins in T-cell recruitment to non-lymphoid tissues and sites of inflammation. *Nat Rev Immunol* **4**, 325-335 (2004).
10. Foreman, K.E.*, et al.* C5a-induced expression of P-selectin in endothelial cells. *J Clin Invest* **94**, 1147-1155 (1994).
11. Kansas, G.S. Selectins and their ligands: current concepts and controversies. *Blood* **88**, 3259-3287 (1996).
12. Foxall, C.*, et al.* The three members of the selectin receptor family recognize a common carbohydrate epitope, the sialyl Lewis(x) oligosaccharide. *J Cell Biol* **117**, 895-902 (1992).
13. Rosen, S.D. Ligands for L-selectin: homing, inflammation, and beyond. *Annual review of immunology* **22**, 129-156 (2004).
14. Alon, R., Hammer, D.A. & Springer, T.A. Lifetime of the P-selectin-carbohydrate bond and its response to tensile force in hydrodynamic flow. *Nature* **374**, 539-542 (1995).
15. Geng, J.G.*, et al.* Rapid neutrophil adhesion to activated endothelium mediated by GMP-140. *Nature* **343**, 757-760 (1990).
16. Bevilacqua, M.P., Stengelin, S., Gimbrone, M.A. & Seed, B. Endothelial leukocyte adhesion molecule 1: an inducible receptor for neutrophils related to complement regulatory proteins and lectins. *Science* **243**, 1160-1165 (1989).
17. Haraldsen, G., Kvale, D., Lien, B., Farstad, I.N. & Brandtzaeg, P. Cytokine-regulated expression of E-selectin, intercellular adhesion molecule-1 (ICAM-1), and vascular cell adhesion molecule-1 (VCAM-1) in human microvascular endothelial cells. *J Immunol* **156**, 2558-2565 (1996).
18. Rivera-Nieves, J.*, et al.* L-selectin, alpha 4 beta 1, and alpha 4 beta 7 integrins participate in CD4+ T cell recruitment to chronically inflamed small intestine. *J Immunol* **174**, 2343-2352 (2005).
19. Laudanna, C., Kim, J.Y., Constantin, G. & Butcher, E. Rapid leukocyte integrin activation by chemokines. *Immunological reviews* **186**, 37-46 (2002).
20. Contento, R.L.*, et al.* Adhesion shapes T cells for prompt and sustained T-cell receptor signalling. *EMBO J* **29**, 4035-4047 (2010).

21. Smith-Garvin, J.E., Koretzky, G.A. & Jordan, M.S. T cell activation. *Annual review of immunology* **27**, 591-619 (2009).
22. Arana, E., Harwood, N.E. & Batista, F.D. Regulation of integrin activation through the B-cell receptor. *J Cell Sci* **121**, 2279-2286 (2008).
23. Van Der Flier, A. & Sonnenberg, A. Function and interactions of integrins. *Cell and Tissue Research* **305**, 285-298 (2001).
24. Gallant, N.D., Michael, K.E. & García, A.J. Cell adhesion strengthening: contributions of adhesive area, integrin binding, and focal adhesion assembly. *Mol Biol Cell* **16**, 4329-4340 (2005).
25. Muller, W.A. Leukocyte-endothelial-cell interactions in leukocyte transmigration and the inflammatory response. *Trends Immunol* **24**, 327-334 (2003).
26. Nourshargh, S., Krombach, F. & Dejana, E. The role of JAM-A and PECAM-1 in modulating leukocyte infiltration in inflamed and ischemic tissues. *J Leukoc Biol* **80**, 714-718 (2006).
27. Korpos, E., Wu, C., Song, J., Hallmann, R. & Sorokin, L. Role of the extracellular matrix in lymphocyte migration. *Cell and Tissue Research* **339**, 47-57 (2010).
28. Stefanelli, T., Malesci, A., De La Rue, S.A. & Danese, S. Anti-adhesion molecule therapies in inflammatory bowel disease: touch and go. *Autoimmun Rev* **7**, 364-369 (2008).
29. Luster, A.D. Chemokines--chemotactic cytokines that mediate inflammation. *N Engl J Med* **338**, 436-445 (1998).
30. Fernandez, E.J. & Lolis, E. Structure, function, and inhibition of chemokines. *Annu Rev Pharmacol Toxicol* **42**, 469-499 (2002).
31. Burke-Gaffney, A., Brooks, A.V.S. & Bogle, R.G. Regulation of chemokine expression in atherosclerosis. *Vascul Pharmacol* **38**, 283-292 (2002).
32. Zlotnik, A. & Yoshie, O. Chemokines: a new classification system and their role in immunity. *Immunity* **12**, 121-127 (2000).
33. Clark-Lewis, I.*, et al.* Structure-activity relationships of chemokines. *J Leukoc Biol* **57**, 703-711 (1995).
34. Comerford, I., Litchfield, W., Harata-Lee, Y., Nibbs, R.J.B. & McColl, S.R. Regulation of chemotactic networks by 'atypical' receptors. *Bioessays* **29**, 237-247 (2007).
35. Locati, M.*, et al.* Silent chemoattractant receptors: D6 as a decoy and scavenger receptor for inflammatory CC chemokines. *Cytokine Growth Factor Rev* **16**, 679-686 (2005).
36. Mantovani, A., Bonecchi, R. & Locati, M. Tuning inflammation and immunity by chemokine sequestration: decoys and more. *Nat Rev Immunol* **6**, 907-918 (2006).
37. Thelen, M. Dancing to the tune of chemokines. *Nat Immunol* **2**, 129-134 (2001).
38. Arai, H. & Charo, I.F. Differential regulation of G-protein-mediated signaling by chemokine receptors. *J Biol Chem* **271**, 21814-21819 (1996).
39. Neptune, E.R. & Bourne, H.R. Receptors induce chemotaxis by releasing the betagamma subunit of Gi, not by activating Gq or Gs. *Proc Natl Acad Sci USA* **94**, 14489-14494 (1997).
40. Tobin, A.B. Phosphorylation of phospholipase C-coupled receptors. *Pharmacol Ther* **75**, 135-151 (1997).
41. Wu, D., Huang, C.K. & Jiang, H. Roles of phospholipid signaling in chemoattractant-induced responses. *J Cell Sci* **113 (Pt 17)**, 2935-2940 (2000).
42. Sotsios, Y. & Ward, S.G. Phosphoinositide 3-kinase: a key biochemical signal for cell migration in response to chemokines. *Immunological reviews* **177**, 217-235 (2000).

43. Weber, C.*, et al.* CCL17-expressing dendritic cells drive atherosclerosis by restraining regulatory T cell homeostasis in mice. *J Clin Invest* **121**, 2898-2910 (2011).
44. Romagnani, S. Cytokines and chemoattractants in allergic inflammation. *Molecular Immunology* **38**, 881-885 (2002).
45. D'Ambrosio, D., Mariani, M., Panina-Bordignon, P. & Sinigaglia, F. Chemokines and their receptors guiding T lymphocyte recruitment in lung inflammation. *Am J Respir Crit Care Med* **164**, 1266-1275 (2001).
46. Nakamoto, N.*, et al.* CCR9+ macrophages are required for acute liver inflammation in mouse models of hepatitis. *Gastroenterology* **142**, 366-376 (2012).
47. Eksteen, B.*, et al.* Hepatic endothelial CCL25 mediates the recruitment of CCR9+ gut-homing lymphocytes to the liver in primary sclerosing cholangitis. *The Journal of Experimental Medicine* **200**, 1511-1517 (2004).
48. Sallusto, F.*, et al.* Rapid and coordinated switch in chemokine receptor expression during dendritic cell maturation. *Eur. J. Immunol.* **28**, 2760-2769 (1998).
49. Cyster, J.G. Chemokines and cell migration in secondary lymphoid organs. *Science* **286**, 2098-2102 (1999).
50. MartIn-Fontecha, A.*, et al.* Regulation of dendritic cell migration to the draining lymph node: impact on T lymphocyte traffic and priming. *The Journal of Experimental Medicine* **198**, 615-621 (2003).
51. Sozzani, S.*, et al.* Differential regulation of chemokine receptors during dendritic cell maturation: a model for their trafficking properties. *J Immunol* **161**, 1083-1086 (1998).
52. Arbonés, M.L.*, et al.* Lymphocyte homing and leukocyte rolling and migration are impaired in L-selectin-deficient mice. *Immunity* **1**, 247-260 (1994).
53. Förster, R.*, et al.* CCR7 coordinates the primary immune response by establishing functional microenvironments in secondary lymphoid organs. *Cell* **99**, 23-33 (1999).
54. Hardtke, S., Ohl, L. & Förster, R. Balanced expression of CXCR5 and CCR7 on follicular T helper cells determines their transient positioning to lymph node follicles and is essential for efficient B-cell help. *Blood* **106**, 1924-1931 (2005).
55. Kerfoot, S.M.*, et al.* Germinal center B cell and T follicular helper cell development initiates in the interfollicular zone. *Immunity* **34**, 947-960 (2011).
56. Viola, A. & Luster, A.D. Chemokines and their receptors: drug targets in immunity and inflammation. *Annu Rev Pharmacol Toxicol* **48**, 171-197 (2008).
57. Charo, I.F. & Ransohoff, R.M. The many roles of chemokines and chemokine receptors in inflammation. *N Engl J Med* **354**, 610-621 (2006).
58. Mantovani, A.*, et al.* The chemokine system in diverse forms of macrophage activation and polarization. *Trends Immunol* **25**, 677-686 (2004).
59. Agace, W. Generation of gut-homing T cells and their localization to the small intestinal mucosa. *Immunol Lett* **128**, 21-23 (2010).
60. Robert, C. & Kupper, T.S. Inflammatory skin diseases, T cells, and immune surveillance. *N Engl J Med* **341**, 1817-1828 (1999).
61. Campbell, J.J.*, et al.* The chemokine receptor CCR4 in vascular recognition by cutaneous but not intestinal memory T cells. *Nature* **400**, 776-780 (1999).
62. Sigmundsdottir, H.*, et al.* DCs metabolize sunlight-induced vitamin D3 to 'program' T cell attraction to the epidermal chemokine CCL27. *Nat Immunol* **8**, 285-293 (2007).
63. Arihiro, S.*, et al.* Differential expression of mucosal addressin cell adhesion molecule-1 (MAdCAM-1) in ulcerative colitis and Crohn's disease. *Pathol Int* **52**, 367-374 (2002).

64. Connor, E.M., Eppihimer, M.J., Morise, Z., Granger, D.N. & Grisham, M.B. Expression of mucosal addressin cell adhesion molecule-1 (MAdCAM-1) in acute and chronic inflammation. *J Leukoc Biol* **65**, 349-355 (1999).
65. Arijs, I.*, et al.* Mucosal Gene Expression of Cell Adhesion Molecules, Chemokines, and Chemokine Receptors in Patients With Inflammatory Bowel Disease Before and After Infliximab Treatment. *The American Journal of Gastroenterology* (2011).
66. Iwata, M.*, et al.* Retinoic acid imprints gut-homing specificity on T cells. *Immunity* **21**, 527-538 (2004).
67. Mebius, R.E. Vitamins in control of lymphocyte migration. *Nat Immunol* **8**, 229-230 (2007).
68. Vicari, A.P.*, et al.* TECK: a novel CC chemokine specifically expressed by thymic dendritic cells and potentially involved in T cell development. *Immunity* **7**, 291-301 (1997).
69. Zabel, B.A.*, et al.* Human G protein-coupled receptor GPR-9-6/CC chemokine receptor 9 is selectively expressed on intestinal homing T lymphocytes, mucosal lymphocytes, and thymocytes and is required for thymus-expressed chemokine-mediated chemotaxis. *The Journal of Experimental Medicine* **190**, 1241-1256 (1999).
70. Kunkel, E.J.*, et al.* Lymphocyte CC chemokine receptor 9 and epithelial thymus-expressed chemokine (TECK) expression distinguish the small intestinal immune compartment: Epithelial expression of tissue-specific chemokines as an organizing principle in regional immunity. *The Journal of Experimental Medicine* **192**, 761-768 (2000).
71. Papadakis, K.A.*, et al.* The role of thymus-expressed chemokine and its receptor CCR9 on lymphocytes in the regional specialization of the mucosal immune system. *J Immunol* **165**, 5069-5076 (2000).
72. Papadakis, K.A.*, et al.* CCR9-positive lymphocytes and thymus-expressed chemokine distinguish small bowel from colonic Crohn's disease. *Gastroenterology* **121**, 246-254 (2001).
73. Zaballos, A., Gutiérrez, J., Varona, R., Ardavín, C. & Márquez, G. Cutting edge: identification of the orphan chemokine receptor GPR-9-6 as CCR9, the receptor for the chemokine TECK. *J Immunol* **162**, 5671-5675 (1999).
74. Yu, C.R., Peden, K.W., Zaitseva, M.B., Golding, H. & Farber, J.M. CCR9A and CCR9B: two receptors for the chemokine CCL25/TECK/Ck beta-15 that differ in their sensitivities to ligand. *J Immunol* **164**, 1293-1305 (2000).
75. Papadakis, K.A.*, et al.* CC chemokine receptor 9 expression defines a subset of peripheral blood lymphocytes with mucosal T cell phenotype and Th1 or T-regulatory 1 cytokine profile. *J Immunol* **171**, 159-165 (2003).
76. Berahovich, R.D., Lai, N.L., Wei, Z., Lanier, L.L. & Schall, T.J. Evidence for NK cell subsets based on chemokine receptor expression. *J Immunol* **177**, 7833-7840 (2006).
77. Wendland, M.*, et al.* CCR9 is a homing receptor for plasmacytoid dendritic cells to the small intestine. *Proc Natl Acad Sci USA* **104**, 6347-6352 (2007).
78. Nakano, H., Yanagita, M. & Gunn, M.D. CD11c(+)B220(+)Gr-1(+) cells in mouse lymph nodes and spleen display characteristics of plasmacytoid dendritic cells. *The Journal of Experimental Medicine* **194**, 1171-1178 (2001).
79. Hadeiba, H.*, et al.* CCR9 expression defines tolerogenic plasmacytoid dendritic cells able to suppress acute graft-versus-host disease. *Nat Immunol* **9**, 1253-1260 (2008).
80. Zhang, Y. & Wang, H. Integrin signalling and function in immune cells. *Immunology* **135**, 268-275 (2012).
81. Stagg, A.J., Kamm, M.A. & Knight, S.C. Intestinal dendritic cells increase T cell expression of alpha4beta7 integrin. *Eur. J. Immunol.* **32**, 1445-1454 (2002).

82. Mora, J.R., *et al.* Selective imprinting of gut-homing T cells by Peyer's patch dendritic cells. *Nature* **424**, 88-93 (2003).
83. Svensson, M., *et al.* Selective generation of gut-tropic T cells in gut-associated lymphoid tissues: requirement for GALT dendritic cells and adjuvant. *Ann N Y Acad Sci* **1029**, 405-407 (2004).
84. Eksteen, B., *et al.* Gut homing receptors on CD8 T cells are retinoic acid dependent and not maintained by liver dendritic or stellate cells. *Gastroenterology* **137**, 320-329 (2009).
85. Duester, G. Families of retinoid dehydrogenases regulating vitamin A function: production of visual pigment and retinoic acid. *Eur J Biochem* **267**, 4315-4324 (2000).
86. Allenby, G., *et al.* Retinoic acid receptors and retinoid X receptors: interactions with endogenous retinoic acids. *Proc Natl Acad Sci USA* **90**, 30-34 (1993).
87. Walters, M.J., *et al.* Characterization of CCX282-B, an orally bioavailable antagonist of the CCR9 chemokine receptor, for treatment of inflammatory bowel disease. *The Journal of pharmacology and experimental therapeutics* **335**, 61-69 (2010).
88. Youn, B.S., Kim, C.H., Smith, F.O. & Broxmeyer, H.E. TECK, an efficacious chemoattractant for human thymocytes, uses GPR-9-6/CCR9 as a specific receptor. *Blood* **94**, 2533-2536 (1999).
89. Youn, B.S., Kim, Y.J., Mantel, C., Yu, K.Y. & Broxmeyer, H.E. Blocking of c-FLIP(L)--independent cycloheximide-induced apoptosis or Fas-mediated apoptosis by the CC chemokine receptor 9/TECK interaction. *Blood* **98**, 925-933 (2001).
90. Saruta, M., *et al.* Phenotype and effector function of CC chemokine receptor 9-expressing lymphocytes in small intestinal Crohn's disease. *J Immunol* **178**, 3293-3300 (2007).
91. Hart, R. & Greaves, D.R. Chemerin contributes to inflammation by promoting macrophage adhesion to VCAM-1 and fibronectin through clustering of VLA-4 and VLA-5. *J Immunol* **185**, 3728-3739 (2010).
92. Aron, J.H. & Bowlus, C.L. The immunobiology of primary sclerosing cholangitis. *Semin Immunopathol* **31**, 383-397 (2009).
93. Pollheimer, M.J., Halilbasic, E., Fickert, P. & Trauner, M. Pathogenesis of primary sclerosing cholangitis. *Best Pract Res Clin Gastroenterol* **25**, 727-739 (2011).
94. Molodecky, N.A., *et al.* Incidence of primary sclerosing cholangitis: a systematic review and meta-analysis. *Hepatology (Baltimore, Md)* **53**, 1590-1599 (2011).
95. Chapman, R.W. Aetiology and natural history of primary sclerosing cholangitis--a decade of progress? *Gut* **32**, 1433-1435 (1991).
96. Holte, K. & Kehlet, H. Postoperative ileus: a preventable event. *Br J Surg* **87**, 1480-1493 (2000).
97. Engel, D.R., *et al.* T helper type 1 memory cells disseminate postoperative ileus over the entire intestinal tract. *Nat Med*, 1-8 (2010).
98. Wurbel, M.A., *et al.* The chemokine TECK is expressed by thymic and intestinal epithelial cells and attracts double- and single-positive thymocytes expressing the TECK receptor CCR9. *Eur. J. Immunol.* **30**, 262-271 (2000).
99. Wurbel, M.-A., Malissen, M., Guy-Grand, D., Malissen, B. & Campbell, J.J. Impaired accumulation of antigen-specific CD8 lymphocytes in chemokine CCL25-deficient intestinal epithelium and lamina propria. *J Immunol* **178**, 7598-7606 (2007).
100. Wurbel, M.A., *et al.* Mice lacking the CCR9 CC-chemokine receptor show a mild impairment of early T- and B-cell development and a reduction in T-cell receptor gammadelta(+) gut intraepithelial lymphocytes. *Blood* **98**, 2626-2632 (2001).

101. Reuter, B.K. & Pizarro, T.T. Mechanisms of tight junction dysregulation in the SAMP1/YitFc model of Crohn's disease-like ileitis. *Ann N Y Acad Sci* **1165**, 301-307 (2009).
102. Rivera-Nieves, J.*, et al.* Antibody blockade of CCL25/CCR9 ameliorates early but not late chronic murine ileitis. *Gastroenterology* **131**, 1518-1529 (2006).
103. Kontoyiannis, D., Pasparakis, M., Pizarro, T.T., Cominelli, F. & Kollias, G. Impaired on/off regulation of TNF biosynthesis in mice lacking TNF AU-rich elements: implications for joint and gut-associated immunopathologies. *Immunity* **10**, 387-398 (1999).
104. Wermers, J.D., McNamee, E.N., Wurbel, M.-A., Jedlicka, P. & Rivera-Nieves, J. The chemokine receptor CCR9 is required for the T cell-mediated regulation of chronic ileitis in mice. *Gastroenterology* (2011).
105. Apostolaki, M.*, et al.* Role of beta7 integrin and the chemokine/chemokine receptor pair CCL25/CCR9 in modeled TNF-dependent Crohn's disease. *Gastroenterology* **134**, 2025-2035 (2008).
106. Wirtz, S., Neufert, C., Weigmann, B. & Neurath, M.F. Chemically induced mouse models of intestinal inflammation. *Nat Protoc* **2**, 541-546 (2007).
107. Wurbel, M.-A., McIntire, M.G., Dwyer, P. & Fiebiger, E. CCL25/CCR9 interactions regulate large intestinal inflammation in a murine model of acute colitis. *PLoS ONE* **6**, e16442 (2011).
108. Mombaerts, P.*, et al.* RAG-1-deficient mice have no mature B and T lymphocytes. *Cell* **68**, 869-877 (1992).
109. Powrie, F., Leach, M.W., Mauze, S., Caddle, L.B. & Coffman, R.L. Phenotypically distinct subsets of CD4+ T cells induce or protect from chronic intestinal inflammation in C. B-17 scid mice. *Int Immunol* **5**, 1461-1471 (1993).
110. Mizuno, S.*, et al.* CCR9(+) plasmacytoid dendritic cells in the small intestine suppress development of intestinal inflammation in mice. *Immunol Lett* **146**, 64-69 (2012).
111. Forbes, A. & Misiewicz, J.J. *Atlas Of Clinical Gastroenterology*, (Elsevier Mosby, 2005).
112. Johnson, L.R. *Physiology of the Gastrointestinal Tract*, (Elsevier Academic Press, 2006).
113. Lacy, E.R. Functional Morphology of the Large Intestine. in *Comprehensive Physiology* (John Wiley & Sons, Inc., 2010).
114. Ross, M.H., Kaye, G.I. & Pawlina, W. *Histology: A Text and Atlas with Cell and Molecular Biology*, (Lippincott Williams & Wilkins, 2003).
115. Kagnoff, M.F. & Eckmann, L. Epithelial cells as sensors for microbial infection. *J Clin Invest* **100**, 6-10 (1997).
116. Keshav, S. Paneth cells: leukocyte-like mediators of innate immunity in the intestine. *J Leukoc Biol* **80**, 500-508 (2006).
117. Jeurissen, S.H., Duijvestijn, A.M., Sontag, Y. & Kraal, G. Lymphocyte migration into the lamina propria of the gut is mediated by specialized HEV-like blood vessels. *Immunology* **62**, 273-277 (1987).
118. Keita, A.V. & Söderholm, J.D. Barrier dysfunction and bacterial uptake in the follicle-associated epithelium of ileal Crohn's disease. *Ann N Y Acad Sci* **1258**, 125-134 (2012).
119. Cunningham, K.E. & Turner, J.R. Myosin light chain kinase: pulling the strings of epithelial tight junction function. *Ann N Y Acad Sci* **1258**, 34-42 (2012).

120. Johansson, M.E.V., Larsson, J.M.H. & Hansson, G.C. The two mucus layers of colon are organized by the MUC2 mucin, whereas the outer layer is a legislator of host-microbial interactions. *Proc Natl Acad Sci USA* **108 Suppl 1**, 4659-4665 (2011).
121. Mantis, N.J., Rol, N. & Corthésy, B. Secretory IgA's complex roles in immunity and mucosal homeostasis in the gut. *Mucosal immunology* **4**, 603-611 (2011).
122. Kumar, H., Kawai, T. & Akira, S. Pathogen recognition by the innate immune system. *Int Rev Immunol* **30**, 16-34 (2011).
123. Uematsu, S. & Fujimoto, K. The innate immune system in the intestine. *Microbiology and Immunology* **54**, 645-657 (2010).
124. Murphy, K.P., Travers, P., Walport, M. & Janeway, C. *Janeway's immunobiology*, (Garland Science, 2008).
125. Pearson, C., Uhlig, H.H. & Powrie, F. Lymphoid microenvironments and innate lymphoid cells in the gut. *Trends Immunol* **33**, 289-296 (2012).
126. Koboziev, I., Karlsson, F. & Grisham, M.B. Gut-associated lymphoid tissue, T cell trafficking, and chronic intestinal inflammation. *Ann N Y Acad Sci* **1207 Suppl 1**, E86-93 (2010).
127. Dangl, J.L.*, et al.* Segmental flexibility and complement fixation of genetically engineered chimeric human, rabbit and mouse antibodies. *The EMBO journal* **7**, 1989-1994 (1988).
128. Chan, A.C. & Carter, P.J. Therapeutic antibodies for autoimmunity and inflammation. *Nature Reviews Immunology* **10**, 301-316 (2010).
129. Weisbart, R.H., Kacena, A., Schuh, A. & Golde, D.W. GM-CSF induces human neutrophil IgA-mediated phagocytosis by an IgA Fc receptor activation mechanism. *Nature* **332**, 647-648 (1988).
130. Girard, J.P. & Springer, T.A. High endothelial venules (HEVs): specialized endothelium for lymphocyte migration. *Immunol Today* **16**, 449-457 (1995).
131. Pickard, J.M. & Chervonsky, A.V. Sampling of the intestinal microbiota by epithelial M cells. *Curr Gastroenterol Rep* **12**, 331-339 (2010).
132. Brodskyn, C.I., DeKrey, G.K. & Titus, R.G. Influence of costimulatory molecules on immune response to Leishmania major by human cells in vitro. *Infection and Immunity* **69**, 665-672 (2001).
133. Lenschow, D.J.*, et al.* Differential up-regulation of the B7-1 and B7-2 costimulatory molecules after Ig receptor engagement by antigen. *Journal of immunology (Baltimore, Md : 1950)* **153**, 1990-1997 (1994).
134. Rodríguez-Pinto, D. ScienceDirect.com - Cellular Immunology - B cells as antigen presenting cells. *Cellular immunology* (2005).
135. Guermonprez, P., Valladeau, J. & Zitvogel, L. Antigen presentation and T cell stimulation by dendritic cells. *Annual review of ...* (2002).
136. Coyle, A.J. & Gutierrez-Ramos, J.-C. The expanding B7 superfamily: Increasing complexity in costimulatory signals regulating T cell function - Nature Immunology. *Nature Immunology* **2**, 203-209 (2001).
137. Khoruts, A., Mondino, A., Pape, K.A., Reiner, S.L. & Jenkins, M.K. A natural immunological adjuvant enhances T cell clonal expansion through a CD28-dependent, interleukin (IL)-2-independent mechanism. *The Journal of Experimental Medicine* **187**, 225-236 (1998).
138. K. Abbas, A. & H. Lichtman, A. Cellular and molecular immunology. 564 (2005).
139. Pamer, E. & Cresswell, P. Mechanisms of MHC class I--restricted antigen processing. *Annual review of immunology* **16**, 323-358 (1998).
140. Rock, K.L. & Shen, L. Cross-presentation: underlying mechanisms and role in immune surveillance. *Immunological reviews* **207**, 166-183 (2005).

141. Stinchcombe, J.C., Bossi, G., Booth, S. & Griffiths, G.M. The immunological synapse of CTL contains a secretory domain and membrane bridges. *Immunity* **15**, 751-761 (2001).
142. Berke, G. The CTL's kiss of death. *Cell* **81**, 9-12 (1995).
143. Kajino, K., Kajino, Y. & Greene, M.I. Fas- and perforin-independent mechanism of cytotoxic T lymphocyte.
144. Ju, S.T.*, et al.* Fas(CD95)/FasL interactions required for programmed cell death after T-cell activation. *Nature* **373**, 444-448 (1995).
145. Suzuki, I. & Fink, P.J. The dual functions of fas ligand in the regulation of peripheral CD8+ and CD4+ T cells. *Proc Natl Acad Sci USA* **97**, 1707-1712 (2000).
146. Müllauer, L.*, et al.* Autoimmune lymphoproliferative syndrome (ALPS) caused by Fas (CD95) mutation mimicking sarcoidosis. *Am J Surg Pathol* **32**, 329-334 (2008).
147. Dowdell, K.C.*, et al.* Somatic FAS mutations are common in patients with genetically undefined autoimmune lymphoproliferative syndrome. *Blood* **115**, 5164-5169 (2010).
148. Billerbeck, E.*, et al.* Analysis of CD161 expression on human CD8+ T cells defines a distinct functional subset with tissue-homing properties. *Proc Natl Acad Sci USA* **107**, 3006-3011 (2010).
149. Chtanova, T., Kemp, R.A., Sutherland, A.P., Ronchese, F. & Mackay, C.R. Gene microarrays reveal extensive differential gene expression in both CD4(+) and CD8(+) type 1 and type 2 T cells. *J Immunol* **167**, 3057-3063 (2001).
150. Dong, T.*, et al.* High pro-inflammatory cytokine secretion and loss of high avidity cross-reactive cytotoxic T-cells during the course of secondary dengue virus infection. *PLoS ONE* **2**, e1192 (2007).
151. Malnati, M.S.*, et al.* Processing pathways for presentation of cytosolic antigen to MHC class II-restricted T cells. *Nature* **357**, 702-704 (1992).
152. Nonoyama, S., Hollenbaugh, D., Aruffo, A., Ledbetter, J.A. & Ochs, H.D. B cell activation via CD40 is required for specific antibody production by antigen-stimulated human B cells. *The Journal of Experimental Medicine* **178**, 1097-1102 (1993).
153. Swain, S.L., Mckinstry, K.K. & Strutt, T.M. Expanding roles for CD4+ T cells in immunity to viruses. *Nat Rev Immunol* **12**, 136-148 (2012).
154. Lee, Y.K.*, et al.* Late Developmental Plasticity in the T Helper 17 Lineage. *Immunity* **30**, 92-107 (2009).
155. Plevy, S.E.*, et al.* A role for TNF-alpha and mucosal T helper-1 cytokines in the pathogenesis of Crohn's disease. *J Immunol* **159**, 6276-6282 (1997).
156. Matsuoka, K.*, et al.* T-bet upregulation and subsequent interleukin 12 stimulation are essential for induction of Th1 mediated immunopathology in Crohn's disease. *Gut* **53**, 1303-1308 (2004).
157. Langrish, C.L.*, et al.* IL-23 drives a pathogenic T cell population that induces autoimmune inflammation. *The Journal of Experimental Medicine* **201**, 233-240 (2005).
158. Kolls, J.K. & Lindén, A. Interleukin-17 family members and inflammation. *Immunity* **21**, 467-476 (2004).
159. Ivanov, I.I.*, et al.* The orphan nuclear receptor RORgammat directs the differentiation program of proinflammatory IL-17+ T helper cells. *Cell* **126**, 1121-1133 (2006).
160. Annunziato, F.*, et al.* Phenotypic and functional features of human Th17 cells. *The Journal of Experimental Medicine* **204**, 1849-1861 (2007).
161. Lee, Y.K., Mukasa, R., Hatton, R.D. & Weaver, C.T. Developmental plasticity of Th17 and Treg cells. *Current opinion in immunology* **21**, 274-280 (2009).

162. Kotake, S.*, et al.* IL-17 in synovial fluids from patients with rheumatoid arthritis is a potent stimulator of osteoclastogenesis. *J Clin Invest* **103**, 1345-1352 (1999).
163. Teunissen, M.B., Koomen, C.W., de Waal Malefyt, R., Wierenga, E.A. & Bos, J.D. Interleukin-17 and interferon-gamma synergize in the enhancement of proinflammatory cytokine production by human keratinocytes. *J Invest Dermatol* **111**, 645-649 (1998).
164. Matusevicius, D.*, et al.* Interleukin-17 mRNA expression in blood and CSF mononuclear cells is augmented in multiple sclerosis. *Mult Scler* **5**, 101-104 (1999).
165. Lock, C.*, et al.* Gene-microarray analysis of multiple sclerosis lesions yields new targets validated in autoimmune encephalomyelitis. *Nat Med* **8**, 500-508 (2002).
166. Amadi-Obi, A.*, et al.* TH17 cells contribute to uveitis and scleritis and are expanded by IL-2 and inhibited by IL-27/STAT1. *Nat Med* **13**, 711-718 (2007).
167. Chi, W.*, et al.* Upregulated IL-23 and IL-17 in Behçet patients with active uveitis. *Invest Ophthalmol Vis Sci* **49**, 3058-3064 (2008).
168. Fujino, S.*, et al.* Increased expression of interleukin 17 in inflammatory bowel disease. *Gut* **52**, 65-70 (2003).
169. Seiderer, J.*, et al.* Role of the novel Th17 cytokine IL-17F in inflammatory bowel disease (IBD): upregulated colonic IL-17F expression in active Crohn's disease and analysis of the IL17F p.His161Arg polymorphism in IBD. *Inflamm Bowel Dis* **14**, 437-445 (2008).
170. Langrish, C.L.*, et al.* IL-12 and IL-23: master regulators of innate and adaptive immunity. *Immunological reviews* **202**, 96-105 (2004).
171. Franke, A.*, et al.* Genome-wide meta-analysis increases to 71 the number of confirmed Crohn's disease susceptibility loci. *Nat Genet* **42**, 1118-1125 (2010).
172. Lees, C.W., Barrett, J.C., Parkes, M. & Satsangi, J. New IBD genetics: common pathways with other diseases. *Gut* **60**, 1739-1753 (2011).
173. Barrett, J.C.*, et al.* Genome-wide association defines more than 30 distinct susceptibility loci for Crohn's disease. *Nat Genet* **40**, 955-962 (2008).
174. Hori, S., Nomura, T. & Sakaguchi, S. Control of regulatory T cell development by the transcription factor Foxp3. *Science* **299**, 1057-1061 (2003).
175. Fontenot, J.D., Gavin, M.A. & Rudensky, A.Y. Foxp3 programs the development and function of CD4+CD25+ regulatory T cells. *Nat Immunol* **4**, 330-336 (2003).
176. Fiorentino, D.F., Zlotnik, A., Mosmann, T.R., Howard, M. & O'Garra, A. IL-10 inhibits cytokine production by activated macrophages. *J Immunol* **147**, 3815-3822 (1991).
177. Ito, S.*, et al.* Interleukin-10 inhibits expression of both interferon alpha- and interferon gamma- induced genes by suppressing tyrosine phosphorylation of STAT1. *Blood* **93**, 1456-1463 (1999).
178. Taga, K. & Tosato, G. IL-10 inhibits human T cell proliferation and IL-2 production. *J Immunol* **148**, 1143-1148 (1992).
179. Scheinin, T., Butler, D.M., Salway, F., Scallon, B. & Feldmann, M. Validation of the interleukin-10 knockout mouse model of colitis: antitumour necrosis factor-antibodies suppress the progression of colitis. *Clin Exp Immunol* **133**, 38-43 (2003).
180. Kullberg, M.C.*, et al.* Bacteria-triggered CD4(+) T regulatory cells suppress Helicobacter hepaticus-induced colitis. *The Journal of Experimental Medicine* **196**, 505-515 (2002).
181. Coombes, J.L., Robinson, N.J., Maloy, K.J., Uhlig, H.H. & Powrie, F. Regulatory T cells and intestinal homeostasis. *Immunological reviews* **204**, 184-194 (2005).
182. Powrie, F.*, et al.* Inhibition of Th1 responses prevents inflammatory bowel disease in scid mice reconstituted with CD45RBhi CD4+ T cells. *Immunity* **1**, 553-562 (1994).

183. Asseman, C., Mauze, S., Leach, M.W., Coffman, R.L. & Powrie, F. An essential role for interleukin 10 in the function of regulatory T cells that inhibit intestinal inflammation. *The Journal of Experimental Medicine* **190**, 995-1004 (1999).
184. Wildin, R.S., Smyk-Pearson, S. & Filipovich, A.H. Clinical and molecular features of the immunodysregulation, polyendocrinopathy, enteropathy, X linked (IPEX) syndrome. *J Med Genet* **39**, 537-545 (2002).
185. Patey-Mariaud de Serre, N.*, et al.* Digestive histopathological presentation of IPEX syndrome. *Mod Pathol* **22**, 95-102 (2009).
186. Maloy, K.J. & Powrie, F. Intestinal homeostasis and its breakdown in inflammatory bowel disease. *Nature* **474**, 298-306 (2011).
187. Molodecky, N.A.*, et al.* Increasing incidence and prevalence of the inflammatory bowel diseases with time, based on systematic review. *Gastroenterology* **142**, 46-54.e42; quiz e30 (2012).
188. Zheng, J.J.*, et al.* Crohn's disease in mainland China: a systematic analysis of 50 years of research. *Chin J Dig Dis* **6**, 175-181 (2005).
189. Sood, A., Midha, V., Sood, N., Bhatia, A.S. & Avasthi, G. Incidence and prevalence of ulcerative colitis in Punjab, North India. *Gut* **52**, 1587-1590 (2003).
190. Loftus, E.V. Clinical epidemiology of inflammatory bowel disease: Incidence, prevalence, and environmental influences. *Gastroenterology* **126**, 1504-1517 (2004).
191. Abraham, C. & Cho, J.H. Inflammatory bowel disease. *N Engl J Med* **361**, 2066-2078 (2009).
192. Cummings, J.R.F., Keshav, S. & Travis, S.P.L. Medical management of Crohn's disease. *BMJ* **336**, 1062-1066 (2008).
193. Bassi, A., Dodd, S., Williamson, P. & Bodger, K. Cost of illness of inflammatory bowel disease in the UK: a single centre retrospective study. *Gut* **53**, 1471-1478 (2004).
194. Semrin, G.*, et al.* Impaired intestinal iron absorption in Crohn's disease correlates with disease activity and markers of inflammation. *Inflamm Bowel Dis* **12**, 1101-1106 (2006).
195. Freeman, H.J. Granuloma-positive Crohn's disease. *Can J Gastroenterol* **21**, 583-587 (2007).
196. Mowat, C.*, et al.* Guidelines for the management of inflammatory bowel disease in adults. *Gut* **60**, 571-607 (2011).
197. Kappelman, M.D.*, et al.* Direct health care costs of Crohn's disease and ulcerative colitis in US children and adults. *Gastroenterology* **135**, 1907-1913 (2008).
198. Kobayashi, T.*, et al.* IL23 differentially regulates the Th1/Th17 balance in ulcerative colitis and Crohn's disease. *Gut* **57**, 1682-1689 (2008).
199. Fuss, I.J.*, et al.* Disparate CD4+ lamina propria (LP) lymphokine secretion profiles in inflammatory bowel disease. Crohn's disease LP cells manifest increased secretion of IFN-gamma, whereas ulcerative colitis LP cells manifest increased secretion of IL-5. *J Immunol* **157**, 1261-1270 (1996).
200. Parronchi, P.*, et al.* Type 1 T-helper cell predominance and interleukin-12 expression in the gut of patients with Crohn's disease. *Am J Pathol* **150**, 823-832 (1997).
201. Fais, S.*, et al.* Spontaneous release of interferon gamma by intestinal lamina propria lymphocytes in Crohn's disease. Kinetics of in vitro response to interferon gamma inducers. *Gut* **32**, 403-407 (1991).
202. Breese, E., Braegger, C.P., Corrigan, C.J., Walker-Smith, J.A. & MacDonald, T.T. Interleukin-2- and interferon-gamma-secreting T cells in normal and diseased human intestinal mucosa. *Immunology* **78**, 127-131 (1993).

203. Monteleone, G.*, et al.* Interleukin 12 is expressed and actively released by Crohn's disease intestinal lamina propria mononuclear cells. *Gastroenterology* **112**, 1169-1178 (1997).
204. Okazawa, A.*, et al.* Th1-mediated intestinal inflammation in Crohn's disease may be induced by activation of lamina propria lymphocytes through synergistic stimulation of interleukin-12 and interleukin-18 without T cell receptor engagement. *The American Journal of Gastroenterology* **97**, 3108-3117 (2002).
205. Fuss, I.J.*, et al.* Nonclassical CD1d-restricted NK T cells that produce IL-13 characterize an atypical Th2 response in ulcerative colitis. *J Clin Invest* **113**, 1490-1497 (2004).
206. Heller, F.*, et al.* Interleukin-13 is the key effector Th2 cytokine in ulcerative colitis that affects epithelial tight junctions, apoptosis, and cell restitution. *Gastroenterology* **129**, 550-564 (2005).
207. Halstensen, T.S. & Brandtzaeg, P. Activated T lymphocytes in the celiac lesion: non-proliferative activation (CD25) of CD4+ alpha/beta cells in the lamina propria but proliferation (Ki-67) of alpha/beta and gamma/delta cells in the epithelium. *Eur. J. Immunol.* **23**, 505-510 (1993).
208. Fell, J.M., Walker-Smith, J.A., Spencer, J. & MacDonald, T.T. The distribution of dividing T cells throughout the intestinal wall in inflammatory bowel disease (IBD). *Clin Exp Immunol* **104**, 280-285 (1996).
209. Feng, T., Wang, L., Schoeb, T.R., Elson, C.O. & Cong, Y. Microbiota innate stimulation is a prerequisite for T cell spontaneous proliferation and induction of experimental colitis. *The Journal of Experimental Medicine* **207**, 1321-1332 (2010).
210. Mottet, C., Uhlig, H.H. & Powrie, F. Cutting edge: cure of colitis by CD4+CD25+ regulatory T cells. *J Immunol* **170**, 3939-3943 (2003).
211. Papadakis, K.A. Chemokines in inflammatory bowel disease. *Current Allergy and Asthma Reports* **4**, 83-89 (2004).
212. Garin, A. & Proudfoot, A.E.I. Chemokines as targets for therapy. *Exp Cell Res* **317**, 602-612 (2011).
213. Nishimura, M., Kuboi, Y., Muramoto, K., Kawano, T. & Imai, T. Chemokines as novel therapeutic targets for inflammatory bowel disease. *Ann N Y Acad Sci* **1173**, 350-356 (2009).
214. Schall, T.J. & Proudfoot, A.E.I. Overcoming hurdles in developing successful drugs targeting chemokine receptors. *Nat Rev Immunol* **11**, 355-363 (2011).
215. Thomas, S. & Baumgart, D.C. Targeting leukocyte migration and adhesion in Crohn's disease and ulcerative colitis. *Inflammopharmacology* (2011).
216. Sisirak, V.*, et al.* CCR6/CCR10-mediated plasmacytoid dendritic cell recruitment to inflamed epithelia after instruction in lymphoid tissues. *Blood* **118**, 5130-5140 (2011).
217. Williams, I.R. CCR6 and CCL20: partners in intestinal immunity and lymphorganogenesis. *Ann N Y Acad Sci* **1072**, 52-61 (2006).
218. Kleinewietfeld, M.*, et al.* CCR6 expression defines regulatory effector/memory-like cells within the CD25(+)CD4+ T-cell subset. *Blood* **105**, 2877-2886 (2005).
219. Rivino, L.*, et al.* CCR6 is expressed on an IL-10-producing, autoreactive memory T cell population with context-dependent regulatory function. *The Journal of Experimental Medicine* **207**, 565-577 (2010).
220. Singh, S.P., Zhang, H.H., Foley, J.F., Hedrick, M.N. & Farber, J.M. Human T cells that are able to produce IL-17 express the chemokine receptor CCR6. *J Immunol* **180**, 214-221 (2008).

221. Demedts, I.K., *et al.* Accumulation of dendritic cells and increased CCL20 levels in the airways of patients with chronic obstructive pulmonary disease. *Am J Respir Crit Care Med* **175**, 998-1005 (2007).
222. McDonald, K.G., *et al.* CC chemokine receptor 6 expression by B lymphocytes is essential for the development of isolated lymphoid follicles. *Am J Pathol* **170**, 1229-1240 (2007).
223. Varona, R., *et al.* CCR6-deficient mice have impaired leukocyte homeostasis and altered contact hypersensitivity and delayed-type hypersensitivity responses. *J Clin Invest* **107**, R37-45 (2001).
224. Salazar-Gonzalez, R.M., *et al.* CCR6-mediated dendritic cell activation of pathogen-specific T cells in Peyer's patches. *Immunity* **24**, 623-632 (2006).
225. Cook, D.N., *et al.* CCR6 mediates dendritic cell localization, lymphocyte homeostasis, and immune responses in mucosal tissue. *Immunity* **12**, 495-503 (2000).
226. Kaser, A., *et al.* Increased expression of CCL20 in human inflammatory bowel disease. *J Clin Immunol* **24**, 74-85 (2004).
227. Hovhannisyan, Z., Treatman, J., Littman, D.R. & Mayer, L. Characterization of IL-17-producing regulatory T cells in inflamed intestinal mucosa from patients with inflammatory bowel diseases. *Gastroenterology* (2010).
228. Teramoto, K., *et al.* Increased lymphocyte trafficking to colonic microvessels is dependent on MAdCAM-1 and C-C chemokine mLARC/CCL20 in DSS-induced mice colitis. *Clin Exp Immunol* **139**, 421-428 (2005).
229. Varona, R., Cadenas, V., Flores, J., Martínez-A, C. & Márquez, G. CCR6 has a non-redundant role in the development of inflammatory bowel disease. *Eur. J. Immunol.* **33**, 2937-2946 (2003).
230. Katchar, K., Kelly, C.P., Keates, S., O'brien, M.J. & Keates, A.C. MIP-3alpha neutralizing monoclonal antibody protects against TNBS-induced colonic injury and inflammation in mice. *Am J Physiol Gastrointest Liver Physiol* **292**, G1263-1271 (2007).
231. Kitamura, K., Farber, J.M. & Kelsall, B.L. CCR6 marks regulatory T cells as a colon-tropic, IL-10-producing phenotype. *J Immunol* **185**, 3295-3304 (2010).
232. Lazarus, N.H., *et al.* A common mucosal chemokine (mucosae-associated epithelial chemokine/CCL28) selectively attracts IgA plasmablasts. *J Immunol* **170**, 3799-3805 (2003).
233. Pan, J., *et al.* A novel chemokine ligand for CCR10 and CCR3 expressed by epithelial cells in mucosal tissues. *J Immunol* **165**, 2943-2949 (2000).
234. Hu, S., Yang, K., Yang, J., Li, M. & Xiong, N. Critical roles of chemokine receptor CCR10 in regulating memory IgA responses in intestines. *Proc Natl Acad Sci USA* **108**, E1035-1044 (2011).
235. Morteau, O., *et al.* An indispensable role for the chemokine receptor CCR10 in IgA antibody-secreting cell accumulation. *J Immunol* **181**, 6309-6315 (2008).
236. Tarlton, N.J., *et al.* Plasmablast frequency and trafficking receptor expression are altered in pediatric ulcerative colitis. *Inflamm Bowel Dis* (2012).
237. Higgins, L.M., Frankel, G., Douce, G., Dougan, G. & MacDonald, T.T. Citrobacter rodentium infection in mice elicits a mucosal Th1 cytokine response and lesions similar to those in murine inflammatory bowel disease. *Infection and Immunity* **67**, 3031-3039 (1999).
238. Loetscher, M., *et al.* Chemokine receptor specific for IP10 and mig: structure, function, and expression in activated T-lymphocytes. *The Journal of Experimental Medicine* **184**, 963-969 (1996).

239. Cole, K.E.*, et al.* Interferon-inducible T cell alpha chemoattractant (I-TAC): a novel non-ELR CXC chemokine with potent activity on activated T cells through selective high affinity binding to CXCR3. *The Journal of Experimental Medicine* **187**, 2009-2021 (1998).
240. Mach, F.*, et al.* Differential expression of three T lymphocyte-activating CXC chemokines by human atheroma-associated cells. *J Clin Invest* **104**, 1041-1050 (1999).
241. Sørensen, T.L.*, et al.* Expression of specific chemokines and chemokine receptors in the central nervous system of multiple sclerosis patients. *J Clin Invest* **103**, 807-815 (1999).
242. Hancock, W.W.*, et al.* Requirement of the chemokine receptor CXCR3 for acute allograft rejection. *The Journal of Experimental Medicine* **192**, 1515-1520 (2000).
243. Ostvik, A.E.*, et al.* Enhanced expression of CXCL10 in inflammatory bowel disease: Potential role of mucosal toll-like receptor 3 stimulation. *Inflamm Bowel Dis* (2012).
244. Hosomi, S.*, et al.* Increased numbers of immature plasma cells in peripheral blood specifically overexpress chemokine receptor CXCR3 and CXCR4 in patients with ulcerative colitis. *Clin Exp Immunol* **163**, 215-224 (2011).
245. Yuan, Y.H.*, et al.* Chemokine receptor CXCR3 expression in inflammatory bowel disease. *Inflamm Bowel Dis* **7**, 281-286 (2001).
246. Sasaki, S.*, et al.* Blockade of CXCL10 protects mice from acute colitis and enhances crypt cell survival. *Eur. J. Immunol.* **32**, 3197-3205 (2002).
247. Wilson, M.S.*, et al.* Colitis and Intestinal Inflammation in IL10−/− Mice Results From IL-13Rα2–Mediated Attenuation of IL-13 Activity. *YGAST* **140**, 254-264.e252 (2010).
248. Singh, U.P., Singh, S., Taub, D.D. & Lillard, J.W. Inhibition of IFN-gamma-inducible protein-10 abrogates colitis in IL-10-/- mice. *J Immunol* **171**, 1401-1406 (2003).
249. Singh, U.P.*, et al.* CXCL10-producing mucosal CD4+ T cells, NK cells, and NKT cells are associated with chronic colitis in IL-10(-/-) mice, which can be abrogated by anti-CXCL10 antibody inhibition. *J Interferon Cytokine Res* **28**, 31-43 (2008).
250. Bazan, J.F.*, et al.* A new class of membrane-bound chemokine with a CX3C motif. *Nature* **385**, 640-644 (1997).
251. Garcia, G.E.*, et al.* NF-kappaB-dependent fractalkine induction in rat aortic endothelial cells stimulated by IL-1beta, TNF-alpha, and LPS. *J Leukoc Biol* **67**, 577-584 (2000).
252. Ludwig, A., Berkhout, T., Moores, K., Groot, P. & Chapman, G. Fractalkine is expressed by smooth muscle cells in response to IFN-gamma and TNF-alpha and is modulated by metalloproteinase activity. *J Immunol* **168**, 604-612 (2002).
253. Greaves, D.R.*, et al.* Linked chromosome 16q13 chemokines, macrophage-derived chemokine, fractalkine, and thymus- and activation-regulated chemokine, are expressed in human atherosclerotic lesions. *Arterioscler Thromb Vasc Biol* **21**, 923-929 (2001).
254. Nishiyori, A.*, et al.* Localization of fractalkine and CX3CR1 mRNAs in rat brain: does fractalkine play a role in signaling from neuron to microglia? *FEBS Lett* **429**, 167-172 (1998).
255. Imai, T.*, et al.* Identification and molecular characterization of fractalkine receptor CX3CR1, which mediates both leukocyte migration and adhesion. *Cell* **91**, 521-530 (1997).
256. Kobayashi, T.*, et al.* Exclusive increase of CX3CR1+CD28-CD4+ T cells in inflammatory bowel disease and their recruitment as intraepithelial lymphocytes. *Inflamm Bowel Dis* **13**, 837-846 (2007).

257. Sans, M.*, et al.* Enhanced recruitment of CX3CR1+ T cells by mucosal endothelial cell-derived fractalkine in inflammatory bowel disease. *Gastroenterology* **132**, 139-153 (2007).
258. Medina-Contreras, O.*, et al.* CX3CR1 regulates intestinal macrophage homeostasis, bacterial translocation, and colitogenic Th17 responses in mice. *J Clin Invest* **121**, 4787-4795 (2011).
259. Kayama, H.*, et al.* Intestinal CX3C chemokine receptor 1(high) (CX3CR1(high)) myeloid cells prevent T-cell-dependent colitis. *Proc Natl Acad Sci USA* **109**, 5010-5015 (2012).
260. TRUELOVE, S.C. & Pena, A.S. Course and prognosis of Crohn's disease. *Gut* **17**, 192-201 (1976).
261. Hench, P.S., Kendall, E.C. & et al. The effect of a hormone of the adrenal cortex (17-hydroxy-11-dehydrocorticosterone; compound E) and of pituitary adrenocorticotropic hormone on rheumatoid arthritis. **24**, 181-197 (1949).
262. Lloyd, M. Philip Showalter Hench, 1896-1965. *Rheumatology (Oxford)* **41**, 582-584 (2002).
263. TRUELOVE, S.C. & WITTS, L.J. Cortisone in ulcerative colitis; preliminary report on a therapeutic trial. *Br Med J* **2**, 375-378 (1954).
264. TRUELOVE, S.C. & WITTS, L.J. Cortisone and corticotrophin in ulcerative colitis. *Br Med J* **1**, 387-394 (1959).
265. Faubion, W.A., Loftus, E.V., Harmsen, W.S., Zinsmeister, A.R. & Sandborn, W.J. The natural history of corticosteroid therapy for inflammatory bowel disease: a population-based study. *Gastroenterology* **121**, 255-260 (2001).
266. Brook, C.G.D. & Marshall, N.J. *Essential Endocrinology*, (John Wiley & Sons, 2001).
267. Hadley, M.E. & Levine, J.E. *Endocrinology*, (Pearson Prentice Hall, 2007).
268. Whitehead, S.A. & Nussey, S.S. *Endocrinology: An Integrated Approach*, (Taylor & Francis, 2001).
269. Rhen, T. & Cidlowski, J.A. Antiinflammatory action of glucocorticoids--new mechanisms for old drugs. *N Engl J Med* **353**, 1711-1723 (2005).
270. Buttgereit, F., Straub, R.H., Wehling, M. & Burmester, G.-R. Glucocorticoids in the treatment of rheumatic diseases: an update on the mechanisms of action. *Arthritis Rheum* **50**, 3408-3417 (2004).
271. Holgate, S.T. & Polosa, R. Treatment strategies for allergy and asthma. *Nat Rev Immunol* **8**, 218-230 (2008).
272. Coutinho, A.E. & Chapman, K.E. The anti-inflammatory and immunosuppressive effects of glucocorticoids, recent developments and mechanistic insights. *Mol Cell Endocrinol* **335**, 2-13 (2011).
273. Barnes, P.J. Glucocorticosteroids: current and future directions. *Br J Pharmacol* (2010).
274. Auphan, N., DiDonato, J.A., Rosette, C., Helmberg, A. & Karin, M. Immunosuppression by glucocorticoids: inhibition of NF-kappa B activity through induction of I kappa B synthesis. *Science* **270**, 286-290 (1995).
275. Ray, A. & Prefontaine, K.E. Physical association and functional antagonism between the p65 subunit of transcription factor NF-kappa B and the glucocorticoid receptor. *Proc Natl Acad Sci USA* **91**, 752-756 (1994).
276. Van Laethem, F.*, et al.* Glucocorticoids attenuate T cell receptor signaling. *The Journal of Experimental Medicine* **193**, 803-814 (2001).

277. Baus, E., Andris, F., Dubois, P.M., Urbain, J. & Leo, O. Dexamethasone inhibits the early steps of antigen receptor signaling in activated T lymphocytes. *J Immunol* **156**, 4555-4561 (1996).
278. Andrade, M.V.M., Hiragun, T. & Beaven, M.A. Dexamethasone suppresses antigen-induced activation of phosphatidylinositol 3-kinase and downstream responses in mast cells. *J Immunol* **172**, 7254-7262 (2004).
279. Tack, G.J., Verbeek, W.H.M., Schreurs, M.W.J. & Mulder, C.J.J. The spectrum of celiac disease: epidemiology, clinical aspects and treatment. *Nat Rev Gastroenterol Hepatol* **7**, 204-213 (2010).
280. Ludvigsson, J.F.*, et al.* The Oslo definitions for coeliac disease and related terms. *Gut* (2012).
281. Olén, O.*, et al.* Coeliac disease characteristics, compliance to a gluten free diet and risk of lymphoma by subtype. *Dig Liver Dis* **43**, 862-868 (2011).
282. Casellas, F., López Vivancos, J. & Malagelada, J.R. Current epidemiology and accessibility to diet compliance in adult celiac disease. *Rev Esp Enferm Dig* **98**, 408-419 (2006).
283. PHR, G.*, et al.* Characteristics of adult celiac disease in the USA: results of a national survey. *The American Journal of Gastroenterology* **96**, 126-131 (2001).
284. Dubé, C.*, et al.* The prevalence of celiac disease in average-risk and at-risk Western European populations: a systematic review. *Gastroenterology* **128**, S57-67 (2005).
285. Sanders. British Society of Gastroenterology. 1-44 (2010).
286. Sollid, L.M. Coeliac disease: dissecting a complex inflammatory disorder. *Nat Rev Immunol* **2**, 647-655 (2002).
287. Schuppan, D., Junker, Y. & Barisani, D. Celiac disease: from pathogenesis to novel therapies. *Gastroenterology* **137**, 1912-1933 (2009).
288. Dieterich, W.*, et al.* Identification of tissue transglutaminase as the autoantigen of celiac disease. *Nat Med* **3**, 797-801 (1997).
289. Di Niro, R.*, et al.* High abundance of plasma cells secreting transglutaminase 2-specific IgA autoantibodies with limited somatic hypermutation in celiac disease intestinal lesions. *Nat Med* **18**, 441-445 (2012).
290. Colombel, J.F.*, et al.* Jejunal immunoglobulin and antigliadin antibody secretion in adult coeliac disease. *Gut* **31**, 1345-1349 (1990).
291. Green, P.H.R. & Cellier, C. Celiac disease. *N Engl J Med* **357**, 1731-1743 (2007).
292. Kaukinen, K., Partanen, J., Mäki, M. & Collin, P. HLA-DQ typing in the diagnosis of celiac disease. *The American Journal of Gastroenterology* **97**, 695-699 (2002).
293. Molberg, O.*, et al.* Tissue transglutaminase selectively modifies gliadin peptides that are recognized by gut-derived T cells in celiac disease. *Nat Med* **4**, 713-717 (1998).
294. Arentz-Hansen, H.*, et al.* The intestinal T cell response to alpha-gliadin in adult celiac disease is focused on a single deamidated glutamine targeted by tissue transglutaminase. *The Journal of Experimental Medicine* **191**, 603-612 (2000).
295. Sjöström, H.*, et al.* Identification of a gliadin T-cell epitope in coeliac disease: general importance of gliadin deamidation for intestinal T-cell recognition. *Scand J Immunol* **48**, 111-115 (1998).
296. van de Wal, Y.*, et al.* Small intestinal T cells of celiac disease patients recognize a natural pepsin fragment of gliadin. *Proc Natl Acad Sci USA* **95**, 10050-10054 (1998).
297. Lundin, K.E.*, et al.* Gliadin-specific, HLA-DQ(alpha 1*0501,beta 1*0201) restricted T cells isolated from the small intestinal mucosa of celiac disease patients. *The Journal of Experimental Medicine* **178**, 187-196 (1993).

298. Nilsen, E.M., *et al.* Gluten specific, HLA-DQ restricted T cells from coeliac mucosa produce cytokines with Th1 or Th0 profile dominated by interferon gamma. *Gut* **37**, 766-776 (1995).
299. Salvati, V.M., *et al.* Interleukin 18 and associated markers of T helper cell type 1 activity in coeliac disease. *Gut* **50**, 186-190 (2002).
300. Monteleone, G., *et al.* Role of interferon alpha in promoting T helper cell type 1 responses in the small intestine in coeliac disease. *Gut* **48**, 425-429 (2001).
301. Gianfrani, C., *et al.* Celiac disease association with CD8+ T cell responses: identification of a novel gliadin-derived HLA-A2-restricted epitope. *J Immunol* **170**, 2719-2726 (2003).
302. Mazzarella, G., *et al.* Gliadin activates HLA class I-restricted CD8+ T cells in celiac disease intestinal mucosa and induces the enterocyte apoptosis. *Gastroenterology* **134**, 1017-1027 (2008).
303. Meresse, B., *et al.* Coordinated induction by IL15 of a TCR-independent NKG2D signaling pathway converts CTL into lymphokine-activated killer cells in celiac disease. *Immunity* **21**, 357-366 (2004).
304. Meresse, B., *et al.* Reprogramming of CTLs into natural killer-like cells in celiac disease. *The Journal of Experimental Medicine* **203**, 1343-1355 (2006).
305. Sakakibara, S., Sakakibara, K. & Tosato, G. NF- B Activation Stimulates Transcription and Replication of Retrovirus XMRV in Human B-Lineage and Prostate Carcinoma Cells. *J Virol* **85**, 3179-3186 (2011).
306. Proudfoot, A.E., Power, C.A., Church, D.J., Soler, D. & Mack, M. Cellular assays of chemokine receptor activation. *Curr Protoc Pharmacol* **Chapter 12**, Unit12.14 (2001).
307. Takahashi, A., Camacho, P., Lechleiter, J.D. & Herman, B. Measurement of intracellular calcium. *Physiol Rev* **79**, 1089-1125 (1999).
308. Dustin, L.B. Ratiometric analysis of calcium mobilization. *Clinical and Applied Immunology Reviews* **1**, 5-15 (2000).
309. Bailey, S. & Macardle, P.J. A flow cytometric comparison of Indo-1 to fluo-3 and Fura Red excited with low power lasers for detecting Ca(2+) flux. *J Immunol Methods* **311**, 220-225 (2006).
310. Livak, K.J. & Schmittgen, T.D. Analysis of Relative Gene Expression Data Using Real-Time Quantitative PCR and the 2−ΔΔCT Method. *Methods* **25**, 402-408 (2001).
311. Middel, P., Raddatz, D., Gunawan, B., Haller, F. & Radzun, H.-J. Increased number of mature dendritic cells in Crohn's disease: evidence for a chemokine mediated retention mechanism. *Gut* **55**, 220-227 (2006).
312. Van Spreeuwel, J.P., *et al.* Morphological and immunohistochemical findings in upper gastrointestinal biopsies of patients with Crohn's disease of the ileum and colon. *J Clin Pathol* **35**, 934-940 (1982).
313. Mahida, Y.R., Patel, S., Gionchetti, P., Vaux, D. & Jewell, D.P. Macrophage subpopulations in lamina propria of normal and inflamed colon and terminal ileum. *Gut* **30**, 826-834 (1989).
314. Hirata, I., Berrebi, G., Austin, L.L., Keren, D.F. & Dobbins, W.O. Immunohistological characterization of intraepithelial and lamina propria lymphocytes in control ileum and colon and in inflammatory bowel disease. *Dig Dis Sci* **31**, 593-603 (1986).
315. Caballero, T., *et al.* Intraepithelial and lamina propria leucocyte subsets in inflammatory bowel disease: an immunohistochemical study of colon and rectal biopsy specimens. *J Clin Pathol* **48**, 743-748 (1995).

316. ChemoCentryx, I. A Study to Evaluate the Efficacy and Safety of CCX282-B in Subjects With Moderate to Severe Crohn's Disease (PROTECT-1). In: ClinicalTrials.gov [Internet]. Bethesda (MD) : National Library of Medicine (US). 2000-[2012 Oct 5]. Available from: http://clinicaltrials.gov/show/NCT00306215 NLM Identifier: NCT00306215.
317. Binda, E.*, et al.* Quantitative isolation of mouse and human intestinal intraepithelial lymphocytes by elutriation centrifugation. *J Immunol Methods* **344**, 26-34 (2009).
318. Keshav, S.*, et al.* A Randomized Controlled Trial of the Efficacy and Safety of CCX282-B, an Orally-Administered Blocker of Chemokine Receptor CCR9, for Patients with Crohn's Disease. *PLoS ONE* **8**, e60094 (2013).
319. Olaussen, R.W., Farstad, I.N., Brandtzaeg, P. & Rugtveit, J. Age-related changes in CCR9+ circulating lymphocytes: are CCR9+ naive T cells recent thymic emigrants? *Scand J Immunol* **54**, 435-439 (2001).
320. Kunkel, E.J.*, et al.* CCR10 expression is a common feature of circulating and mucosal epithelial tissue IgA Ab-secreting cells. *J Clin Invest* **111**, 1001-1010 (2003).
321. Holness, C.L. & Simmons, D.L. Molecular cloning of CD68, a human macrophage marker related to lysosomal glycoproteins. *Blood* **81**, 1607-1613 (1993).
322. Strobl, H.*, et al.* Identification of CD68+lin- peripheral blood cells with dendritic precursor characteristics. *J Immunol* **161**, 740-748 (1998).
323. Senju, M., Wu, K.C., Mahida, Y.R. & Jewell, D.P. Coexpression of CD4 and CD8 on peripheral blood T cells and lamina propria T cells in inflammatory bowel disease by two colour immunofluorescence and flow cytometric analysis. *Gut* **32**, 918-922 (1991).
324. Mizukami, T.*, et al.* CCR9(+) macrophages are required for eradication of peritoneal bacterial infections and prevention of polymicrobial sepsis. *Immunol Lett* (2012).
325. Su, C., Lichtenstein, G.R., Krok, K., Brensinger, C.M. & Lewis, J.D. A meta-analysis of the placebo rates of remission and response in clinical trials of active Crohn's disease. *Gastroenterology* **126**, 1257-1269 (2004).
326. Ghosh, S.*, et al.* Natalizumab for active Crohn's disease. *N Engl J Med* **348**, 24-32 (2003).
327. Targan, S.R.*, et al.* Natalizumab for the treatment of active Crohn's disease: results of the ENCORE Trial. *Gastroenterology* **132**, 1672-1683 (2007).
328. Kane, S.V.*, et al.* Natalizumab for moderate to severe Crohn's disease in clinical practice: The Mayo Clinic Rochester experience. *Inflamm Bowel Dis* (2012).
329. Bannai, M.*, et al.* Abundance of unconventional CD8(+) natural killer T cells in the large intestine. *Eur. J. Immunol.* **31**, 3361-3369 (2001).
330. Kelly, E., Bailey, C.P. & Henderson, G. Agonist-selective mechanisms of GPCR desensitization. *British Journal of Pharmacology* **153**, S379-S388 (2009).
331. Mariani, M., Lang, R., Binda, E., Panina-Bordignon, P. & D'Ambrosio, D. Dominance of CCL22 over CCL17 in induction of chemokine receptor CCR4 desensitization and internalization on human Th2 cells. *Eur. J. Immunol.* **34**, 231-240 (2004).
332. Meiser, A.*, et al.* The chemokine receptor CXCR3 is degraded following internalization and is replenished at the cell surface by de novo synthesis of receptor. *J Immunol* **180**, 6713-6724 (2008).
333. Proudfoot, A.E.I., Power, C.A., Church, D.J., Soler, D. & Mack, M. Cellular Assays of Chemokine Receptor Activation. in *Current Protocols in Pharmacology* (John Wiley & Sons, Inc., 2001).
334. White, G.E. & Greaves, D.R. Fractalkine: a survivor's guide: chemokines as antiapoptotic mediators. *Arterioscler Thromb Vasc Biol* **32**, 589-594 (2012).

335. Karpus, W.J*., et al.* Differential CC chemokine-induced enhancement of T helper cell cytokine production. *J Immunol* **158**, 4129-4136 (1997).
336. Burns, J.M*., et al.* A novel chemokine receptor for SDF-1 and I-TAC involved in cell survival, cell adhesion, and tumor development. *The Journal of Experimental Medicine* **203**, 2201-2213 (2006).
337. Xanthou, G., Williams, T.J. & Pease, J.E. Molecular characterization of the chemokine receptor CXCR3: evidence for the involvement of distinct extracellular domains in a multi-step model of ligand binding and receptor activation. *Eur. J. Immunol.* **33**, 2927-2936 (2003).
338. Sarra, M., Pallone, F., Macdonald, T.T. & Monteleone, G. IL-23/IL-17 axis in IBD. *Inflamm Bowel Dis* **16**, 1808-1813 (2010).
339. Sullivan, K.E*., et al.* Measurement of cytokine secretion, intracellular protein expression, and mRNA in resting and stimulated peripheral blood mononuclear cells. *Clin Diagn Lab Immunol* **7**, 920-924 (2000).
340. Schroeder, A*., et al.* The RIN: an RNA integrity number for assigning integrity values to RNA measurements. *BMC Mol Biol* **7**, 3 (2006).
341. Zachar, V., Mikulecky, M., Mayer, V., Mackay, I. & Frazer, I. A biometrical view on normal values of CD4 and CD8 lymphocyte counts in peripheral blood. *Pathology* **20**, 358-360 (1988).
342. Grakoui, A*., et al.* The immunological synapse: a molecular machine controlling T cell activation. *Science* **285**, 221-227 (1999).
343. Springer, T.A. & Dustin, M.L. Integrin inside-out signaling and the immunological synapse. *Current Opinion in Cell Biology* **24**, 107-115 (2012).
344. Fan, S.T*., et al.* CD11a/CD18 (LFA-1) integrin engagement enhances biosynthesis of early cytokines by activated T cells. *Cell Immunol* **148**, 48-59 (1993).
345. van Rheenen, P.F., Van de Vijver, E. & Fidler, V. Faecal calprotectin for screening of patients with suspected inflammatory bowel disease: diagnostic meta-analysis. *BMJ* **341**, c3369 (2010).
346. Souza, H.S., Elia, C.C., Spencer, J. & MacDonald, T.T. Expression of lymphocyte-endothelial receptor-ligand pairs, alpha4beta7/MAdCAM-1 and OX40/OX40 ligand in the colon and jejunum of patients with inflammatory bowel disease. *Gut* **45**, 856-863 (1999).
347. Ando, T*., et al.* Inflammatory cytokines induce MAdCAM-1 in murine hepatic endothelial cells and mediate alpha-4 beta-7 integrin dependent lymphocyte endothelial adhesion in vitro. *BMC Physiol* **7**, 10 (2007).
348. Roozendaal, R. & Mebius, R.E. Stromal cell-immune cell interactions. *Annual review of immunology* **29**, 23-43 (2011).
349. Szabo, M.C., Butcher, E.C. & McEvoy, L.M. Specialization of mucosal follicular dendritic cells revealed by mucosal addressin-cell adhesion molecule-1 display. *J Immunol* **158**, 5584-5588 (1997).
350. Grant, A.J., Lalor, P.F., Hübscher, S.G., Briskin, M. & Adams, D.H. MAdCAM-1 expressed in chronic inflammatory liver disease supports mucosal lymphocyte adhesion to hepatic endothelium (MAdCAM-1 in chronic inflammatory liver disease). *Hepatology (Baltimore, Md)* **33**, 1065-1072 (2001).
351. Yang, Y.-X. & Lichtenstein, G.R. Corticosteroids in Crohn's disease. *The American Journal of Gastroenterology* **97**, 803-823 (2002).
352. Ashwell, J.D., Lu, F.W. & Vacchio, M.S. Glucocorticoids in T cell development and function. *Annual review of immunology* **18**, 309-345 (2000).

353. Kunicka, J.E., *et al.* Immunosuppression by glucocorticoids: inhibition of production of multiple lymphokines by in vivo administration of dexamethasone. *Cell Immunol* **149**, 39-49 (1993).
354. Almawi, W.Y., Beyhum, H.N., Rahme, A.A. & Rieder, M.J. Regulation of cytokine and cytokine receptor expression by glucocorticoids. *J Leukoc Biol* **60**, 563-572 (1996).
355. Vacca, A., *et al.* Glucocorticoid receptor-mediated suppression of the interleukin 2 gene expression through impairment of the cooperativity between nuclear factor of activated T cells and AP-1 enhancer elements. *The Journal of Experimental Medicine* **175**, 637-646 (1992).
356. Penton-Rol, G., *et al.* Up-regulation of CCR2 chemokine receptor expression and increased susceptibility to the multitropic HIV strain 89.6 in monocytes exposed to glucocorticoid hormones. *J Immunol* **163**, 3524-3529 (1999).
357. Okutsu, M., Suzuki, K., Ishijima, T., Peake, J. & Higuchi, M. The effects of acute exercise-induced cortisol on CCR2 expression on human monocytes. *Brain Behav Immun* **22**, 1066-1071 (2008).
358. Curnow, S.J., *et al.* Topical glucocorticoid therapy directly induces up-regulation of functional CXCR4 on primed T lymphocytes in the aqueous humor of patients with uveitis. *J Immunol* **172**, 7154-7161 (2004).
359. Okutsu, M., Ishii, K., Niu, K.J. & Nagatomi, R. Cortisol-induced CXCR4 augmentation mobilizes T lymphocytes after acute physical stress. *Am J Physiol Regul Integr Comp Physiol* **288**, R591-599 (2005).
360. Wang, J., *et al.* IL-4 and a glucocorticoid up-regulate CXCR4 expression on human CD4+ T lymphocytes and enhance HIV-1 replication. *J Leukoc Biol* **64**, 642-649 (1998).
361. Ghosh, M.C., *et al.* Dexamethasone augments CXCR4-mediated signaling in resting human T cells via the activation of the Src kinase Lck. *Blood* **113**, 575-584 (2009).
362. Nagase, H., *et al.* Glucocorticoids preferentially upregulate functional CXCR4 expression in eosinophils. *J Allergy Clin Immunol* **106**, 1132-1139 (2000).
363. Dimitrov, S., *et al.* Cortisol and epinephrine control opposing circadian rhythms in T cell subsets. *Blood* **113**, 5134-5143 (2009).
364. Lu, N.Z., *et al.* International Union of Pharmacology. LXV. The pharmacology and classification of the nuclear receptor superfamily: glucocorticoid, mineralocorticoid, progesterone, and androgen receptors. *Pharmacol Rev* **58**, 782-797 (2006).
365. Numakawa, T., *et al.* Glucocorticoid receptor interaction with TrkB promotes BDNF-triggered PLC-gamma signaling for glutamate release via a glutamate transporter. *Proc Natl Acad Sci USA* **106**, 647-652 (2009).
366. Committee, J.F. British Medical Association and the Royal Pharmaceutical Society of Great Britain. British National Formulary. 58th ed. UK: BMJ Publishing Group. 2009. (2009).
367. Hafezi-Moghadam, A., *et al.* Acute cardiovascular protective effects of corticosteroids are mediated by non-transcriptional activation of endothelial nitric oxide synthase. *Nat Med* **8**, 473-479 (2002).
368. Kremer, K.N., *et al.* Stromal cell-derived factor-1 signaling via the CXCR4-TCR heterodimer requires phospholipase C-{beta}3 and phospholipase C-{gamma}1 for distinct cellular responses. *J Immunol* **187**, 1440-1447 (2011).
369. Gosling, J., *et al.* Cutting edge: identification of a novel chemokine receptor that binds dendritic cell- and T cell-active chemokines including ELC, SLC, and TECK. *J Immunol* **164**, 2851-2856 (2000).

370. Townson, J.R. & Nibbs, R.J.B. Characterization of mouse CCX-CKR, a receptor for the lymphocyte-attracting chemokines TECK/mCCL25, SLC/mCCL21 and MIP-3beta/mCCL19: comparison to human CCX-CKR. *Eur. J. Immunol.* **32**, 1230-1241 (2002).
371. Heinzel, K., Benz, C. & Bleul, C.C. A silent chemokine receptor regulates steady-state leukocyte homing in vivo. *Proc Natl Acad Sci USA* **104**, 8421-8426 (2007).
372. Schweickart, V.L., Epp, A., Raport, C.J. & Gray, P.W. CCR11 is a functional receptor for the monocyte chemoattractant protein family of chemokines. *J Biol Chem* **275**, 9550-9556 (2000).
373. Yamamoto, J.*, et al.* Differential expression of the chemokine receptors by the Th1- and Th2-type effector populations within circulating CD4+ T cells. *J Leukoc Biol* **68**, 568-574 (2000).
374. Kim, C.H.*, et al.* Rules of chemokine receptor association with T cell polarization in vivo. *J Clin Invest* **108**, 1331-1339 (2001).
375. Sauty, A.*, et al.* The T cell-specific CXC chemokines IP-10, Mig, and I-TAC are expressed by activated human bronchial epithelial cells. *J Immunol* **162**, 3549-3558 (1999).
376. Groom, J.R. & Luster, A.D. CXCR3 ligands: redundant, collaborative and antagonistic functions. *Immunology and cell biology* **89**, 207-215 (2011).
377. Krakauer, T. Differential inhibitory effects of interleukin-10, interleukin-4, and dexamethasone on staphylococcal enterotoxin-induced cytokine production and T cell activation. *J Leukoc Biol* **57**, 450-454 (1995).
378. Sallusto, F., Lenig, D., Mackay, C.R. & Lanzavecchia, A. Flexible programs of chemokine receptor expression on human polarized T helper 1 and 2 lymphocytes. *The Journal of Experimental Medicine* **187**, 875-883 (1998).
379. Visser, J.*, et al.* Differential regulation of interleukin-10 (IL-10) and IL-12 by glucocorticoids in vitro. *Blood* **91**, 4255-4264 (1998).
380. Ramírez, F., Fowell, D.J., Puklavec, M., Simmonds, S. & Mason, D. Glucocorticoids promote a TH2 cytokine response by CD4+ T cells in vitro. *J Immunol* **156**, 2406-2412 (1996).
381. Brinkmann, V. & Kristofic, C. Regulation by corticosteroids of Th1 and Th2 cytokine production in human CD4+ effector T cells generated from CD45RO- and CD45RO+ subsets. *J Immunol* **155**, 3322-3328 (1995).
382. Richards, D.F., Fernandez, M., Caulfield, J. & Hawrylowicz, C.M. Glucocorticoids drive human CD8(+) T cell differentiation towards a phenotype with high IL-10 and reduced IL-4, IL-5 and IL-13 production. *Eur. J. Immunol.* **30**, 2344-2354 (2000).
383. Van Laethem, F., Baus, E., Andris, F., Urbain, J. & Leo, O. A novel aspect of the anti-inflammatory actions of glucocorticoids: inhibition of proximal steps of signaling cascades in lymphocytes. *Cell Mol Life Sci* **58**, 1599-1606 (2001).
384. Rutgeerts, P.*, et al.* A comparison of budesonide with prednisolone for active Crohn's disease. *N Engl J Med* **331**, 842-845 (1994).
385. Edsbäcker, S. & Andersson, T. Pharmacokinetics of budesonide (Entocort EC) capsules for Crohn's disease. *Clin Pharmacokinet* **43**, 803-821 (2004).
386. Berlin, C.*, et al.* alpha 4 integrins mediate lymphocyte attachment and rolling under physiologic flow. *Cell* **80**, 413-422 (1995).
387. Miles, A., Liaskou, E., Eksteen, B., Lalor, P.F. & Adams, D.H. CCL25 and CCL28 promote alpha4 beta7-integrin-dependent adhesion of lymphocytes to MAdCAM-1 under shear flow. *Am J Physiol Gastrointest Liver Physiol* **294**, G1257-1267 (2008).
388. Akobeng, A.K. & Thomas, A.G. Systematic review: tolerable amount of gluten for people with coeliac disease. *Aliment Pharmacol Ther* **27**, 1044-1052 (2008).

389. Meresse, B., Malamut, G. & Cerf-Bensussan, N. Celiac Disease: An Immunological Jigsaw. *Immunity* **36**, 907-919 (2012).
390. ChemoCentryx, I. A Phase II Study of CCX282-B in Patients With Celiac Disease. In: ClinicalTrials.gov [Internet]. Bethesda (MD) : National Library of Medicine (US). 2000-[2012 Oct 5]. Available from: http://clinicaltrials.gov/show/NCT00540657 NLM Identifier: NCT00540657.
391. ChemoCentryx, I. Safety and Activity Study of an Oral Medication to Treat Moderate to Severe Crohn's Disease. In: ClinicalTrials.gov [Internet]. Bethesda (MD) : National Library of Medicine (US). 2000-[2012 Oct 5]. Available from: http://clinicaltrials.gov/show/NCT00102921 NLM Identifier: NCT00102921.
392. Tiittanen, M., Westerholm-Ormio, M., Verkasalo, M., Savilahti, E. & Vaarala, O. Infiltration of forkhead box P3-expressing cells in small intestinal mucosa in coeliac disease but not in type 1 diabetes. *Clin Exp Immunol* **152**, 498-507 (2008).
393. Vorobjova, T.*, et al.* Increased FOXP3 expression in small-bowel mucosa of children with coeliac disease and type I diabetes mellitus. *Scand J Gastroenterol* **44**, 422-430 (2009).
394. Hmida, N.B.*, et al.* Impaired control of effector T cells by regulatory T cells: a clue to loss of oral tolerance and autoimmunity in celiac disease? *The American Journal of Gastroenterology* **107**, 604-611 (2012).
395. Zanzi, D.*, et al.* IL-15 Interferes With Suppressive Activity of Intestinal Regulatory T Cells Expanded in Celiac Disease. *The American Journal of Gastroenterology* **106**, 1308-1317 (2011).
396. Soper, D.S. A-priori Sample Size Calculator for Student t-Tests (Online Software). http://www.danielsoper.com/statcalc3. (2012).
397. Mosley, R.L., Whetsell, M. & Klein, J.R. Proliferative properties of murine intestinal intraepithelial lymphocytes (IEL): IEL expressing TCR alpha beta or TCR tau delta are largely unresponsive to proliferative signals mediated via conventional stimulation of the CD3-TCR complex. *Int Immunol* **3**, 563-569 (1991).
398. Nilsen, E.M.*, et al.* Gluten induces an intestinal cytokine response strongly dominated by interferon gamma in patients with celiac disease. *Gastroenterology* **115**, 551-563 (1998).
399. Troncone, R.*, et al.* Majority of gliadin-specific T-cell clones from celiac small intestinal mucosa produce interferon-gamma and interleukin-4. *Dig Dis Sci* **43**, 156-161 (1998).
400. GlaxoSmithKline. Open-Label Extension Study of GSK1605786A (SHIELD-3). In: ClinicalTrials.gov [Internet]. Bethesda (MD) : National Library of Medicine (US). 2000-[2012 Oct 5]. Available from: http://clinicaltrials.gov/show/NCT01318993 NLM Identifier: NCT01318993.
401. GlaxoSmithKline. GSK1605786A in the Maintenance of Remission in Subjects With Crohn's Disease (SHIELD-2). In: ClinicalTrials.gov [Internet]. Bethesda (MD) : National Library of Medicine (US). 2000-[2012 Oct 5]. Available from: http://clinicaltrials.gov/show/NCT01316939 NLM Identifier: NCT01316939.
402. Danese, S. New therapies for inflammatory bowel disease: from the bench to the bedside. *Gut* **61**, 918-932 (2012).
403. Vermeire, S.*, et al.* The mucosal addressin cell adhesion molecule antibody PF-00547,659 in ulcerative colitis: a randomised study. *Gut* **60**, 1068-1075 (2011).
404. Strandberg, K., Blidberg, K., Sahlander, K., Palmberg, L. & Larsson, K. Effect of formoterol and budesonide on chemokine release, chemokine receptor expression and chemotaxis in human neutrophils. *Pulmonary Pharmacology & Therapeutics* **23**, 316-323 (2010).

405. Kato, A.*, et al.* Dexamethasone and FK506 inhibit expression of distinct subsets of chemokines in human mast cells. *J Immunol* **182**, 7233-7243 (2009).

APPENDIX 1: Solutions used in this thesis

Cell culture

Complete growth media: 10% FCS, 50 U/ml penicillin, 50 µg/ml streptomycin, RPMI-1640 or DMEM.

Freezing medium: 10% DMSO, 80% FCS.

Red blood cell lysis buffer: 155 mM NH_4Cl, 12 mM $NaHCO_3$, 0.1 mM EDTA.

Immunohistochemistry

Blocking Solution: 10% human serum, D-PBS.

Citrate buffer: 10 mM Citric acid (anhydrous), pH 6.

Tris-EDTA buffer: 10 mM Tris Base, 1 mM EDTA, pH 9.

Peroxidase block: 3% H_2O_2 in ddH_2O.

Washing buffer: PBS ± 0.1% Tween-20.

Flow Cytometry

FACS buffer: 0.1% BSA, 0.1% NaN_3, D-PBS.

Cell sorting

Labeling buffer (for live cell isolation): 0.1% BSA, D-PBS.

Chemotaxis

Chemotaxis buffer: 0.1% BSA, 25mM HEPES, RPMI-1640.

Calcium flux

HEPES Buffered Saline Solution: 1 mM $CaCl_2$, 0.5 mM $MgCl_2$, 0.1% BSA,10 mM HEPES, HBSS.

Pluronic F-127: 20% weight/volume in DMSO.

Western blotting

Serum Free Medium: 0.1% BSA, RPMI-1640.

1% NP-40 buffer: 1% NP-40, 50 nM TRIS (pH 7.4), 150 nM NaCL, 1mM EDTA

Lysis buffer: 1 mM Sodium Orthovanadate ($NaVO_4$), 1 mM Sodium fluoride (NaF), 1 tablet of Protease inhibitor (Roche), 1% NP-40 buffer (note: activate $NaVO_4$ by heating to 100°C for 5 minutes and always make lysis buffer fresh).

TBS-T: 10 mM Tris-HCL, 68 mM NaCl, 0.05% Tween 20.

Stripping buffer: 67 mM Tris HCl, 2% SDS, 100 mM 2-mercaptoethanol.

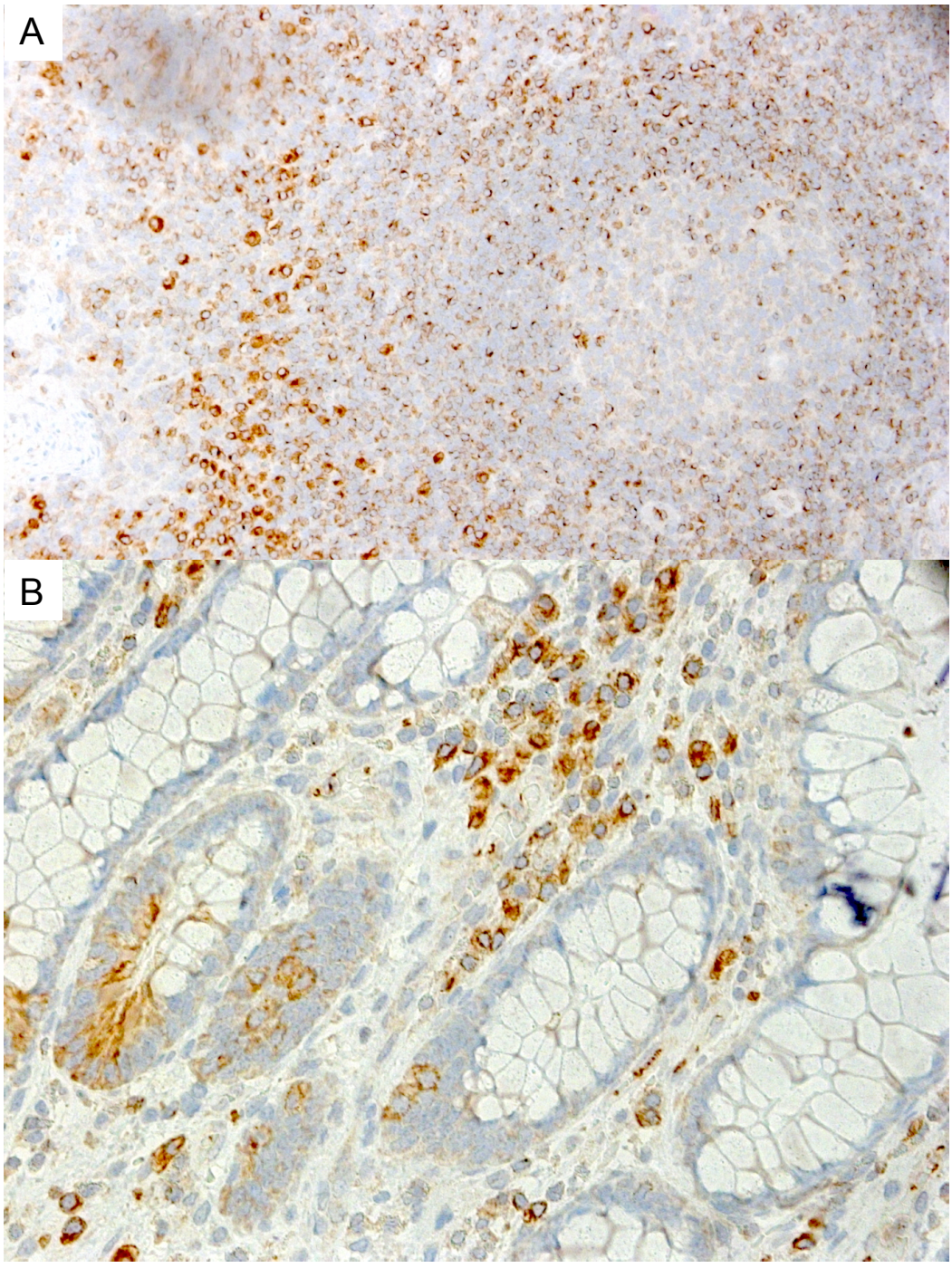
APPENDIX 2: Manuscripts and published work

Wendt, E., White, G., Ferry, H., Huhn, M., Schall, T, Greaves, D. R., Keshav, S. (2012) Glucocorticoids inhibit CCR9-mediated signalling in human T lymphocytes. *Manuscript.*

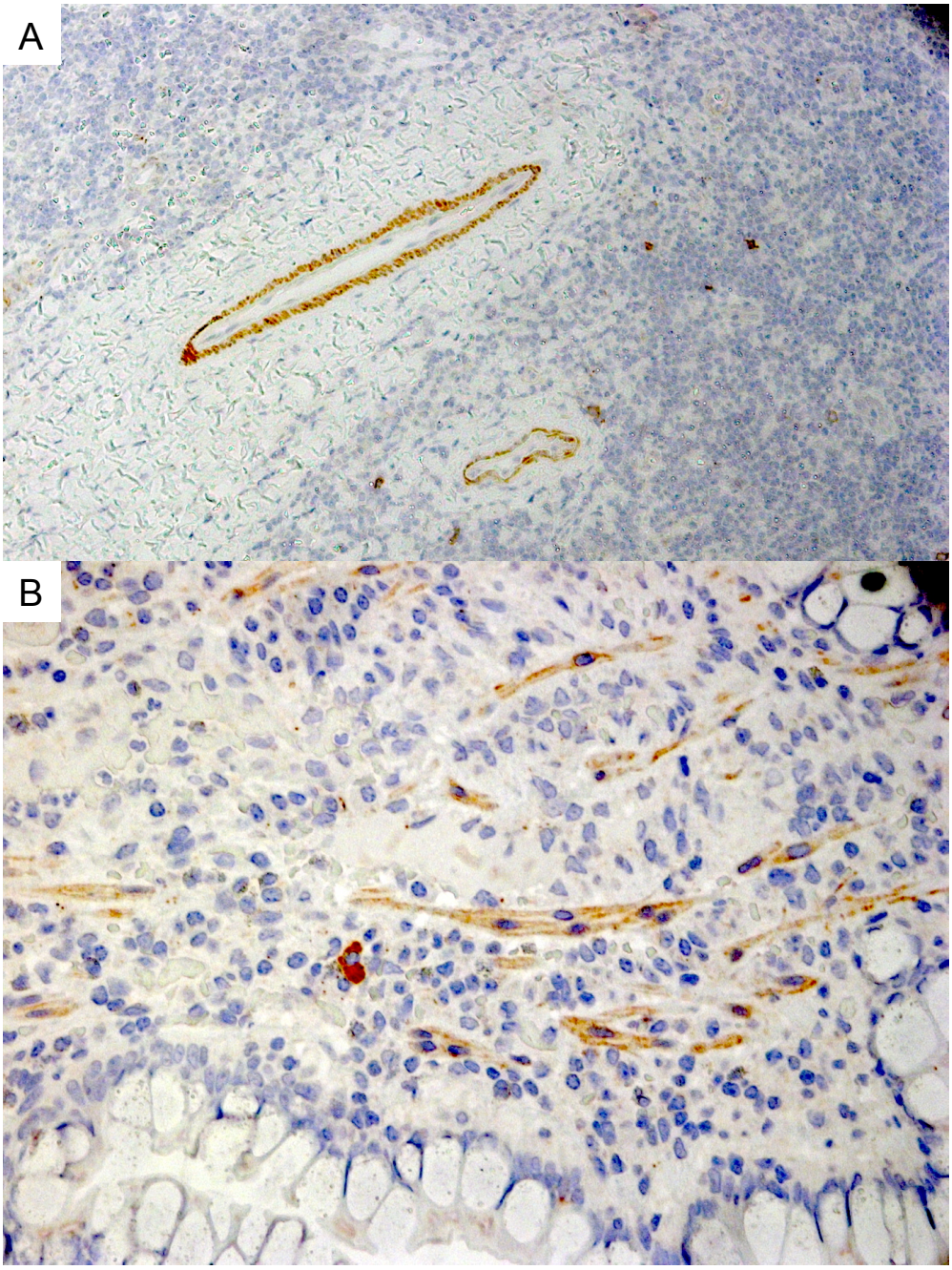
Walters, M., Wang, Y., Lai, N., Baumgart, T., Zhao, B., Dairaghi, D. J., Bekker, P., Ertl, L. S., Penfold, M. E. T., Jaej, J. C. Keshav, S., **Wendt, E**., Pennell, A., Ungashe, S., Wei, Z., Wright, J. J. K. & Schall, T. J. (2010) Characterization of CCX282-B, an Orally Bioavailable Antagonist of the CCR9 Chemokine Receptor, for Treatment of Inflammatory Bowel Disease. *The Journal of pharmacology and experimental therapeutics* 335: 61-69.

Vignuzzi, M., **Wendt, E**. & Andino, R. (2008) Engineering attenuated virus vaccines by controlling replication fidelity. *Nature Medicine* 14**:** 154-61.

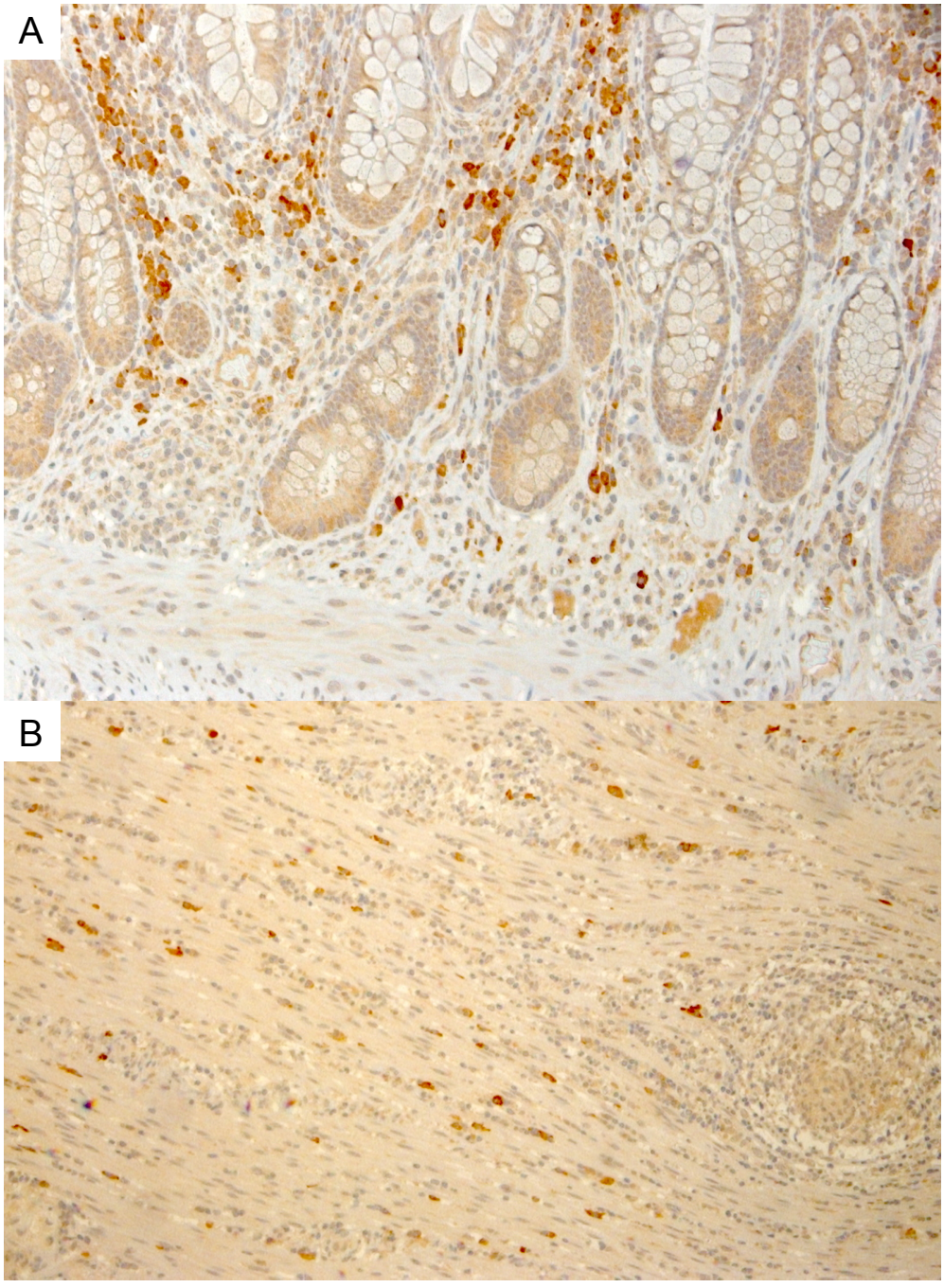
APPENDIX 3: Anti-human CCR9 antibodies rejected from used by IHC



CCR9 R&D Clone 248605.111
A: Paraffin embedded human tonsil.
B: Paraffin embedded, terminal ileum. Crohn's disease biopsy.
Conclusion: non-specific staining. Stained high proportion of cells in tonsil and Paneth cells in the small intestine.

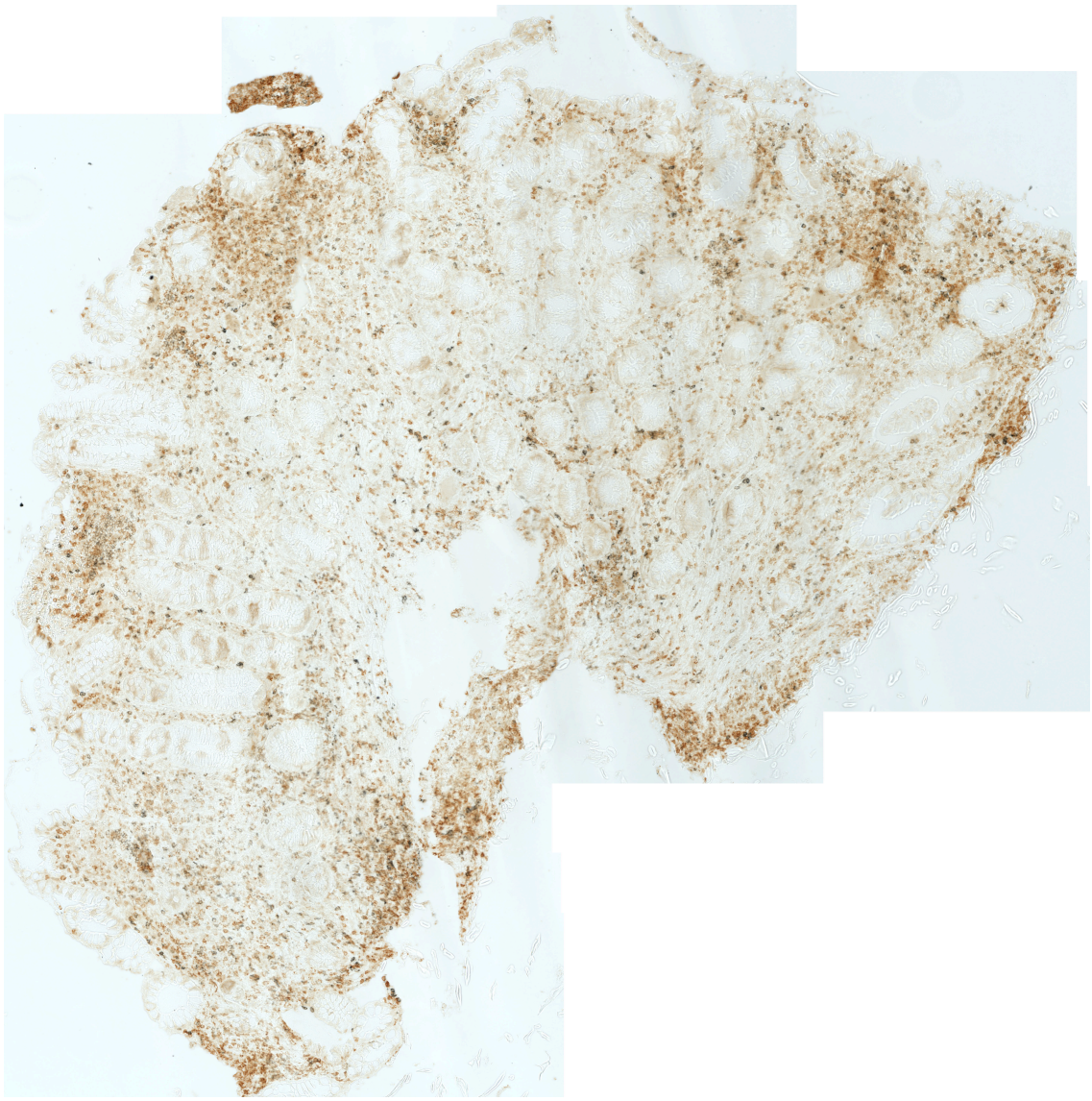


CCR9 R&D Clone 96-1.5
A: Paraffin embedded human tonsil.
B: Paraffin embedded, terminal ileum. Crohn's disease biopsy.
Conclusion: non-specific staining of vascular endothelial cells (A) and fibroblasts (B).

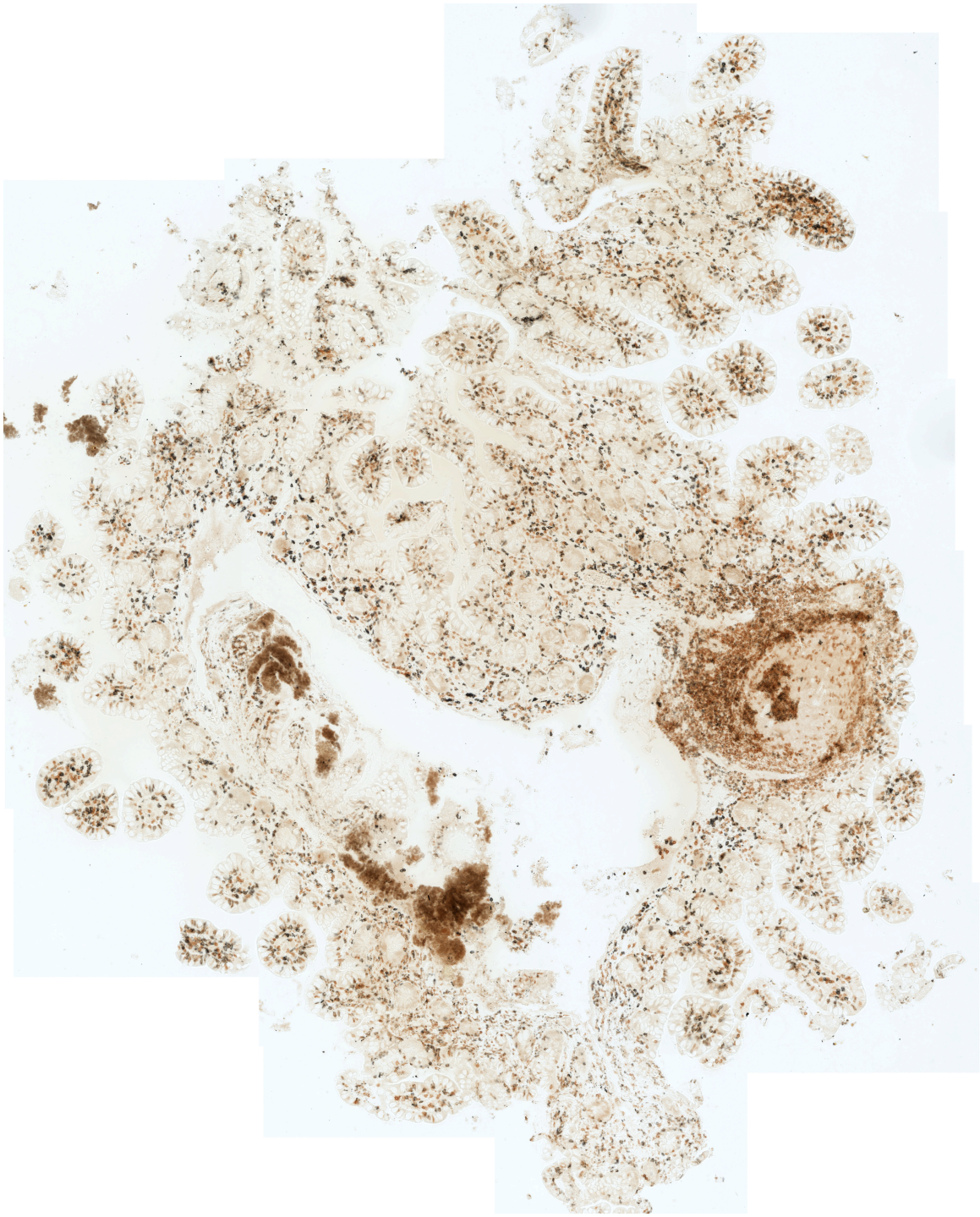


CCR9 R&D Clone 248601
A: Paraffin embedded, terminal ileum. Crohn's disease biopsy.
B: Muscularis externa of TI.
Conclusion: non-specific staining of intestinal epithelial cells (A) and within the muscularis externa (B).

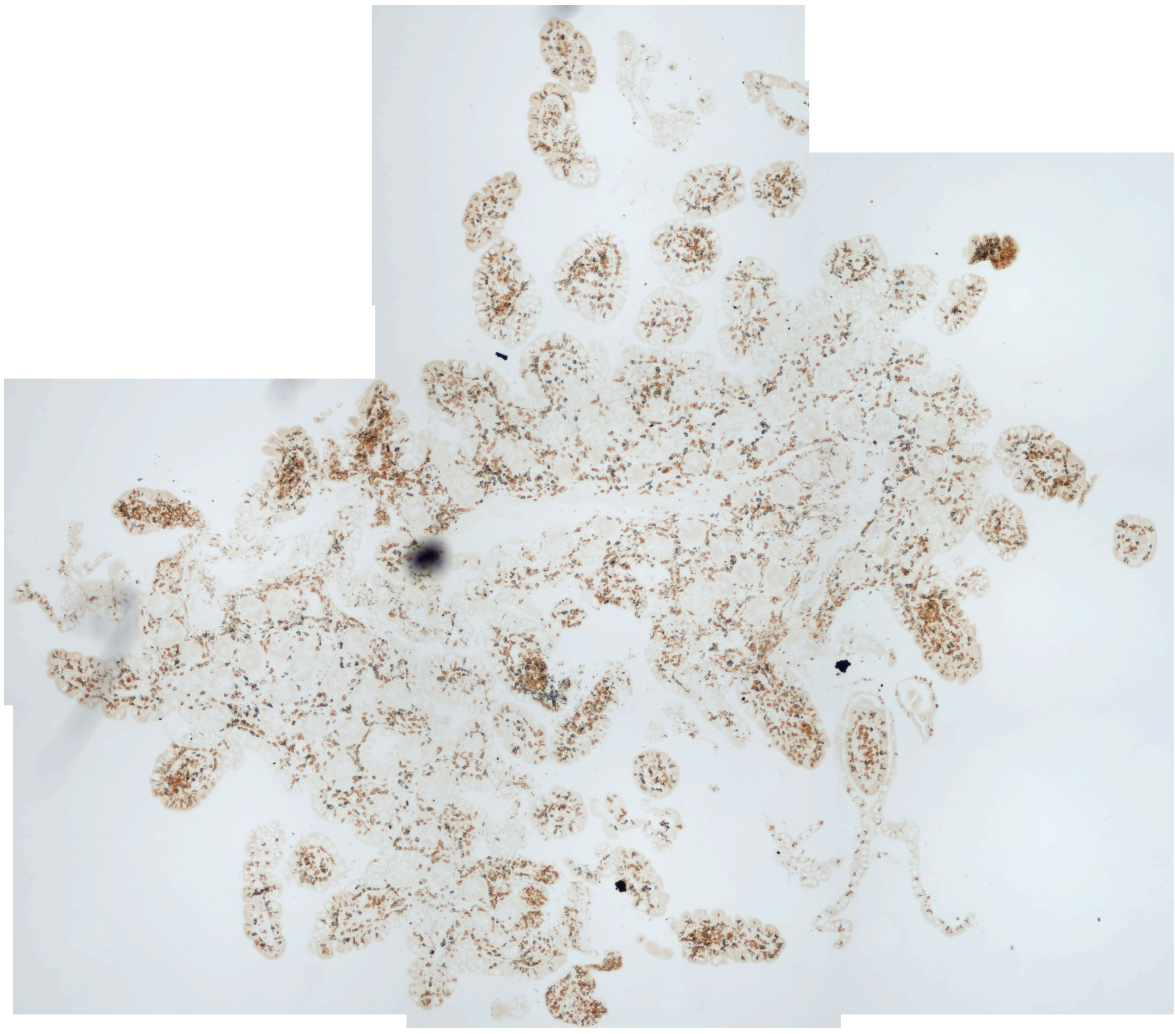
APPENDIX 4: Representative PROTECT-1 biopsies



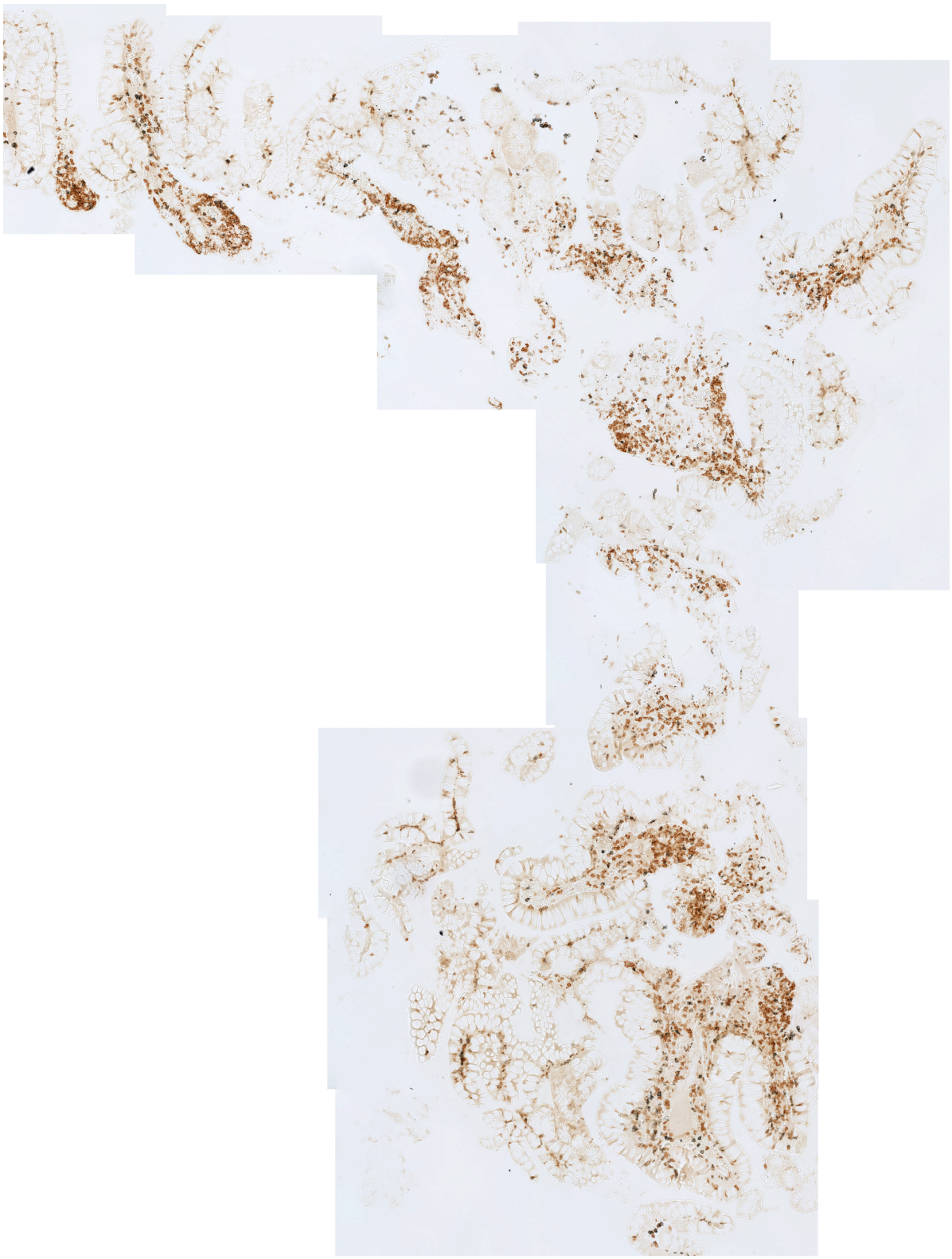
Representative PROTECT-1 clinical trial biopsy (1 of 6)



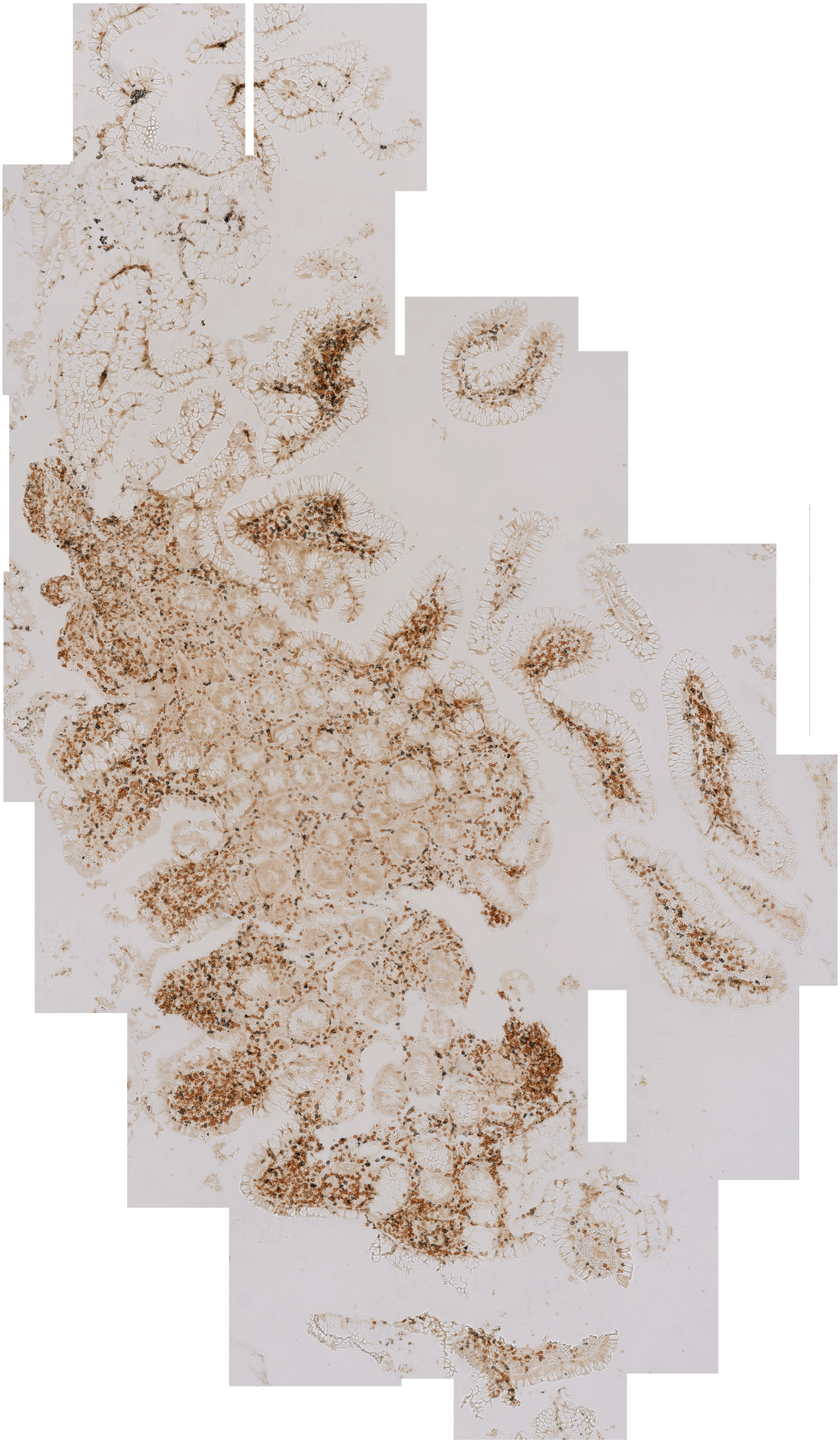
Representative PROTECT-1 clinical trial biopsy (2 of 6)



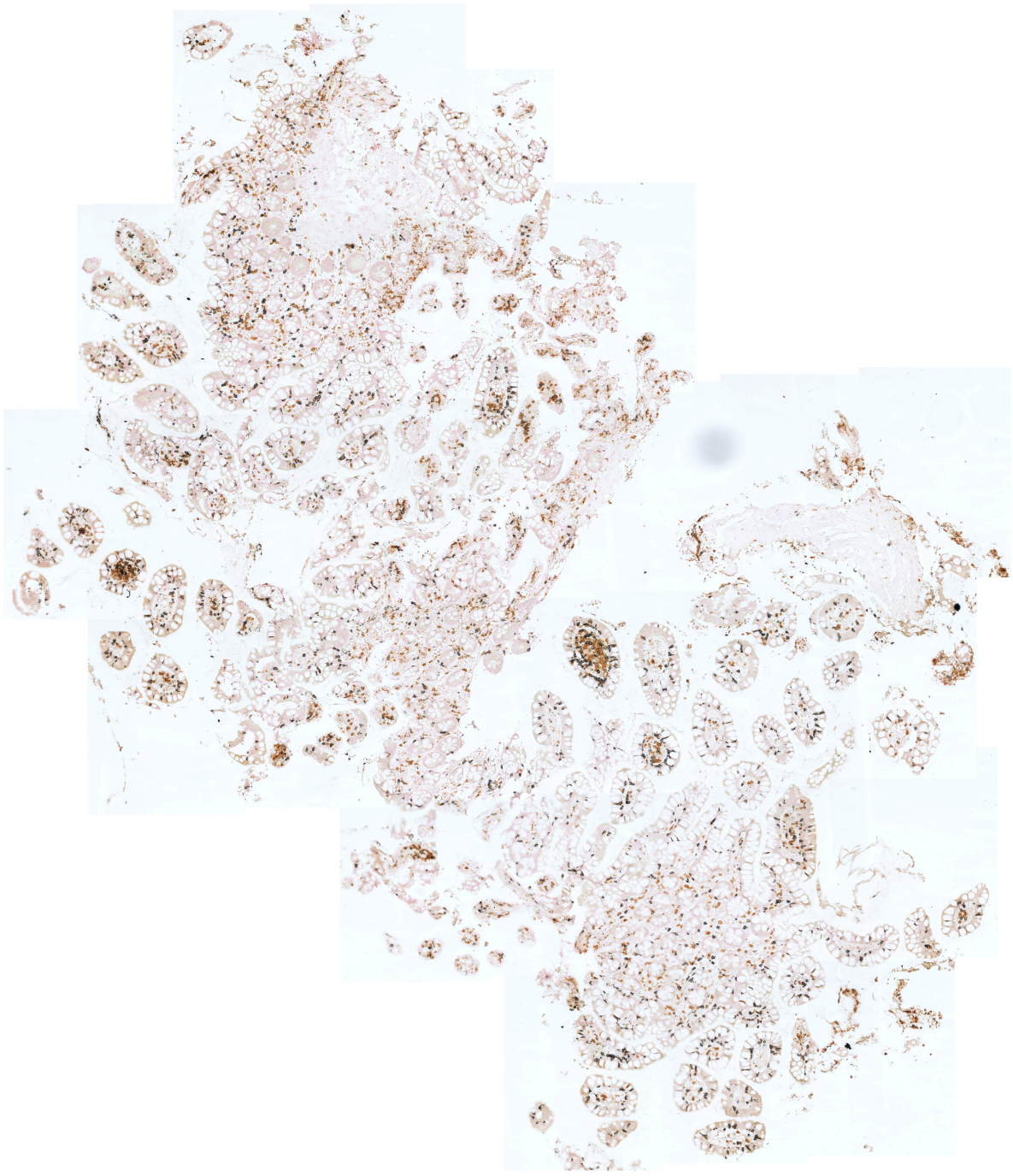
Representative PROTECT-1 clinical trial biopsy (3 of 6)



Representative PROTECT-1 clinical trial biopsy (4 of 6)

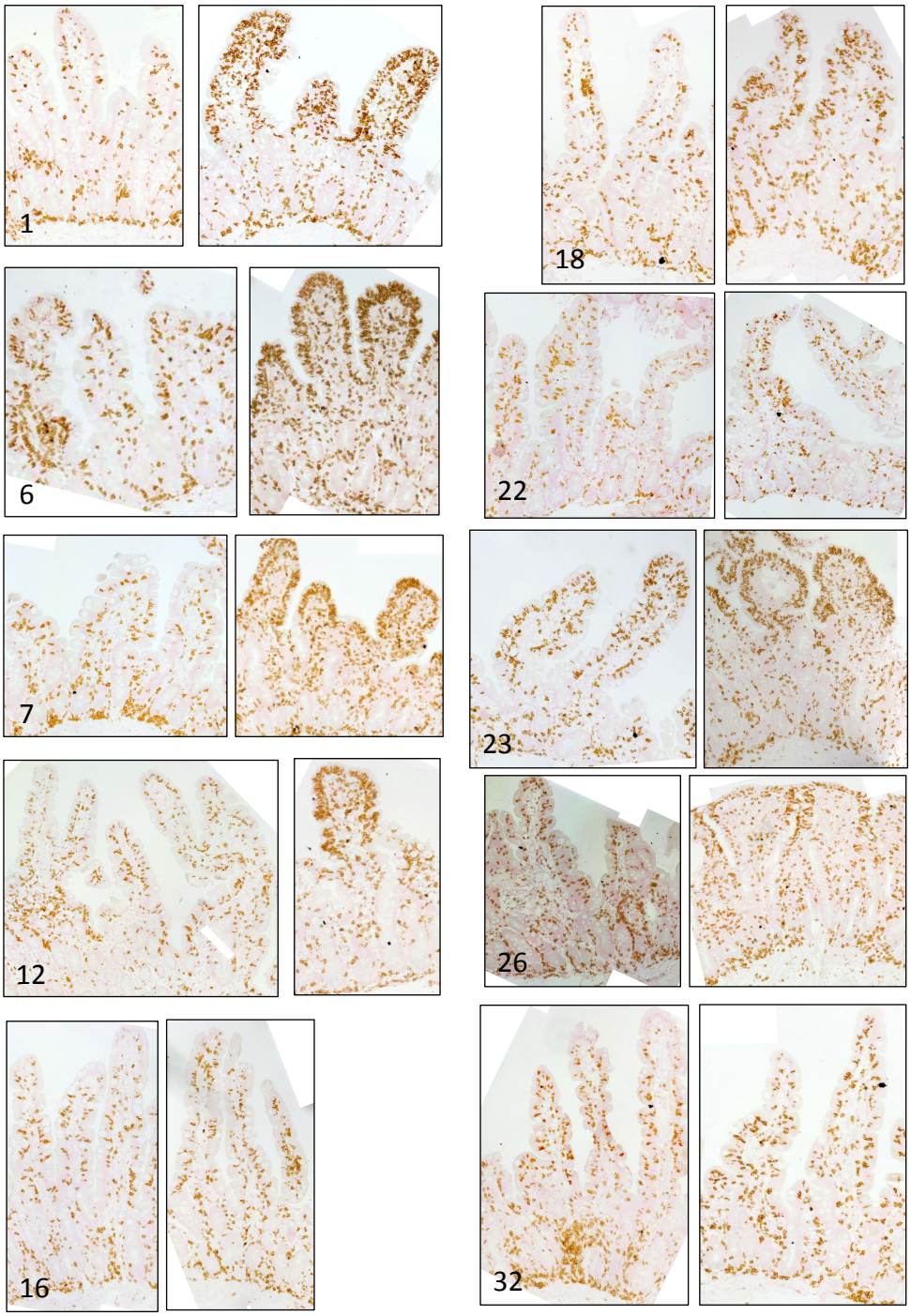


Representative PROTECT-1 clinical trial biopsy (5 of 6)

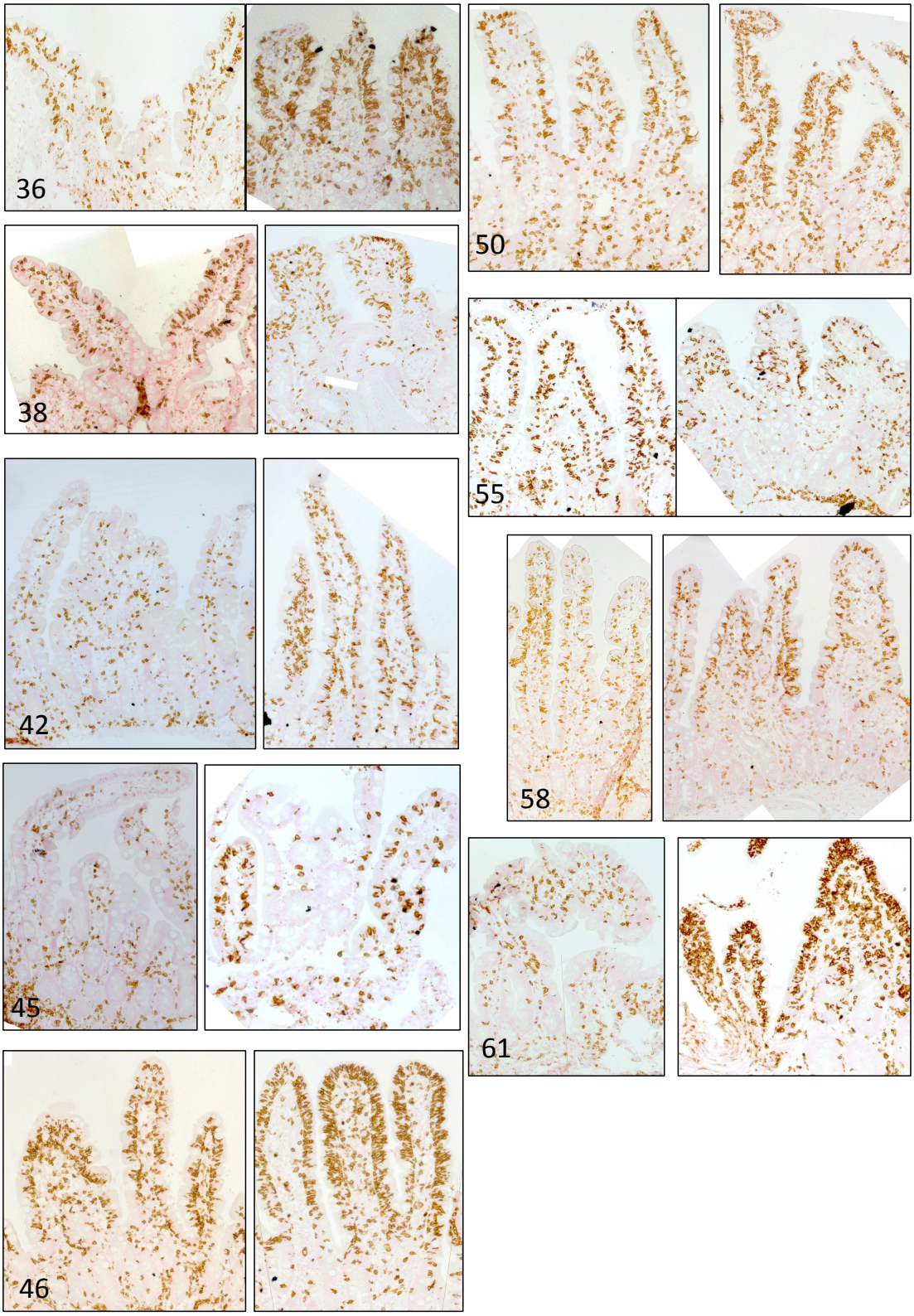


Representative PROTECT-1 clinical trial biopsy (6 of 6)

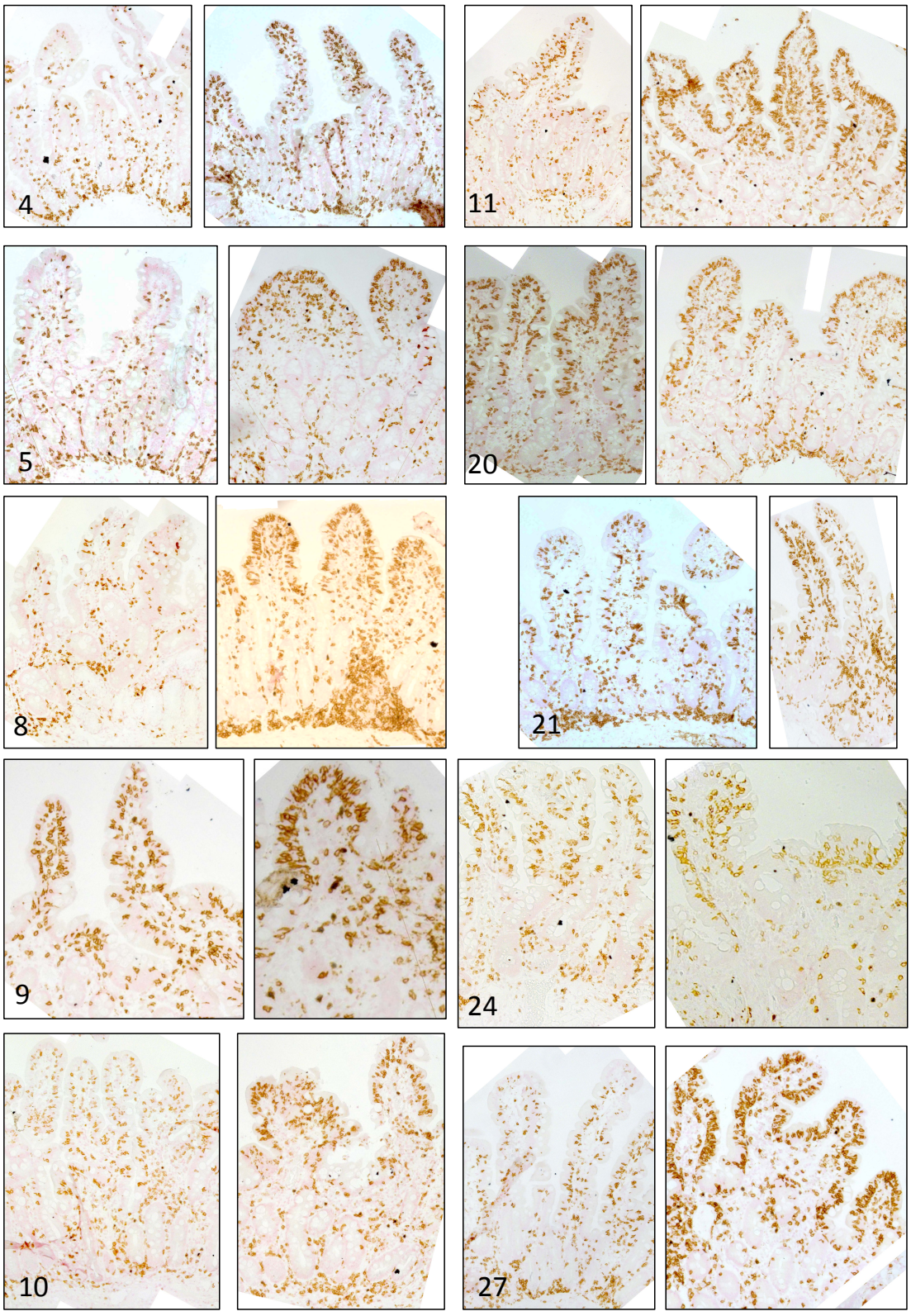
APPENDIX 5: Representative biopsies from the duodenum (Clinical trial in coeliac disease)



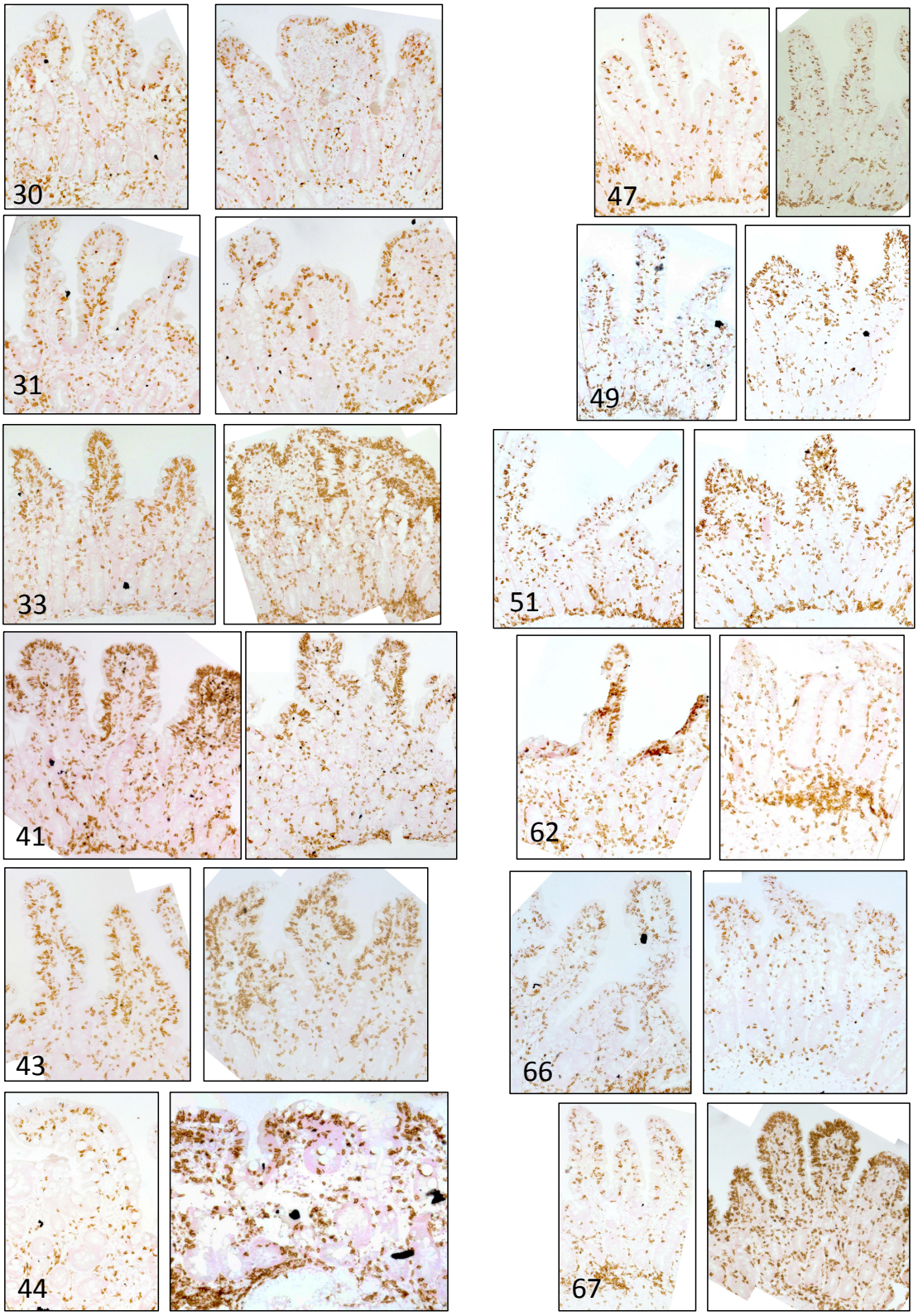
Matched Coeliac patient biopsies page 1 of 2 (placebo treatment).
Number is randomized identification for unique patient. Left biopsy is from Baseline (Gluten free diet, prior to treatment), right biopsy is following 91 days of gluten challenge (Day 91).



Matched Coeliac patient biopsies page 2 of 2 (placebo treatment)



Matched Coeliac patient biopsies page 1 of 2 (CCX282-B treatment)
Number is randomized identification for unique patient. Left biopsy is from Baseline (Gluten free diet, prior to treatment), right biopsy is following 91 days of gluten challenge (Day 91).



Matched Coeliac patient biopsies page 2 of 2 (CCX282-B treatment)